A quantum statistical approach to quantum correlations in many-body systems

Irénée Frerot

Numéro National de Thèse : 2017LYSEN061

THESE de DOCTORAT DE L'UNIVERSITE DE LYON
opérée par
l'Ecole Normale Supérieure de Lyon

Ecole Doctorale N°52
Physique et Astrophysique de Lyon (PHAST)
Discipline : Physique

Soutenue publiquement le 09/10/2017, par:

Irénée Frérot

Corrélations quantiques : une approche de physique statistique

A quantum-statistical approach to quantum correlations in many-body systems

---

Devant le jury composé de :

Antoine Browaeys, DR CNRS, Institut d'Optique (Palaiseau), Examinateur
Pascal Degiovanni, DR CNRS, Ecole Normale Supérieure de Lyon, Examinateur
Nicolas Laflorencie, CR CNRS Université Paul Sabatier (Toulouse), Rapporteur
Luca Tagliacozzo, Lecturer, University of Strathclyde (Glasgow), Examinateur
Anna Sanpera Trigueros, Professeur ICREA, Universitat Autonoma Barcelona, Rapportrice
Tommaso Roscilde, Maître de Conférence, Ecole Normale Supérieure de Lyon, Directeur
Augusto Smerzi, DR INO-CNR, QSTAR et LENS, University of Florence, Examinateur

Remerciements

Mes remerciements s'adressent en premier lieu à mon directeur de thèse, Tommaso Roscilde. Son enthousiasme sans faille et sa curiosité insatiable ont été le carburant précieux de nos échanges. "Tout commence par la mystique, disait Péguy, et tout finit par la politique". Autrement dit, on commence par mourir pour, et on finit par vivre de. Je sais que Tommaso ne laissera jamais la politique passer avant la mystique, alors merci.

Merci aussi à mon père, qui m'a transmis son émerveillement pour la nature qui est au commencement et à l'aboutissement de toute science, et qui fut, avec mon grand-père, mon premier professeur.

Au cours de cette thèse, j'ai pu profiter des conseils avisés de nombreux collègues, tant à Lyon qu'ailleurs. Je souhaite ainsi remercier les anciens postdocs du labo Adam Rançon et Laurent De Forges De Parny, les anciens doctorants Louis-Paul Henry, Daniele Malpetti et Piero Naldesi ; les collègues de Villetaneuse Bruno Laburthe-Tolra, Laurent Vernac et Paolo Pedri ; Nicolas Laflorencie à Toulouse ; Luca Tagliacozzo à Glasgow ; Maxime Clusel, parti trop tôt. Au laboratoire de physique, il me faut remercier les collègues de Matière Condensée : Pascal Degiovanni, Peter Holdsworth, David Carpentier, Edmond Orignac, Andrej Fedorenko, Krzysztof Gawedzki, Clément Dutreix, Pierre Delplace. Les doctorants Benjamin Roussel, Arnaud Baguet, Thibaud Louvet, Clément Cabart, Jérôme Thibaut, Raphaël Menu, Alexandre Feller, Christoph Charles, Robin Guichardaz, Yannick Herfray, Sylvain Lacroix, Baptiste Pezelier, Valentin Raban, Kumar Upreti Lavi, ainsi que Thibault Lestang, Antoine Renaud et Géraldine Davis. Je remercie également mes amis lyonnais Romain et Vladimir.

Je tiens enfin à remercier les membres de mon jury de thèse Anna Sanpera, Antoine Browaeys et Augusto Smerzi, en plus de ceux déjà cités.

Contents

Part I

Coherent fluctuations and quantum correlations in many-body systems: generalities

Toutes choses acquièrent de la profondeur — plus que de la profondeur, quelque chose comme une quatrième dimension.

Henri Bergson

Chapter 1

Quantum coherence and quantum uncertainty

1.1 Quantum uncertainty and thermal de Broglie wavelength

The concept of *coherent fluctuations* (or *quantum fluctuations*) is intimately related to the wave-particle duality at the heart of quantum theory. In the early years of the 20^{th} century, the experimental observations on the black-body radiation and the photoelectric effect led Einstein (1905) to postulate the existence of light corpuscles, or photons, in apparent contradiction with the representation of light as a wave phenomenon (see, for instance, the book of Jammer (1966) for an historical overview of the conceptual development of quantum mechanics). Reversing the logic, de Broglie (1924) made the hypothesis that massive particles have in turn a wave-like nature. The experimental confirmation of the wave-like behaviors of electrons by Davisson and Germer (1928) firmly established the wave-particle duality as a basic concept to understand natural phenomena. This duality between wave-like and particle-like behavior of matter has then been rooted into the formal structure of quantum mechanics by Schrödinger equation for the wavefunction (Schrödinger, 1926), and Born's statistical interpretation of the latter (Born, 1926). The wave-particle duality is one of the facets of Heisenberg uncertainty principle (Heisenberg, 1927), from which Bohr (1928) elaborated the more philosophical concept of complementarity.

In which situations can we expect wave-like effects to play a significant role in the behavior of a many-particle ensemble, for instance a cloud of atoms at thermal equilibrium? Following the original intuition of de Broglie (1924), to each atom of

mass m and velocity v we associate a wavelength

$$\lambda_{dB} = \frac{h}{mv} \tag{1.1}$$

with h the Planck constant. Using that $mv^2 \sim k_B T$, T being the temperature of the gas and k_B Boltzmann constant, we arrive at

$$\lambda_{dB} \sim \frac{h}{\sqrt{m k_B T}} \,. \tag{1.2}$$

If the inter-particle distance d is much larger than the thermal de Broglie wavelength λ_{dB}, particles can be considered as classical, distinguishable objects, while in the regime where $d \lesssim \lambda_{dB}$, the wavepackets associated to each particle start to overlap, leading to interference phenomena which significantly alter the behavior of the gas with respect to the predictions of classical mechanics. In this regime, quantum fluctuations (namely, the coherent superposition of different positions in the state vector of each particle) cannot be ignored, and the particles start to develop non-classical forms of correlations – they become *entangled*[1]. In summary, this analysis shows that quantum mechanics adds a new length scale to the problem, the thermal de Broglie wavelength, as the typical distance that particles can explore coherently. The thermal de Broglie wavelength is different from 1) the interparticle distance; and 2) the typical distance that particles can explore (coherently and incoherently) — namely the size of the cloud.

1.2 The harmonic oscillator example

To gain intuition about the physical origin of the coherent superposition of an atom over different positions, we consider the simple example of a particle of mass m confined in a harmonic potential, in contact with a heat bath at temperature T. We are interested in the uncertainty of the particle position inside the trap. This uncertainty has two origins 1) thermal fluctuations and 2) intrinsic quantum fluctuations which subsist even at $T = 0$. The total (squared) uncertainty, resulting from thermal and quantum effects together, can be quantified by the variance of the position

$$\langle \delta^2 x \rangle_{\rm tot} = \langle x^2 \rangle - \langle x \rangle^2 \,. \tag{1.3}$$

Elementary algebra shows that[2]

$$\langle \delta^2 x \rangle_{\rm tot} = x_0^2 \left(\bar{n} + \frac{1}{2} \right) \,. \tag{1.5}$$

[1] The word "entangled", synonym for "non-separable", has a mathematical definition to be given in Section 2.1, translating the idea of *correlated quantum superposition*.

[2] The Hamiltonian is

$$H = \frac{p^2}{2m} + \frac{1}{2} m\omega^2 x^2 = \hbar\omega \left(a^\dagger a + \frac{1}{2} \right) \tag{1.4}$$

with $x_0^2 = \hbar/m\omega$, and $\bar{n}$ is the mean number of energy quanta. Using Bose-Einstein formula for $\bar{n}$, we arrive at

$$\langle \delta^2 x \rangle_{\rm tot} = \frac{\hbar}{m\omega} \left(\frac{1}{e^{\hbar\omega/k_B T} - 1} + \frac{1}{2} \right) . \tag{1.6}$$

At high temperature ($\hbar\omega \ll k_B T$), the classical prediction of the equipartition theorem $\langle \delta^2 x \rangle_{\rm tot} = k_B T/m\omega^2$ is recovered, while in the opposite limit the variance of the position saturates to $\hbar/2m\omega$ due to the residual zero-point motion of the particle. In fact, classical mechanics predicts that $\langle \delta^2 x \rangle_{\rm tot} = k_B T/m\omega^2$ at any temperature. It is then tempting to interpret $k_B T/m\omega^2$ as the thermal contribution to the uncertainty of the position, the remainder being the quantum uncertainty, or, more accurately, the *quantum variance* of the position

$$\langle \delta^2 x \rangle_{\rm tot} = \langle \delta^2 x \rangle_{\text{equipartition (classical)}} + \langle \delta^2 x \rangle_Q . \tag{1.7}$$

It is natural to expect that quantum fluctuations are reduced by thermal agitation, and in fact the quantum variance of the position is proportional to $\lambda_{dB}^2 = h^2/mk_B T$ at low trap frequency ($\hbar\omega \ll k_B T$). In this respect, the thermal de Broglie wavelength may be interpreted as the quantum uncertainty of the position of a particle in a cloud, in addition to the prediction of classical mechanics.

1.3 Coherent *vs.* incoherent uncertainty

The analysis of the previous section conveys the general idea that the uncertainty of physical quantities has two sources:

1. The uncertainty on the experimental preparation of the system generates a certain randomness in the microstate $|\psi\rangle$. To take into account the uncertainty on the preparation, one introduces a *statistical ensemble of states* $\{p_i, |\psi_i\rangle\}$, where p_i is the probability for having actually prepared the microstate $|\psi_i\rangle$. This statistical ensemble is incorporated in the density operator (or matrix) $\rho = \sum_i p_i |\psi_i\rangle\langle\psi_i|$, often called simply "the state ρ". The uncertainty on the actual microstate is a source of *incoherent fluctuations*. When the preparation consists of placing the system in contact with a heat bath, incoherent fluctuations are equivalently called "thermal fluctuations".

with $a = \frac{\tilde{x}+i\tilde{p}}{\sqrt{2}}$, $a^\dagger = \frac{\tilde{x}-i\tilde{p}}{\sqrt{2}}$, $\tilde{x} = x\sqrt{m\omega/\hbar} = x/x_0$ and $\tilde{p} = p/\sqrt{m\hbar\omega} = p/p_0$. Operators a and $a^\dagger$ satisfy the bosonic commutation relations $[a, a^\dagger] = 1$. Using $x = x_0 \frac{a+a^\dagger}{\sqrt{2}}$ and $\langle a^{(\dagger)} \rangle = \langle [a^{(\dagger)}]^2 \rangle = 0$, we obtain the desired result with $\bar{n} = \langle a^\dagger a \rangle$.

2. Even when the system is in a particular microstate $|\psi\rangle$, observables may have an intrinsic *quantum uncertainty*. This happens whenever $|\psi\rangle$ is not an eigenstate of the observable in question. The quantum uncertainty cannot be traced back to a lack of accuracy during the preparation of the system, and is absent in classical physics. It is the source of *coherent fluctuations*.

In the present work we show that the two contributions can be formally separated in the form of an incoherent and a coherent contribution to the variance of any observable, both of which are measurable in the case of thermal equilibrium. In general we expect that an observable $\mathcal{O}$ possesses quantum fluctuations in a state ρ if and only if $\mathcal{O}$ and ρ do not commute with each other. This expectation may be promoted to a general principle:

Quantum uncertainty principle

$$[\mathcal{O}, \rho] \neq 0 \iff \begin{array}{l}\mathcal{O} \text{ has quantum fluctuations} \\ \text{if the system is in the state } \rho\end{array} \tag{1.8}$$

In the specific case of thermal equilibrium states, this is equivalent to the condition $[\mathcal{O}, \mathcal{H}] \neq 0$, where $\mathcal{H}$ is the Hamiltonian of the system. In fact, it is tempting to regard the "Quantum uncertainty principle" as one of the facets of Heisenberg uncertainty relations, and we might use the term "Heisenberg uncertainty" as a synonym for "quantum uncertainty".

In conclusion of this section, three main questions can be identified.

- How to isolate, both in computations and in experiments, quantum fluctuations from incoherent uncertainties?
- Under which conditions can a function $\mathcal{C}(\rho, \mathcal{O})$ be said to quantify the coherence of the state ρ with respect to the eigenstates of the observable $\mathcal{O}$?
- What are the interference phenomena associated to quantum fluctuations which justify the term "coherent fluctuations"?

It is the purpose of the following sections to address these questions.

1.4 Quantum coherence and interferometry

1.4.1 A simple example of interferometer

In the previous section, we introduced quantum fluctuations as fluctuations which cannot be understood from the perspective of a statistical ensemble, but rather as

a manifestation of the quantum uncertainty principle for non-conserved quantities (namely: for observables which do not commute with the density operator). In this section, we introduce an *a priori* independent notion of quantum fluctuations from the perspective of interference phenomena. However, the two notions turn out to be equivalent. This equivalence is elaborated in Sections 1.5 and 1.7. Rather generally, an interference experiment can be sketched as follows: 1) we consider an input state $|\psi\rangle = \lambda_0|0\rangle + \lambda_1|1\rangle$, where $|\lambda_0|^2 + |\lambda_1|^2 = 1$, and $|0\rangle$ and $|1\rangle$ represent the two arms of the interferometer (we consider real and positive λ_0, λ_1 and absorb possible phases into the definition of $|0\rangle$ and $|1\rangle$); and 2) a phase is accumulated along each arm to yield $|\psi(\phi_0, \phi_1)\rangle = \lambda_0 e^{i\phi_0}|0\rangle + \lambda_1 e^{i\phi_1}|1\rangle$. Finally, an observable is measured on $|\psi(\phi_0, \phi_1)\rangle$, for instance $S^x = (|1\rangle\langle 0| + |0\rangle\langle 1|)/2$, whose average value is

$$\begin{aligned} s &= \langle\psi(\phi_0, \phi_1)|S^x|\psi(\phi_0, \phi_1)\rangle \\ &= \lambda_0\lambda_1 \cos(\phi_0 - \phi_1) \, . \end{aligned} \tag{1.9}$$

The signal s oscillates as a function of the phase difference on the two arms $\phi = \phi_0 - \phi_1$. The visibility of the interference fringes $V = 2\lambda_0\lambda_1$ is nothing else than (twice) the standard deviation (defined as the square root of the variance) of $S^z = (|0\rangle\langle 0| - |1\rangle\langle 1|)/2$, quantifying the superposition of $|\psi\rangle$ in the basis $(|0\rangle, |1\rangle)$, the eigenstates of S^z[3]. It is the variance of S^z which is related to the visibility because S^z is the so-called *generator* of the transformation of $|\psi\rangle$ in the interferometer (namely, the evolution in the interferometer can be written, up to a global phase, as $|\psi(\phi_0, \phi_1)\rangle = e^{iS^z\phi}|\psi\rangle$). But the variance of S^z cannot in general quantify the visibility of the interference fringes, for the state could have the same variance without any coherence between $|0\rangle$ and $|1\rangle$[4]. If one imagines a situation of partial dephasing of ρ

$$\rho_\alpha(\phi) = \lambda_0^2|0\rangle\langle 0| + \lambda_1^2|1\rangle\langle 1| + \alpha\,(\lambda_0\lambda_1 e^{i\phi}|0\rangle\langle 1| + \text{h.c.}) \tag{1.10}$$

with $0 < \alpha < 1$ and h.c. denoting the hermitian conjugate, a calculation of $\langle S^x\rangle$ gives

$$\text{Tr}[\rho_\alpha(\phi)S^x] = \alpha\lambda_0\lambda_1 \cos\phi \, , \tag{1.11}$$

so that the visibility is now reduced by a factor α. For any α, the variance of S^z is $(\lambda_0\lambda_1)^2$, but only part of this variance comes from coherent fluctuations, which manifest themselves in interference phenomena. It is then natural to split the variance

[3] Indeed $\langle\delta^2 S^z\rangle = \langle\psi|(S^z)^2|\psi\rangle - \langle\psi|S^z|\psi\rangle^2 = (1/4)[1 - (\lambda_0^2 - \lambda_1^2)^2] = (\lambda_0\lambda_1)^2$ where we used that $1 = \lambda_0^2 + \lambda_1^2$.

[4] If $\rho = |\psi\rangle\langle\psi| \to \rho^{\text{decoh}} = \lambda_0^2|0\rangle\langle 0| + \lambda_1^2|1\rangle\langle 1|$, then $\rho^{\text{decoh}}(\phi) = e^{iS^z\phi}\rho^{\text{decoh}}e^{-iS^z\phi} = \rho^{\text{decoh}}$ (the state is unable to show any interference effect), while $\langle\delta^2 S^z\rangle(\rho^{\text{decoh}}) = \langle\delta^2 S^z\rangle(|\psi\rangle) = (\lambda_0\lambda_1)^2$ (the uncertainty on σ^z, now fully of incoherent origin, is the same as before decoherence had been introduced).

into an incoherent and a coherent part, the latter being responsible for interference phenomena

$$\langle \delta^2 S^z \rangle_{\text{tot}} = \langle \delta^2 S^z \rangle_{\text{incoh}} + \langle \delta^2 S^z \rangle_{\text{coh}} \, . \tag{1.12}$$

The coherent part is suppressed in favor of the incoherent one by the noise on the relative phase between $|0\rangle$ and $|1\rangle$.

More generally, one can conceive an interferometer with more than two arms

$$|\psi\rangle = \lambda_1 |\psi_1\rangle + \lambda_2 |\psi_2\rangle \cdots + \lambda_n |\psi_n\rangle \tag{1.13}$$

$$|\psi(\phi_1 \ldots \phi_n)\rangle = \sum_k \lambda_k e^{i\phi_k} |\psi_k\rangle \, . \tag{1.14}$$

Intuitively, interference effects are going to be significant if the number of relevant λ_k's is large. This raises the following questions:

- How to quantify the number of relevant $|\psi_k\rangle$'s over which the state of the system extends coherently (especially if the state is mixed)?
- How is it related to the visibility of interference phenomena?

The first question turns out to be the same as the question raised at the end of the previous Section 1.1 (namely, "How to define, compute and measure quantum fluctuations?"), and an answer will be provided in the following Sections 1.5 and 1.7. Concerning the visibility in interference experiments, the question may be a bit too general to be given a simple answer: we now have n phases instead of 2, and the very meaning of "visibility of the fringes" in this high-dimensional space is not clear (see however von Prillwitz, Rudnicki, and Mintert (2015) and Biswas, García Díaz, and Winter (2017) for studies in that direction). Nonetheless, the interferometric point of view provides an elegant mathematical framework to quantify coherent fluctuations, as shown in Section 1.5. Also, quantifying the coherent extent of a state on a family of other states, in relationship with the visibility in interference experiments, is a question of high experimental and even technological significance if the state ρ is intended to serve as a probe for estimating the phase difference on the arms of an interferometer (Pezzè et al., 2016). In the following paragraph, we introduce a central quantity in the context of phase estimation, the *quantum Fisher information* (Pezzè and Smerzi, 2014).

1.4.2 Quantum Fisher information

Phase estimation. As a special case of the multipath interferometer, we consider the situation in which one aims at measuring with great accuracy the value of a field

ϕ (a magnetic field, a gravity field, a local acceleration field, and so on). A probe quantum system in the state ρ is sent into the region where the field is to be measured, and, neglecting dissipative processes, it undergoes the unitary evolution

$$\rho(\phi) = e^{-i\phi\mathcal{O}}\rho e^{i\phi\mathcal{O}} \,. \tag{1.15}$$

If a magnetic field of magnitude ϕ in the z direction is present, the observable $\mathcal{O} = S^z$ is the z component of the magnetic moment of the quantum system; if a gravitational potential ϕz is present, then $\mathcal{O} = z$ is the z-coordinate of the constituents of the quantum system, and so on. Now, after the unitary evolution, some measurement A is performed on the probe, yielding the result a with probability $p_\phi(a)$. If this probability depends on ϕ, measuring A provides information on the actual strength of the field. If one is to evaluate the sensitivity of the interferometer, it is meaningful to determine its ability to discriminate between closely separated values of ϕ, say ϕ and $\phi + d\phi$. So the question is the following: how well can we distinguish the probability distribution p_ϕ from $p_{\phi+d\phi}$ by measuring A several times? Of course, if the value of the field ϕ is perfectly stable, and the measurement repeated an infinite number of times, the statistics of the results will exactly coincide with p_ϕ for one, and only one value of ϕ (unless $p_\phi = p_{\phi'}$, in which case there is no way to discriminate between ϕ and ϕ' by measuring A). So in this idealized situation, one is able to discriminate arbitrarily close values of ϕ, however similar p_ϕ and $p_{\phi+d\phi}$ can be. But what if only a finite, albeit very large, number N of measurements can be performed?

Fisher information and the Cramér-Rao bound. This is a basic question of estimation theory, and the answer is given by the Cramér-Rao bound (Pezzè and Smerzi, 2014): the variance $\Delta^2\phi_{\text{est}}$ on the estimation of ϕ is lower bounded by the inverse of N times the Fisher information of p_ϕ

$$\Delta^2\phi_{\text{est}} \geq \frac{1}{NI[\phi, A]} \tag{1.16}$$

and the bound is asymptotically reachable in the limit $N \to \infty$. The Fisher information

$$I[\phi, A] = \sum_a \frac{[\partial_\phi p_\phi(a)]^2}{p_\phi(a)} \tag{1.17}$$

is a measure of the distinguishability $\mathcal{D}[p_\phi, p_{\phi+d\phi}]$ between p_ϕ and $p_{\phi+d\phi}$ in the limit $d\phi \to 0$[5]

$$\mathcal{D}[p_\phi, p_{\phi+d\phi}] = \frac{1}{2} I[\phi, A](d\phi)^2 \,. \tag{1.20}$$

[5] as quantified by the relative entropy (Vedral, 2002). The relative entropy (or Kullback-Leibler divergence) between two probability distributions p and q is defined as $S_{\text{rel}}(p|q) = \sum_a p(a)\log[p(a)/q(a)]$.

The intuitive meaning of this result is that the more different the probability distribution p_ϕ is from $p_{\phi+d\phi}$, the more information we obtain on the value of ϕ by measuring A. The amount of information about ϕ contained in p_ϕ is quantified by the Fisher information, and the Cramér-Rao bound provides the quantitative link between this amount of information, and the precision on the value of ϕ we obtain by measuring A.

Quantum Fisher information. Now, the precision of the evaluation of ϕ depends on the measurement A performed on the probe. In order to obtain the best possible precision, the Fisher information has to be maximized over all possible measurements, yielding the so-called quantum Cramér-Rao bound

$$\Delta^2\phi_{\rm est} \geq \frac{1}{NF_Q}\,. \tag{1.21}$$

The quantum Fisher information (QFI)

$$F_Q = \max_{\rm meas.A} I[\phi, A] \tag{1.22}$$

where the max is over all the possible measurements, is thus the fundamental property of the input state ρ of the system which quantifies its ability to probe the field ϕ very accurately in an interferometric setup[6]. Interestingly, F_Q does not depend any more on ϕ, although the optimal measurement A to perform might do so. This important property will be discussed in Section 1.5. The QFI is then only a property of the state ρ, and of the observable $\mathcal{O}$ which couples to ϕ in the interferometer.

One has

$$\begin{aligned}\log\left[\frac{p_{\phi+d\phi}(a)}{p_\phi(a)}\right] &= \log\left(1+\frac{d\phi}{p_\phi(a)}\partial_\phi p_\phi(a)+\frac{(d\phi)^2}{2p_\phi(a)}\partial_\phi^2 p_\phi(a)+O[(d\phi)^3]\right)\\ &= \frac{d\phi}{p_\phi(a)}\partial_\phi p_\phi(a)+\frac{(d\phi)^2}{2p_\phi(a)}\partial_\phi^2 p_\phi(a)\\ &\quad -\frac{1}{2}\left(\frac{d\phi}{p_\phi(a)}\partial_\phi p_\phi(a)\right)^2+O[(d\phi)^3]\,.\end{aligned} \tag{1.18}$$

Hence, the relative entropy between p_ϕ and $p_{\phi+d\phi}$ is

$$\begin{aligned}S_{\rm rel}(p_\phi|p_{\phi+d\phi}) &= -\sum_a p_\phi(a)\log[p_{\phi+d\phi}(a)/p_\phi(a)]\\ &= -d\phi\partial_\phi\sum_a p_\phi(a)-\frac{(d\phi)^2}{2}\partial_\phi^2\sum_a p_\phi(a)+\frac{(d\phi)^2}{2}\sum_a\frac{[\partial_\phi p_\phi(a)]^2}{p_\phi(a)}\end{aligned} \tag{1.19}$$

As $\sum_a p_\phi(a)=1$ for all ϕ, the first two terms vanish and we obtained the result of Eq. (1.20).

[6] Or, more generally, when the system undergoes an arbitrary evolution parametrized by the field ϕ. Our focus is here on interferometry because we elaborate on the concept of coherence, but the theory of parameter estimation is not restricted to interferometric setups.

Quantum Fisher information for pure states. Quite remarkably, if ρ is a pure state, the QFI takes the physically transparent expression (Pezzè and Smerzi, 2014)

$$F_Q[\rho, \mathcal{O}] = 4\langle \delta^2 \mathcal{O} \rangle_{\rho=|\psi\rangle\langle\psi|} = 4(\langle\psi|\mathcal{O}^2|\psi\rangle - \langle\psi|\mathcal{O}|\psi\rangle^2) \, . \tag{1.23}$$

In full agreement with the qualitative discussion at the beginning of this section, the variance of $\mathcal{O}$ in the state $|\psi\rangle$ directly quantifies the ability of $|\psi\rangle$ to exhibit high-visibility interference phenomena with respect to the eigenstates of $\mathcal{O}$. The physical intuition behind this observation is that if p_ϕ changes very rapidly with ϕ, it means that $\rho(\phi) = e^{-i\phi\mathcal{O}}\rho e^{i\phi\mathcal{O}}$ changes very rapidly with ϕ. If ρ is a pure state $|\psi\rangle$, this is achieved when $|\psi\rangle$ is not an eigenstates of $\mathcal{O}$, so that the transformation $e^{-i\phi\mathcal{O}}|\psi\rangle$ transforms $|\psi\rangle$ significantly. In this case, the extent of $|\psi\rangle$ over the spectrum of $\mathcal{O}$ is quantified the variance. If instead ρ is a mixed state, the coherent extent of ρ over the spectrum of $\mathcal{O}$ is rather quantified by the QFI, which is thus a kind of *quantum variance* (QV)[7].

1.4.3 Uncertainty relations

We argued that coherent fluctuations are a manifestation of the quantum uncertainty principle. It is legitimate to ask if they are involved in some analog of the Heisenberg uncertainty relation for two non-commuting observables A and B

$$\langle \delta^2 A \rangle \langle \delta^2 B \rangle \geq \frac{1}{4} |\langle [A, B] \rangle|^2 \, . \tag{1.24}$$

The answer is yes, as we show in this section. In fact, it is a basic result of estimation theory that the Fisher information $I(\phi, A)$ [Eq. (1.17)] of the probability distribution $p_\phi(a)$ for the eigenvalues a of A, is lower bounded by the following expression

$$I(\phi, A) \geq \frac{|\partial_\phi \langle A \rangle|^2}{\langle \delta^2 A \rangle(\phi)} \, . \tag{1.25}$$

Inequality (1.25) can be proved using Cauchy-Schwarz inequality[8]. The meaning of this inequality is simple. Let us imagine that the probability distribution $p_\phi(a)$ is

[7] The very same idea lies behind the concept of "quantum speed limit". In interferometry, if ϕ is very small, one needs a very large coherent extent of ρ across the eigenstates of $\mathcal{O}$ in order for $\rho(\phi) = e^{-i\phi\mathcal{O}}\rho e^{i\phi\mathcal{O}}$ to be distinguishable from ρ — a very large QV. Conversely, if the QV is small, the time needed for $\rho(t) = e^{-it\mathcal{O}}\rho e^{it\mathcal{O}}$ to become distinguishable from ρ is large — at least larger than some bound specified by the quantum speed limit. For a study of quantum speed limits in connection with the coherence content of the ρ, see Pires et al. (2016) and references therein.

[8] The following proof is suggested in a footnote of Pezzé and Smerzi (2009). It is essentially identical to the proof of the Cramér-Rao bound (Pezzè and Smerzi, 2014). By definition of $\langle A \rangle$, for any value of ϕ we have

$$\int da \, p_\phi(a)[a - \langle A \rangle(\phi)] = 0 \, . \tag{1.26}$$

peaked around $\bar{a} = \langle A \rangle(\phi)$ with a standard deviation (std) $\Delta A = \sqrt{\langle \delta^2 A \rangle}(\phi)$. If A is measured and if the value a is obtained, we expect it to be close to $\bar{a}(\phi)$ (within the std). Our confidence interval $\Delta\phi_{\rm est}$ for ϕ is thus fixed by

$$\Delta\phi_{\rm est} |\partial_\phi \langle A \rangle| = \Delta A \, . \tag{1.30}$$

The Cramér-Rao bound, Eq. (1.16) imposes that this confidence interval be larger than $I(\phi, A)^{-1/2}$, which corresponds to Eq. (1.25)[9]. Basically, replacing A with any power of A, inequality (1.25) states that the Fisher information is larger than the rate of change of any one of the moments of $p_\phi(a)$: it contains information on the rate of change of the full distribution $p_\phi(a)$, capturing the rate of change of all the moments together.

Like in previous section, we specify our attention to the case where the parameter ϕ enters in a unitary transformation $U(\phi) = e^{-i\phi B}$ generated by some observable B, so that

$$\partial_\phi \langle A \rangle = i[B, A] \, . \tag{1.31}$$

Given that the QFI is the upper bound to the Fisher information associated to all possible observables A that could be measured, we finally obtain

$$F_Q(B) \langle \delta^2 A \rangle \geq |\langle [A, B] \rangle|^2 \, . \tag{1.32}$$

Eq. (1.32) reduces to the standard Heisenberg inequality, Eq. (1.24), for pure states, for which $F_Q(B) = 4\langle \delta^2 B \rangle$. For mixed states, it is more stringent than the latter, since in general $F_Q(B) \leq 4\langle \delta^2 B \rangle$ [namely, Eq. (1.32) *implies* Eq. (1.24)].

In conclusion, Eq. (1.32) represents an interesting complementarity relation between the quantum and total fluctuations of two non-commuting observables, the quantum fluctuations being quantified by the QFI.

Differentiating with respect to ϕ, we obtain

$$\int da \, \partial_\phi p_\phi(a) [a - \langle A \rangle(\phi)] = \int da \, p_\phi(a) \partial_\phi \langle A \rangle(\phi) \, . \tag{1.27}$$

The r.h.s is $\partial_\phi \langle A \rangle(\phi)$, since $\langle A \rangle(\phi)$ is independent of a, and since the probability distribution $p_\phi(a)$ is normalized to 1. Then, using that $\partial_\phi p_\phi(a) = p_\phi(a) \partial_\phi \ln p_\phi(a)$, we obtain

$$\int da \, p_\phi(a) [\partial_\phi \ln p_\phi(a)] [a - \langle A \rangle(\phi)] = \partial_\phi \langle A \rangle(\phi) \, . \tag{1.28}$$

Applying Cauchy-Scharz inequality $|\langle XY \rangle|^2 \leq \langle X^2 \rangle \langle Y^2 \rangle$, valid for any pair of random variables $X(a)$ and $Y(a)$, to $X(a) = \partial_\phi \ln p_\phi(a)$ and $Y(a) = a - \langle A \rangle(\phi)$, we finally obtain inequality (1.25) with the Fisher information of the distribution p_ϕ

$$I(\phi, A) = \int da \, p_\phi(a) [\partial_\phi \ln p_\phi(a)]^2 \, . \tag{1.29}$$

[9] $\Delta\phi^2_{\rm est} = \langle \delta^2 A \rangle / |\partial_\phi \langle A \rangle|^2 \geq 1/I(\phi, A) \Leftrightarrow I(\phi, A) \geq |\partial_\phi \langle A \rangle|^2 / \langle \delta^2 A \rangle$.

Finally, we notice that when considering a gaussian state for the two quadratures p and q of a bosonic mode, the inequality of Eq. (1.32) is saturated:

$$F_Q(p)\langle\delta^2 q\rangle = \hbar^2 \quad \text{(gaussian states)}. \tag{1.33}$$

This result generalizes to mixed gaussian states the well-known property of the minimal-uncertainty states obtained as ground states of harmonic-oscillator Hamiltonians. In the present context, it is simply a consequence of the fact that inequality (1.25) is saturated for a gaussian probability distribution.

1.5 Mathematical approach to quantum coherence

In Section 1.1, we showed that the de Broglie wavelength, quantifying the spatial extent over which particles are coherently spread at thermal equilibrium, can be interpreted as the quantum contribution to the uncertainty of the position, in addition to the prediction of the equipartition theorem, valid for classical systems only. This idea will be given a much wider significance in Section 1.7 where the *quantum variance* is introduced for any observable. In Section 1.4.2, we approached the more general question of estimating the coherent extent of an arbitrary state over the eigenstates of an arbitrary observable. This question was approached from the point of view of interference phenomena, and it was proposed that the quantum Fisher information (QFI) precisely measures this quantum uncertainty. In particular, in the case of pure states, the QFI reduces to (four times) the variance of the observable in question. The physical intuition behind this result was that the more widely a state ρ coherently extends over the eigenvectors of $\mathcal{O}$, the more rapidly it evolves with ϕ in a unitary transformation $U(\phi) = e^{-i\phi\mathcal{O}}$ generated by $\mathcal{O}$, and parametrized by ϕ. "Rapidly" means here that there exists some (ϕ-dependent) observable whose probability distribution in the state $\rho(\phi)$ is very different from its probability distribution in the state $\rho(\phi + d\phi)$. The QFI precisely quantifies this "speed of evolution".

To avoid confusion, we note that the concept of coherence discussed here is sometimes called *asymmetry* in the literature. The study of coherence, both from a physical and a mathematical point of view, is still a vivid area of research, and several concepts are not set in stone. The interested reader is referred to Marvian and Spekkens (2016) for a discussion on various notions of coherence, and to Streltsov, Adesso, and Plenio (2016) for a review on coherence as a resource.

In the remainder of this section, we shall first discuss a mathematical framework settled to quantify coherence. Then we will construct a whole family of coherence measures, to which the QFI belongs, based on the intuition that a state evolves rapidly

under a unitary transformation if and only if it possesses a large coherence with respect to the generator of the transformation. Finally, we will show that all these coherence quantifiers can be measured through to the dynamical structure factor for thermal equilibrium states.

1.5.1 Axiomatic framework

To justify more rigorously that the QFI, or any other quantity, is a coherence measure, it is reasonable to introduce a set of mathematical conditions that any coherence measure $\mathcal{C}(\rho, \mathcal{O})$ should fulfill (Streltsov, Adesso, and Plenio, 2016). This approach highlights several physical and mathematical aspects behind the general concept of coherence. Proposed conditions are the following:

(i) Quantum uncertainty principle:

$$\mathcal{C}(\rho, \mathcal{O}) \neq 0 \Longleftrightarrow [\rho, \mathcal{O}] \neq 0 \, . \tag{1.34}$$

If ρ can be decomposed as an incoherent mixture of eigenstates of $\mathcal{O}$, all fluctuations of $\mathcal{O}$ are of incoherent origin, and $\mathcal{C}(\rho, \mathcal{O}) = 0$. Coherent fluctuations are a manifestation of the quantum uncertainty principle, and can only be present if $[\mathcal{O}, \rho] \neq 0$. By convention, coherence measures are chosen non-negative, $\mathcal{C}(\rho, \mathcal{O}) \geq 0$.

(ii) Monotonicity under operations which conserve $\mathcal{O}$:

$$\mathcal{C}(\mathcal{L}(\rho), \mathcal{O}) \leq \mathcal{C}(\rho, \mathcal{O}) \tag{1.35}$$

if $\mathcal{L}\left(e^{-it\mathcal{O}}\rho e^{it\mathcal{O}}\right) = e^{-it\mathcal{O}}\mathcal{L}(\rho)e^{it\mathcal{O}}$, and $\mathcal{L}$ is an arbitrary linear evolution for quantum states [more precisely, $\mathcal{L}$ is a completely positive, trace preserving (CPTP) linear transformation (Wiseman and Milburn, 2010)]. In particular, if $\mathcal{L}$ is a unitary transformation of inverse $\mathcal{L}^{-1}$, the coherence is preserved throughout the unitary evolution[10,11]. This condition corresponds to the intuition that only operations which do not conserve $\mathcal{O}$ can create coherence between the eigenstates of $\mathcal{O}$. In the case of a unitary transformation which commutes with $\mathcal{O}$, the probability distribution for the fluctuations of $\mathcal{O}$ is conserved throughout the evolution, and we may legitimately expect that the putative distribution for *quantum* fluctuations of $\mathcal{O}$ is also conserved (Marvian and Spekkens, 2014).

[10] Indeed, $\mathcal{C}(\rho, \mathcal{O}) \geq \mathcal{C}(\mathcal{L}(\rho), \mathcal{O}) \geq \mathcal{C}(\mathcal{L}^{-1}[\mathcal{L}(\rho)], \mathcal{O}) = \mathcal{C}(\rho, \mathcal{O})$, so that $\mathcal{C}(\rho, \mathcal{O}) = \mathcal{C}(\mathcal{L}(\rho), \mathcal{O})$.

[11] The QFI satisfies this condition. This is the reason why the optimal precision that can be reached in the evaluation of the small field ϕ in an interferometric framework is independent of ϕ, see Section 1.4.2.

(iii) Convexity with respect to ρ:

$$\mathcal{C}\left(\sum_i p_i \rho_i, \mathcal{O}\right) \leq \sum_i p_i \mathcal{C}(\rho_i, \mathcal{O}) \ . \tag{1.36}$$

This condition translates the idea that incoherently mixing states can only lead to a decrease of coherence. In order to create coherence, one needs to coherently superpose states, not to mix them incoherently.

(iv-a) Additivity under tensor product:

$$\mathcal{C}(\rho_A \otimes \rho_B, \mathcal{O}_A + \mathcal{O}_B) = \mathcal{C}(\rho_A, \mathcal{O}_A) + \mathcal{C}(\rho_B, \mathcal{O}_B) \ , \tag{1.37}$$

where A and B are two quantum systems, and $\mathcal{O}_{A(B)}$ is an observable related to $A(B)$ degrees of freedom[12]. If the combined state ρ_{AB} of two systems A and B is a tensor product $\rho_A \otimes \rho_B$, they are uncorrelated: fluctuations on A and B are independent, and so are quantum fluctuations.

Actually, anticipating over the developments of the following sections, one could argue that a more stringent condition should apply to measures of coherence, namely, that if A and B only share classical correlations (to be defined later), then quantum fluctuations on A and B should be independent, leading to the condition

(iv-b)

$$\mathcal{C}(\rho_{AB}, \mathcal{O}_A + \mathcal{O}_B) = \mathcal{C}(\rho_A, \mathcal{O}_A) + \mathcal{C}(\rho_B, \mathcal{O}_B) \tag{1.38}$$

if ρ_{AB} is a classical-quantum or a quantum-classical state (defined in Section 2.1), with

$$\rho_{A(B)} = \mathrm{Tr}_{B(A)} \rho_{AB} \ . \tag{1.39}$$

As this condition has not been considered in the litrature so far, we leave this as an optional stronger requirement, which is indeed fulfilled by the measures of coherence discussed in this manuscript.

To these requirements widely accepted in the literature (apart from (iv-b) which had not been proposed), we suggest to add the following physically motivated one:

(v) Absence of divergent behavior at thermal phase transitions. Thermal (*i.e.* finite temperature) phase transitions are driven by thermal (namely incoherent) fluctuations, and quantum fluctuations should not become critical at such transitions.

[12] The mathematically oriented reader should like to read $\mathcal{O}_A \otimes I_B$ instead of $\mathcal{O}_A$, where I_B denotes the identity operator acting on B Hilbert space, and similarly for $\mathcal{O}_B$. Throughout this manuscript, we follow the physicist notations and always omit the "$\otimes I_{\text{everything else}}$" factors.

1.5.2 A family of coherence measures

We now show that measures of coherence in the above sense can be constructed by translating mathematically the physical intuition that a state ρ evolves swiftly with t under a unitary transformation $U(t) = e^{-it\mathcal{O}}$ if, and only if it possesses a large coherence with respect to $\mathcal{O}$. That is, we show that if $\mathcal{D}_f[\rho, \rho(dt)]$ is a measure of distinguishability (parametrized by a function f which satisfies certain properties to be discussed shortly) between ρ and $\rho(dt) = \rho - i[\mathcal{O}, \rho]dt + O(dt^2)$ then

$$\mathcal{D}_f[\rho, \rho(dt)] = \frac{1}{2}\mathcal{C}_f(\rho, \mathcal{O})(dt)^2 \tag{1.40}$$

defines a measure of coherence $\mathcal{C}_f$ satisfying (i)-(v). Mathematically, a measure of distinguishability $\mathcal{D}(\rho_1, \rho_2)$ is a non-negative function which contracts under any evolution of the states (*i.e.* under any CPTP linear operation $\mathcal{L}$): $\mathcal{D}[\mathcal{L}(\rho_1), \mathcal{L}(\rho_2)] \leq \mathcal{D}(\rho_1, \rho_2)$ (Bengtsson and Zyczkowski, 2007). In particular, if $\mathcal{L}$ is a unitary evolution, the distinguishability between ρ_1 and ρ_2 is conserved throughout the evolution[13]. Pictorially speaking, the space of quantum states rotates as a rigid body under a unitary evolution. In general, loss of distinguishability under evolution comes from the fact that noise and dissipation lead to a loss of structure of ρ_1 and ρ_2, and thus to a decrease of our ability to distinguish them from each other[14]. Among the distinguishability measures, of particular interest are those based on a *metric*, that is, an infinitesimal notion of distance. If g is a metric, then the infinitesimal squared length from ρ to $\rho + d\rho$ is

$$ds^2 = g_{\mu\nu} d\rho^\mu d\rho^\nu \tag{1.41}$$

where summation over repeated indices is understood, and $\mu, \nu = 1, \ldots D^2$ label the entries of the $D \times D$ density-matrix ρ. Then, the distance between ρ_1 and ρ_2 along a path γ joining ρ_1 and ρ_2 in the Hilbert space is

$$\mathcal{D}_\gamma(\rho_1, \rho_2) = \int_\gamma ds \ . \tag{1.42}$$

The distinguishability between ρ_1 and ρ_2 is then defined as the length of the shortest path joining them (the *geodesic* distance) $\mathcal{D}(\rho_1, \rho_2) = \min_\gamma \mathcal{D}_\gamma(\rho_1, \rho_2)$. Petz (1996) showed that any metric contractive under evolution must be of the form (up to a

[13] $\mathcal{D}(\rho_1, \rho_2) = \mathcal{D}(\mathcal{L}[\mathcal{L}^{-1}(\rho_1)], \mathcal{L}[\mathcal{L}^{-1}(\rho_2)] \leq \mathcal{D}[\mathcal{L}(\rho_1), \mathcal{L}(\rho_2)] \leq \mathcal{D}(\rho_1, \rho_2)$, so that the inequalities are in fact equalities.

[14] For classical probability distributions p_1 and p_2, this corresponds to the fact that, for instance, under a stochastic map, p_1 and p_2 flow towards some fixed point, and thus become less and less distinguishable from each other.

multiplicative constant)[15]

$$ds^2 = \frac{f(0)}{2} \sum_{i,j} \frac{|d\rho_{ij}|^2}{p_i f(p_j/p_i)} \tag{1.43}$$

with $\rho = \sum_i p_i |i\rangle\langle i|$, and $d\rho_{ij} = \langle i|d\rho|j\rangle$. $f(x) \geq 0$ is a function which fulfills a set of conditions, among which

a) $f(x) = xf(1/x)$;

b) $f(1) = 1$.

The diagonal terms $i = j$ of Eq. (1.43) reconstruct the Fisher information for the probability distribution p_i, see Eq. (1.17). Here, $d\rho = -i[\mathcal{O}, \rho]dt$, so that $|d\rho_{ij}|^2 = |[\mathcal{O}, \rho]_{ij}|^2 (dt)^2 = |\langle i|\mathcal{O}|j\rangle|^2 (p_j - p_i)^2 (dt)^2$. In particular, $d\rho_{ii} = 0$ for all i. This leads us to introduce the following measure of coherence

$$\mathcal{C}_f(\rho, \mathcal{O}) = \frac{f(0)}{2} \sum_{i \neq j} \frac{(p_i - p_j)^2}{p_i f(p_j/p_i)} |\langle i|\mathcal{O}|j\rangle|^2 \, . \tag{1.44}$$

If ρ is a pure state $|\psi\rangle\langle\psi|$, $\mathcal{C}_f$ is just the variance of $\mathcal{O}$[16], but it is otherwise smaller that the variance. It can be proved that $\mathcal{C}_f$ satisfies conditions (i)-(v):

(i) Nonnegativity is manifest, and $\mathcal{C}_f(\rho, \mathcal{O}) = 0$ iff $\forall i, j \ (d\rho)_{ij} = 0$ iff $[\rho, \mathcal{O}] = 0$.

(ii) and (iii) are proved in the Appendix of Zhang et al. (2016).

(iv-b) is proved in Appendix A.

(v) is discussed in Section 1.9.

In particular, the quantum Fisher information is equal to $4\mathcal{C}_F$ with $F(x) = (1 + x)/2$ (Pezzè and Smerzi, 2014), which obviously satisfies the conditions a) and b). Another example is provided by the quantum variance introduced in Section 1.7. Finally, we note the following inequalities, valid for any f (Gibilisco, Imparato, and Isola, 2009)

$$\mathcal{C}_f \leq \mathcal{C}_F \leq \frac{1}{2f(0)} \mathcal{C}_f \tag{1.45}$$

which imply, in particular, that all members of the family have the same properties as far as the scaling behavior with system size, or temperature dependence for equilibrium

[15] The prefactor $f(0)/2$ is chosen in such a way that the corresponding coherence measure is the variance for pure states. Different normalization choices can be found in the literature.

[16] Indeed, noting $|\psi\rangle = |i = 1\rangle$ and $(|i\rangle)$ an orthonormal basis of the Hilbert space, $p_1 = 1$ and $p_{i\neq 1} = 0$, $\mathcal{C}_f(|\psi\rangle\langle\psi|, \mathcal{O}) = \frac{f(0)}{2} 2 \sum_{i\neq 1} \frac{1}{f(0)} |\langle\psi|\mathcal{O}|i\rangle|^2 = \langle\psi|\mathcal{O}(\mathbb{1} - |\psi\rangle\langle\psi|)\mathcal{O}|\psi\rangle = \langle\psi|\mathcal{O}^2|\psi\rangle - \langle\psi|\mathcal{O}|\psi\rangle^2$.

states, are concerned. These inequalities confirm that all the coherence measures of the family quantify the same physical property of the system: the width over which it extends coherently in the space of the eigenvalues of $\mathcal{O}$, or in other words, the coherent fluctuations of $\mathcal{O}$.

1.6 Coherent fluctuations and dynamical structure factor

As a further unifying aspect for the coherence measures introduced in Section 1.5.2, we show that if ρ is a thermal equilibrium state at inverse temperature $\beta = (k_B T)^{-1}$, $\rho = e^{-\beta\mathcal{H}}/Z$, all of them can be related to the *dynamical structure factor* for the fluctuations of $\mathcal{O}$[17] (Forster, 1995; Täuber, 2014)

$$S_{\mathcal{O}\mathcal{O}}(\omega) = \int_{-\infty}^{+\infty} dt\, e^{i\omega t} \langle \delta\mathcal{O}(t)\delta\mathcal{O}(0)\rangle \tag{1.46}$$

where $\delta\mathcal{O} = \mathcal{O} - \langle\mathcal{O}\rangle$ and $\mathcal{O}(t) = e^{it\mathcal{H}/\hbar}\mathcal{O}e^{-it\mathcal{H}/\hbar}$. In particular, the variance of $\mathcal{O}$ is the integral over all frequencies of the dynamical structure factor

$$\langle \delta^2\mathcal{O}\rangle_{\rm tot} = \langle \delta\mathcal{O}(0)\delta\mathcal{O}(0)\rangle = \int_{-\infty}^{+\infty} \frac{d\omega}{2\pi} S_{\mathcal{O}\mathcal{O}}(\omega)\ . \tag{1.47}$$

The coherence measure $\mathcal{C}_f$ takes the following expression

$$\mathcal{C}_f(\rho,\mathcal{O}) = \int_0^{\infty} \frac{d\omega}{2\pi}\, h_f^Q(\beta\hbar\omega)(1-e^{-\beta\hbar\omega})\, S_{\mathcal{O}\mathcal{O}}(\omega) \tag{1.48}$$

where h_Q^f is a *quantum filter*

$$h_f^Q(x) = f(0)\frac{1-e^{-x}}{f(e^{-x})} \tag{1.49}$$

parametrized by the function f[18]. As $h_f^Q(x) \sim x$ at small x, it filters out the low frequencies $\omega \ll k_B T/\hbar$ in the ω-integral of Eq. (1.48). At $T = 0$ ($\beta \to \infty$), $h_f^Q = 1$,

[17] The expression of the QFI in terms of the dynamical structure factor was first proved by Hauke et al. (2016). Here, we generalize this result to any member $\mathcal{C}_f$ of the family of coherence measures.

[18] We obtain Eq. (1.48) as follows. First, denoting $\rho = \sum_i p_i|i\rangle\langle i|$, such that $\mathcal{H}|i\rangle = E_i|i\rangle$ and $p_i = e^{-\beta E_i}/Z$, we obtain the following expression for the dynamical structure factor

$$\begin{aligned} S_{\mathcal{O}\mathcal{O}}(\omega) &= \int_{-\infty}^{+\infty} dt\, e^{i\omega t} \sum_{i,j} p_i\, e^{\frac{it}{\hbar}(E_i-E_j)} \langle i|\delta\mathcal{O}|j\rangle\langle j|\delta\mathcal{O}|i\rangle \\ &= \sum_{i,j} p_i\, 2\pi\delta[\omega + (E_i-E_j)/\hbar]\, |\langle i|\delta\mathcal{O}|j\rangle|^2 \end{aligned} \tag{1.50}$$

and the total variance is recovered[19]. This result is intuitive, in that only frequencies such that $\hbar\omega \gg k_B T$ are sensitive to quantum-mechanical effects, and are thus the only ones to contribute to the coherent fluctuations of $\mathcal{O}$, while the frequencies such that $\hbar\omega \ll k_B T$ contribute to the incoherent fluctuations. Alternatively, the dynamical structure factor may be expressed in terms of the imaginary part of the dynamical susceptibility via the fluctuation-dissipation theorem (Callen and Welton, 1951; Forster, 1995)

$$S_{\mathcal{O}\mathcal{O}}(\omega) = \frac{2\hbar}{1 - e^{-\beta\hbar\omega}} \chi''_{\mathcal{O}\mathcal{O}}(\omega) \tag{1.55}$$

where $\chi''_{\mathcal{O}\mathcal{O}}(\omega)$ is the imaginary part of the dynamical susceptibility $\chi_{\mathcal{O}\mathcal{O}}(\omega)$, characterizing the average increase of $\langle \mathcal{O} \rangle(t)$ at frequency ω if a small periodic forcing in the form of $-\epsilon(\mathcal{O}e^{i\omega t} + \text{h.c.})/2$ added to the Hamiltonian is exerted

$$\langle \delta\mathcal{O} \rangle(\omega) = \epsilon \chi_{\mathcal{O}\mathcal{O}}(\omega) + O(\epsilon^2) \,, \tag{1.56}$$

where $\langle \delta\mathcal{O} \rangle(t) = \langle \mathcal{O} \rangle_\epsilon(t) - \langle \mathcal{O} \rangle_{\epsilon=0}$.

The imaginary part $\chi''_{\mathcal{O}\mathcal{O}}(\omega > 0)$ characterizes energy absorption by the system under the driving force. Using the fluctuation-dissipation theorem, Eq. (1.55), the coherence measure $\mathcal{C}_f$ can then be expressed as

$$\mathcal{C}_f(\rho, \mathcal{O}) = \hbar \int_0^\infty \frac{d\omega}{\pi} \, h_f^Q(\beta\hbar\omega) \, \chi''_{\mathcal{O}\mathcal{O}}(\omega) \,. \tag{1.57}$$

In particular, the critical behavior of quantum fluctuations at a phase transition can be traced back to the low frequency behavior of χ'', and of the quantum filter $f(0)(1 -$

Since, for $\omega \neq 0$, we may keep only $i \neq j$ in the sum, we replace $|\langle i|\delta\mathcal{O}|j\rangle|^2$ by $|\langle i|\mathcal{O}|j\rangle|^2$. This expression of $S_{\mathcal{O}\mathcal{O}}(\omega)$ is to be compared with the expression of $\mathcal{C}_f$, Eq. (1.44)

$$\mathcal{C}_f = \sum_{i,j} p_i \, g_f(p_j/p_i) |\langle i|\mathcal{O}|j\rangle|^2 \tag{1.51}$$

with $g_f(x) = \frac{f(0)}{2} \frac{(1-x)^2}{f(x)}$. Since $p_j/p_i = e^{-\beta(E_j - E_i)}$, we have that

$$g_f(p_j/p_i) = \int_{-\infty}^{+\infty} d\omega \, \delta[\omega + (E_i - E_j)/\hbar] \, g_f(e^{-\beta\hbar\omega}) \tag{1.52}$$

and hence the expression

$$\mathcal{C}_f = \int_{-\infty}^{+\infty} \frac{d\omega}{2\pi} \, g_f(e^{-\beta\hbar\omega}) \, S_{\mathcal{O}\mathcal{O}}(\omega) \,. \tag{1.53}$$

Then, using $S_{\mathcal{O}\mathcal{O}}(-\omega) = e^{-\beta\hbar\omega} S_{\mathcal{O}\mathcal{O}}(\omega)$ and $g_f(x) = x g_f(1/x)$, we conclude that

$$\mathcal{C}_f = \int_0^{+\infty} \frac{d\omega}{2\pi} \left[g_f(e^{-\beta\hbar\omega}) \, S_{\mathcal{O}\mathcal{O}}(\omega) + g_f(e^{\beta\hbar\omega}) \, S_{\mathcal{O}\mathcal{O}}(-\omega) \right] = \int_0^{+\infty} \frac{d\omega}{2\pi} \, 2 g_f(e^{-\beta\hbar\omega}) \, S_{\mathcal{O}\mathcal{O}}(\omega) \,. \tag{1.54}$$

This expression coincides with Eq. (1.48) with the quantum filter $h_f^Q(x) = 2g_f(e^{-x})/(1 - e^{-x}) = f(0)(1 - e^{-x})/f(e^{-x})$.

[19] Note that $S(\omega < 0) = 0$ at $T = 0$.

$e^{-\beta\hbar\omega})/f(e^{-\beta\hbar\omega})$ which is linear at small ω. On the other hand, the total variance of $\mathcal{O}$ is

$$\langle\delta^2\mathcal{O}\rangle_{\rm tot} = \hbar\int_0^\infty \frac{d\omega}{\pi}\,\coth(\beta\hbar\omega/2)\,\chi''_{\mathcal{O}\mathcal{O}}(\omega)\,, \tag{1.58}$$

where the function $\coth(\beta\hbar\omega/2)$ behaves as $1/\omega$ at small ω, namely it enhances the low frequency part of the integrand.

1.7 Quantum coherence and thermodynamics: the quantum variance

Considerations of previous Section 1.5 lead to criteria that a good measure of coherence is expected to satisfy. These criteria are motivated both by physical and mathematical considerations. There exists a whole family of coherence measures fulfilling these criteria, and some of them (like the quantum Fisher information) have additional, special physical meaning which translates into experimental significance. In this section, we introduce another member of this family of coherence measures, the *quantum variance* (QV), by considering the effect of the quantum uncertainty principle onto the equilibrium fluctuations of an observable for a system in contact with a heat bath. In the case of a particle confined in a harmonic potential $\frac{1}{2}m\omega^2x^2$, we proposed in Section 1.2 to define the QV of the position $\langle\delta^2x\rangle_Q$ as

$$\langle\delta^2x\rangle_{\rm tot} = \langle\delta^2x\rangle_{\rm equipartition} + \langle\delta^2x\rangle_Q \tag{1.59}$$

where $\frac{1}{2}m\omega^2\langle\delta^2x\rangle_{\rm equipartition} = \frac{1}{2}k_BT$, with k_B the Boltzmann constant and T the temperature. Namely: the QV quantifies the amount by which a thermodynamic identity valid for classical systems is violated. The equipartition theorem is in fact a special instance of the more general fluctuation-dissipation theorem (FDT), valid for classical systems at thermal equilibrium for any observable $\mathcal{O}$:

$$\langle\delta^2\mathcal{O}\rangle \underset{\text{classical FDT}}{=} k_BT\chi^{\rm stat}_{\mathcal{O}\mathcal{O}} \tag{1.60}$$

where $\chi^{\rm stat}_{\mathcal{O}\mathcal{O}}$ is the static susceptibility of $\langle\mathcal{O}\rangle$ with respect to the application of a small field ϵ coupled to the same observable $\mathcal{O}$. If $\mathcal{H}$ is the Hamiltonian of the system, the definition of $\chi^{\rm stat}_{\mathcal{O}\mathcal{O}}$ is the following:

$$\mathcal{H} \;\to\; \mathcal{H} - \epsilon\mathcal{O} \tag{1.61}$$

$$\langle\mathcal{O}\rangle \;\xrightarrow{\epsilon}\; \langle\mathcal{O}\rangle + \epsilon\chi^{\rm stat}_{\mathcal{O}\mathcal{O}} + O(\epsilon^2)\,. \tag{1.62}$$

For instance, if $\mathcal{O} = M^z$ is the magnetization along the direction z, ϵ is a small magnetic field along z, and $\chi^{\rm stat}_{\mathcal{O}\mathcal{O}} = \frac{\partial\langle M^z\rangle}{\partial\epsilon}\Big|_{\epsilon=0}$. If $\mathcal{O}_k = \int dx\; e^{ikx}n(x)$ is some

Fourier component of the density, then ϵ is a potential oscillating in space at the same wave-vector k, and $\chi^{\rm stat}_{\mathcal{O}\mathcal{O}}(k) = \left.\frac{\partial\langle O_k\rangle}{\partial\epsilon}\right|_{\epsilon=0}$, and so on.

This simple relation between the static susceptibility and the variance of $\mathcal{O}$ at equilibrium cannot hold in general for quantum systems, as the example of the harmonic oscillator illustrates. Furthermore, the classical FDT predicts that all fluctuations vanish at $T = 0$ — provided that $\chi^{\rm stat}_{\mathcal{O}\mathcal{O}}$ does not diverge at low T[20]. But according to quantum mechanics, at $T = 0$ almost all observables continue to fluctuate — in fact, any observable which does not commute with the Hamiltonian continues to fluctuate, since the ground state is generally not one of its eigenstates. What the classical FDT ignores are precisely these fluctuations related to Heisenberg principle, which are the only one subsisting down to $T = 0$. In other words, the classical FDT neglects the possibility for a quantum system to be in a *coherent superposition* of several classical configurations, or in short, the classical FDT ignores coherent fluctuations. We are thus lead to define the QV of $\mathcal{O}$ as the part of fluctuations not captured by the classical FDT

$$\langle\delta^2\mathcal{O}\rangle_Q = \langle\delta^2\mathcal{O}\rangle_{\rm tot} - k_BT\chi^{\rm stat}_{\mathcal{O}\mathcal{O}}\,. \tag{1.63}$$

As we shall see, $\langle\delta^2\mathcal{O}\rangle_Q \geq 0$ by construction.

1.7.1 QV and Heisenberg principle

The nonzero value of $\langle\delta^2\mathcal{O}\rangle_Q$ can be directly traced back to the noncommutativity of $\mathcal{O}$ with the Hamiltonian, $[\mathcal{O},\mathcal{H}] \neq 0$. Indeed, if they commute, the eigenstates of $\mathcal{H}$ can be chosen among the eigenstates of $\mathcal{O}$, and the classical reasoning holds[21]. More generally, the susceptibility $\chi^{\rm stat}_{\mathcal{O}\mathcal{O}}$ takes the following expression in terms of the

[20] Quantum-mechanically one could envision that $\chi^{\rm stat} \to \infty$ when $T \to 0$ but one can prove that $k_BT\chi^{\rm stat} \to 0$ for non-degenerate ground states.

[21] The origin of the FDT $\langle\delta^2\mathcal{O}\rangle = k_BT\chi^{\rm stat}_{\mathcal{O}\mathcal{O}}$ for classical systems is that upon the application of $-\epsilon\mathcal{O}$, each microscopic configuration $\mathcal{C}$ of the system is shifted in energy by an amount $-\epsilon\mathcal{O}(\mathcal{C})$, where $\mathcal{O}(\mathcal{C})$ is the value that the observable $\mathcal{O}$ takes in the microscopic configuration $\mathcal{C}$. Then, the average value of $\mathcal{O}$ in the presence of the perturbation reads

$$\langle\mathcal{O}\rangle(\epsilon) = \frac{1}{Z(\epsilon)}\sum_{\mathcal{C}}\mathcal{O}(\mathcal{C})e^{-\beta[E(\mathcal{C})-\epsilon\mathcal{O}(\mathcal{C})]} \tag{1.64}$$

where $E(\mathcal{C})$ is the energy of the configuration $\mathcal{C}$ in the absence of the perturbation, and $\beta = (k_BT)^{-1}$. $Z(\epsilon) = \sum_{\mathcal{C}} e^{-\beta[E(\mathcal{C})-\epsilon\mathcal{O}(\mathcal{C})]}$ is the partition function. The classical FDT then follows by differentiating $\langle\mathcal{O}\rangle(\epsilon)$ with respect to ϵ:

$$\chi^{\rm stat}_{\mathcal{O}\mathcal{O}} = \left.\frac{\partial\langle\mathcal{O}\rangle}{\partial\epsilon}\right|_{\epsilon=0} = \beta\frac{1}{Z}\sum_{\mathcal{C}}\mathcal{O}(\mathcal{C})^2e^{-\beta E(\mathcal{C})} - \langle\mathcal{O}\rangle\,\frac{1}{Z}\left.\frac{\partial Z}{\partial\epsilon}\right|_{\epsilon=0} = \beta[\langle\mathcal{O}^2\rangle - \langle\mathcal{O}\rangle^2]\,. \tag{1.65}$$

The partition function in the quantum case is $Z(\epsilon) = {\rm Tr}[e^{-\beta(\mathcal{H}-\epsilon\mathcal{O})}]$. If $|\mathcal{C}\rangle$ denote the common eigenstates of $\mathcal{H}$ and $\mathcal{O}$, with eigenvalues $E(\mathcal{C})$ and $\mathcal{O}(\mathcal{C})$, the partition function takes the same expression as in the classical case $Z(\epsilon) = \sum_{\mathcal{C}}\langle\mathcal{C}|e^{-\beta(\mathcal{H}-\epsilon\mathcal{O})}|\mathcal{C}\rangle = \sum_{\mathcal{C}} e^{-\beta[E(\mathcal{C})-\epsilon\mathcal{O}(\mathcal{C})]}$.

so-called imaginary-time correlations of $\mathcal{O}$

$$\chi^{\text{stat}}_{\mathcal{O}\mathcal{O}} = \int_0^\beta d\tau \, \langle \mathcal{O}(\tau)\mathcal{O}(0)\rangle - \langle \mathcal{O}\rangle^2 \tag{1.66}$$

where $\mathcal{O}(\tau) = e^{\tau\mathcal{H}}\mathcal{O}e^{-\tau\mathcal{H}}$. Averages are taken at termal equilibrium $\langle\cdot\rangle = \text{Tr}(\cdot\, e^{-\beta\mathcal{H}})/Z$[22]. In general, $k_BT\chi^{\text{stat}}_{\mathcal{O}\mathcal{O}} \leq \langle\delta^2\mathcal{O}\rangle$, with the equality holding iff $[\mathcal{O},\mathcal{H}] = 0$[23]. So finally we have that

$$\boxed{\langle\delta^2\mathcal{O}\rangle_Q \geq 0 \text{ and } \langle\delta^2\mathcal{O}\rangle_Q = 0 \text{ iff } [\mathcal{O},\mathcal{H}] = 0\,.} \tag{1.69}$$

The QV thus quantifies the contribution of the quantum uncertainty principle, Eq. (1.8), to equilibrium fluctuations of the observable $\mathcal{O}$. We still have to show that the QV satisfies the reasonable requirements identified in Section 1.5 that any measure of coherence should fulfill, and we are going to do so by showing that the QV belongs to the family of measures of coherence derived from the notion of distinguishability between ρ and $\rho(t) = e^{-it\mathcal{O}}\rho e^{it\mathcal{O}}$ introduced in Section 1.5. Before doing so, we give another intuitive meaning of the QV in terms of *imaginary-time fluctuations* within the path-integral formulation of quantum statistical mechanics (Feynman and Hibbs, 1965; Frérot and Roscilde, 2016b; Malpetti, 2016)

1.7.2 QV and path integrals

For classical systems, the partition function $Z = \text{Tr}(e^{-\beta\mathcal{H}})$ is a sum over the microscopic configurations of the system, each configuration being weighted by a Boltzmann factor $e^{-\beta E(\mathcal{C})}$. As we discussed, this calculation ignores the possibility for a quantum

[22] The proof is as follows. We consider $\mathcal{H}_1 = \mathcal{H} - V$, and $g(\beta) = e^{\beta\mathcal{H}}e^{-\beta\mathcal{H}_1}$. g obeys the differential equation $\partial_\beta g = e^{\beta\mathcal{H}}(\mathcal{H} - \mathcal{H}_1)e^{-\beta\mathcal{H}_1} = e^{\beta\mathcal{H}}Ve^{-\beta\mathcal{H}_1}$, and the solution is (since $g(0) = 1$) $g(\beta) = 1 + \int_0^\beta d\tau\, e^{\tau\mathcal{H}}Ve^{-\tau\mathcal{H}_1}$. So we have that

$$e^{-\beta\mathcal{H}_1} = e^{-\mathcal{H}} + \int_0^\beta d\tau\, e^{-\beta\mathcal{H}}V(\tau) + O(V^2)\,. \tag{1.67}$$

From this equation, we get that $Z_1 = \text{Tr}e^{-\beta\mathcal{H}_1} = Z(1 + \beta\langle V\rangle) + O(V^2)$. On the other hand, we have that $\text{Tr}(e^{-\beta\mathcal{H}_1}\mathcal{O}) = \text{Tr}(e^{-\beta\mathcal{H}}\mathcal{O}) + \int_0^\beta d\tau\, \text{Tr}(e^{-\beta\mathcal{H}}V(\tau)\mathcal{O}) + O(V^2)$. Finally, we arrive at the desired result

$$\langle\mathcal{O}\rangle(V) = \langle\mathcal{O}\rangle(0) + \int_0^\beta d\tau\, [\langle V(\tau)\mathcal{O}(0)\rangle - \langle V\rangle\langle\mathcal{O}\rangle] \tag{1.68}$$

and Eq. (1.66) follows by taking $V = \epsilon\mathcal{O}$.

[23] We show that $\forall\tau\ \langle\mathcal{O}(\tau)\mathcal{O}(0)\rangle \leq \langle\mathcal{O}^2\rangle$. Introducing $X = \mathcal{O}(\tau) - \mathcal{O}(0)$, we have $\langle XX^\dagger\rangle \geq 0$ with equality iff $X = 0$. Since $X^\dagger = \mathcal{O}(-\tau) - \mathcal{O}$, this is is equivalent to $\langle\mathcal{O}(\tau)\mathcal{O}(-\tau)\rangle + \langle\mathcal{O}^2\rangle \geq \langle\mathcal{O}(\tau)\mathcal{O}(0)\rangle + \langle\mathcal{O}(0)\mathcal{O}(-\tau)\rangle$. Since $\langle\mathcal{O}(\tau_1)\mathcal{O}(\tau_2)\rangle = \langle\mathcal{O}(\tau_1 - \tau_2)\mathcal{O}(0)\rangle$, we finally have $\langle\mathcal{O}(\tau)\mathcal{O}(0)\rangle \leq \frac{1}{2}\left(\langle\mathcal{O}^2\rangle + \langle\mathcal{O}(2\tau)\mathcal{O}(0)\rangle\right)$. Iterating this relation, we find that $\langle\mathcal{O}(\tau)\mathcal{O}(0)\rangle \leq \left[\sum_{i=1}^\infty (1/2)^i\right]\langle\mathcal{O}^2\rangle = \langle\mathcal{O}^2\rangle$. Then, the equality $(\beta\hbar)^{-1}\int_0^{\beta\hbar}\langle\mathcal{O}(\tau)\mathcal{O}(0)\rangle = \langle\mathcal{O}^2\rangle$ holds iff $\forall\tau\ \mathcal{O}(\tau) = \mathcal{O}$ iff $[\mathcal{O},\mathcal{H}] = 0$.

system to coherently spread across several microscopic configurations. In the framework of path-integrals, this coherent spreading can be cast in the form of a so-called imaginary-time dynamics: instead of sampling microscopic configurations, one has to sample *paths* $\mathcal{C}(\tau)$ of microscopic configurations, and the dynamics along the paths correspond to the coherent delocalization of the system in the space of configurations. The paths have a duration $\beta\hbar$ in the extra imaginary-time dimension, and are periodic $\mathcal{C}(\beta\hbar) = \mathcal{C}(0)$. Each path is weighted by a Boltzmann weight $e^{-(1/\hbar)S[\mathcal{C}(\tau),\, \partial_\tau \mathcal{C}(\tau),\, ...]}$. A major subtlety comes from the fact that these weights might be complex numbers, so that the interpretation in terms of "weight" is less clear. In the end, taking the trace in a basis $\mathcal{C}$ where $\mathcal{O}$ is diagonal, the partition function may be cast in the form (Feynman and Hibbs, 1965; Frérot and Roscilde, 2016b; Malpetti, 2016)

$$Z = \int_{\mathcal{C}(0)=\mathcal{C}(\beta\hbar)} \mathcal{D}[\mathcal{C}(\tau)] e^{-\frac{1}{\hbar} S[\mathcal{C}(\tau),\, \partial_\tau \mathcal{C}(\tau),\, ...]} \,. \tag{1.70}$$

The variance of $\mathcal{O}$ is then

$$\langle \delta^2 \mathcal{O} \rangle_{\text{tot}} = \left\langle \frac{1}{\beta\hbar} \int_0^{\beta\hbar} [\mathcal{O}(\tau) - \langle \mathcal{O} \rangle]^2 d\tau \right\rangle_{\text{paths}} \tag{1.71}$$

and $\langle \dots \rangle_{\text{paths}}$ denotes an average over an ensemble of paths weighted by $e^{-S/\hbar}$. $\mathcal{O}(\tau)$ is a shorthand for $\mathcal{O}[\mathcal{C}(\tau)]$. Now, we see that $\mathcal{O}$ fluctuates for two reasons 1) the average value of $\mathcal{O}(\tau)$ along a path $\bar{\mathcal{O}} = (\beta\hbar)^{-1} \int_0^{\beta\hbar} \mathcal{O}(\tau) d\tau$ (also called *path centroid*) fluctuates from path to path and 2) for a given path, the value of $\mathcal{O}(\tau)$ fluctuates along the imaginary time dimension with respect to the path centroid $\bar{\mathcal{O}}$. Quite remarkably, the splitting between incoherent and coherent fluctuations, as leading to the definition of the QV, exactly coincides with the above two sources of fluctuations within the path integral formalism

$$\langle \delta^2 \mathcal{O} \rangle_{\text{tot}} = \underbrace{\left\langle (\bar{\mathcal{O}} - \langle \mathcal{O} \rangle)^2 \right\rangle_{\text{paths}}}_{k_B T \chi_{\mathcal{O}}} + \underbrace{\left\langle \frac{1}{\beta\hbar} \int_0^{\beta\hbar} [\mathcal{O}(\tau) - \bar{\mathcal{O}}]^2 d\tau \right\rangle_{\text{paths}}}_{\langle \delta^2 \mathcal{O} \rangle_Q} . \tag{1.72}$$

As illustrated on Fig. 1.1, this provides a very intuitive account for the origin of incoherent and coherent fluctuations at thermal equilibrium: to sample paths, one can first sample the mean value along the path (the path centroid), and the statistics of this mean value provides the probability for *incoherent* (or thermal) fluctuations, and then, for each given value of the path centroid, sample the paths which fluctuate in imaginary time with respect to this path centroid, providing the probability for

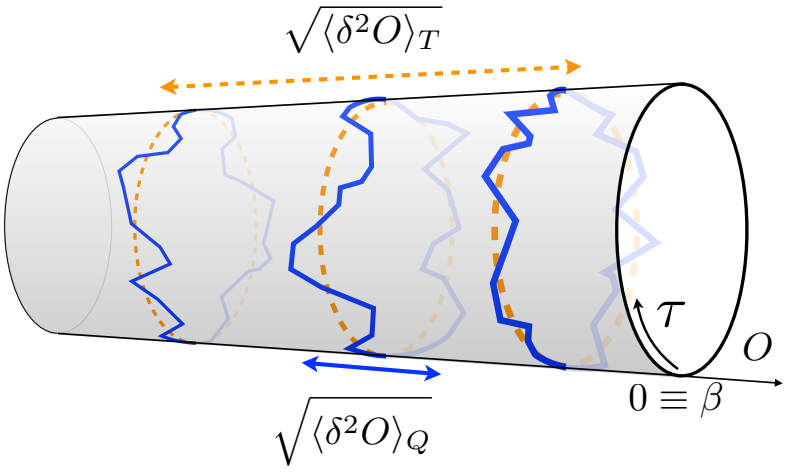

Figure 1.1: **Thermal vs. quantum fluctuations.** Different imaginary-time paths $\mathcal{O}(\tau)$ in the space of eigenvalues of the observable $\mathcal{O}$ are shown, associated with the path-integral representation of a generic mixed state ρ. While the thermal/incoherent fluctuations $\langle \delta^2 \mathcal{O} \rangle_{\mathrm{T}}$ are associated with the fluctuations of the centroid of the paths (dashed yellow lines), the quantum/coherent fluctuations $\langle \delta^2 \mathcal{O} \rangle_Q$ are associated with the fluctuations of the paths around their centroids (solid blue lines). Figure courtesy of T. Roscilde.

coherent (or quantum) fluctuations. In short

$$\text{thermal variance} \quad = \quad \left\{ \begin{array}{c} \text{variance (from path to path)} \\ \text{of the mean (along a path);} \end{array} \right. \tag{1.73}$$

$$\text{quantum variance} \quad = \quad \left\{ \begin{array}{c} \text{mean (over the paths)} \\ \text{of the variance (along a path).} \end{array} \right. \tag{1.74}$$

1.7.3 QV and "skew information"

The QV has a natural meaning in the context of equilibrium fluctuations only, but its definition can be extended to arbitrary states by the following mathematical expression

$$\langle \delta^2 \mathcal{O} \rangle_Q = \mathrm{Tr}(\rho \mathcal{O}^2) - \int_0^1 d\alpha \, \mathrm{Tr}(\rho^{1-\alpha} \mathcal{O} \rho^\alpha \mathcal{O}) \tag{1.75}$$

where we made the change of variable $\tau \to \alpha\beta$ in Eq. (1.66) and used the fact that $\rho = (1/Z) e^{-\beta \mathcal{H}}$. To prove that the QV is a member of the family of coherence measures introduced in Section 1.5, we note that the quantity $I_\alpha(\rho, \mathcal{O}) = \mathrm{Tr}(\rho \mathcal{O}^2) - \mathrm{Tr}(\rho^{1-\alpha} \mathcal{O} \rho^\alpha \mathcal{O})$, known as the Dyson-Wigner-Yanase skew information in the literature (Wigner and Yanase, 1963), belongs to it for any $0 < \alpha < 1$ (Hansen, 2008). The QV, being the averaged of I_α over α

$$\langle \delta^2 \mathcal{O} \rangle_Q = \int_0^1 I_\alpha(\rho, \mathcal{O}) d\alpha \, , \tag{1.76}$$

automatically inherits this property, and thus the mathematical properties (i, ... v) of Section 1.5.1. Note also that it is immediate to see from Eq. (1.75) that if ρ is a pure state, so that $\rho = |\psi\rangle\langle\psi| = \rho^\alpha = \rho^{1-\alpha}$, the quantum variance coincides with the total variance. In particular, for thermal equilibrium states, this proves that if the ground state is unique

$$k_B T \chi^{\rm stat}_{\mathcal{O}\mathcal{O}} = \langle \delta^2 \mathcal{O} \rangle_{\rm tot} - \langle \delta^2 \mathcal{O} \rangle_Q \underset{T\to 0}{\to} 0 \, . \tag{1.77}$$

Note that this proof requires the ground state to be separated from excited states by a nonzero energy gap. While this is true by definition on a finite size system if the ground state is unique, this may not hold in the thermodynamic limit. In fact, when considering the behavior of fluctuations above a quantum critical point in Part III, we shall precisely encounter a situation where Eq. (1.77) does not hold.

1.7.4 Expression of the QV for arbitrary states

We can derive from Eq. (1.75) another useful expression of the quantum variance by evaluating the trace in a basis of eigenstates of ρ, $\rho = \sum_i p_i |i\rangle\langle i|$:

$$\begin{aligned}
\langle \delta^2 \mathcal{O} \rangle_Q &= \sum_i p_i \langle i|\mathcal{O}^2|i\rangle - \int_0^1 d\alpha \sum_{i,j} p_i^{1-\alpha} p_j^\alpha |\langle i|\mathcal{O}|j\rangle|^2 \\
&= \sum_{i,j} p_i \left(1 - \frac{p_j/p_i - 1}{\ln(p_j/p_i)} \right) |\langle i|\mathcal{O}|j\rangle|^2 \\
&= \sum_{i,j} p_i \left(\frac{1+x}{2} - \frac{x-1}{\ln x} \right) |\langle i|\mathcal{O}|j\rangle|^2 \, ,
\end{aligned} \tag{1.78}$$

with $x = p_j/p_i$. This expression, of the form given in Eq. (1.44), may be used to evaluate the QV when it is possible to diagonalize exactly the density matrix — or, equivalently, the Hamiltonian for thermal equilibrium states.

1.7.5 QV and dynamical susceptibility

Finally, the QV can be expressed as an integral over frequencies of the dynamical susceptibility, weighted by a "quantum filter" (see Section 1.5)

$$\langle \delta^2 \mathcal{O} \rangle_Q = \hbar \int_0^\infty \frac{d\omega}{\pi} \, h_{\rm QV}(\beta\hbar\omega) \, \chi''_{\mathcal{O}\mathcal{O}}(\omega) \tag{1.79}$$

with the quantum filter given by the so-called "Langevin function"

$$h_{\rm QV}(x) = \coth(x/2) - \frac{2}{x} \, . \tag{1.80}$$

This expression can be proved using Eq. (1.58) for the total variance, and the following expression for the static susceptibility

$$\chi^{\rm stat}_{\mathcal{O}\mathcal{O}} = 2\int_0^\infty \frac{d\omega}{\pi}\frac{\chi''_{\mathcal{O}\mathcal{O}}(\omega)}{\omega}\,, \tag{1.81}$$

which follows itself by inserting the dynamical structure factor $S_{\mathcal{O}\mathcal{O}}(\omega)$, defined in Eq. (1.46), into Eq. (1.66) for the static susceptibility:

$$\langle\mathcal{O}(\tau)\mathcal{O}(0)\rangle - \langle\mathcal{O}\rangle^2 = \int_{-\infty}^\infty \frac{d\omega}{2\pi} S_{\mathcal{O}\mathcal{O}}(\omega)e^{-\tau\hbar\omega}\,. \tag{1.82}$$

Using the identity $S_{\mathcal{O}\mathcal{O}}(-\omega) = e^{-\beta\hbar\omega}S_{\mathcal{O}\mathcal{O}}(\omega)$, performing the integration over τ, and using the fluctuation-dissipation theorem, Eq. (1.55), to express $S_{\mathcal{O}\mathcal{O}}(\omega)$ in terms of $\chi''_{\mathcal{O}\mathcal{O}}(\omega)$, we finally obtain Eq. (1.81).

1.8 Inequalities between the QV, the QFI and the skew information

It is informative to compare the expression for the QV in terms of dynamical susceptibilities, Eq. (1.79), to a similar expression for the quantum Fisher information (QFI), proved by Hauke et al. (2016) and derived in Section 1.6

$$F_Q[\rho,\mathcal{O}]/4 = \hbar\int_0^\infty \frac{d\omega}{\pi}\, h_{\rm QFI}(\beta\hbar\omega)\,\chi''_{\mathcal{O}\mathcal{O}}(\omega) \tag{1.83}$$

with the quantum filter given by

$$h_{\rm QFI}(x) = \tanh(x/2)\,. \tag{1.84}$$

We also have a similar expression for the "skew information" (Wigner and Yanase, 1963) $I_\alpha[\rho,\mathcal{O}] = {\rm Tr}(\rho\mathcal{O}^2) - {\rm Tr}(\rho^{1-\alpha}\mathcal{O}\rho^\alpha\mathcal{O})$, where the quantum filter is given by

$$h_\alpha(x) = \frac{\cosh(x/2) - \cosh[(\alpha-1/2)x]}{\sinh(x/2)}\,. \tag{1.85}$$

All these expressions for the quantum filters may be recovered from Eq. (1.49) by noting that the QV, the QFI, and the skew information can be expressed as in Eq. (1.44) with for f the following functions:

$$f_{\rm QV}(x) = \frac{(1-x)^2/6}{1+x+2(1-x)/\ln x} \tag{1.86}$$

$$f_{\rm QFI}(x)/4 = (1+x)/2 \tag{1.87}$$

$$f_\alpha(x) = \frac{\alpha(1-\alpha)(1-x)^2}{1+x-x^\alpha-x^{1-\alpha}} \tag{1.88}$$

A direct comparison of $f_{\rm QFI}$, $f_{1/2}$ and $f_{\rm QV}$ reveals the following chain of inequalities

$$\langle\delta^2\mathcal{O}\rangle_Q(\rho) \leq I_{1/2}[\rho,\mathcal{O}] \leq \frac{F_Q[\rho,\mathcal{O}]}{4} \leq 2I_{1/2}[\rho,\mathcal{O}] \leq 3\langle\delta^2\mathcal{O}\rangle_Q(\rho) \quad (1.89)$$

$$I_\alpha[\rho,\mathcal{O}] \leq \frac{F_Q[\rho,\mathcal{O}]}{4} \leq \frac{1}{2\alpha(1-\alpha)} I_\alpha[\rho,\mathcal{O}] \,, \quad (1.90)$$

where the inequalities with the QFI can also be viewed as special instances of Eq. (1.45). As both the QV and the skew information can be expressed in terms of imaginary-time correlations, themselves more easily accessed in numerical and field-theory computations than the dynamical structure factor, these inequalities may be used in practice to bound the QFI, relevant to interferometric questions.

1.9 Behavior of quantum fluctuations at thermal critical points

We conclude this first chapter by showing that quantum fluctuations are not expected to diverge at a thermal (namely finite-temperature) critical point where, instead, the total fluctuations diverge. In this section, we consider the fluctuations of the order parameter of a critical phase transition, typically some component of the magnetization in the magnetic language of "standard models" for second-order phase transitions (Collins, 1989). In Part III, we come back in much more details to the critical behavior of quantum fluctuations at both thermal and quantum critical points; in this section, we only derive this general prediction.

In order to do so, we resort to generic scaling arguments for the dynamical response close to a critical point (Hohenberg and Halperin, 1977; Collins, 1989; Täuber, 2014; Kamenev, 2011).

Quantum fluctuations and dynamical susceptibility. We recall the expression of quantum fluctuations in terms of the dynamical susceptibility $\chi''(\omega)$ (see Section 1.6)

$$\mathcal{C}_f = \hbar \int_0^\infty \frac{d\omega}{\pi} h_f^Q(\beta\hbar\omega)\chi''_{\mathcal{O}\mathcal{O}}(\omega) \,, \quad (1.91)$$

where h_f^Q is a *quantum filter*. Close to the critical point, $\mathcal{C}_f$ is composed of a regular part, varying smoothly across the phase transition, and of a singular part whose singularity descends from the singular part of $\chi''_{\mathcal{O}\mathcal{O}}$

$$\mathcal{C}_f = \mathcal{C}_f^{\rm reg} + \mathcal{C}_f^{\rm sing} \,. \quad (1.92)$$

Critical behavior of the static susceptibility. The static susceptibility $\chi_{\mathcal{O}\mathcal{O}}$ of the order parameter diverges upon approaching the critical temperature T_c according to

$$\chi_{\mathcal{O}\mathcal{O}} \sim t^{-\gamma_{\mathrm{T}}} \tag{1.93}$$

where $t = |T/T_c - 1|$, T being the temperature and γ_{T} a critical exponent (we denote with a subscript T the critical exponents associated to a thermal phase transition). In virtue of Eq. (1.81), which we repeat here for completeness

$$\chi_{\mathcal{O}\mathcal{O}} = 2\int_0^\infty \frac{d\omega}{\pi} \frac{\chi''_{\mathcal{O}\mathcal{O}}(\omega)}{\omega} \,, \tag{1.94}$$

the static response may be viewed as stemming from fluctuations at all frequencies, weighted by $\chi''_{\mathcal{O}\mathcal{O}}(\omega)/\omega$.

Critical slowing down. We expect that, close to the critical point, $\chi''_{\mathcal{O}\mathcal{O}}(\omega)$ is peaked around $\omega = 0$, with a characteristic width ω_c having the physical meaning of a relaxation rate. This relaxation rate is generically observed to vanish upon approaching the critical point as a power law (Hohenberg and Halperin, 1977; Collins, 1989; Täuber, 2014; Kamenev, 2011)

$$\omega_c \sim \xi^{-z_{\mathrm{T}}} \tag{1.95}$$

where ξ is the correlation length for the fluctuations of the order parameter, and z_{T} the *dynamical critical exponent*. Given that $\xi \sim t^{-\nu_{\mathrm{T}}}$, this scaling law is equivalent to

$$\omega_c \sim t^{\nu_{\mathrm{T}} z_{\mathrm{T}}} \,. \tag{1.96}$$

The divergence of ω^{-1} at the critical point induces the so-called *critical slowing down* of the dynamics.

Dynamical scaling hypothesis. The dynamical scaling hypothesis amounts to postulate the following behavior for the singular part of the dynamical susceptibility

$$\chi''_{\mathcal{O}\mathcal{O}}(\omega) = g\left(\frac{\omega}{\omega_c}\right) \chi_{\mathcal{O}\mathcal{O}} \tag{1.97}$$

with g some scaling function.

Critical scaling of the singular part of quantum fluctuations. As a consequence, quantum fluctuations acquire a singular part of the form

$$\mathcal{C}_f^{\mathrm{sing}} = \hbar\chi_{\mathcal{O}\mathcal{O}} \int_0^\infty \frac{d\omega}{\pi}\, h_f^Q(\beta\hbar\omega) g(\omega/\omega_c) \,. \tag{1.98}$$

Close to the critical point, the scaling function g selects frequencies close to zero, such that $\hbar\omega \ll k_B T$. This implies that we may approximate the quantum filter h_f^Q by its linear behavior at small ω. Making the change of variables $x = \omega/\omega_c$, we arrive at the expression

$$\mathcal{C}_f^{\text{sing}} = \frac{(\hbar\omega_c)^2}{k_B T} \chi_{\mathcal{O}\mathcal{O}} \mathcal{I}_f \tag{1.99}$$

where

$$\mathcal{I}_f = \int_0^\infty \frac{dx}{\pi}\, h_f^Q(x) g(x)\ . \tag{1.100}$$

Recalling the scaling behaviors $\chi_{\mathcal{O}\mathcal{O}} \sim t^{-\gamma_{\text{T}}}$ and $\omega_c \sim t^{\nu_{\text{T}} z_{\text{T}}}$, and using the relation $\gamma_{\text{T}} = (2 - \eta_{\text{T}})\nu_{\text{T}}$ with η_{T} the critical exponent of the correlation function (Collins, 1989), we may finally predict that the singular part of the quantum fluctuations scales according to

$$\mathcal{C}_f^{\text{sing}} \sim t^{2\nu_{\text{T}}(z_{\text{T}} + \eta_{\text{T}}/2 - 1)}\ . \tag{1.101}$$

This prediction is the main result of the present section.

Criterion for the absence of divergence of quantum fluctuations at the thermal phase transition. Noting that $\nu_{\text{T}} \geq 0$, we can conclude that this singular part is non-divergent if and only if

$$z_{\text{T}} \geq 1 - \eta_{\text{T}}/2\ . \tag{1.102}$$

The values of z_{T} reported in the literature are always larger than 1 (Hohenberg and Halperin, 1977; Collins, 1989; Täuber, 2014; Kamenev, 2011), so that this condition is fulfilled for all models studied so far (note that $\eta_{\text{T}} \geq 0$). On the other hand, we may expect that temperature-derivatives of $\mathcal{C}_f$ of sufficiently high degree are singular at the critical point. For instance, the gaussian theory for a non-conserved order parameter (Hohenberg and Halperin, 1977; Collins, 1989; Täuber, 2014; Kamenev, 2011) predicts $\nu_{\text{T}} = 1/2$, $z_{\text{T}} = 2$ and $\eta_{\text{T}} = 0$, so that $\mathcal{C}_f^{\text{sing}} \sim t$. For systems belonging to this universality class, we can thus predict a singularity of $\partial_T \mathcal{C}_f$, and indeed, we shall encounter such an example in Part III.

We note that it may happen that $z_{\text{T}} = 1 - \eta_{\text{T}}$, although this situation would be very pathological. For instance, we may have $z_{\text{T}} = 1$ and $\eta_{\text{T}} = 0$. In this case, we expect from Eq. (1.101) a discontinuity of the quantum fluctuations across the phase transition. If the discontinuity vanishes, the singular behavior stems from the cubic term in $h_f^Q(\beta\hbar\omega)$ (assuming that it is an odd function). In this case, repeating the steps leading to Eq. (1.101), we obtain that

$$\mathcal{C}_f^{\text{sing}} \sim t^{2\nu_{\text{T}}(2z_{\text{T}} + \eta_{\text{T}}/2 - 1)}\ . \tag{1.103}$$

Discussion. In view of Eq. (1.91), it is not surprising that quantum fluctuations bear the signature of the dynamical critical exponent z_{T}. However, we emphasize that the quantum variance was *not* defined by Eq. (1.91), but as the difference between total fluctuations and the static susceptibility (see Section 1.7). In principle, neither the total fluctuations nor the static susceptibility need dynamical probes to be measured. We have thus shown that the difference between two static physical quantities, namely physical quantities whose investigation do not require any dynamical measurement, bears the signature of the dynamical critical exponent, associated to the critical slowing down at a thermal transition.

In light of the link between the quantum fluctuations and the dynamical susceptibility via Eq. (1.91), this conclusion is important both conceptually and experimentally. From a computational perspective, taking for $\mathcal{C}_f$ the quantum variance, our result also shows that the dynamical exponent z_{T} is contained in the *imaginary-time* dynamics alone (see Section 1.7), without the need to actually calculate the response at real frequencies.

1.10 Conclusion

In this first chapter, we introduced the notion of coherent fluctuations from two different perspectives: 1) the effect of Heisenberg principle, through the non-commutativity of an observable $\mathcal{O}$ with the state ρ, onto the fluctuations of that observable. For states at thermal equilibrium, we introduced the quantum variance, quantifying the fluctuations of $\mathcal{O}$ which exceed the prediction of a classical fluctuation-dissipation theorem (valid only if $[\mathcal{O}, \rho] = 0$); 2) the interference effects exhibited by ρ when it undergoes a unitary transformation $U(\phi) = e^{-i\phi\mathcal{O}}$ generated by the observable $\mathcal{O}$, and parametrized by ϕ. We introduced the quantum Fisher information, quantifying the ultimate precision one can get on the estimation of ϕ by measuring ρ after this unitary evolution. The quantum Fisher information and the quantum variance were shown to belong to a wider family of coherence measures, as they both quantify the speed of evolution of ρ under a unitary transformation $U(\phi)$, although for different measures of distinguishability between ρ and $\rho(\phi)$. In particular, all the coherence measures of this family where expressed in terms of the dynamical susceptibility $\chi_{\mathcal{O}\mathcal{O}}(\omega)$ if the system is at thermal equilibrium.

Despite similarities, we emphasize the specificity of the quantum variance, which is, to our knowledge, the only measure of coherence defined in purely physical terms, namely, as the difference between the variance of $\mathcal{O}$ and ($k_B T$ times) the static susceptibility of $\mathcal{O}$ with respect to a perturbation which couples to $\mathcal{O}$. This aspect

has a tremendous impact in terms of the computability of the quantum variance via state-of-the-art analytical and numerical approaches to quantum many-body systems, as well as its potential accessibility to experiments. In the following Chapter 2, we show that quantum correlations can be naturally quantified in a similar spirit.

Chapter 2

Quantum covariance

2.1 Quantum correlations: entanglement and beyond

2.1.1 Non-locality

Over the past decades, it has been progressively recognized that quantum mechanics predicts correlations among degrees of freedom that would do not admit a classical counterpart. Whether correlations in specific situations should be considered as genuinely quantum depends on what is understood as a classical framework. The most extreme form of non-classicality is manifested by the impossibility to reproduce some predictions of quantum mechanics with a *local* "hidden-variable" (LHV) model. In short, if two measurements, respectively x and y, are performed on two systems A and B yielding the results a and b with probability $p(ab|xy)$, locality is defined as the existence of a "hidden-variable" λ, whose value is independent of the chosen measurements x and y (this is the locality hypothesis), and occurs with probability $q(\lambda)$, such that

$$p(ab|xy) = \int d\lambda \; q(\lambda) \; p(a|x,\lambda) \; p(b|y,\lambda) \tag{2.1}$$

for any pair of measurements (x, y) and any pair of results (a, b). Eq. (2.1) expresses the fact that correlations among the results of measurement on A and B can be interpreted as resulting from 1) an interaction between the two systems during which the shared value of λ is determined (possibly randomly), and 2) an evolution during which A and B do not influence each other any longer, and behave as two independent bodies. Then, correlations between measurement results on A and B can be fully traced back to the common value of λ, without any further reciprocal influence. The incompatibility of such LHV hypothesis with some predictions of quantum mechanics

was first discovered by Bell (1964), following the careful scrutiny of the famous EPR paper (Einstein, Podolsky, and Rosen, 1935) by Bohm (1952). The experimental confirmation of the predictions of quantum mechanics first by Aspect, Grangier, and Roger (1982) and many subsequent experimental tests of non-locality, up to the very recent triplet of 2015 loophole-free experiments (Hensen et al., 2015; Giustina et al., 2015; Shalm et al., 2015), definitely ruled out the possibility to build a consistent physical theory of nature based on purely local objects (Brunner et al., 2014).

2.1.2 Non-separabiliy or entanglement

Non-locality, namely the impossibility to express the probability of measurement results on two systems A and B as in Eq. (2.1), is an extreme form of non-separability (synonymous with entanglement in the present day terminology). The term "entanglement" was originally introduced by Schrödinger (1935) to qualify a situation where (in his words) :

> "Maximal knowledge of a total system does not include total knowledge of all its parts, not even when these are separated from each other and at the moment not influencing each other at all." (Schrödinger, 1935)

Werner (1989) realized that this "entanglement of predictions" (Schrödinger, 1935) reflects the impossibility that A and B, prepared in distant laboratories by means of local operations and classical communications (LOCC) only, reproduce all the forms of correlations predicted by quantum mechanics. In this LOCC paradigm (Horodecki et al., 2009), only combined states ρ_{AB} of the form

$$\rho_{AB}^{\text{sep}} = \sum_i p_i \, \sigma_i^A \otimes \sigma_i^B \quad \text{(separable state)} \tag{2.2}$$

can be produced. Here $\sigma_i^{A(B)}$ is an arbitrary density-matrix for $A(B)$ subsystem, and p_i is the probability that the two distant laboratories where A and B are manipulated prepare the joint state $\sigma_i^A \otimes \sigma_i^B$. A state ρ_{AB} failing to admit such decomposition is called *non-separable* or *entangled* (Horodecki et al., 2009). Non-locality is an extreme form of non-separability in that any separable state, Eq. (2.2), admits a LHV model (where the hidden variable λ is just the label i in the sum on the r.h.s of Eq. (2.2)), so that non-separability is necessary for non-locality, while the converse is not true: there exists non-separable states which nevertheless admit a LHV model (Werner, 1989; Augusiak, Demianowicz, and Acín, 2014)[1].

[1] Quantum steering is yet another layer of refinement, lying in-between non-separability and non-locality (Cavalcanti and Skrzypczyk, 2017).

2.1.3 Non-classicality and the quantum discord

A more recent breakthrough came when Ollivier and Zurek (2001) and Henderson and Vedral (2001) realized that even for separable states, correlations between measurements on A and B may exhibit non-classical features. This happens whenever the states $\{\sigma_i^A\}$ (or $\{\sigma_i^B\}$) in Eq. (2.2) are not fully distinguishable from one another, a possibility offered by the superposition principle. The non-classicality is expressed by the fact that two different ways of characterizing the correlations between A and B, equivalent for classical systems where the statistical properties are represented by a probability distribution $p(a,b)$ in a phase-space, may be inequivalent when transposed to quantum systems, where such representation is in general impossible. The two quantities are here

1. The information contained in the correlations between A and B (or mutual information), quantified by the sub-additive behavior of entropy

$$I(A:B) = S_A + S_B - S_{AB} \tag{2.3}$$

   where $S(\{p_i\}) = -\sum_i p_i \log p_i$ stands for the Shannon entropy of the probability distribution p_i. For A, one takes $p(a) = \sum_b p(a,b)$, and similarly for B.

2. The average information gained on the state of B by knowing the state of A:

$$J(A:B) = S_B - \sum_a p(a) S(B|a) \tag{2.4}$$

   where $S(B|a) = S(\{p(b|a)\})$.

The equality of $I(A:B)$ and $J(A:B)$ for classical probability distributions is a simple consequence of Bayes' rule $p(b|a) = p(a,b)/p(a)$. For quantum systems, "knowing the state of A" has an unambiguous meaning only if a measurement M_A on A is specified, whose outcome modifies the entropy of B. J then becomes measurement-dependent, and asymmetric in A and B. On the other hand, $I(A:B)$ keeps the same expression as in Eq. (2.3), provided Shannon entropy is replaced by von Neumann entropy $-\mathrm{Tr}\rho\log\rho$, and the reduced states for $A(B)$ is obtained by tracing over the degrees of freedom of $B(A)$: $\rho_{A(B)} = \mathrm{Tr}_{B(A)}\rho_{AB}$. In general, $J(M_A:B) < I(A:B)$, and this is so for any measurement M_A unless the state ρ_{AB} is of the form

$$\rho_{AB}^{C-Q} = \sum_i p_i \, |e_i^A\rangle\langle e_i^A| \otimes \sigma_i^B \quad \underline{\text{(classical-quantum state)}} \, , \tag{2.5}$$

where $\{|e_i^A\rangle\}$ forms an orthogonal family of states. If this is so, measuring a non-degenerate observable diagonal in $\{|e_i^A\rangle\}$ maximizes the information gained on B, so that the upper bound $J(M_A : B) = I(A : B)$ is reached. These considerations led Ollivier and Zurek (2001) and Henderson and Vedral (2001) to define the *quantum discord* as

$$D(A : B) = I(A : B) - \max_{\text{meas.}M_A} J(M_A : B) \tag{2.6}$$

where the maximum is taken over all possible measurements on A. The quantum discord cannot be negative, and reaches zero iff the state ρ_{AB} is classical-quantum, Eq. (2.5) (Modi et al., 2012). Non-classical features of correlations between A and B in a state which is not classical-quantum are grouped under the generic name of *quantum correlations*, which is thus, strictly speaking, a more general concept than entanglement (Adesso, Bromley, and Cianciaruso, 2016).

2.1.4 Hierarchy of quantum correlations

In conclusion of this first section, we have the following hierarchy of non-classical correlations

$$\text{quantum correlations} < \left\{ \begin{array}{c} \text{non-separability} \\ \text{entanglement} \end{array} \right. < \text{non-locality} \, . \tag{2.7}$$

The above hierarchy means that in order to exhibit non-locality (in the sense of the non-existence of a LHV model which reproduces the correlations between A and B, Eq. (2.1)), ρ_{AB} needs to be non-separable (*i.e.* not of form given in Eq. (2.2)), and hence, obviously, quantum-mechanically correlated (*i.e* not of the form given in Eq. (2.5)). The converse is not true: some states are quantum-mechanically correlated (or, equivalently, *discordant* in the sense of a non-zero discord), while actually being separable, and some non-separable states admit a LHV model (Werner, 1989). Finally, we note that for pure states, any correlation is a quantum effect, and the above hierarchy collapses onto a single notion (Brunner et al., 2014)

$$\text{correlations} = \text{quantum correlations} = \left\{ \begin{array}{c} \text{non-separability} \\ \text{entanglement} \end{array} \right. = \text{non-locality} \, . \tag{2.8}$$

2.2 Quantum correlations as correlations among Heisenberg uncertainties

2.2.1 Quantum variance versus the quantum discord

The considerations leading Henderson and Vedral (2001) and Ollivier and Zurek (2001) to introduce the quantum discord (see Section 2.1) have a flavor similar to our

considerations of Section 1.7, leading to the introduction of the quantum variance (QV). According to Modi et al. (2012)

> " Quantum discord encapsulates the idea that two equivalent ways of looking at correlations in classical information theory give different results when generalized to quantum information theory. In quantum physics, we can have classical correlations, but we also have correlations that exceed them." (Modi et al., 2012)

Recalling the definition of the QV of an arbitrary observable $\mathcal{O}$, Eq. (1.63)

$$\langle \delta^2 \mathcal{O} \rangle_{\text{tot}} = k_B T \chi_{\mathcal{O}} + \langle \delta^2 \mathcal{O} \rangle_Q$$

with $\chi_{\mathcal{O}}$ the static susceptibility of $\langle \mathcal{O} \rangle$, k_B Boltzmann constant and T the temperature (see Section 1.7), we could rephrase this statement for quantum fluctuations. Indeed, we showed in Section 1.7 that the QV encapsulates the idea that two equivalent ways of looking at fluctuations in classical statistical mechanics (namely fluctuations at equilibrium, and linear response to a perturbation) give different results when generalized to quantum statistical mechanics. In quantum physics, we have classical (incoherent) fluctuations, but we also have quantum (coherent) fluctuations in addition.

Despite a similar flavor, we must bear in mind several fundamental differences between the quantum discord and the QV. First, while the former is based on information-theoretic quantities ("information gained on B by making measurements on A"), the latter is defined in purely physical terms, without explicit reference to the underlying mathematical theory. Indeed, the QV can be defined and measured even without knowing anything about quantum mechanics, a very different situation from an information-theoretic quantity like the quantum discord. Second, according to the quantum discord, even pure states share classical correlations (as quantified by $J(M_A : B)$, see Eq. (2.4)), while according to the QV, any fluctuation in a pure state is a quantum effect, and several arguments supporting this conclusion were given in Section 1.4.2, 1.5 and 1.7. Similarly, according to the natural concept of quantum correlations which we are about to derive from the QV, any correlation in a pure state has a quantum origin, in agreement with the fact that any form of correlations in a pure state implies that the state is entangled, see Eq. (2.8).

2.2.2 The quantum covariance

The concept of quantum (or coherent) fluctuations introduced in Section 1 calls for a natural concept of quantum correlations, completely independent of the one discussed in the previous Section 2.1.

Here and in the rest of this manuscript, *quantum correlations* are understood as *correlations among coherent fluctuations*.

To give to this statement a mathematical meaning, we specify two observables $\mathcal{O}_A$ and $\mathcal{O}_B$. The quantum covariance of $\mathcal{O}_A$ and $\mathcal{O}_B$ is then defined as

$$\mathrm{covar}_Q(\mathcal{O}_A,\mathcal{O}_B)=\langle\delta\mathcal{O}_A\delta\mathcal{O}_B\rangle_Q=\frac{1}{2}\left[\langle\delta^2(\mathcal{O}_A+\mathcal{O}_B)\rangle_Q-\langle\delta^2\mathcal{O}_A\rangle_Q-\langle\delta^2\mathcal{O}_B\rangle_Q\right] \tag{2.9}$$

where $\langle\delta^2(\mathcal{O}_A+\mathcal{O}_B)\rangle_Q$, $\langle\delta^2\mathcal{O}_A\rangle_Q$ and $\langle\delta^2\mathcal{O}_B\rangle_Q$ are the quantum variances of $\mathcal{O}_A+\mathcal{O}_B$, $\mathcal{O}_A$ and $\mathcal{O}_B$ respectively. This is just the transposition to the quantum fluctuations setting of the definition of the (total) covariance in terms of the (total) variances[2]

$$\langle\delta\mathcal{O}_A\delta\mathcal{O}_B\rangle_{\mathrm{tot}}=\frac{1}{2}\left[\langle\delta^2(\mathcal{O}_A+\mathcal{O}_B)\rangle_{\mathrm{tot}}-\langle\delta^2\mathcal{O}_A\rangle_{\mathrm{tot}}-\langle\delta^2\mathcal{O}_B\rangle_{\mathrm{tot}}\right] \tag{2.12}$$

In all this manuscript, we shall always consider two observables $\mathcal{O}_A$ and $\mathcal{O}_B$ related to two subsystems A and B which are disjoint portions of a bigger one, so that $\mathcal{O}_A$ and $\mathcal{O}_B$ commute. In this case, an equivalent definition for the quantum covariance is

$$\begin{aligned}\langle\delta\mathcal{O}_A\delta\mathcal{O}_B\rangle_Q &= \langle\delta\mathcal{O}_A\delta\mathcal{O}_B\rangle_{\mathrm{tot}}-k_BT\chi_{AB} &(2.13)\\ &= \langle\mathcal{O}_A\mathcal{O}_B\rangle-\frac{1}{\beta}\int_0^\beta d\tau\,\langle\mathcal{O}_A(\tau)\mathcal{O}_B(0)\rangle &(2.14)\\ &= \mathrm{Tr}(\rho\mathcal{O}_A\mathcal{O}_B)-\int_0^1 d\alpha\,\mathrm{Tr}(\rho^{1-\alpha}\mathcal{O}_A\rho^\alpha\mathcal{O}_B) &(2.15)\end{aligned}$$

with $\chi_{AB}=\frac{\partial\langle\mathcal{O}_A\rangle}{\partial f_B}=\frac{\partial\langle\mathcal{O}_B\rangle}{\partial f_A}$ the cross-susceptibility — namely the susceptibility of $\langle\mathcal{O}_A\rangle$ with respect to the application of a small perturbation on B in the form of $-f_B\mathcal{O}_B$ added to the Hamiltonian (obviously, the definition is symmetric upon exchanging the role of A and B, see Section 1.7). We have noted $\mathcal{O}(\tau)=e^{\tau\mathcal{H}}\mathcal{O}e^{-\tau\mathcal{H}}$ and $\rho=e^{-\beta\mathcal{H}}/Z$. This equivalent expression, which makes no reference to the

[2] We focus here on the quantum covariance based on the non-additivity of the QV. The definition can be immediately extended to any measure of coherence $\mathcal{C}_f$ discussed in Section 1.5 as

$$\mathcal{C}_f(\mathcal{O}_A+\mathcal{O}_B,\rho)=\mathcal{C}_f(\mathcal{O}_A,\rho)+\mathcal{C}_f(\mathcal{O}_B,\rho)+2\,\mathrm{covar}_Q^f(\mathcal{O}_A,\mathcal{O}_B)\,. \tag{2.10}$$

In fact, if the quantum Fisher information (Section 1.4.2) is the quantity of interest, the associated quantum covariance is known in the literature as the "quantum Fisher information matrix" (QFIM). We are not aware of an interpretation of the QFIM in terms of quantum correlations, but we suggest to do so. In Chapter 8 and 11, we compare the QFIM to the quantum covariance for, respectively, a free fermions system and a quantum Ising chain. The quantum f-covariance is given by

$$\mathrm{covar}_Q^f(\rho,O_A,O_B)=\frac{f(0)}{2}\sum_{ij}\frac{(p_i-p_j)^2}{p_if(p_j/p_i)}\langle i|O_A|j\rangle\langle j|O_B|i\rangle \tag{2.11}$$

where p_i and $|i\rangle$ are the eigenvalues and eigenstates of the total density matrix ρ (in general different from the reduced density matrix ρ_{AB}).

QV, is another instance of the violation of a classical fluctuation-dissipation relation ($\langle \delta\mathcal{O}_A \delta\mathcal{O}_B \rangle_{\rm tot} = k_B T \chi_{AB}$), in the case of quantum systems. The third expression, Eq. (2.15), makes no reference to the Hamiltonian, and extends the definition of the quantum covariance to arbitrary states ρ.

The path-integral framework (see Section 1.7 for details) provides a third, complementary picture

$$\langle \delta\mathcal{O}_A \delta\mathcal{O}_B \rangle_Q = \left\langle \frac{1}{\beta\hbar} \int_0^{\beta\hbar} d\tau \, [\mathcal{O}_A(\tau) - \bar{\mathcal{O}}_A][\mathcal{O}_B(\tau) - \bar{\mathcal{O}}_B] \right\rangle_{\rm paths} \tag{2.16}$$

where $\bar{\mathcal{O}} = (\beta\hbar)^{-1} \int_0^{\beta\hbar} \mathcal{O}(\tau)$ denotes the path centroid, and the average is taken over paths weighted by the action $e^{-S/\hbar}$. The above expression Eq. (2.16) shows that the quantum covariance is nothing else than the correlation function for imaginary-time fluctuations with respect to the path centroid (Malpetti and Roscilde, 2016). As discussed in Section 1.7, quantum fluctuations for a system at thermal equilibrium are the fluctuations in imaginary-time of the path-integral. Similarly, quantum correlations of two observables are the correlations among their respective imaginary-time fluctuations.

The quantum covariance will be studied on model examples of many-body systems, and in the vicinity of (thermal and quantum) phase transitions in Part III. In particular, the quantum covariance may exhibit a behavior in total discrepancy with the total covariance (Malpetti and Roscilde, 2016), especially in the vicinity of thermal phase transitions, where the total covariance may exhibit a singular behavior, while the quantum covariance nearly insensitive to the very presence of a phase transition.

2.3 Quantum covariance within quantum information theory

Considerations on Heisenberg principle and on the physical notion of coherent fluctuations, as quantified by the quantum variance, the quantum Fisher information, or any member $\mathcal{C}_f$ of the family of coherence measures discussed in Section 1.5, naturally lead us to a physically meaningful concept of quantum correlations— quantum correlations between two observables $\mathcal{O}_A$ and $\mathcal{O}_B$, concerning degrees of freedom located in two subsystems A and B, are the correlations which may exist between the quantum uncertainties of $\mathcal{O}_A$ and $\mathcal{O}_B$. *A priori*, this physical concept of quantum correlations need not be related to the information-theoretic concept of quantum correlations discussed in Section 2.1. For instance, can the quantum covariance serve a "measure of quantum correlations", in the sense of quantum information thoery

(Adesso, Bromley, and Cianciaruso, 2016), just as the quantum variance can serve as a "measure of coherence" (Streltsov, Adesso, and Plenio, 2016), as defined in Section 1.5? Leaving this question open to future studies, we simply raise the question

- What is the relationship (if any) between the physical and the information-theoretic concepts of quantum correlations?

This question remains largely open, but several elements are worth mentioning. We have to distinguish between two situations

1) The bipartite case: subsystems A and B exhaust the whole system of interest. A and B may be coherently coupled (*i.e.* the state of A and the state of B may share some well-defined phase relationship), but they are incoherently coupled to their environment.

2) The multipartite case: A and B are immersed in a larger quantum system ABC. In this case, A and B are coherently coupled to each other (either directly of via C), and are also coherently coupled to C. However, they are incoherently coupled to the environment of ABC.

2.3.1 Bipartite case

In the bipartite case, we have the following result[3].

$$\rho_{AB} \text{ is classical-quantum, Eq. (2.5)} \Longrightarrow \forall \mathcal{O}_A, \mathcal{O}_B \ \mathrm{covar}_Q(\mathcal{O}_A, \mathcal{O}_B) = 0 \ . \quad (2.17)$$

In a classical-quantum state (c-q) Eq. (2.5), coherent fluctuations on A and B are completely uncorrelated, and this holds for any pair of observables. This situation is much more satisfactory than for the quantum discord (Section 2.1): in the sense of the quantum discord, almost all measurements on A are "discordant", even for a c-q state, since $J(M_A : B) < I(A : B)$ unless the optimal measurement is picked up. Instead, it is enough to exhibit a single pair of observables $\mathcal{O}_A$, $\mathcal{O}_B$ whose quantum fluctuations are not independent to conclude that the state cannot be c-q. The definition of the quantum covariance does not require any optimization, which in turn makes the quantum discord exceedingly difficult to estimate as soon as A and B become bigger than single qubits. Furthermore, the quantum covariance is defined in terms of physical quantities which can, in principle, be measured in experiments. Finally, we conjecture that the inverted implication of Eq. (2.17) holds; namely, that if the

[3] The proof is given in Appendix A. In particular, even if our emphasis is on the quantum covariance derived from the physically motivated quantum variance, the result holds if the quantum covariance is derived from another coherence measure of Section 1.5.

state is not c-q, there exists at least one pair of observables for which the quantum covariance is nonzero. It is natural to expect that if the quantum covariance is very large, then the state ρ_{AB} must be very far from being c-q. This expectation takes the form of a theorem, namely, the quantum covariance cannot exceed certain threshold value unless the state is entangled. This follows from the following inequality, valid for any member $\mathcal{C}_f$ of the family of coherence measures discussed in Section 1.5. If ρ_{AB} is separable

$$\mathcal{C}_f(\mathcal{O}_A + \mathcal{O}_B) \leq \frac{1}{2}(o_{\max} - o_{\min})^2 \tag{2.18}$$

where the spectrum of $\mathcal{O}_A$ and $\mathcal{O}_B$ is assumed to be bounded between $o_{\min}$ and $o_{\max}$[4]. As $2\text{covar}_Q^f(\mathcal{O}_A, \mathcal{O}_B) \leq \mathcal{C}_f(\mathcal{O}_A) + \mathcal{C}_f(\mathcal{O}_B)$[5], we conclude that, for separable states:

$$\begin{aligned} 4\text{covar}_Q^f(\mathcal{O}_A, \mathcal{O}_B) &\leq \mathcal{C}_f(\mathcal{O}_A) + \mathcal{C}_f(\mathcal{O}_B) + 2\text{covar}_Q^f(\mathcal{O}_A, \mathcal{O}_B) \\ &= \mathcal{C}_f(\mathcal{O}_A + \mathcal{O}_B) \\ &\leq \frac{1}{2}(o_{\max} - o_{\min})^2 \end{aligned} \tag{2.21}$$

where the first inequality holds in full generality, and the second if ρ_{AB} is separable. On the other hand, if for any f the f-quantum covariance exceeds the bound $\frac{1}{8}(o_{\max} - o_{\min})^2$, then the state ρ_{AB} is necessarily entangled.

2.3.2 Multipartite case

In the multipartite case, the fundamental departure of the physical notion of quantum correlations from the information-theoretic one is that the splitting between classical and quantum correlations is not any more a property of the reduced state ρ_{AB} alone, but depends on the full state ρ_{ABC} in which A and B are immersed. For instance, if ρ_{ABC} is a pure state, it is not legitimate, according to the physical notion of quantum correlations, to split the correlations between $\mathcal{O}_A$ and $\mathcal{O}_B$ into a classical and a quantum part: the classical part vanishes identically even if ρ_{AB} is a mixed state. This

[4] This was first proved by Hyllus et al. (2012) and Tóth (2012) for the quantum Fisher information. As the only ingredient is that the latter is convex in ρ and is additive for product states, the proof immediately carries over to any measure of coherence $\mathcal{C}_f$. If $\rho = \sum_i p_i \sigma_i^A \otimes \sigma_i^B$

$$\mathcal{C}_f(\mathcal{O}_A + \mathcal{O}_B, \rho) \leq \sum_i p_i \mathcal{C}_f(\mathcal{O}_A + \mathcal{O}_B, \sigma_i^A \otimes \sigma_i^B) \tag{2.19}$$

$$= \sum_i p_i [\mathcal{C}_f(\mathcal{O}_A, \sigma_i^A) + \mathcal{C}_f(\mathcal{O}_B, \sigma_i^B)] \,. \tag{2.20}$$

Without loss of generality, $\sigma_i^{A(B)}$ can be chosen as pure states, for which C_f is just the variance. If the spectrum of $\mathcal{O}_{A(B)}$ is contained in $[o_{\min}, o_{\max}]$, then the variance is maximal if the state is the equal weight superposition of the eigenvectors corresponding to $o_{\min}$ and $o_{\max}$, for which the variance is $(o_{\max} - o_{\min})^2/4$, hence the result of Eq. (2.18).

[5] This follows from the fact that $\mathcal{C}_f(\mathcal{O}_A - \mathcal{O}_B) = \mathcal{C}_f(\mathcal{O}_A) + \mathcal{C}_f(\mathcal{O}_B) - 2\text{covar}_Q^f(\mathcal{O}_A, \mathcal{O}_B) \geq 0$.

situation has severe consequences when considering, for instance, the correlations between two spins in a many-spin system (Malpetti and Roscilde, 2016). For instance, according to the quantum discord, quantum correlations among two spins may exhibit singularities at *thermal* phase transitions. As thermal phase transitions are driven by incoherent fluctuations, this result appears to be unphysical. On the contrary, according to the physical notion of quantum correlations provided by the quantum covariance, quantum correlations among two spins are non-singular across thermal phase transitions, a much more sensible statement. We elaborate further on the critical behavior of quantum correlations in Chapter III.

Overall, these observations call into question the relevance of the quantum discord in the context of many-body systems. The physically consistent picture provided by the concept of quantum correlations as correlations among coherent fluctuations offers instead a very plausible physical basis for the study of quantum correlations in many-body systems.

Part II

Entanglement thermodynamics

Fools, they do not even know how
much more is the half than the whole.

Hesiod

Summary of Part II. In this part, we develop a thermodynamic understanding of entanglement in many-body ground states. The *entanglement thermodynamics* point of view is elaborated in Chapter 3, where the central *entanglement temperature* hypothesis is proposed. Chapter 4 is then devoted to the study of entanglement in simple free fermion models in $d = 1$ and $d = 2$ from the perspective of the entanglement temperature hypothesis. In the following Chapters 5, 6 and 7 of this part, we focus on the various phases of the paradigmatic Bose-Hubbard model, describing strongly correlated bosons on a lattice. A general semi-classical approach (the *slave-boson* approach) is presented, and applied to the Bose-Hubbard model. Technical considerations about the structure of entanglement within the slave-boson approach are also discussed (Chapter 5). The structure of entanglement in the superfluid phase is studied in Chapter 6, while the Mott-insulator/superfluid phase transition is investigated, from the perspective of entanglement, in Chapter 7, and conclusions are drawn in Section 7.3. This part is largely based on the results published in Frérot and Roscilde (2015) and Frérot and Roscilde (2016a), but contains mainly new developments, particularly for what concerns the entanglement temperature hypothesis.

Chapter 3

Entanglement thermodynamics: general aspects

3.1 Introduction

When an extended, many-body quantum system is in a perfectly well-defined microstate (pure state), entanglement implies that a generic subsystem, instead, cannot be assigned a well-defined microstate. It admits only an ensemble (mixed-state) description, with a finite entropy — the *entanglement entropy*. This is of course very reminiscent of systems in contact with an energy (and/or particle) reservoir at equilibrium, and yet, it bears fundamental differences for ground states of several important many-body Hamiltonians, in that the entanglement entropy is generally sub-extensive (*i.e.* unlike thermodynamic entropy, it is not proportional to the volume of the subsystem).

In the present part of the manuscript, we explore the possibility of capturing (ground-state) entanglement and quantum fluctuations in a subsystem (A) within an effective thermodynamic description, in which the complement of A (B) plays the role of the reservoir. The ensuing "entanglement thermodynamics" is obviously very different from ordinary thermodynamics, due to the sub-extensive nature of some of its thermodynamic fluctuations.

Entanglement entropy is introduced in Section 3.2, and the thermodynamic picture is elaborated in the subsequent sections. We shall argue that the thermodynamic analogy provides a way to predict approximate "equations of states" for quantum-fluctuation properties, namely constituent relationships involving the fluctuations of

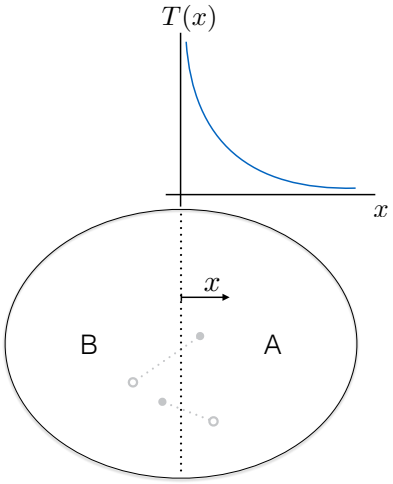

Figure 3.1: Illustration of the local entanglement temperature. The global system A-B lies in its ground state, and the entanglement temperature decays when moving away from the boundary between A and B.

local observables[1], as well as entanglement entropy. We shall do so in a variety of models of high experimental relevance. For a broader overview on the study of entanglement in many-body systems, see Amico et al. (2008), and Eisert, Cramer, and Plenio (2010) and Laflorencie (2016) for reviews more focused on ground-state entanglement properties.

State of the art. Our contribution lies at the convergence point of three lines of research that have been undertaken recently.

1) The first one aims at establishing rigorous relations between entanglement entropy and local fluctuations, typically the number of particles in atomic gases or some component of the magnetization in certain spin models (see Song et al. (2012) for an important contribution in this sense). Up to now, such relationships have been established only for noninteracting fermions in any dimension (Calabrese, Mintchev, and Vicari, 2012) and Luttinger liquid theory describing one-dimensional conductors (Laflorencie and Rachel, 2014), but it does not seem easy to extend these results to, *e.g.* a bosonic superfluid in dimensions $d \geq 2$ (see below).

2) The purpose of the second line of research is to find a microscopic account for the special sub-extensive scaling of entanglement entropy, and in order to do so, the latter should be decomposed as a sum of local contributions. In this perspective, a

[1] By "local", we mean that the observable is restricted to degrees of freedom of a (generally extended) subsystem, not necessarily to a single site in a lattice model, or to a local field in some continuum approach. We use the term "global" for observables related to the entire system.

central concept is the *entanglement contour* ($\mathcal{C}_s$) introduced by Chen and Vidal (2014), such that

$$S_A = \int_A d^d x \, \mathcal{C}_s(x) \tag{3.1}$$

where S_A is the entanglement entropy of subsystem A. In a previous work (Frérot and Roscilde, 2015), we extended the notion of contour to fluctuations, and explored the link between the fluctuation and entanglement contours as a way to obtain a deeper, more microscopic understanding of the link between the entanglement entropy and local quantum fluctuations.

3) Swingle and McGreevy (2015) have proposed an illuminating insight into the origin of area laws of entanglement entropy. They argued that the reduced density matrix of A could be well approximated by

$$\rho_A \approx \exp - \int_A d^d x \, \frac{\mathcal{H}(x)}{T(x)}, \tag{3.2}$$

or equivalently, that the "entanglement Hamiltonian" $-\log \rho_A$ is well approximated by the physical Hamiltonian $\mathcal{H}(x)$ modulated spatially by a *local entanglement temperature* $T(x)$ at position x (this situation is pictorially illustrated on Fig. 3.1). We emphasize that, although the viewpoint of an effective local temperature is very convenient to account for the structure of entanglement in many-body systems, the situation is very different from A being thermalized with a series of local thermostats at temperature $T(x)$. In fact, this situation would bring the subsystem A out of equilibrium, and the ensuing state would not be described by an equilibrium Boltzmann form as in Eq. (3.2). Hence, the rigorous point of view is that A is effectively thermalized at some uniform, fixed temperature, but the energy scales of the constituents of A (masses, interaction energies, etc.) are modulated in space by $T(x)$. Nonetheless, we shall find the idea of local thermostats extremely useful.

Extending the entanglement thermodynamics ideas. In this context, our original contribution is to show that the approach of Swingle and McGreevy (2015) does in fact provide a way to link entanglement entropy with observable fluctuations in a generic manner. The basic idea is to supplement the Ansatz of Eq. (3.2) for the reduced density-matrix by a so-called *local equilibrium approximation*. This amounts to decompose the subsystem A into mesoscopic uncorrelated subregions, each of them being thermalized at the local temperature $T(x)$, and contributing $\approx \langle \delta^2 \mathcal{O} \rangle [T(x)]$ to the variance of $\mathcal{O}$ and $\approx S[T(x)]$ to entanglement entropy, where $\langle \delta^2 \mathcal{O} \rangle (T)$ and $S(T)$ are respectively the (thermal) variance of $\mathcal{O}$ and the (thermal) entropy at temperature T. Furthermore, we propose a procedure, based on the notion of contours, to reconstruct

the local entanglement temperature $T(x)$ from the correlations of $\mathcal{O}$ in the ground state and the knowledge of $\langle \delta^2 \mathcal{O} \rangle(T)$.

Entanglement entropy is introduced in Section 3.2, and the "entanglement temperature" (ET) hypothesis is motivated and developed in Section 3.3.2 on general grounds. The central concept of *contours* is introduced, and constitutive "entanglement equations of states" are proposed (Section 3.3.3). The remaining Chapters 4, 5, 6 and 7 of Part II are devoted to the study of paradigmatic examples of many-body Hamiltonians, namely free fermions, and bosons described by the Bose-Hubbard model.

3.2 Entanglement entropy

3.2.1 Information theory approach

A central goal of the present part is the investigation of the relationship between an information-theoretic notion of quantum correlations (namely entanglement entropy), and the physical notion of quantum correlations introduced in the first chapter (see Section 2.2) for many-body systems at zero temperature. As the global many-body wave-function is a pure state, the situation is conceptually simple: all correlations are quantum correlations, and all forms of quantum correlations are a manifestation of entanglement. Physically, correlations are correlations among the fluctuations of two observables $\mathcal{O}_A$ and $\mathcal{O}_B$, as quantified for instance by the covariance

$$\langle \delta\mathcal{O}_A \delta\mathcal{O}_B \rangle = \langle \mathcal{O}_A \mathcal{O}_B \rangle - \langle \mathcal{O}_A \rangle \langle \mathcal{O}_B \rangle \, . \tag{3.3}$$

In information theory, correlations are quantified by the mutual information.

Von Neumann entropy. Considering a system in a state $\rho = \sum_i p_i |\psi_i\rangle\langle\psi_i|$, where $|\psi_i\rangle$ are orthogonal to each other, and $\sum_i p_i = 1$, the picture is that the system is in an incoherent mixture of pure states $|\psi_i\rangle$ with probabilities p_i. The lack of information on the actual microstate is then quantified by the Shannon entropy of the probability distribution

$$S(\rho) = -\sum_i p_i \ln p_i \, . \tag{3.4}$$

Shannon entropy is interpreted as the average information gained when the system is measured (more specifically: when the actual microstate i is uncovered).

Alternatively, one could consider an arbitrary (complete, non-degenerate) observable $\mathcal{O} = \sum_i o_i |o_i\rangle\langle o_i|$, and study the probability distribution for observing the results o_i if $\mathcal{O}$ is measured, $p_i^{\mathcal{O}} = \langle o_i|\rho|o_i\rangle$. The Shannon entropy of this probability

distribution will be minimal if $\mathcal{O}$ and ρ commute, which leads us to the following definition of von Neumann entropy

$$S(\rho) = \min_{\mathcal{O} \text{ complete}} -\sum_i p_i^{\mathcal{O}} \ln p_i^{\mathcal{O}} \tag{3.5}$$

$$= -\mathrm{Tr}(\rho \ln \rho) \, . \tag{3.6}$$

Von Neumann entropy is the "minimal uncertainty", as quantified by Shannon entropy, among all possible observables. This minimal uncertainty cannot be attributed to the fact that, for instance, ρ is a pure state, but one is measuring an observable for which it is not an eigenstate. Von Neumann entropy is thus considered as the intrinsic entropy of the state, which vanishes if the state is pure, even though a generic observable, because of quantum fluctuations, has a nonzero Shannon entropy.

Mutual information. From now on, unless possible ambiguity, we will use the term "entropy" to refer to von Neumann entropy. An important property of entropy is its sub-additivity: if ρ_{AB} is the state of a combined system formed of two parts A and B, then

$$S(\rho_{AB}) \leq S(\rho_A) + S(\rho_B) \tag{3.7}$$

with $\rho_A = \mathrm{Tr}_B \rho_{AB}$ is the reduced-density matrix of A obtained after tracing over the degrees of freedom of B, and similarly for ρ_B (Lieb and Ruskai, 1973). Sub-additivity translates the fact that observing A and B separately instead of jointly generally yields redundant information — precisely because of the possible existence of correlations between them. The mutual information

$$I(A:B) = S(\rho_A) + S(\rho_B) - S(\rho_{AB}) \geq 0 \tag{3.8}$$

is then defined as the information contained in $A - B$ correlations[2].

Entanglement. Furthermore, for separable states Eq. (2.2) (and thus for classical probability distributions), it always holds that

$$S(\rho_A) \leq S(\rho_{AB}) \quad \text{(separable states)}. \tag{3.9}$$

This property[3] translates the intuitive statement according to which one cannot be more ignorant about the state of a subsystem, than we are about the state of the total

[2] Alternatively, $I(A:B) = \mathcal{D}(\rho_{AB}|\rho_A \otimes \rho_B)$ where the relative entropy $\mathcal{D}(\rho|\sigma) = \mathrm{Tr}[\rho(\ln \rho - \ln \sigma)]$ quantifies our ability to distinguish ρ (the actual density-matrix ρ_{AB}) from σ (the uncorrelated state $\rho_A \otimes \rho_B$) by making measurements on ρ (Vedral, 2002).

[3] Inequality (3.9) is an immediate consequence of the concavity of $S(\rho_{AB}) - S(\rho_A)$ with respect to ρ_{AB}, proved by Lieb and Ruskai (1973). Indeed, if $\rho_{AB} = \sum_i p_i \, \sigma_i^A \otimes \sigma_i^B$ (separable state), concavity implies that $S(\rho_{AB}) - S(\rho_A) \geq \sum_i p_i [S(\sigma_i^A \otimes \sigma_i^B) - S(\sigma_i^A)]$. Then, using that $S(\sigma_i^A \otimes \sigma_i^B) = S(\sigma_i^A) + S(\sigma_i^B)$, and the fact that $S(\sigma_i^B) \geq 0$, we conclude that $S(\rho_{AB}) \geq S(\rho_A)$.

system. However intuitive this statement may seem, it does not hold in general for quantum system, as a manifestation of entanglement (Schrödinger, 1935).

Conversely, the violation of Eq. (3.9) witnesses the presence of entanglement between A and B. This violation has been reported in the experiment of Islam et al. (2015), on systems of a few ultra-cold bosons on a lattice (strictly speaking, they measured the order-2 Rényi entropy, for which Eq. (3.9) is also valid (Horodecki and Horodecki, 1996)).

The situation is especially dramatic if ρ_{AB} is a pure state, for instance the ground-state of some Hamiltonian, for which $S(\rho_{AB}) = 0$. In this case, any nonzero entropy on a subsystem A is a manifestation of entanglement, stemming purely from quantum correlations with its complement B

$$I(A:B) = S(\rho_A) + S(\rho_B) = 2S(\rho_A)\,, \tag{3.10}$$

where the second equality comes from the fact that, for a pure state, $S(\rho_A) = S(\rho_B)$[4]. In this context, $S(\rho_A)$ is called the *entanglement entropy* of A, and quantifies the amount of quantum correlations shared by A and B (in the information-theoretic sense (Horodecki et al., 2009)).

3.2.2 Entanglement entropy *vs.* thermodynamic entropy

The question we are raising is the following:

- Is there any relationship between the information-theoretic entanglement entropy of pure states and the thermodynamic entropy of equilibrium statistical mechanics?

The answer to this very natural question is far from obvious. Usually, our physical understanding of the non-vanishing entropy of a system is the presence of a bath. The common picture is then that the system acts as a bath to itself through quantum fluctuations. On the one hand, it is immediate to see that the existence of quantum correlations in a pure state (namely the existence of at least a pair of observables of subsystems A and B which exhibit a nonzero covariance) implies that entanglement entropy is nonzero[5]. Yet going beyond this simple observation and establish a more

[4] This may be viewed as a consequence of the following inequality $S(\rho_{AB}) \geq |S(\rho_A) - S(\rho_B)|$ (Araki and Lieb, 1970), so that $S(\rho_{AB}) = 0 \Rightarrow S(\rho_A) = S(\rho_B)$, but is physically a consequence of the fact that for a pure state, nonzero entropy of the subsystems is only a correlation effect, in which A and B play a symmetric role. The Schmidt decomposition makes this A-B symmetry manifest, regardless of their respective size.

[5] Indeed, a pure state is separable iff it is a product state, and a product state exhibits no correlation between its subsystems. Hence, if some correlations exist in a pure state, it cannot be separable: it must be entangled.

systematic understanding of the behavior of entanglement entropy in terms of quantum correlations/fluctuations is not obvious. We are thus lead to raise the following questions:

- What quantum correlations/fluctuations imply the existence of entanglement among the subparts of a many-body system?
- Can we construct equations of states for entanglement thermodynamics, in connection with experiments?

Local fluctuations of globally conserved quantities. The first question calls for an identification of the physical mechanism(s) driving the existence of entanglement among the different subsystems, and is the leitmotiv pertaining to all the studies conducted during this thesis. The answer will obviously depend on the physical system under examination, but some general understanding can be gained for a specific class of systems, namely the ones possessing a globally conserved quantity, which nonetheless fluctuates locally — typically the number of particles in an atomic gas, but the conclusions are not restricted to this example (Song et al., 2012).

Considering an extended quantum system in d spatial dimensions, which we divide into two portions A and B, we show that, under global particle-number conservation, local particle number fluctuations *imply* entanglement between A and B. We assume that the Hamiltonian $\mathcal{H}_{AB}$ describing the whole system conserves the total number of particles $N = N_A + N_B$, and consider any one of its eigenstates $|\Psi\rangle$ (for instance the ground state). The Schmidt decomposition of $|\Psi\rangle$ with respect to an AB bipartition reads (Nielsen and Chuang, 2000)

$$|\Psi\rangle = \sum_{\alpha} \lambda_\alpha |\psi_\alpha\rangle_A \otimes |\phi_\alpha\rangle_B \tag{3.11}$$

where the basis $(|\psi_\alpha\rangle_A)$ diagonalizes the reduced density matrix $\rho_A = \mathrm{Tr}_B(\rho_{AB})$, and $\rho_{AB} = |\Psi\rangle\langle\Psi|$. Since N is a good quantum number of $\mathcal{H}_{AB}$, any eigenstate of $\mathcal{H}_{AB}$ is a simultaneous eigenstate of N, whence $[\rho_{AB}, N_A + N_B] = 0$. This in turn implies that

$$\mathrm{Tr}_B[\rho_{AB}, N_A + N_B] = [\mathrm{Tr}_B(\rho_{AB}), N_A] = 0 \,, \tag{3.12}$$

so that the states $|\psi_\alpha\rangle_A = |N_A^{(\alpha)}, \{k^{(\alpha)}\}\rangle_A$ can be chosen to be a basis of eigenstates of N_A (where $\{k^{(\alpha)}\}$ are the other quantum numbers labeling the states)

$$|\Psi\rangle = \sum_{\alpha} \lambda_\alpha \, |N_A^{(\alpha)}, \{k^{(\alpha)}\}\rangle_A \otimes |N - N_A^{(\alpha)}, \{k'^{(\alpha)}\}\rangle_B \,. \tag{3.13}$$

Hence for any eigenstate $|\Psi\rangle$ the existence of a finite uncertainty on the local particle number N_A implies a Schmidt decomposition with at least two terms, and a finite entanglement entropy $S_A = -\mathrm{Tr}\rho_A \ln \rho_A = -\sum_\alpha \lambda_\alpha \ln \lambda_\alpha$. This establishes coherent particle-number exchange as a fundamental mechanism of entanglement. A similar reasoning applies to any model possessing a globally conserved quantity $\mathcal{O}$, and exhibiting fluctuations of the corresponding local quantity $\mathcal{O}_A$. An important example is that of quantum spin systems possessing an axial symmetry: fluctuations of the local magnetization along the symmetry axis imply entanglement. The above analysis is based on two caveats: 1) the system must be in an eigenstate of the Hamiltonian. Otherwise, as discussed in the first chapter (see in particular Section 1.7), fluctuations have both a thermal and a quantum origin, and only the latter are responsible for entanglement. We come back to the study of quantum fluctuations at finite temperature in Part III; and 2) there must be some globally conserved quantity on which to base the analysis. In general, local fluctuations of observables which are not globally conserved have both intrinsic fluctuations, and correlation-induced fluctuations, and only the correlation part is associated to entanglement.

Area law of entanglement entropy in ground states. From now on, we specify our attention to ground states of many-body Hamiltonians. The second question (Can we establish equations of states for entanglement thermodynamics?) is necessarily a subtle point. As a matter of fact, in ground states, entanglement entropy is typically a sub-extensive quantity: in contrast to the thermal entropy, it generically scales as the boundary area of A

$$S(\rho_A) = S_A(l) \sim l^{d-1} \tag{3.14}$$

if l is the linear size of A (Eisert, Cramer, and Plenio, 2010). The intuitive explanation for this so-called area-law scaling of entanglement entropy is that it is a correlation property only. Generally, we may expect that $S(\rho_A) + S(\rho_B)$ differs from $S(\rho_{AB})$ by at most a term proportional to the area of the boundary separating A and B. The general expectation is then that $I(A:B) = S(\rho_A) + S(\rho_B) - S(\rho_{AB})$ obeys an area-law scaling, provided correlations are short-ranged. This is the reason why we expect that in ground-states, where $S(\rho_A) = I(A:B)/2$, entanglement entropy obeys an area-law scaling. This property is generally lost at finite energy density, where the entanglement entropy of a subsystem is equal (up to boundary terms) to the thermodynamic entropy corresponding to that energy.

Note that it often happens that correlations are *not* short-ranged in ground-states of many-body systems. Paradigmatic examples in this sense are offered by the Fermi-liquid metallic phase, and the bosonic superfluid, where density correlations decay as

a power-law with distance. We may expect violations of the area law for entanglement entropy in such critical phases, and it is indeed well-known that the area law is corrected by a multiplicative $\log l$ factor in the Fermi-liquid regime (Calabrese and Cardy, 2004; Gioev and Klich, 2006; Wolf, 2006). Instead, the area law is not violated in critical bosonic systems (at least not in dimension $d \geq 2$), and it is one of the purposes of the following sections to explain why the area law is violated for critical fermions, and not for critical bosons.

3.3 Entanglement thermodynamics

In this section, we introduce the concept of entanglement thermodynamics. We first discuss the possibility to approximate the reduced density-matrix of a subsystem by an equilibrium state of the same subsystem connected to a thermal bath (Section 3.3.1). The limitations of this "global temperature" approach are discussed, and lead us to introduce a refined "local temperature" Ansatz to the reduced density-matrix, partly based on the Bisognano-Wichmann theorem for Lorentz invariant field theories (Section 3.3.2). A local equilibrium hypothesis for this refined Ansatz leads us to the concept of local entanglement thermodynamics, providing us a systematic way to relate entanglement properties with more standard observables (Section 3.3.3).

3.3.1 Global entanglement temperature

Model example: free fermions. To introduce the main concepts of this chapter with a simple example, we focus on a gas of fermions in the Fermi-liquid regime (equivalent to non-interacting fermions as far as the qualitative behavior is concerned), and consider them on a d-dimensional hyper-cubic lattice. They are described by the Hamiltonian

$$\mathcal{H} = \sum_{\boldsymbol{k}} (\epsilon_{\boldsymbol{k}} - \mu) c^\dagger_{\boldsymbol{k}} c_{\boldsymbol{k}} \tag{3.15}$$

where $c_{\boldsymbol{k}} = V^{-1/2} \sum_i e^{-i\boldsymbol{k}\cdot\boldsymbol{r}_i} c_i$ destroys a fermion in the single particle state of momentum $\boldsymbol{k}$. Here, $\boldsymbol{r}_i$ denotes the position of the site i on the lattice, which contains V sites. Periodic boundary conditions are assumed for simplicity, so that $\epsilon_k = -2J \sum_{p=1}^{d} \cos(k_p a)$, with J the hopping amplitude and a the lattice spacing (set to 1 in the following, *i.e.* distances are measured in units of a). The chemical potential μ sets the Fermi energy at $T = 0$. Our concern is to develop a thermodynamic understanding of the entanglement entropy of a large subsystem A, of linear size l, when the total system is in the ground state of $\mathcal{H}$. Since A is not isolated — due to the coherent exchange of particles with its complement B—, the number of particles in A

is not fixed (only the average density is fixed) while the number of particles in the total system is fixed (by μ). The subsystem A is thus described by some grand-canonical ensemble.

Entanglement Hamiltonian. Without loss of generality, the reduced density matrix of A may be written as

$$\rho_A = e^{-\mathcal{H}_A^{\rm ent}} \tag{3.16}$$

for some *entanglement Hamiltonian* $\mathcal{H}_A^{\rm ent}$. Indeed, if ρ is diagonalized as $\sum_i p_i |i\rangle\langle i|$, then $\rho = e^{-\mathcal{H}}$ for $\mathcal{H} = \sum \epsilon_i |i\rangle\langle i|$, with $p_i = e^{-\epsilon_i}$. So at least formally, entanglement entropy of A is just the thermal entropy of some fictitious system of fermions whose dynamics is governed by the entanglement Hamiltonian, and thermalized at some fictitious temperature arbitrarily set to 1 (the global energy scale of the entanglement Hamiltonian is just a matter of convention).

A "global entanglement temperature" Ansatz. On physical grounds, for a sufficiently large A subsystem, one expects the entanglement Hamiltonian to resemble the "physical" Hamiltonian for the fermions hopping on the lattice. After all, ρ_A is expected to be close to the ground state of the physical Hamiltonian $\mathcal{H}_A^{\rm phys}$ (the hopping Hamiltonian for the free fermions, but involving only the matrix elements within the subsystem A), denoted $|{\rm GS}_A\rangle$, and to deviate from it mainly near the boundary of A

$$\rho_A = |{\rm GS}_A\rangle\langle {\rm GS}_A| + \text{ boundary terms }. \tag{3.17}$$

Of course, the boundary terms are essential to describe entanglement between A and B. Then, a possible Ansatz for the entanglement Hamiltonian is to take the physical Hamiltonian of A divided by some very low *entanglement temperature*

$$\mathcal{H}_A^{\rm ent} \approx \frac{\mathcal{H}_A^{\rm phys}}{T_{\rm ent}} \tag{3.18}$$

naively translating the idea that there is entanglement between A and B because the system acts as a heat bath to its subsystems. We call Eq. (3.18) the *global entanglement temperature* hypothesis (GET), as opposed to the *local entanglement temperature* hypothesis (LET) to be introduced in Section 3.3.2. The GET hypothesis cannot systematically reproduce the expectation that the degrees of freedom of A contributing to entanglement with B are located in the vicinity of the boundary between A and B. Indeed, this happens only if the low-lying excitations of $\mathcal{H}_A^{\rm phys}$ are boundary states, as for instance in topological phases. In certain cases, it has rather been suggested that $\mathcal{H}_A^{\rm ent} \approx \mathcal{H}_{\rm boundary}^{\rm phys}$, where $\mathcal{H}_{\rm boundary}^{\rm phys}$ is the physical Hamiltonian of A, restricted to

the degrees of freedom at the boundary between A and B (Li and Haldane, 2008). This would naturally account for the area law, since the entanglement Hamiltonian would describe a system of boundary degrees of freedom in $d-1$ dimensions in thermal equilibrium, exhibiting an entropy proportional to l^{d-1}. We shall see in Section 7.1 that the LET hypothesis partly justifies this point of view when dealing with gapped phases.

A sub-intensive entanglement temperature. According to the GET hypothesis, if the entanglement entropy of an extensive subsystem obeys a sub-extensive scaling law (typically an area law), then the entanglement temperature must be a sub-intensive quantity, namely

$$T_{\rm ent} \xrightarrow{l\to\infty} 0 \; . \tag{3.19}$$

The GET hypothesis can either be tested directly by calculating the entanglement Hamiltonian[6], and comparing it to the physical Hamiltonian, or, more constructively, it can be tested for its consequences.

Consequence of the GET Ansatz for entanglement thermodynamics. Direct consequences of the GET hypothesis are that 1) the (quantum) variance of any local observable $\mathcal{O}_A$ in the ground-state of AB equals the (quantum[7] and thermal) variance that $\mathcal{O}_A$ would take if A were thermalized, in the absence of its complement B, at temperature $T_{\rm ent}$, in the grand-canonical ensemble; and 2) (entanglement) entropy of A in the ground-state of AB equals the (thermal) entropy of $\mathcal{H}_A^{\rm physical}$ at temperature $T_{\rm ent}$. In the case of a gas, one thus predicts

$$S_A = l^d s(T_{\rm ent}) \tag{3.20}$$

$$\langle \delta^2 N_A \rangle = l^d k_B T_{\rm ent} \frac{\partial \langle n \rangle}{\partial \mu} \tag{3.21}$$

where l is the linear size of subsystem A, $s(T)$ is the entropy per unit volume at temperature T, and we have used the fluctuation-response relation between the particle-number variance $\langle \delta^2 N \rangle$ and the (isothermal) compressibility $\partial \langle n \rangle / \partial \mu$. Under the GET hypothesis, one could then measure $\langle \delta^2 N_A \rangle$, and deduce the entanglement temperature using Eq. (3.21). If the thermodynamic function $s(T)$ is known, entanglement entropy

[6] This is in general a very difficult task, even for the free fermion Hamiltonian, in part because one needs to know precisely *all* the entanglement energies. They are extracted as $-\log(p_i)$ with p_i the eigenvalues of the reduced density matrix, and many p_i's lie exponentially close to 0 when l increases, so that the required accuracy on the p_i's grows exponentially with l. A few exact results exist, which form the basis of the LET hypothesis discussed in Section 3.3.2.

[7] A quantum contribution to the variance of $\mathcal{O}_A$ is expected also at finite temperature if $\mathcal{O}_A$ is not a conserved quantity, see Chapter 1.

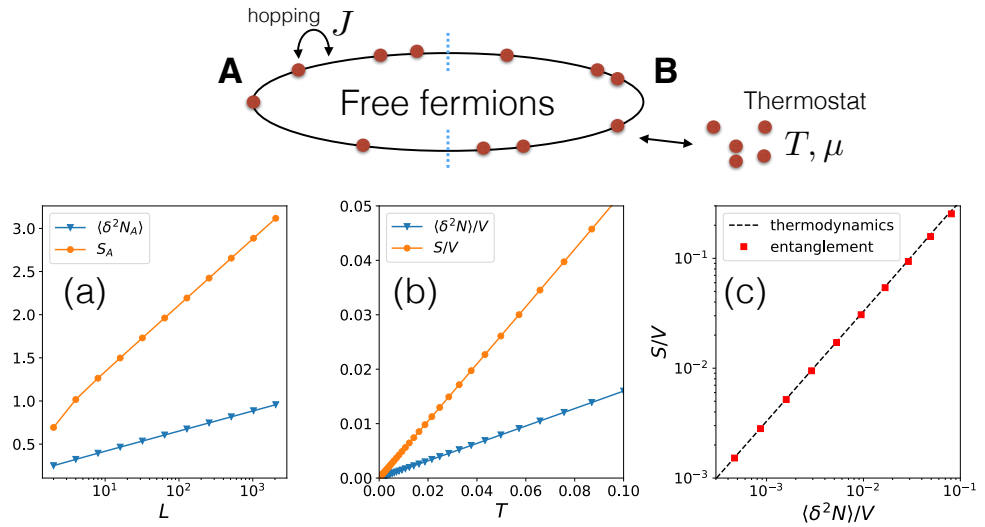

Figure 3.2: GET hypothesis for the free fermions. (a) Entanglement entropy S_A and variance of the number of fermions $\langle\delta^2 N_A\rangle$ at $T = 0$ and $\mu = 0$ (half-filling). A is half of a line of $V = 2l$ sites with periodic boundary conditions (PBC), for $l = 4, 8, 16 \ldots 2048$. Note the logarithmic scale on the horizontal axis. (b) Thermal entropy S and thermal variance of the number of particles $\langle\delta^2 N\rangle$ (both per site) as a function of temperature, for $\mu = 0$. The system is a line of 2×10^4 sites with PBC. (c) Squares: entanglement entropy as a function of the variance of the number of fermions in subsystem A (both per site), extracted from panel (a). Dashed-line: thermal entropy as a function of the thermal variance in the grand-canonical ensemble, extracted from panel (b), showing a slope of $\pi^2/3$ (see text).

can then be deduced through Eq. (3.20). Alternatively, one can avoid the detour through the entanglement temperature if the thermodynamic relation $S(\langle\delta^2 N\rangle)$ is known in the grand-canonical ensemble: the entanglement entropy is just estimated as $S_A = S(\langle\delta^2 N_A\rangle)$.

Test of the GET thermodynamic relations for gapless free fermions. As illustrated on Fig. 3.2, in the case of gapless free fermions with a $d-1$ dimensional Fermi surface, the GET hypothesis enables one to predict quantitatively the value of the entanglement entropy of subsystem A, based on the knowledge of the thermodynamic relation $S(\langle\delta^2 N\rangle)$, and on the measurement of the particle number variance in A. This remarkable result is well known in the literature. It can be proven (to leading order in the scaling behavior) for free fermions in any dimension (Calabrese, Mintchev, and Vicari, 2012) and carries over to interacting fermions and bosons in one dimension in the Luttinger-liquid regime (Laflorencie and Rachel, 2014). In all these situations, entanglement entropy and the variance of the number of particles in a subsystem of

linear size l scale as

$$S_A, \langle \delta^2 N_A \rangle \sim l^{d-1} \log l \, . \tag{3.22}$$

For the above-cited systems, since at low temperature in the grand-canonical ensemble, both quantities are extensive and linear in T, one deduces that the entanglement temperature must scale as

$$T_{\rm ent} \sim \frac{\log l}{l} \tag{3.23}$$

which is sub-intensive, in agreement with the general arguments given so far. For free fermions (in the gapless metallic phase), the relationship between $\langle \delta^2 N_A \rangle$ and S_A is remarkably simple (Calabrese, Mintchev, and Vicari, 2012)

$$S_A = \frac{\pi^2}{3} \langle \delta^2 N_A \rangle + O(1) \tag{3.24}$$

where $O(1)$ denotes subdominant constant terms. It is not difficult to see that this relationship is exactly the same in the grand-canonical ensemble at low temperature (Huang, 1987; Diu, Lederer, and Roulet, 1996)

$$S/V = \frac{\pi^2}{3} \rho(\mu) T + O(T^3) \tag{3.25}$$

$$\langle \delta^2 N \rangle / V = \rho(\mu) T + O(T^3) \tag{3.26}$$

where $\rho(\mu)$ is the density of states at Fermi energy[8]. These results give encouraging support to the thermodynamic understanding of ground-state entanglement entropy, and to the physical picture behind the Ansatz of Eq. (3.18) for the entanglement Hamiltonian.

Inconsistency of the GET Ansatz for superfluid bosons. Unfortunately, the same hypothesis is inconsistent when applied to bosons in a superfluid regime in dimension $d \geq 2$, as a simple scaling comparison shows. As a matter of fact, at thermal equilibrium, entropy and fluctuations behave as

$$S \sim V T^d \tag{3.28}$$

$$\langle \delta^2 N \rangle \sim V T \, . \tag{3.29}$$

Here, we assume that the superfluid is in the Bogoliubov regime (Pitaevskii and Stringari, 2003), where the entropy is carried by the linearly dispersing phonons,

[8] In particular, in $d = 1$, entanglement entropy in the ground state grows as $(\ln l)/3$ for a line of length l in an infinite chain (Calabrese and Cardy, 2004). As in $d = 1$, $\rho(\mu) = [2J\pi \sin(\pi n)]^{-1}$ with n the density, the entanglement temperature is

$$T_{\rm ent} = \frac{2J \sin(\pi n)}{\pi} \frac{\log l}{l} \, . \tag{3.27}$$

which are noninteracting bosonic quasiparticles, whence the result $S \sim T^d$ (Huang, 1987; Diu, Lederer, and Roulet, 1996) (a proof is given in the footnote 5 of Chap. 6).

On the other hand, in the ground-state it is found that entanglement entropy and local fluctuations of the number of bosons scale as[9]

$$S_A \sim l^{d-1} \tag{3.30}$$

$$\langle \delta^2 N_A \rangle \sim l^{d-1} \log l \, . \tag{3.31}$$

Hence, the thermal analogy for S suggests that $T_{\rm ent}^d \sim 1/l$ and $T_{\rm ent} \sim (\log l)/l$ for $\langle \delta^2 N \rangle$, two scalings manifestly incompatible One thus has to face the following questions

- Why is the GET hypothesis working for fermions, and not for bosons?
- More specifically, why is the area law violated by a multiplicative $\log l$ for fermions, and not for bosons?

This latter question is especially relevant in view of the fact that for fermions and bosons alike, the local variance of the number of particles obeys the same scaling $\langle \delta^2 N_A \rangle \sim l^{d-1} \log l$. We will see in Section 3.3.2 how the LET hypothesis answers these questions, but at this point, a closer look to the structure of the entanglement Hamiltonian is in order. The GET hypothesis, Eq. (3.18), makes in particular a very simple prediction for the spectrum of $\mathcal{H}_{\rm ent}$: it should be simply the spectrum of $\mathcal{H}_A^{\rm phys}$ rescaled by the entanglement temperature.

Entanglement spectrum *vs.* physical spectrum for free fermions. If the physical Hamiltonian describes free fermions, the entanglement Hamiltonian is also a free-fermion Hamiltonian

$$\mathcal{H}_{\rm ent} = \sum_\alpha E_{\rm ent}^{(\alpha)} c_\alpha^\dagger c_\alpha \tag{3.32}$$

where c_α destroys a fermion in the entanglement eigenmode α (technical details on the entanglement properties of free-fermion Hamiltonian will be given in see Section 4.1). The (single particle) entanglement spectrum $E_{\rm ent}^{(\alpha)}$ is deduced from the eigenvalues n_α of the correlation matrix $C_{ij} = \langle c_i^\dagger c_j \rangle$ for $i, j \in A$ as

$$n_\alpha = \frac{1}{e^{E_{\rm ent}^{(\alpha)}} + 1} \, . \tag{3.33}$$

[9] For the scaling of the particle number variance, see Astrakharchik, Combescot, and Pitaevskii (2007) and Klawunn et al. (2011). The area law scaling for entanglement entropy has been observed in spin and bosonic models with a spontaneously broken continuous symmetry ($U(1)$ or $SU(2)$), both with quantum Monte Carlo calculations (Hastings et al., 2010; Kallin et al., 2011; Humeniuk and Roscilde, 2012; Herdman et al., 2016) and semi-classical methods (Song et al., 2011; Luitz et al., 2015; Frérot and Roscilde, 2015). See Laflorencie (2016) for a review.

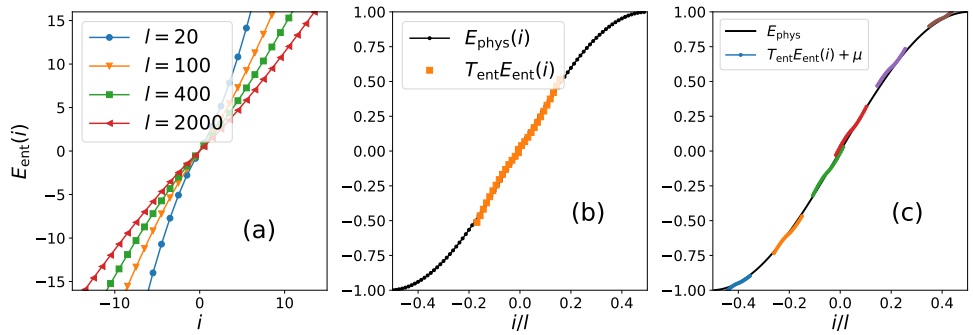

Figure 3.3: Entanglement spectrum vs. physical spectrum for 1d free fermions. (a) Single particle entanglement spectrum. A is a line of l sites in a chain of $50l$ sites with PBC at half filling. i labels the entanglement eigenstates, shifted to be centered at $i = 0$. (b) Square symbols: entanglement spectrum rescaled by $T_{\rm ent} = (2J/\pi)(\ln l/l)$ (only the lowest levels are shown); dots: physical spectrum (in units of $2J$). A same as in (a) with $l = 80$. (c) Same as in (b) for $\mu = -0.95, -0.6, -0.15, 0.15, 0.6, 0.95$, and $T_{\rm ent} = (\ln l)/[l\pi^2\rho(\mu)]$ with $\rho(\mu) = [2J\pi\sin(\pi n)]^{-1}$, n being the density. In all panels, we set $J = 1/2$

n_α, the mean occupation of the entanglement eigenmode α, is just a Fermi distribution for the entanglement energies[10]. The entanglement spectrum for $1d$ free fermions is plotted on Fig. 3.3(a). The GET hypothesis predicts that

$$E_{\rm ent}^{(\alpha)} = \frac{E_{\rm phys}^{(\alpha)} - \mu}{T_{\rm ent}} \,. \tag{3.34}$$

As shown on Fig. 3.3(b) and (c), this relation is well verified for the low-lying entanglement energies, near $E_{\rm ent} = 0$. In the thermodynamic limit, $T_{\rm ent} \to 0$ and the relevant entanglement energies are given by Eq. (3.34) with an increasingly good accuracy, as shown by Peschel and Eisler (2009). As $\langle \delta^2 N_A \rangle$ and S_A depend only on the density of states close to the Fermi energy $E_{\rm ent} = 0$, this justifies the thermodynamic relation between them illustrated on Fig. 3.2(c). However, it is already apparent on Fig. 3.3(b,c) that the GET prediction of Eq. (3.34) only applies to the part of the entanglement spectrum lying close to the Fermi level, while deviations are apparent further away from the Fermi level.

Necessity of a refined Ansatz for the entanglement Hamiltonian. Unfortunately, a comparison between the entanglement spectrum (ES) and the physical spectrum (PS) beyond the $1d$ free fermions case shows even stronger limitations of the GET

[10] In particular, the variance of the local particle number is $\langle \delta^2 N_A \rangle = \sum_\alpha n_\alpha(1 - n_\alpha)$ and the entanglement entropy is $S_A = -\sum_\alpha [n_\alpha \ln n_\alpha + (1 - n_\alpha)\ln(1 - n_\alpha)]$.

hypothesis. For instance, as it will be discussed shortly, for a $2d$ bosonic superfluid, the dispersion relation of the entanglement spectrum shows a *logarithmic* dispersion relation $E_{\rm ent}(k_\parallel) \sim 1/|\ln k_\parallel|$ ($k_\parallel$ denotes the wavevector parallel to the cut between A and B), while the physical spectrum is linearly dispersing, $E(k) \sim k$. A global rescaling of the spectrum cannot turn a linear dispersion into a logarithmic one.

Furthermore, the GET Ansatz suffers from another fundamental limitation. Indeed, the system of interest is translationally invariant, so that correlations depends only on the relative distance, namely

$$\langle \mathcal{O}_i \mathcal{O}_j \rangle = \langle \mathcal{O}_0, \mathcal{O}_{|i-j|} \rangle \, . \tag{3.35}$$

However, this property is lost in the GET Ansatz because of the introduction of sharp boundaries.

This calls for a more refined Ansatz for the entanglement Hamiltonian, provided by the *local entanglement temperature* (LET) hypothesis.

3.3.2 The local entanglement temperature hypothesis

The idea of the LET Ansatz is to restore the translational invariance of the system of interest by imposing soft boundary conditions on the entanglement Hamiltonian.

An Ansatz for the entanglement Hamiltonian. According to the LET hypothesis (Swingle and McGreevy, 2015), a quantitative understanding of the entanglement features (and in particular, as we shall see, of the relationship between entanglement and quantum correlations of observable quantities) in the ground-state of many-body lattice Hamiltonians is provided by the following Ansatz

$$\begin{aligned} \rho_A &\approx (1/Z) e^{-\mathcal{H}_A^{\rm ent}} \\ \mathcal{H}_A^{\rm ent} &= \sum_{i \in A \text{ (sites)}} \frac{\mathcal{H}_i^{\rm phys}}{T_{\rm ent}(i)} + \sum_{b \in A \text{ (bonds)}} \frac{\mathcal{H}_b^{\rm phys}}{T_{\rm ent}(b)} \, . \end{aligned} \tag{3.36}$$

Here, $\mathcal{H}_i^{\rm phys}$ is the physical Hamiltonian acting on the site i, containing the local potentials and the local interaction terms, for instance $U n_i(n_i-1)/2 - V_i n_i$ for a Hubbard Hamiltonian, with U the onsite interaction strength and V_i a local potential. Likewise, $\mathcal{H}_b^{\rm phys}$ denotes a "bond" term in the Hamiltonian, for instance a hopping term $J c_i^\dagger c_j + \text{h.c.}$ or an interaction term $V_{ij} n_i n_j$ if b is linking sites i and j. $T_{\rm ent}$ is a local entanglement temperature, typically going from higher values near the boundary of A (so that the fluctuations of the boundary degrees of freedom are enhanced), to smaller values in the bulk of A (so that the corresponding degrees of freedom

are increasingly frozen out), in accordance with the picture by which the quantum fluctuations contributing to entanglement between A and B are located in the vicinity of the $A - B$ boundary.

According to the LET hypothesis expressed in Eq. (3.36), the entanglement Hamiltonian takes a particularly suggestive form: it is simply the physical Hamiltonian modulated in space by some local entanglement temperature. Again, the LET hypothesis should not be taken as an exact statement — in fact, exact calculations on lattice models show that it cannot hold as an equality, since the entanglement Hamiltonian typically involves longer-ranged hopping than the physical Hamiltonian — but rather as a useful heuristic viewpoint which should be tested for its predictions. Nonetheless, it is noteworthy that the LET hypothesis takes the form of a theorem for certain field theories — namely Lorentz-invariant field theories — which are relevant descriptions of the low-energy properties of important lattice many-body systems, suggesting in particular that the entanglement temperature should decay as $1/x$, x being the distance to the $A - B$ boundary.

The Bisognano-Wichmann theorem. The study of the entanglement content of the vacuum of quantum field theories — the continuum counterpart to the study of entanglement in ground states of many-body quantum Hamiltonians on a lattice — was partly stimulated by Hawking prediction of black holes evaporation (Hawking, 1974), a consequence of the pumping of gravitational energy to create particles out of the vacuum of quantum fields, and in particular, out of the electromagnetic vacuum (Unruh, 1976). A related result is the prediction by Bekenstein (1973) that a black hole has an entropy proportional to its area $\mathcal{A}$ (in units of the squared Planck length, $l_P = G\hbar^2/c^3$, the Bekenstein-Hawking black-hole entropy is $S_{\rm BH} = \mathcal{A}/4l_P^2$). These results can be viewed as special consequences of the entanglement content of the vacuum of quantum field theories (Susskind and Lindesay, 2005). In this context, a very important result, directly motivating the Ansatz of Eq. (3.36) (Swingle and McGreevy, 2015), was obtained by Bisognano and Wichmann (1976), who showed that the reduced-density matrix for a half-infinite space A ($t = 0$, $x_1 > 0$ and $x_i \in \mathbb{R}$ for $i = 2, \ldots, d$) obtained after tracing out the degrees of freedom in the complementary half-infinite space ($t = 0$, $x_1 < 0$ and $x_i \in \mathbb{R}$ for $i = 2, \ldots, d$), in the ground-state of a Lorentz-invariant quantum field theory is

$$\rho_A = \frac{1}{Z} \exp\left[- \int_{x \in A, x_1 > a} d^d x \, \frac{2\pi x_1}{\hbar c} \mathcal{H}(x) \right] \tag{3.37}$$

where $\mathcal{H}(x)$ is the Hamiltonian density, c the speed of light, and a some short-distance ultraviolet cutoff, set by the underlying lattice spacing for instance (Susskind and

Lindesay, 2005). Z is such that $\mathrm{Tr}\rho_A = 1$. Eq. (3.37) shows that the entanglement Hamiltonian for a half-space in the vacuum of a Lorentz-invariant quantum field theory is exactly the field-theory Hamiltonian modulated in space by a local entanglement temperature

$$T_{\mathrm{ent}} = \frac{\hbar c}{2\pi x_1} \tag{3.38}$$

where x_1 is the distance to the boundary between A and B. The Bisognano-Wichmann theorem is extremely relevant to the study of entanglement in ground-states of condensed matter systems, as the Lorentz invariance of the field theory it relies upon is often a good approximation to the low-energy physics of the model of interest. In physical systems, one encounters both situations where the Lorentz invariance is a low-energy property of the Hamiltonian (Bose-Hubbard model), and situations where it is not (free fermions in $d \geq 2$, spins with power-law decaying interactions with a sufficiently small decay exponent), and we will see that even in the absence of Lorentz invariance, the local temperature hypothesis may work very well (though with a decay with the distance to the boundary possibly different from $T_{\mathrm{ent}} \sim 1/x_1$).

The local entanglement temperature on the lattice. Coming back to our subject of interest – the entanglement Hamiltonian for a lattice many-body systems – the Bisognano-Wichmann theorem suggests that, under Lorentz invariance of the effective field-theory description, the entanglement temperature is $c/2\pi x_1$, with x_1 the distance to the $A-B$ cut. We choose units where $\hbar = 1$, and measure the distance in units of the lattice spacing a. To be precise, in the following, we shall focus on square lattices (or cubic in $d = 3$) with periodic boundary conditions. To begin with, let us imagine that the total system is defined on a cylinder $L_x \times L^{d-1}$ periodic along $x_2, \ldots x_d$, with $L_x \gg 1$. If we define A as containing all sites such that $x_1 \geq 1$, and B with all sites such that $x_1 \leq 0$, the $A-B$ cut is between $x_1 = 0$ and $x_1 = 1$, centered on $x_1 = 1/2$. A site at position $(x_1, \ldots, x_d)$ is thus at a distance $x_1 - 1/2$ from the boundary, and similarly for a link parallel to the $A-B$ boundary. On the other hand, a link between $(x_1, x_2, \ldots, x_d)$ and $(x_1+1, x_2, \ldots, x_d)$ is at distance x_1 from the boundary. Finally, if the system is periodic also along x_1, so that A is a cylinder of dimensions $l \times L^{d-1}$ cut out of a torus of dimensions $L_x \times L^{d-1}$, having now two boundaries with B, we conjecture that the local temperature is the sum of the temperatures induced by each of the boundaries[11]

$$T_{\mathrm{site}}(x) = \frac{c}{2\pi}\left[\frac{1}{x_1 - 1/2} + \frac{1}{l - x_1 + 1/2}\right] \tag{3.39}$$

[11] This conjecture is motivated by the fact that it is an exact result in the context of $1d$ conformal field theory (Wong et al., 2013).

and similarly

$$\frac{2}{T_{\rm link}(x,x')} = \frac{1}{T_{\rm site}(x)} + \frac{1}{T_{\rm site}(x')} \tag{3.40}$$

In any case, we shall propose a way to extract the local entanglement temperature from correlation functions in the ground-state.

3.3.3 From local temperature to local thermodynamics

Physical meaning of the LET Ansatz. At first sight, such an Ansatz like Eq. (3.36) seems "obviously wrong", since the reduced density matrix must reproduce all the properties of a homogeneous system : after all, singling out a subsystem is an arbitrary operation. In particular, the average value of any local observable $\langle \mathcal{O}_i \rangle$ related to the degrees of freedom on a given site i, is independent of i, and any correlation function $\langle \delta\mathcal{O}_i \delta\mathcal{O}_j \rangle$ depends only on the relative position of i and j. But how could a Hamiltonian modulated in space give rise to homogeneous properties? The idea is that one may reproduce the statistical properties of a *homogeneous system without boundaries at zero temperature* with those of an *inhomogeneous system with boundaries at finite temperature*. Roughly speaking, as the fluctuations in a system with boundaries are typically suppressed near the boundaries[12], a higher "local" temperature is needed in order to compensate for this effect.

To avoid confusion, it should be stressed that Eq. (3.36) corresponds to an equilibrium state, and does not describe a physical situation where the region A is in contact with a series of thermostats at temperatures $T(x)$. Indeed, this situation would produce stationary currents circulating throughout A, and lead to a non-equilibrium steady state which could not be described by a Boltzmann form. The correct image is that of a system whose energy scales (mass, interaction strength, external potentials) are modulated by $T(x)$, and in contact with a unique thermostat at a temperature arbitrarily set to 1, so what really happens is that the (softer) degrees of freedom near the edges are more subject to thermal fluctuations, while the (harder) degrees of freedom in the bulk of A are completely frozen to their ground state. This happens in such a fine-tuned way that, at temperature 1, all observables are translationally invariant. In particular, the *ground state* (or any eigenstate) of the Ansatz Hamiltonian Eq. (3.36) have no reason to be, and in general are *not*, translationally invariant. We shall illustrate this point on explicit examples in the remainder of this section (see, for instance, Fig. 4.3).

[12] A prominent counter-example is represented by gapped topological phases, where the low energy dynamics takes place at the boundaries.

Local equilibrium approximation. In spite of these precautions, we will see that it is extremely convenient to regard $T(x)$ as the local temperature of the subsystem A. Indeed, $T(x)$ does play the pivot role of a *local entanglement temperature*, relating the contribution of a site at x to entanglement entropy, to its contribution to quantum fluctuations. The latter assumption is physically motivated by a *local equilibrium approximation* (LEA) on the reduced density matrix Eq. (3.36). The LEA can be formulated as follows

$$\langle \mathcal{O}_i \rangle (\rho = e^{-\beta(\sum_i \mathcal{H}_i)}) \approx \langle \mathcal{O} \rangle (\rho = e^{-\beta(\mathcal{H} \equiv \mathcal{H}_i)}) \tag{3.41}$$

and expresses the fact that, at equilibrium, the average value of a local observable $\mathcal{O}_i$, in an inhomogeneous system having a position-dependent Hamiltonian $\mathcal{H}_i$, is given by the average value that the same observable $\mathcal{O}$ would have in a homogeneous system, where the Hamiltonian would be uniformly equal to $\mathcal{H}_i$, thermalized at the same temperature $T = 1/\beta$. The LEA is widely used in the context of cold atoms, where it allows for the experimental reconstruction of equations of state. Even though the LEA was originally formulated for the density (hence the traditional terminology of *local density approximation* – LDA), it is straightforwardly generalized to any local observable.

Area laws and their violation from the LEA. In the context of entanglement, the LEA can be used in a straightforward manner (Susskind and Lindesay, 2005; Wong et al., 2013; Swingle, 2013; Swingle and McGreevy, 2015) to give an estimate for entanglement entropy

$$S \approx \sum_{i \in A} s\left(T_i\right) \tag{3.42}$$

where $s(T)$ is the thermal entropy per unit of volume, and T_i the local entanglement temperature. Remarkably, for conformally invariant models, the formula Eq. (3.42) provides the leading term of the entanglement entropy with the correct prefactor (Swingle, 2013; Wong et al., 2013). More generally, if one accepts that the local entanglement temperature decays as $T(x) \sim 1/x$ with x the distance from the boundary between A and B, as proven for Lorentz-invariant quantum field theories (Bisognano and Wichmann, 1976), one easily understands the origin of the area law, and its possible logarithmic violation.

- For gapped phases, the area law is straightforward to derive : as $s[T(x)] \sim e^{-\Delta/T(x)} \sim e^{-x\Delta}$, the terms contributing to the sum in Eq. (3.42) are exponentially localized in a layer of width $1/\Delta$ near the boundary, hence the area law.

- For gapless free fermions, regardless of the number d of dimensions of space, $s[T(x)] \sim T(x) \sim 1/x$, hence the logarithmic violation of the area law $S \sim l^{d-1} \log l$.

- For a system of linearly dispersing bosons, $s[T(x)] \sim T(x)^d \sim 1/x^d$, so that the area law is strict for $d \geq 2$, and logarithmically violated in $d = 1$.

The first figure of merit of the local entanglement thermodynamics approach is hence to give a coherent picture for the area laws and their possible violation encountered in a variety of situations (Swingle and McGreevy, 2015). But the second, and perhaps more important one, appears when one follows the same line of reasoning to account for the scaling of fluctuations.

For concreteness, consider the number of particles in region A : $N_A = \sum_{i \in A} n_i$. The variance of N_A can be decomposed as $\langle N_A^2 \rangle - \langle N_A \rangle^2 = \sum_{i \in A} [\langle n_i N_A \rangle - \langle n_i \rangle \langle N_A \rangle] = \sum_{i \in A} \langle \delta n_i \delta N_A \rangle$, where $\delta \mathcal{O} = \mathcal{O} - \langle \mathcal{O} \rangle$. The LEA is then applied to $\langle \delta n_i \delta N_A \rangle$ — that we call later the "contour of density fluctuations" —, by assuming that the correlation between the site i and the region A approximates the correlation we would find in a homogeneous system with temperature T_i. Explicitly:

$$\langle \delta n_i \delta N_A \rangle \approx \frac{1}{V} \langle \delta^2 N \rangle (T_i) \tag{3.43}$$

where the r.h.s represents the variance of the number of particles per unit volume of a large system of volume V, at a uniform temperature T_i. Knowing the scaling of the thermal fluctuations with the temperature in a homogeneous system, one is then able to predict the scaling of the quantum fluctuations with the linear size l of a subsystem at zero temperature from the knowledge of the local entanglement temperature. For instance, the scaling of $\langle \delta^2 N \rangle$ with T is the same for bosons and fermions : they are exponentially activated for gapped phases, and are proportional to T in Bose superfluids and Fermi liquid phases. This can be shown through the thermodynamic identity $\langle \delta^2 N \rangle / V = T \partial n / \partial \mu$, where the susceptibility $\partial n / \partial \mu$ of the density to a change of chemical potential behaves as $e^{-\Delta/T}$ in a gapped, incompressible phase, and tends to a finite value at zero temperature in a gapless Fermi liquid and a superfluid alike. This implies, through the hypothesis $T(x) \sim 1/x$ and the LEA (3.43) on the reduced density matrix (3.36), that the area law for particle number fluctuations is strict for gapped phases, and logarithmically violated for gapless phases, which matches the observations.

LEA and "contours". But more importantly, we are now able to give an indirect, yet experimentally meaningful way to estimate entanglement entropy. Indeed, under

the assumptions that 1) the thermodynamic equation of state relating entropy and density fluctuations $s = s(\langle \delta^2 N \rangle / V)$ is known; and 2) one can calculate/measure the density-density correlations; then one can estimate the entanglement entropy as

$$S \approx \sum_{i \in A} s(\mathcal{C}_N(i)) \tag{3.44}$$

where $\mathcal{C}_N(i) = \langle \delta n_i \delta N_A \rangle$ defines the *fluctuation contour* (Frérot and Roscilde, 2015). But the *entanglement contour* $\mathcal{C}_s$ (that will be introduced in Section 4.1) has been precisely defined by Chen and Vidal (2014) to achieve this spatial decomposition of entanglement entropy : $S = \sum_{i \in A} \mathcal{C}_s(i)$, so that the central conjecture (3.44) can be formulated in a stronger form :

$$\begin{aligned} S(T) &\overset{f}{\longleftrightarrow} \langle \delta^2 \mathcal{O} \rangle \\ \mathcal{C}_s(i) &\overset{f}{\longleftrightarrow} \mathcal{C}_{\mathcal{O}}(i) \end{aligned} \tag{3.45}$$

where the f above the arrows means that the contours are linked by the same functional relation than their thermal counterparts. We conjecture, and will show on several explicit examples in the following sections, that the correspondence formulated in Eq. (3.45) holds, at least in an approximate manner, for several local observable $\mathcal{O}$.

Discussion. We have now introduced all the basic tools needed for the microscopic understanding of the entanglement structure in many-body ground states, based on usual thermodynamic concepts. The following Chapters 4, 5, 6 and 7 will be devoted to the explicit study of model systems, against which to test the general considerations and approximations discussed so far. At this point, we wish to emphasize that while the LET Ansatz for the entanglement Hamiltonian, Eq. (3.36) combined with the LEA Eq. (3.41) *imply* the thermodynamic relations between the contours, Eq. (3.45), the converse is not true. Namely, we shall encounter situations where the correspondence between the contours, Eq. (3.45), holds, while the LET Ansatz of Eq. (3.36) is not at all a good approximation to the entanglement Hamiltonian (free fermions in $d \geq 2$)[13].

[13] Similarly, while the Bisognano-Wichmann theorem for quantum field theories, Eq. (3.37), relies on the hypothesis of Lorentz invariance, situations are encountered where the Lorentz invariance is not a good approximation at low energy, but where the entanglement Hamiltonian is well approximated by the LET Ansatz of Eq. (3.36), though with a decay of the local temperature with the distance x_1 to the boundary different from $1/x_1$. This situation is realized by certain spin models with power-law decaying interactions, although it shall not be elaborated further in this manuscript.

Chapter 4

Entanglement thermodynamics: Free fermions

Introduction. In this chapter, the spatial structure of entanglement in a gas of free fermions (FF) at zero temperature is investigated. Section 4.1 is devoted to general considerations, valid for arbitrary FF models, and definitions of the entanglement and fluctuations contour are given. Section 4.2 studies the simplest case of $1d$ gapless FF, for which we exhibit a very accurate Ansatz for the entanglement Hamiltonian in the form of the lattice version of the Bisognano-Wichmann theorem, Eq. (3.37), valid for field theories in the continuum. We also show that the local equilibrium point of view for the spatial structure of entanglement, discussed on general grounds in Section 3.3.3, is extremely meaningful in this case. Section 4.3 is then devoted to $2d$ FF, for which the naive LET Ansatz of Eq. (3.36) is incorrect. We trace this inefficiency back to the absence of Lorentz invariance in $d = 2$, and show that, nevertheless, a local equilibrium hypothesis is still meaningful at the level of the contours. Conclusions and outlooks on FF models are finally proposed in Section 4.4.

4.1 Generalities

In this section, we provide technical details necessary to study the structure of entanglement in FF models (as proposed originally by Peschel and Eisler (2009)), and introduce the concept of *contours* for entanglement and for the variance of an observable.

4.1.1 Entanglement Hamiltonian

We consider an arbitrary FF Hamiltonian

$$\mathcal{H} = \sum_{i,j} c_i^\dagger h_{ij} c_j \tag{4.1}$$

where i, j denote the sites of a lattice of arbitrary geometry and arbitrary dimension. $c_i^{(\dagger)}$ are fermionic operators satisfying the anti-commutation relations

$$\left\{ \begin{array}{rcl} \{c_i, c_j^\dagger\} & = & \delta_{ij} \\ \{c_i, c_j\} & = & 0\,. \end{array} \right. \tag{4.2}$$

The $V \times V$ hermitian matrix h_{ij} is the one-body Hamiltonian, which is diagonalized by a unitary transformation $h = UEU^\dagger$ with $UU^\dagger = U^\dagger U = \mathcal{I}$, and $E = \mathrm{diag}(\epsilon_1, \ldots, \epsilon_V)$. The diagonal form of $\mathcal{H}$ is thus

$$\begin{aligned} \mathcal{H} &= \sum_{\alpha=1}^{V} \sum_{i,j=1}^{V} U_{i\alpha} \epsilon_\alpha U_{j\alpha}^* c_i^\dagger c_j \\ &= \sum_{\alpha=1}^{V} f_\alpha^\dagger f_\alpha \epsilon_\alpha \end{aligned} \tag{4.3}$$

where

$$f_\alpha^\dagger = \sum_{i=1}^{V} U_{i\alpha} c_i^\dagger \tag{4.4}$$

creates a particle, delocalized on the lattice, in the single-particle wavefunction (or "mode") $\psi_\alpha(i) = U_{i\alpha}$. The (many-body) ground state of $\mathcal{H}$ is obtained by filling all energy levels up to the Fermi energy $\epsilon_F = 0$[1]. A thermal state

$$\rho = \frac{1}{Z} e^{-\mathcal{H}/k_B T} \tag{4.5}$$

is obtained by populating each single-particle mode with an average number of fermions

$$\begin{aligned} n_\alpha &= \langle f_\alpha^\dagger f_\alpha \rangle \\ &= \frac{1}{1 + e^{\epsilon_\alpha / k_B T}}\,. \end{aligned} \tag{4.6}$$

Such a state is a Gaussian state, namely the exponential of a quadratic form

$$\rho = \frac{1}{Z} \prod_\alpha e^{-\beta \epsilon_\alpha f_\alpha^\dagger f_\alpha} \tag{4.7}$$

[1] Note that we set the density by absorbing the chemical potential term $-\mu N = -\mu \sum_i c_i^\dagger c_i$ into the diagonal part of h_{ij}, so that the Fermi energy is by definition at $\epsilon_F = 0$. Usually, one sets $\epsilon_F = \mu$, but this simply corresponds to a global shift of the single-particle energies.

and therefore it satisfies Wick's theorem[2], which implies that this state is completely characterized by the one-body correlation matrix

$$\begin{aligned} C_{ij} &= \langle c_i^\dagger c_j \rangle \\ &= \sum_{\alpha,\beta} U_{i\alpha}^* \langle f_\alpha^\dagger f_\beta \rangle U_{j\beta} \\ &= (U^* N U^T)_{ij} \end{aligned} \tag{4.8}$$

where $N = \mathrm{diag}(n_1, \ldots, n_V)$ and U^T denotes the transpose of U. If we restrict our observations to a subsystem A, containing an arbitrary subset of the sites of the lattice, we may keep only

$$C_A = (C_{ij})_{i,j\in A} \, . \tag{4.9}$$

Since all correlation functions related to A degrees of freedom factorize according to the prescriptions of Wick's theorem, we know that the reduced density matrix ρ_A is also a Gaussian state, which can be written as the exponential of a FF Hamiltonian h_A (Peschel and Eisler, 2009)

$$\left\{ \begin{array}{rcl} \rho_A &=& e^{-\mathcal{H}_A} \\ \mathcal{H}_A &=& \sum_{i,j\in A} c_i^\dagger c_j (h_A)_{ij} \, . \end{array} \right. \tag{4.10}$$

In particular, Eq. (4.8) implies that C_A^* and h_A are diagonal in the same basis $U^{(A)} = (U_{i\alpha}^{(A)})$. Furthermore, the eigenvalues $n_\alpha^{(A)}$ of C_A^* are related to the eigenvalues $\epsilon_\alpha^{(A)}$ of h_A by

$$n_\alpha^{(A)} = \frac{1}{1 + e^{\epsilon_\alpha^{(A)}}} \tag{4.11}$$

$$\epsilon_\alpha^{(A)} = \ln\left(\frac{1}{n_\alpha^{(A)}} - 1 \right) \, . \tag{4.12}$$

In particular, if one works with the ground state of $\mathcal{H}$ (or, more generally, any pure state obtained by populating certain single-particle modes α with one fermion, and the other ones with zero fermion), h_A is the (one-body) entanglement Hamiltonian, and $\epsilon_\alpha^{(A)}$ the (one-body) entanglement spectrum. In principle, the entanglement Hamiltonian could be reconstructed by diagonalizing the one-body density matrix C_A^* containing only degrees of freedom within region A

$$C_A^* = U^{(A)} N_A (U^{(A)})^\dagger \tag{4.13}$$

[2] More generally, any state obtained by populating the one-particle states independently of each other is a Gaussian state. Formally, this can be thought of as a thermal state, although with a different temperature for each mode α. Wick's theorem is proved and extensively discussed in the book of Blaizot and Ripka (1986).

but in practice, this is possible only for relatively small systems (up to about 30 sites), because many $n_\alpha^{(A)}$ lie exponentially close to 0 or 1, so that it is very hard to get a sufficient precision on the associated $\epsilon_\alpha^{(A)}$ and to reconstruct the entanglement Hamiltonian. On the other hand, most physical quantities of interest are insensitive to the modes whose occupation lie close to 0 or 1. For instance, entanglement entropy of A is the thermal entropy associated to the occupation n_α^A of the entanglement eigenmodes. Any mode is occupied (with probability $n_\alpha^{(A)}$) or empty (with probability $1 - n_\alpha^{(A)}$) independently of the others, yielding an entropy of

$$S_A = \sum_\alpha s(n_\alpha^{(A)}) \tag{4.14}$$

$$s(n) = -n \ln n - (1-n)\ln(1-n) \, . \tag{4.15}$$

As $s(n)$ is 0 for $n = 0, 1$, the entanglement entropy is mostly sensitive to the highly fluctuating modes such that $n_\alpha^{(A)} \approx 1/2$.

4.1.2 Contours

A key concept in the study of the spatial structure of entanglement in many-body systems is the *entanglement contour*, first introduced by Chen and Vidal (2014), and further elaborated by us (Frérot and Roscilde, 2015) and by Coser, De Nobili, and Tonni (2017). The basic idea of the entanglement contour is to decompose entanglement entropy as a sum of local contributions

$$S_A = \sum_{i \in A} \mathcal{C}_s(i) \tag{4.16}$$

where $\mathcal{C}_s(i)$ is the contribution of site i to the entanglement of A with B. In view of the fact that S_A is a sum of independent contributions stemming from the different entanglement eigenmodes, Eq. (4.14), it is natural to seek a decomposition of the form

$$S_A = \sum_{i \in A} \underbrace{\sum_\alpha s(n_\alpha^{(A)}) w_\alpha(i)}_{\mathcal{C}_s(i)} \tag{4.17}$$

where $w_\alpha(i)$ is weighting the contribution of site i to $s(n_\alpha^{(A)})$, the contribution of the entanglement mode α to entanglement entropy. In particular, for all α

$$\sum_i w_\alpha(i) = 1 \, . \tag{4.18}$$

Here, the most obvious choice is given by the weight of the entanglement mode α on site i

$$w_\alpha(i) = |U_{i\alpha}^{(A)}|^2 \tag{4.19}$$

so that the entanglement contour reads

$$\mathcal{C}_s(i) = \sum_\alpha |U^{(A)}_{i\alpha}|^2 s(n^{(A)}_\alpha) \; . \tag{4.20}$$

This definition of the entanglement contour satisfies several natural desiderata (Chen and Vidal, 2014), and in particular the sum rule Eq. (4.17). In a similar spirit (Frérot and Roscilde, 2015), we define the fluctuation (or density) contour as

$$\mathcal{C}_N(i) = \langle n_i N_A \rangle - \langle n_i \rangle \langle N_A \rangle \; , \tag{4.21}$$

such that

$$\langle \delta^2 N_A \rangle = \sum_{i \in A} \mathcal{C}_N(i) \; . \tag{4.22}$$

As $N_A = \sum_\alpha c^\dagger_\alpha c_\alpha$ and $n_i = \sum_{\alpha,\beta} (U^{(A)})^*_{i\alpha} U^{(A)}_{i\beta} c^\dagger_\alpha c_\beta$, we can write

$$\begin{aligned} \mathcal{C}_N(i) &= \sum_{\alpha,\beta} |U^{(A)}_{i\alpha}|^2 \left[\langle n_\alpha n_\beta \rangle - \langle n_\alpha \rangle \langle n_\beta \rangle \right] \\ &= \sum_\alpha |U^{(A)}_{i\alpha}|^2 [\langle (n^{(A)}_\alpha)^2 \rangle - \langle n^{(A)}_\alpha \rangle^2] \end{aligned} \tag{4.23}$$

where $\langle n^2 \rangle - \langle n \rangle^2 = n(1-n)$ since $n = 0$ or 1. Here, we have used the fact that the populations $n_\alpha = c^\dagger_\alpha c_\alpha$ are conserved, and that they fluctuate independently for $\alpha \neq \beta$. Note the similarity of the expression of Eq. (4.23) for the fluctuation contour with Eq. (4.20) for the entanglement contour.

4.1.3 Contour and structure factor

In the special case of a translationally invariant system, it is convenient to relate the fluctuation contour of an observable to the structure factor. Considering an arbitrary local observable $\mathcal{O}_i$, the structure factor is defined as

$$S_{\mathcal{O}}(\boldsymbol{k}) = \sum_j e^{-i\boldsymbol{k}\cdot(\boldsymbol{r}_j - \boldsymbol{r}_i)} \langle \delta\mathcal{O}_i \delta\mathcal{O}_j \rangle \; . \tag{4.24}$$

In particular, the corresponding contour is

$$\begin{aligned} \mathcal{C}_{\mathcal{O}}(i) &= \sum_{j \in A} \langle \delta\mathcal{O}_i \delta\mathcal{O}_j \rangle \\ &= \frac{1}{N} \sum_{\boldsymbol{k}} e^{-i\boldsymbol{k}\cdot\boldsymbol{r}_i} S_{\mathcal{O}}(\boldsymbol{k}) \sum_{j \in A} e^{i\boldsymbol{k}\cdot\boldsymbol{r}_j} \\ &= \frac{1}{N} \sum_{\boldsymbol{k}} e^{-i\boldsymbol{k}\cdot\boldsymbol{r}_i} S_{\mathcal{O}}(\boldsymbol{k}) T_A(\boldsymbol{k})^* \end{aligned} \tag{4.25}$$

where we have introduced the form factor for the subsystem A

$$T_A(\boldsymbol{k}) = \sum_{j \in A} e^{-i\boldsymbol{k}\cdot\boldsymbol{r}_j} \; . \tag{4.26}$$

4.1.4 Discussion

We emphasize that the above treatment applies to *any* free fermion Hamiltonian. It relies solely on the validity of Wick's theorem. This includes arbitrary hopping amplitudes (including complex ones to implement, for instance, magnetic fields on free hopping electrons) and arbitrary onsite potentials. Furthermore, if the state satisfies Wick's theorem at some initial time, and is evolved through a free fermion Hamiltonian (possibly time-dependent), it satisfies Wick's theorem at any later time as well. This property is easy to prove in the Heisenberg picture for the $c_i^{(\dagger)}$ operators

$$i\hbar\partial_t c_i = [c_i, \mathcal{H}] = \sum_j h_{ij} c_j \tag{4.27}$$

so that $c_i(t)$ is a linear combination of the $c_j(0)$'s ($= c_j$). Since any linear combination of operators which satisfy Wick's theorem also satisfies Wick's theorem, we immediately realize that the evolved state is amenable to the same treatment as the initial one. Hence, all sorts of questions related to the effect of gauge fields, disorder, time evolution, finite temperature, etc, onto the structure of entanglement in free fermion models can be investigated at a minimal computational effort.

These properties have been used by Chen and Vidal (2014) to investigate the real-time dynamics of entanglement contours, and by us (Frérot and Roscilde, 2015) to investigate fluctuation and entanglement contours of fermions in the brick-wall lattice (which has similar properties to the graphene lattice), or in topological bands.

4.2 Free fermions in one dimension

In this section, we introduce the FF Hamiltonian in $d = 1$ and the "local entanglement termodynamics" (LET) Ansatz for the entanglement Hamiltonian [Eq. (4.42)] inspired by the Bisognano-Wichmann theorem, Eq. (3.37). We show that the LET Ansatz and the actual entanglement Hamiltonian have striking similarities (exact same eigenvectors, very similar energies, see Fig. 4.1). We then argue in favor of the validity of the local temperature picture by comparing the contours of several quantities and their thermal counterparts (Fig. 4.2). Finally, we briefly emphasize again the subtle but essential point that the reduced density-matrix is a thermal state of the entanglement Hamiltonian at a very specific temperature.

4.2.1 Free fermions on a line

In this section, we investigate again the simplest situation: free fermions hopping on a homogeneous $1d$ lattice. The Hamiltonian in second-quantized form is

$$\mathcal{H} = -J \sum_{x=1}^{N} (c_x^\dagger c_{x+1} + c_{x+1}^\dagger c_x) - \mu \sum_{x=1}^{N} c_x^\dagger c_x \tag{4.28}$$

where we identify $x = N + 1$ with $x = 1$ (periodic boundary conditions). $\mathcal{H}$ is diagonalized by a Fourier transform

$$\begin{aligned} c_k &= \frac{1}{\sqrt{N}} \sum_x e^{-ikx} c_x & (4.29)\\ \epsilon_k &= -2J \cos k - \mu & (4.30)\\ \mathcal{H} &= \sum_k \epsilon_k c_k^\dagger c_k \, . & (4.31) \end{aligned}$$

The one-body spectrum ϵ_k is symmetric with respect to $k \leftrightarrow -k$. It is convenient to introduce the Fermi wavevector $k_F \geq 0$ such that

$$\begin{aligned} \epsilon_{k_F} &= 0 & (4.32)\\ \mu &= -2J \cos k_F \, . & (4.33) \end{aligned}$$

The speed of light in the Bisognano-Wichmann theorem Eq. (3.37) is replaced here by the Fermi velocity

$$\begin{aligned} v_F &= \left. \frac{\partial \epsilon_k}{\partial k} \right|_{k=k_F} & (4.34)\\ &= 2J \sin k_F \, . & (4.35) \end{aligned}$$

At low energy ($|\epsilon_k| \ll J$), the spectrum is approximately linear

$$\begin{aligned} \epsilon_{k_F+q} &= -2J \cos(k_F + q) + 2J \cos(k_F) & (4.36)\\ &= q v_F + O(q^2) & (4.37) \end{aligned}$$

so that $q = k - k_F > 0$ can be thought of as the momentum of relativistic massless fermions ($E_q = \sqrt{m^2c^4 + q^2c^2} = |q|c$ if $m = 0$) where v_F plays the role of c. This linear dispersion at low energy, $\epsilon_{k_F+q} \approx v_F q$, is the origin of the Lorentz invariance of the effective field theory which describes the low-energy / long-wavelength behavior of this free fermion gas on the lattice. Finally, the one-body correlation matrix in the

ground state is

$$C_{xx'} = \langle c_x^\dagger c_{x'} \rangle \tag{4.38}$$
$$= \frac{1}{N} \sum_k \langle c_k^\dagger c_k \rangle e^{ik(x'-x)} \tag{4.39}$$
$$\overset{N\to\infty}{\longrightarrow} \int_{-k_F}^{k_F} \frac{dk}{2\pi} e^{ik(x'-x)} \tag{4.40}$$
$$= \frac{\sin[k_F(x'-x)]}{\pi(x'-x)} \tag{4.41}$$

which depends only on the relative position $x' - x$ since we work with periodic boundary conditions. We have taken the thermodynamic limit $N \to \infty$.

4.2.2 Entanglement Hamiltonian

We consider a subsystem A containing all the sites from $x = 1$ to $x = l$. The one-body entanglement Hamiltonian h_A is obtained by diagonalizing the correlation matrix C_A^* ($= C_A = (C_{ij})_{i,j\in A}$), see Section 4.1: h_A and C_A^* have the same eigenvectors, and their spectra are related by Eq. (4.12). The "local entanglement temperature" Ansatz (see Section 3.3.2) for the entanglement Hamiltonian is

$$\mathcal{H}_A^{\mathrm{LET}} = -\frac{2\pi}{v_F} J \sum_{x=1}^{l-1} \beta_{x,x+1} (c_x^\dagger c_{x+1} + c_{x+1}^\dagger c_x) - \frac{2\pi}{v_F} \mu \sum_{x=1}^{l} \beta_x \mu c_x^\dagger c_x \,. \tag{4.42}$$

With all β's equal to $v_F/2\pi$, this would just be the physical Hamiltonian restricted to the subsystem A (note in particular that we now have *open* boundary conditions). Here, we have (as introduced in Section 3.3.2, paragraph "local entanglement temperature on the lattice")

$$\beta_r = (r - 1/2)\left(1 - \frac{r-1/2}{l}\right) \tag{4.43}$$
$$\beta_{r,r+1} = r(1 - r/l) \tag{4.44}$$

Miraculously, h_A^{LET} and C_A are found to commute, so that they have the same eigenvectors[3]. In particular, h_A and h_A^{LET} have also the same eigenvectors, denoted $\psi_\alpha(x)$, and possibly differ only in their spectrum, denoted respectively ϵ_α and $\epsilon_\alpha^{\mathrm{LET}}$

$$h_A \psi_\alpha = \epsilon_\alpha \psi_\alpha \tag{4.45}$$
$$h_A^{\mathrm{LET}} \psi_\alpha = \epsilon_\alpha^{\mathrm{LET}} \psi_\alpha \,, \tag{4.46}$$

[3] This can be checked by a lengthy but straightforward comparison of the matrix elements of $C_A h_A^{\mathrm{LET}}$ and $h_A^{\mathrm{LET}} C_A$.

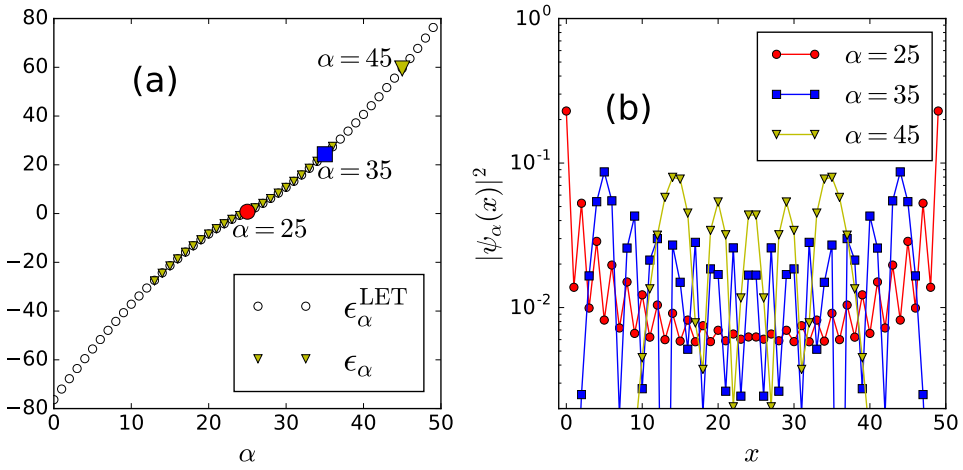

Figure 4.1: Entanglement Hamiltonian for $1d$ free fermions ($l = 50$, $N = 5000$, $\mu = 0$). (a) Comparison between the entanglement spectrum (filled yellow triangles) with the spectrum of $h_A^{\rm LET}$, Eq. (4.42) (empty circles). Only the lowest levels (near $\alpha = l/2 = 25$) are plotted for the entanglement spectrum because of the already-cited limitations in the numerical precision (see Section 3.3.1). Large symbols at $\alpha = 25, 35, 45$ indicate the eigenvalues associated to the eigenstates plotted on panel (b). (b) Spatial weight $|\psi_\alpha(x)|^2$ of the eigenstates of the one-body entanglement Hamiltonian, for $\alpha = 25, 35, 45$. Highest modes (contributing a smaller amount to entanglement entropy) are located far in the bulk of A, while lowest modes (giving the largest contributions to entanglement entropy) have more weight close to the boundaries. Notice the logarithmic scale on the vertical axis.

so that the reduced density matrix for A is

$$\rho_A = \frac{1}{Z} \exp\left\{ -\sum_\alpha (c_\alpha^{(A)})^\dagger c_\alpha^{(A)} \epsilon_\alpha \right\} \tag{4.47}$$

where $1/Z$ ensures the normalization $\mathrm{Tr}(\rho_A) = 1$ and we have introduced

$$c_\alpha^{(A)} = \sum_{x \in A} \psi_\alpha(x)^* c_x \ . \tag{4.48}$$

Similarly, the approximate reduced density matrix provided by the LET Ansatz is

$$\rho_A^{\rm LET} = \frac{1}{Z'} \exp\left\{ -\sum_\alpha (c_\alpha^{(A)})^\dagger c_\alpha^{(A)} \epsilon_\alpha^{\rm LET} \right\} \ . \tag{4.49}$$

As shown on Fig. 4.1(a), the spectra of h_A and $h_A^{\rm LET}$ are very similar, which makes $h_A^{\rm LET}$ and excellent approximation of h_A, since they have exactly the same eigenvectors. However, even though it is not visible on Fig. 4.1(a), we emphasize that

they are different, even in the asymptotic limit $l \to \infty$, as h_A contains further hopping terms beyond nearest neighbor, absent from h_A^{LET}, which persist for arbitrary large l (Eisler and Peschel, 2017). Interestingly, as shown on Fig. 4.1(b) the eigenvectors $\psi_\alpha(x)$ associated to entanglement energies close to $\epsilon_\alpha = 0$ (which give the largest contribution to entanglement entropy), are mainly localized near the edges of A, while the eigenvectors associated to increasingly high entanglement energies (which contribute increasingly less to entanglement entropy), have their weight located increasingly far from the boundary.

Somehow illustrating the origin of the are law of entanglement entropy (logarithmically violated in this case), the entanglement modes which contribute the most to entanglement entropy involve degrees of freedom in the vicinity of the boundary of A. There is nothing rigorous in this last remark, since strictly speaking, entanglement entropy is only sensitive to the entanglement energies, and not to the spatial structure of the associated entanglement modes. The connection between the spatial structure of entanglement eigenstates and the scaling of entanglement entropy can be made more rigorous by the analysis of the spatial structure of the entanglement contours, which are sensitive to both entanglement energies (dictating the mode populations) and to the spatial structure of the modes. Contrary to the entanglement spectrum, and to the entanglement eigenstates, the contours have a robust structure in the thermodynamic limit.

4.2.3 Relations between the contours

Expression of the contours. We now wish to investigate the "local entanglement temperature" hypothesis discussed on general grounds in Section 3.3.3 in the specific case at hand: free fermions hopping on a line. In this context, the two central quantities (introduced in Section 4.1) are the *entanglement contour*

$$\mathcal{C}_s(x) = \sum_\alpha s(n_\alpha) |\psi_\alpha(x)|^2 \,, \tag{4.50}$$

where $n_\alpha = [1 + \exp(\epsilon_\alpha)]^{-1}$ and $s(n) = -n \ln n - (1-n)\ln(1-n)$; and the *density-fluctuations contour*

$$\begin{aligned} \mathcal{C}_N(x) &= \sum_{x'=1}^{l} \langle \delta n_x \delta n_{x'} \rangle & (4.51) \\ &= \sum_\alpha \langle \delta^2 n_\alpha \rangle |\psi_\alpha(x)|^2 \,, & (4.52) \end{aligned}$$

where $\langle \delta^2 n \rangle = n(1-n)$. More generally, we can consider the fluctuation contour associated to other Fourier components of the density

$$\mathcal{C}_k(x) = \sum_{x'=1}^{l} \langle \delta n_x \delta n_{x'} \rangle \cos[k(x-x')] \tag{4.53}$$

such that, integrating over the whole subsystem A, we obtain the local structure factor (times the number l of sites)

$$\sum_x \mathcal{C}_k(x) = \sum_{x,x' \in A} e^{ik(x-x')} \langle \delta n_x \delta n_{x'} \rangle \equiv l S_A(k) \; . \tag{4.54}$$

The variance of the number of particles, $\langle \delta^2 N_A \rangle$, corresponds to the special case $k = 0$, while the case $k = \pi$ corresponds to the variance of the staggered density in A

$$N_{\text{stagg}} = N_{\text{even}} - N_{\text{odd}} \; , \tag{4.55}$$

also called "imbalance" in the literature, where N_{even} counts the number of particles on the sites such that x is even, and N_{odd} on the remaining ones.

Spatial structure of the contours *vs.* thermal behavior of the corresponding thermodynamic fluctuations. Fig. 4.2(a) shows the contours of entanglement $\mathcal{C}_s$, of density fluctuations $\mathcal{C}_N = \mathcal{C}_{k=0}$, and of imbalance fluctuations $\mathcal{C}_\pi$ for a subsystem of 100 sites in a chain of 5000 sites. Clearly, the contours are symmetric with respect to the center of A. Furthermore, both the entanglement and density-fluctuations contour decay when moving away from the boundary of A (note the logarithmic scale on the vertical axis). This corresponds to fact that both $S_A = \sum_{x \in A} \mathcal{C}_s(x)$ and $\langle \delta^2 N_A \rangle = \sum_{x \in A} \mathcal{C}_N(x)$ are sub-extensive in the size of A: if the contours would decay to a nonzero (an size-independent) value in the bulk of A, their integral would scale linearly in the volume of A. Remarkably, both $\mathcal{C}_s$ and $\mathcal{C}_N$ decay as $1/x$ in the bulk of A, giving rise to the logarithmic violation of the area law observed for gapless free fermions, and they do so in such a way that

$$\frac{\mathcal{C}_s}{\mathcal{C}_N} \to \frac{\pi^2}{3} \tag{4.56}$$

showing that the relation

$$\frac{S_A}{\langle \delta^2 N_A \rangle} \approx \frac{\pi^2}{3} \tag{4.57}$$

is simply inherited by the same relation existing already at the level of the contours (Frérot and Roscilde, 2015). This is a first illustration of the validity of the local temperature picture discussed on general grounds in Section 3.3.3, and further illustrated on panels (b), (c) and (d) of Fig. 4.2.

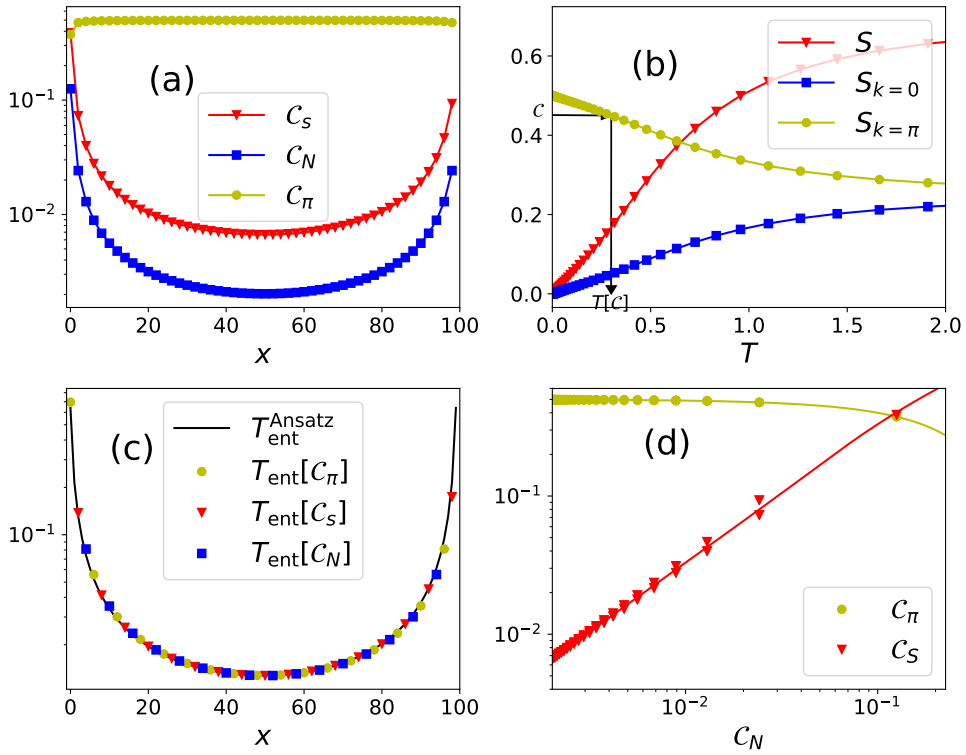

Figure 4.2: Local entanglement temperature for $1d$ free fermions. A is a line of 100 sites in a chain of 5000 sites with PBC, at half filling. (a) Entanglement contour (red triangles), density-fluctuations contour (blue squares) and imbalance-fluctuations contour(yellow circles) as a function of position in subsystem A (see text for the definitions). (b) Entropy density, structure factor at $k = 0$ and at $k = \pi$ (see text for the definition), as a function of temperature. Same symbols as for the corresponding contours in panel (a). Black arrows illustrate the manner in which the local entanglement temperature may be reconstructed from the knowledge of the contour [panel (a)], and the knowledge of the thermal behavior of the corresponding fluctuations [panel (b)]: one chooses $T_{\rm ent}(x)$ such that $\mathcal{C}_{\mathcal{O}}(x) = \langle \delta^2 \mathcal{O} \rangle [T_{\rm ent}(x)]/V$. (c) Entanglement temperature as a function of the position, extracted by the above-mentioned procedure, from the entanglement, density and imbalance contours [same symbols as for the associated contours in panel (a)]. Solid black line: prediction of Eq. (3.39) with $c = v_F$. (d) Entanglement contour (red triangles) and imbalance-fluctuations contour (yellow circles) as a function of the density-fluctuations contours [data extracted from panel (a)]. Solid lines are the corresponding entropy density and structure factor at $k = \pi$, as a function of the structure factor at $k = 0$, at thermal equilibrium [data extracted from panel (b)].

On the other hand, the imbalance-fluctuations contour slightly increases near the boundaries of A, and quickly reaches a plateau value, independent of the size of A, corresponding to the fact the $\langle \delta^2 N^A_{\text{stagg}} \rangle$ scales linearly with the volume of A; namely it exhibits a *volume-law scaling*. The slight decrease of $\mathcal{C}_\pi$ when approaching the boundaries of A nicely matches the expectation that the entanglement temperature is higher near the boundaries. Indeed, in Fig. 4.2(b) we have plotted the structure factors at $k = 0$ (equal to $\langle \delta^2 N \rangle / V$, V being the total number of sites in the system), and at $k = \pi$ (equal to $\langle \delta^2 N_{\text{stagg}} \rangle / V$), and the entropy density as a function of temperature. While the variance of N and the entropy both increase linearly at low temperature (the prefactor relating them being precisely $\pi^2/3$), and then reach a shot-noise limit at high temperature ($S/V \to \ln 2$ and $\langle \delta^2 N \rangle / V \to n(1-n) = 1/4$ for $n = 1/2$), corresponding to uncorrelated fluctuations on all the sites, the imbalance fluctuations actually *increase* when moving towards lower temperature[4]. As a consequence of the entanglement temperature going to zero in the bulk, the imbalance-fluctuations contour is hence larger in the bulk than on the edges of A. This in contrasts with the entanglement and density-fluctuations contours, which go to zero in the bulk of A, reflecting the fact that both the variance of the density and the entropy go to zero at low temperature.

Thermodynamic relations between the contours and local entanglement temperature. Now, from the hypothesis that the contours depend on the local entanglement temperature in the same way as the global fluctuations do on the true temperature,

$$\mathcal{C}_{\mathcal{O}}(T_{\text{ent}}) \approx \frac{\langle \delta^2 \mathcal{O} \rangle}{V}(T_{\text{ent}}) \, , \tag{4.58}$$

we can extract T_{ent} from: 1) the knowledge of the equation $\langle \delta^2 \mathcal{O} \rangle(T)$ (which could be measured in an experiment); and 2) the knowledge of the contour $\mathcal{C}_{\mathcal{O}}$ (which could also be measured whenever the correlations of $\mathcal{O}$ are accessible). The small black arrows on Fig. 4.2(b) illustrate the procedure to extract T_{ent} from 1) and 2). In principle, the entanglement temperature obtained in this way is observable-dependent. However, as shown on Fig. 4.2(c), the temperature obtained from $\mathcal{C}_s$[5], $\mathcal{C}_N$ and $\mathcal{C}_\pi$ are extremely close to each other, and furthermore, they are extremely close to the entanglement temperature which modulates in space the Ansatz Hamiltonian of Eq. (4.42)

$$T^{\text{Ansatz}}_{\text{ent}}(x) = \frac{v_F}{2\pi} \left(\frac{1}{x - 1/2} + \frac{1}{l - x + 1/2} \right) \tag{4.59}$$

[4] This highly non-classical behavior is a consequence of the imbalance fluctuations being strongly affected by the *quantum* (or coherent) contribution to the fluctuations, see Frérot and Roscilde (2016b) and Section III.

[5] Although the entanglement contour is *a priori* not a measurable quantity, we also illustrate the procedure for it for the sake of completeness.

if $x = 1 \dots l$ denotes the position of the sites of A (recall that the two boundaries between A and B are at positions $1/2$ and $l + 1/2$ respectively). This further validates the local equilibrium approximation (LEA), discussed in Section 3.3.3, according to which the subsystem A may be viewed as being in local thermal equilibrium at the temperature $T_{\rm ent}(x)$ (independent of the observable). One then sees that the local contribution of the site x to the variance of an observable $\mathcal{O}$, as extracted from the LEA on the Ansatz Hamiltonian, is just the contour $\mathcal{C}_{\mathcal{O}}(x)$.

The validity of the LEA is not at all obvious a priori, since we know that the state has an infinite correlation length. One could argue that what matters in this context is not the correlation length ξ in the ground state, but the correlation length $\xi(x)$ at the local temperature $T_{\rm ent}(x)$. The physical intuition would be that we can divide the subsystem A into patches of linear size $\xi(x)$, on which the temperature is approximatetly constant, and which are uncorrelated from each other. In the present case of free fermions, $\xi(T) \approx v_F/(2\pi T)$, and $T(x) \approx v_F/(2\pi x)$ so that $\xi(x) \approx x$. If one wants the temperature to be approximately constant across a patch of size $\xi(x) \approx x$, one needs the gradient of $T(x)$ to be sufficiently small

$$\frac{\Delta T}{T(x)} \ll 1 \quad \Leftrightarrow \quad \frac{\xi \partial_x T}{T(x)} \ll 1 \tag{4.60}$$

$$\Leftrightarrow \quad \frac{x \frac{v_F}{2\pi x^2}}{\frac{v_F}{2\pi x}} \ll 1 \tag{4.61}$$

$$\Leftrightarrow \quad 1 \ll 1 \tag{4.62}$$

which is not a good approximation. So it seems difficult to justify the LEA on physical grounds, especially in view of the fact that the "patches" we consider in practice, are single lattice sites. However, we are somehow forced to admit that it indeed provides a correct account for the thermodynamic relations observed between the contours.

Note that the picture of local thermal equilibrium must be manipulated with caution: all local observables are really translationally invariant. The contours are *not*, because they are *not* local quantities (they depend on the very definition of A), and therefore are able to detect the (non-uniform) entanglement temperature. The balance between the idea of local equilibrium and the nonlocal nature of entanglement is somewhat embodied in the local *and* nonlocal nature of the contours.

Finally, we illustrate on Fig. 4.2(d) how the detour through the entanglement temperature can be circumvented by directly comparing the contours of different observables. Indeed, a direct consequence of Eq. (4.58) is that, considering two observables $\mathcal{O}_1$ and $\mathcal{O}_2$, the associated contours obey

$$\mathcal{C}_{\mathcal{O}_1}(\mathcal{C}_{\mathcal{O}_2}) \approx \langle \delta^2 \mathcal{O}_1 / V \rangle \left(\langle \delta^2 \mathcal{O}_2 \rangle / V \right) \tag{4.63}$$

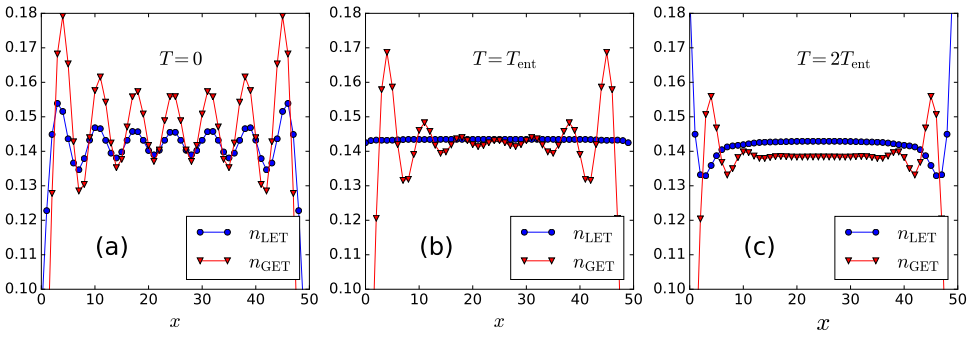

Figure 4.3: Homogeneity of the Ansatz states. Comparison of the density profile between the GET Ansatz (red triangles) and the LET Ansatz (blue circles) at various temperatures, for $\mu/J = -1.8$ (density $n = 0.1434$). (a) At $T = 0$; (b) At $T = T_{\rm ent}$, chosen such that the (thermal) entropy matches the entanglement entropy that the system would have if it were immersed in an infinitely large ground state. (c) At $T = 2T_{\rm ent}$. Friedel oscillations at wavevector k_F, induced by the presence of boundaries, are strongly suppressed only at $T = T_{\rm ent}$ for the LET Hamiltonian, Eq. (4.42), while they survive up to large temperatures for the GET Hamiltonian (namely, the physical Hamiltonian with open boundaries).

where, on the r.h.s, we have the relation between the variances of $\mathcal{O}_1$ and $\mathcal{O}_2$ per site at thermal equilibrium. We illustrate this prediction by showing how the entanglement contour and imbalance contour could be reconstructed from the knowledge of the density contour, together with the thermal behavior of the entropy and of the structure factors at $k = 0$ and π (plotted on Fig. 4.2(b)), without the need to actually measure the temperature, which can be a delicate task in the context of cold atoms.

4.2.4 Homogeneity of the Ansatz state

Before moving on to the $d = 2$ situation, we briefly comment on the seemingly paradoxical observation that a thermal state of a manifestly inhomogeneous Hamiltonian, as proposed in Eq. (4.42) (LET Ansatz), reproduces much better the properties of a homogeneous system (since subsystem A is immersed in a homogeneous system, it is itself perfectly translationally invariant), than of a more homogeneous Hamiltonian, as proposed in Eq. (3.18) (GET Ansatz, namely, the physical Hamiltonian with open boundaries). To gain insight into this issue, we briefly study the behavior of the spatial density for these two Ansatz Hamiltonians, varying the temperature. The subtle point here is that even if the GET Hamiltonian is homogeneous, the mere presence of boundaries induces strong Friedel oscillations of the density at wavevector k_F near the edges. As is already visible on Fig. 4.3(a), these boundary-induced oscillations are less pronounced in the ground state of the LET Hamiltonian, than in the ground

state of the GET Hamiltonian. The ground state of the LET Hamiltonian has per se no physical meaning, but this observation somehow anticipate the fact that at $T = T_{\text{ent}}$[6] [Fig. 4.3(b)], the density profile for the LET Hamiltonian is nearly perfectly flat. On the other hand, the GET Ansatz continues to exhibit strong Friedel oscillations of the density at this temperature (where its thermal entropy matches the ground state entanglement entropy of A), and up to relatively high temperatures [Fig. 4.3(c)]. Furthermore, at $T > T_{\text{ent}}$, the LET Ansatz exhibits again spatial inhomogeneities: only at $T = T_{\text{ent}}$ does the LET Hamiltonian accurately mimic the reduced-density matrix ρ_A in the ground-state of the physical Hamiltonian. To conclude this discussion, we may say that the inhomogeneous entanglement Hamiltonian is perfectly fined tuned to mimic the ground state properties *when studied at a very specific temperature*. It is not only the structure of the entanglement Hamiltonian itself which matters, but also the fact that the statistical properties associated to it are evaluated at a special temperature. Similar considerations have led Chandran, Khemani, and Sondhi (2014) to question the common belief according to which the low energy entanglement Hamiltonian contains universal signatures of the phase of matter characterizing the physical ground state $|\text{GS}_{\text{phys}}\rangle$. They argued that the low energy physics of the entanglement Hamiltonian need not correspond to the actual properties of $|\text{GS}_{\text{phys}}\rangle$, and in especially pathologic models, there might even be (finite temperature) phase transitions between the ground state of the entanglement Hamiltonian, $|\text{GS}_{\text{ent.Ham.}}\rangle$, and the state at temperature 1, which describes the physical ground state $|\text{GS}_{\text{phys}}\rangle$ under examination.

4.3 Free fermions in $d \geq 2$

We now turn to the richer case of free fermions in $d = 2$. After introducing the model, we show that for a subsystem A consisting of a cylinder cut out of a torus, the entanglement Hamiltonian decouples as a sum of $1d$ FF systems, each of them having its own Fermi velocity. In each sector, we can use the results of Section 4.2 in $d = 1$, but the validity of the LET hypothesis for the entanglement Hamiltonian, which would require a unique Fermi velocity, breaks down. In spite of this breakdown, we show that a local equilibrium point of view, understood as a relation among the contours, continues to hold.

[6] The entanglement temperature T_{ent} is chosen in such a way that the thermal entropy coincides with the entanglement entropy of the reduced state ρ_A in the ground state of the infinite free fermion chain.

4.3.1 Free fermions on a torus

We consider free fermions hopping on a square lattice, and work with periodic boundary conditions (PBC, the system is thus defined on a torus). The Hamiltonian is

$$\mathcal{H} = -\sum_{x=1}^{L_x}\sum_{y=1}^{L_y} c_{x,y}^\dagger \left[J(c_{x,y+1} + c_{x,y-1} + c_{x-1,y} + c_{x+1,y}) + \mu c_{x,y}\right] \ , \tag{4.64}$$

where we identify $x = L_x + 1$ with $x = 1$ and $y = L_y + 1$ with $y = 1$ (PBC). As usual, μ is the chemical potential (fixing the density), and J the hopping amplitude. The Hamiltonian is diagonalized by Fourier transform

$$\begin{aligned} c_{k_x,k_y} &= \frac{1}{\sqrt{L_x L_y}} \sum_{x,y} e^{-i\boldsymbol{k}\cdot\boldsymbol{r}} c_{x,y} && (4.65)\\ \epsilon_{\boldsymbol{k}} &= -2J(\cos k_x + \cos k_y) - \mu && (4.66)\\ \mathcal{H} &= \sum_{\boldsymbol{k}} \epsilon_{\boldsymbol{k}} c_{\boldsymbol{k}}^\dagger c_{\boldsymbol{k}} \ , && (4.67) \end{aligned}$$

where $\boldsymbol{k} = (k_x, k_y)$ and $\boldsymbol{r} = (x, y)$. We consider the ground state of $\mathcal{H}$, filling all energy levels up to the Fermi energy $\epsilon_F = 0$ (again, we incorporate the chemical potential as a shift of energy levels). The one-body correlation function is (with $V = L_x L_y$)

$$C_{\boldsymbol{r}\boldsymbol{r}'} = \langle c_{\boldsymbol{r}}^\dagger c_{\boldsymbol{r}'} \rangle = \frac{1}{V} \sum_{\boldsymbol{k}} e^{i\boldsymbol{k}\cdot(\boldsymbol{r}'-\boldsymbol{r})} f_{\mathrm{FD}}(\epsilon_{\boldsymbol{k}}) \tag{4.68}$$

with $f_{\mathrm{FD}}(\epsilon) = 1$ if $\epsilon < \epsilon_F$, and 0 if $\epsilon > \epsilon_F$ (the Fermi-Dirac distribution at zero temperature).

4.3.2 Entanglement Hamiltonian for a cylinder

Block-diagonalization of the correlation matrix. We consider a subsystem A in the form of a cylinder $l_x \times L_y$. This geometry enables us to use the translational invariance along the y direction. In particular, it will be convenient not to work directly with the correlation matrix $(C_{\boldsymbol{r}\boldsymbol{r}'})_{\boldsymbol{r},\boldsymbol{r}'\in A}$, but to remain in Fourier space for the y direction. Defining

$$c_{x,k_y} = \frac{1}{\sqrt{L_y}} \sum_{y=1}^{L_y} e^{-ik_y y} c_{x,y} \ , \tag{4.69}$$

we have the correlation matrix

$$\begin{aligned}\langle c^\dagger_{x,k_y} c_{x',k'_y}\rangle &= \frac{1}{L_x}\sum_{k_x,k'_x=1}^{L_x} e^{-i(k_x x - k'_x x')} \underbrace{\langle c^\dagger_{k_x,k_y} c_{k'_x,k'_y}\rangle}_{\delta_{k_x,k'_x}\delta_{k_y,k'_y} f_{\mathrm{FD}}(\epsilon_{\boldsymbol{k}})} \\ &= \delta_{k_y,k'_y}\frac{1}{L_x}\sum_{k_x} e^{-ik_x(x-x')} f_{\mathrm{FD}}(\epsilon_{\boldsymbol{k}}) \\ &\equiv \delta_{k_y,k'_y} C_{xx'}(k_y)\ . \end{aligned} \tag{4.70}$$

This calculation shows that the correlation matrix is block-diagonal with respect to the k_y index. Since the subsystem A is also translationally invariant in the y direction (having the geometry of a cylinder), the same holds for the correlation matrix restricted to sites in A. To diagonalize it, and thereby gain access to the entanglement properties (see Section 4.1 and 4.2 for more details), we can then just work in each k_y sector successively, in which we diagonalize the matrix

$$[C_{xx'}(k_y)]_{xx'\in A}\ . \tag{4.71}$$

Moreover, one sees that in each k_y sector, the correlation matrix is *exactly* the correlation matrix for a $1d$ system of free fermions, Eq. (4.41), although with a k_y-dependent chemical potential

$$\mu(k_y) \equiv 2J\cos[k_F(k_y)] = 2J\cos k_y + \mu\ , \tag{4.72}$$

where we introduced the k_y-dependent Fermi wavevector $k_F(k_y)$ (which we choose between 0 and π for convenience).

Entanglement Hamiltonian. We thus realize that all the analyses we have made on the entanglement structure in $1d$ in Section 4.2 can just be repeated here in each k_y sector. Note that we also have a k_y-dependent Fermi velocity

$$v_F(k_y) = 2J\sin[k_F(k_y)]\ , \tag{4.73}$$

which plays an important role for the entanglement properties, as the prefactor of the entanglement temperature, see for instance Eq. (4.59). In particular, we expect that the entanglement Hamiltonian is very well approximated by

$$\mathcal{H}_A^{\mathrm{Ansatz}} = \sum_{k_y=1}^{L_y} \mathcal{H}_A^{\mathrm{LET}}(k_y) \tag{4.74}$$

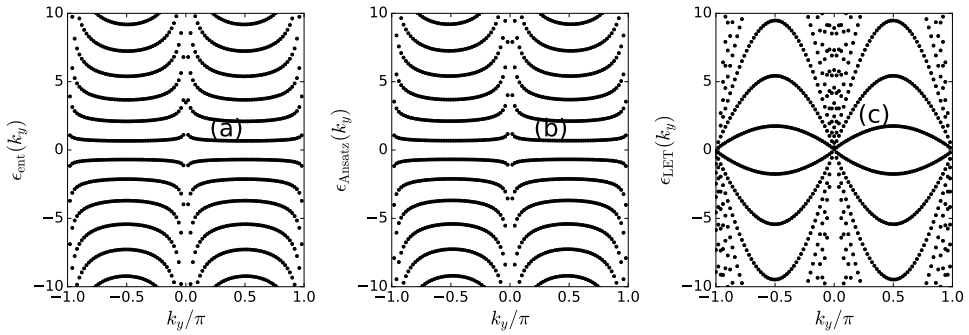

Figure 4.4: Entanglement spectrum for free fermions in $d = 2$. A is a 100×100 cylinder in a 100×10^4 torus, and $\mu/J = 0$. (a) Entanglement spectrum; (b) Spectrum of the Hamiltonian Eq. (4.75); (c) Spectrum of the LET Hamiltonian, Eq. (4.78) (namely the same as in (b), but with a k_y-independent Fermi velocity, see text).

where the one-body entanglement Hamiltonian in the k_y sector is given by Eq. (4.42), which we repeat here for completeness:

$$\begin{aligned} \mathcal{H}_A^{\rm LET}(k_y) &= -\frac{2\pi}{v_F(k_y)} J \sum_{x=1}^{l-1} \beta_{x,x+1} (c^\dagger_{k_y,x} c_{k_y,x+1} + c^\dagger_{k_y,x+1} c_{k_y,x}) \\ &\quad -\frac{2\pi}{v_F} \mu(k_y) \sum_{x=1}^{l} \beta_x \mu c^\dagger_{k_y,x} c_{k_y,x} \end{aligned} \tag{4.75}$$

where the β coefficients are given by

$$\beta_x = (x - 1/2)\left(1 - \frac{x - 1/2}{l_x}\right) \tag{4.76}$$

$$\beta_{x,x+1} = x(1 - x/l_x)\,. \tag{4.77}$$

We know that the eigenfunctions of $h_A^{\rm LET}(k_y)$ are exactly the eigenfunctions of the one-body entanglement Hamiltonian (this is just the same argument as in $1d$, see the discussion after Eq. (4.41)), and we expect that their spectrum are very similar, since in each k_y sector we have a $1d$ free fermion gas, for which we have already noticed how similar the entanglement spectrum and the spectrum of the Ansatz Hamiltonian are (see for instance Fig. 4.1).

Entanglement spectrum. As illustrated on Fig. 4.4(b), the spectrum of $h_A^{\rm LET}(k_y)$ indeed reproduces closely the exact entanglement spectrum, Fig. 4.4(a). For comparison, we have plotted on Fig. 4.4(c) the spectrum of the LET Ansatz Hamiltonian we

could have proposed to describe the entanglement properties

$$\mathcal{H}_{\rm LET} = -\frac{2\pi}{v_F^{\rm eff}} \sum_{x=1}^{l_x} \sum_{y=1}^{L_y} c^\dagger_{x,y} \left[J(\beta_x c_{x,y+1} + \beta_x c_{x,y-1} + \right. \\ \left. \beta_{x-1,x} c_{x-1,y} + \beta_{x,x+1} c_{x+1,y}) + \beta_x \mu c_{x,y} \right] , \tag{4.78}$$

where $v_F^{\rm eff}$ is some effective Fermi velocity, chosen in such a way that the entanglement entropy of $\mathcal{H}_{\rm LET}$ at temperature 1 equals the entanglement entropy of A. Clearly, Fig. 4.4(c) shows that this LET Ansatz completely misses the structure of the entanglement spectrum. Indeed, there is no reason to expect that the LET Ansatz of Eq. (4.78) is a good approximation to the entanglement Hamiltonian, since such an Ansatz is motivated by the Bisognano-Wichmann theorem (see Section 3.3.2) which relies on the hypothesis of Lorentz invariance. However, contrary to the $1d$ case, the $2d$ free fermion gas is *not* Lorentz invariant at low energy. For instance there is not a single Fermi velocity, but a different one at each point of the Fermi surface. And, as we just showed, it is a much better approximation to consider the $2d$ free fermion gas as a collection of $1d$ systems, each being Lorentz invariant (and even conformally invariant) at low energy, and each having its own Fermi velocity. It would be interesting to generalize this picture to arbitrary geometries for the subsystem A, and propose a more general Ansatz entanglement Hamiltonian. This perspective resonates with the arguments of Swingle (2010), who proposed an interpretation of the entanglement entropy of free-fermion systems as an integral over the Fermi surface of a collection of $1d$ systems. We leave this question open to future studies.

4.3.3 Local entanglement temperature for $2d$ free fermions

Despite the fact that one cannot approximate the entanglement Hamiltonian by the physical Hamiltonian modulated in space by a unique entanglement temperature (instead, one has a different entanglement temperature in each k_y sector, proportional to the k_y-dependent Fermi velocity $v_F(k_y)$), the thermodynamic relations among the contours continue to hold. This is illustrated on Fig. 4.5. Panel (a) shows the contours of entanglement, density fluctuations and imbalance fluctuations (see Section 4.2 for definitions), and panel (b) shows the entropy density, and the structure factor at $\boldsymbol{k} = (0,0)$ and $\boldsymbol{k} = (\pi,\pi)$ as a function of temperature. The validity of the local entanglement temperature hypothesis is illustrated on panel (c), where we have extracted the local temperature for the three contours of panel (a), using the temperature dependence of the associated thermodynamic quantities of panel (b). The

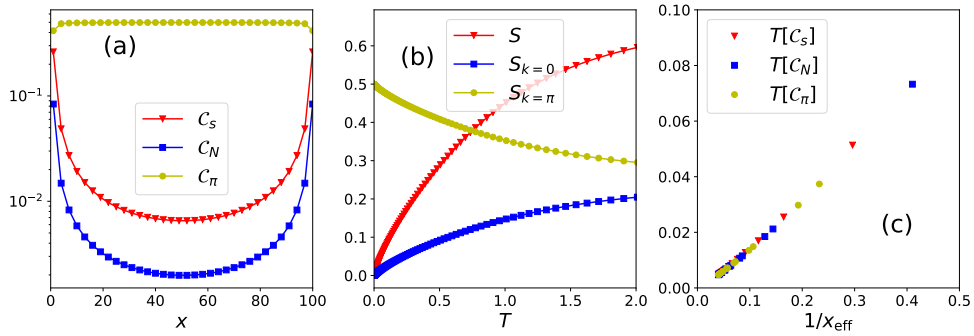

Figure 4.5: Local entanglement thermodynamics for $2d$ free fermions. A is a cylinder of size 100×100 in a torus of size 5000×100, and we worked at half-filling ($\mu = 0$). (a) Entanglement (red triangles), density (blue squares) and imbalance (yellow circles) contours as a function of position in subsystem A (see text). (b) Entropy density, structure factor at $\boldsymbol{k} = (0, 0)$ and at $\boldsymbol{k} = (\pi, \pi)$ as a function of temperature. Same symbols as for the corresponding contours in panel (a). (c) Local entanglement temperature extracted from the contours of panel (a), and the temperature dependency of the associated thermodynamic quantities of panel (b). Same symbols as for the contours on panel (a).

local temperature is plotted as a function of

$$\frac{1}{x_{\text{eff}}} = \frac{1}{x - 1/2} + \frac{1}{l - x + 1/2} \equiv \frac{1}{\beta_x} \tag{4.79}$$

where β_x has been defined in Eq. (4.77). The linear behavior of T as a function of $1/x_{\text{eff}}$ shows that the local temperature takes the form

$$T_{\text{eff}} = \frac{c_{\text{eff}}}{2\pi x_{\text{eff}}} \tag{4.80}$$

where c_{eff} is some effective Fermi velocity.

The fact that the three different ways to extract the local temperature are essentially equivalent shows that each of the three contours of panel (a), combined with the knowledge of the thermodynamic relations of panel (b), could be used to reconstruct the two others, and, presumably, the contour related to any other observable.

4.3.4 Discussion

The $2d$ free fermion case is thus an interesting situation where the local entanglement temperature hypothesis completely misses the structure of the entanglement spectrum (Fig. 4.4), but correctly predicts the thermodynamic relations observed among the contours (Fig. 4.5), showing that the two things need not be related.

The validity of the local thermodynamic relations between the contours in the $2d$ free fermion gas could have been anticipated. In fact, if the subsystem A is a cylinder,

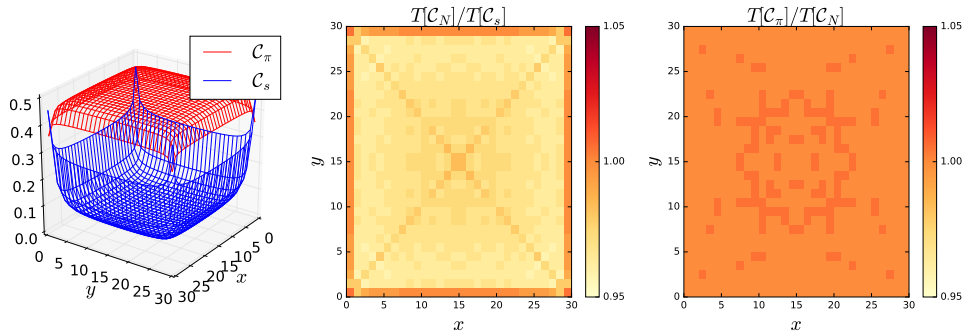

Figure 4.6: Local entanglement thermodynamics for $2d$ free fermions. A is a square of size 30×30 in a torus of size 1500×1500, and we worked at half-filling ($\mu = 0$). (a) Entanglement (blue) and imbalance (red) contours as a function of the position (x, y) in subsystem A. (b) Ratio of the local temperature extracted from the density contour to the one extracted from the entanglement contour. (c) Ratio of the local temperature extracted from the imbalance contour to the one extracted from the density contour.

we have seen that the reduced density matrix describes a collection of independent $1d$ free fermion gases, each having its own Fermi velocity $v_F(k_y)$. In this case, the contours take the form

$$\mathcal{C} = \sum_{k_y} \mathcal{C}(k_y) \, . \tag{4.81}$$

Since at low entanglement temperature, the contours depend *linearly* on each other, reflecting the fact that the associated thermodynamic quantities depend linearly on temperature [see, for instance, Fig. 4.2(b)], the k_y-sector contributions to the contours are related linearly to each other (at least in the bulk of A, where the entanglement temperature goes to zero). But a sum of linear dependences gives also rise to a linear dependence. Hence, the thermodynamic relations between the contours holds also in $2d$, inherited from the same relations being valid in $1d$. Nonetheless, we emphasize that the thermodynamic relations among the contours seem to hold for arbitrary shapes. For instance, on Fig. 4.6 we have plotted the contours for a square subsystem. In this case, we cannot invoke the translational invariance to reduce the problem to that of a collection of independent $1d$ Fermi gases. However, the local temperatures extracted from the entanglement, density or imbalance contours are the same within 5% [panels (b), (c)].

The robustness of the thermodynamic relations among the contours for gapless free fermions can be understood in the following manner. Let us postulate that the entanglement Hamiltonian has the form

$$\mathcal{H}_E = \sum_i \mathcal{H}_i \tag{4.82}$$

where $\mathcal{H}_i$ is a free fermion Hamiltonian consisting of hopping between sites in the vicinity of i. Then, according to the local equilibrium approximation, the entanglement contour and density-fluctuations contour are approximately given by

$$\mathcal{C}_s \approx s(\mathcal{H}_i) \quad ; \quad \mathcal{C}_N \approx \langle \delta^2 N \rangle (\mathcal{H}_i)/V \ . \tag{4.83}$$

Then, if $\mathcal{H}_i$ corresponds to a gapless free-fermion Hamiltonian, we know that

$$\mathcal{C}_s \approx \frac{\pi^2}{3} \mathcal{C}_N \tag{4.84}$$

regardless of the microscopic details. For the imbalance-fluctuation contour, we do not know the general relation between S and $\langle \delta^2 N_{\text{stagg}} \rangle$, but such a general relation presumably exists in order to explain the robustness of the relations among the contours.

4.4 Conclusion on free fermions models

In this chapter, we have investigated the spatial structure of entanglement in simple gapless free fermion (FF) models in $d = 1$ and $d = 2$, and we have done so from the perspective of the local entanglement temperature (LET) hypothesis introduced in Section 3.3.2. We have distinguished two levels of interpretation regarding the LET hypothesis: 1) as an Ansatz for the entanglement Hamiltonian, represented by Eq. (3.36); and 2) as a set of relations among the contours. On general grounds, 2) may be viewed as a consequence of 1) through the local equilibrium approximation (LEA, see Section 3.3.3). For FF in $d = 1$, we showed that both 1) and 2) are valid, but we also showed that the LEA should not be expected to be correct *a priori*, so that the validity of 2) does not appears as a trivial consequence of 1). In passing, we emphasized that not only the structure of the entanglement Hamiltonian is important, but also the fact that it is evaluated at a very specific temperature: for instance, Fig. 4.3 shows that only at that temperature, the density is homogeneous.

FF in $d = 2$ represent a surprising example where the LET Ansatz for the entanglement Hamiltonian completely misses its actual structure, but where the relationships among the contours continue to hold. It appears desirable to deepen our understanding in $d = 2$. One could, inspired for instance by the explanation of Swingle (2010) of the behavior of entanglement entropy, propose a generalization of the Ansatz of Eq. (4.75) for the entanglement Hamiltonian, to arbitrary shapes of the subsystem A, and propose an explanation for the validity of 2) based on the form of this Ansatz.

Consequence for the experimental study of entanglement in equilibrium many-body systems. The general expectation concerning FF models, is that all the information about the structure of entanglement is essentially contained in the density correlations. To study entanglement itself is not expected to provide any new fundamental insight into these simple models, beyond the one provided by standard observables. Indeed, from density-fluctuation contours (measurable with quantum gas microscopes (Bakr et al., 2009; Preiss et al., 2015; Preiss, 2015)), one can extract the local entanglement temperature T_i, and hence the entanglement contour via

$$\mathcal{C}_s(i) = s(T_i) \tag{4.85}$$

with $s(T)$ the thermal entropy density.

Possible extensions. Besides conducting similar studies on more complex free-fermion models, it could also be interesting to develop a similar understanding of the relationship between entanglement and fluctuations during the unitary dynamics following a quantum quench. In the simplest examples, one expects the dynamics of the fluctuation contours to closely follow the dynamics of the entanglement contours, as studied by Chen and Vidal (2014).

Experimental relevance of free-fermion models. In this chapter, fermions were supposed without interactions. In fact, the Pauli principle makes a system of fermions extremely robust to repulsive interactions. The theory developed by Landau (Nozieres and Pines, 1999) shows that a Fermi liquid is essentially a free fermion system, albeit with effective masses which may differ significantly from the masses of the original fermions. Furthermore, we tacitly assumed that the fermions were *spinless*. Of course, fermions have always a half-integer spin, but if interactions are neglected, a gas of multiple-spin-component free fermions may just be treated as a mixture of independent spinless-fermion systems. Furthermore, weak attraction among spin-1/2 fermions can lead to superconductivity through pairing, but we have not considered this possibility. In Chapters 5, 6 and 7, we shall instead consider the similar — though not identical — phenomenon of superfluidity for weakly repulsive bosons. We also know that strong interactions among spin-1/2 fermions on a lattice may drive a phase transition from the metallic phase to a so-called Mott-insulating (MI) phase. We have completely neglected this possibility in our study of free fermion systems of Section 4. In fact, the very understanding of the phase diagram of interacting spinful fermions on a lattice is considered one of the most difficult open problems of theoretical condensed matter. In recent years, great experimental effort has been devoted to build cold-atom experiments simulating the behavior of spin-1/2 band electrons in solids, and

promising results concerning the observation of antiferromagnetic ordering in the MI phase have been reported (Parsons et al., 2016; Boll et al., 2016).

Chapter 5

Slave-boson approach to the Bose-Hubbard model

Introduction. In Chapter 4, we have explored various aspects of the local entanglement temperature (LET) hypothesis on free-fermion lattice systems. We have in particular introduced the concept of *contours* as central quantities to develop a thermodynamic understanding of the structure of entanglement in many-body ground states: the relations between the contours of different observables reflect the thermodynamic relations between the corresponding observables at thermal equilibrium. In $1d$, we have also shown that the entanglement Hamiltonian is very well approximated by a LET Ansatz, namely, as the physical Hamiltonian modulated in space by a local temperature, and that this local temperature is precisely the origin of the thermodynamic relations among the contours (Section 4.2). In the present chapter and the following Chapters 6 and 7, we continue our study and focus on bosonic particles on a lattice, inspired by cold-atom experiments realizing the Bose-Hubbard model (Bloch, Dalibard, and Zwerger, 2008). In particular, such experiments realize the bosonic analog of the interaction-induced phase transition from a superfluid to a Mott insulator, as first reported by Greiner et al. (2002). In the remainder of this Chapter, we present a powerful quasiparticle approach (the slave-boson approach) to the study of the Bose-Hubbard model. By doing so, we shall set the context and discuss the technical details necessary to conduct the study of the entanglement structure in the superfluid phase (Chapters 6) and across the superfluid-insulator phase transition (Chapter 7).

5.1 The Bose-Hubbard model

In this section, we introduce the Bose-Hubbard (BH) model describing interacting bosons on a lattice (Fisher et al., 1989; Bloch, Dalibard, and Zwerger, 2008).

For a recent experimental investigation of the entanglement structure in Bose-Hubbard systems, see the thesis of Preiss (2015).

The Hamiltonian describing interacting bosons on a lattice contains two parts. The first part is the one-body (kinetic) Hamiltonian

$$\mathcal{H}_{\text{kin}} = -\sum_{i,j} t_{ij} b_i^\dagger b_j \tag{5.1}$$

where $t_{ij} = t_{ji}^*$ is the hopping matrix. b_i, b_j are bosonic operators satisfying the commutation relations $[b_i, b_j] = 0$ and $[b_i, b_j^\dagger] = \delta_{ij}$. If the only hopping mechanism is between nearest-neighbor sites, $t_{ij} = t$ if i and j are nearest-neighbors, and 0 otherwise. We shall mainly focus on this situation, although the slave-boson treatment is valid for an arbitrary hopping matrix. In experiments, there is always an external confining potential V_i. We neglect this term here, and focus on a homogeneous system with periodic boundary conditions (PBC). If the system contains N noninteracting bosons, the ground state of $\mathcal{H}_{\text{kin}}$ is a Bose-Einstein condensate (BEC) containing all atoms in the one-particle ground-state (the lowest-energy wavefunction of the matrix $-t_{ij}$). The perfect BEC is unstable to arbitrarily weak attractive interactions. Therefore, we focus on repulsive interactions. For simplicity, we neglect interactions between bosons when they are on different sites. When two bosons are on the same site, the energy cost is denoted U, so that the interaction term is

$$\mathcal{H}_{\text{int}} = U \sum_i \frac{n_i(n_i - 1)}{2} \tag{5.2}$$

where $n_i = b_i^\dagger b_i$ is the number of bosons on site i. The factor $\frac{n_i(n_i-1)}{2} = \binom{n_i}{2}$ simply counts the number of pairs of bosons on site i, each pair contributing an interaction energy U. The Bose-Hubbard Hamiltonian is the sum of the kinetic and interaction Hamiltonians

$$\mathcal{H}_{\text{BH}} = \mathcal{H}_{\text{kinetic}} + \mathcal{H}_{\text{int}} \,. \tag{5.3}$$

If the number N of bosons is incommensurate with the number V of sites (namely, if the density $\langle n \rangle = N/V$ is not an integer), the system is always a superfluid condensate (throughout this thesis, we use the concepts of condensation and of superfluidity interchangeably, as they coincide for the models of our interest). This includes the weak-interaction limit, accurately described by Bogoliubov theory (Pitaevskii and

Stringari, 2003), and the hardcore limit, accurately described by a semi-classical approach after a mapping to an equivalent XY spin model (Coletta, Laflorencie, and Mila, 2012). If the density is an integer, a sufficiently strong interaction is always able to destroy the superfluidity, driving the system towards a Mott insulating phase (Fisher et al., 1989; Greiner et al., 2002). This phase transition is driven by the ratio t/U of the kinetic to interaction energy: the kinetic part favors the delocalization of the particles across the lattice (if the density is an integer, this implies that several bosons must be allowed to occupy the same lattice site), while the interaction part favors configurations where all sites contain as few bosons as allowed by the filling. If t/U is very small, local fluctuations of the number of bosons per site become too expensive energetically, and superfluidity, which requires the coherent delocalization of the bosons all across the lattice, is destroyed.

For theoretical purposes, it is more convenient to work at fixed chemical potential rather than at fixed density, because the chemical potential appears explicitly as a Hamiltonian parameter. The grand-canonical Hamiltonian takes the form

$$\mathcal{H}_{\mathrm{BH}} = -\sum_{i,j} t_{ij} b_i^\dagger b_j + \sum_i \left(U \frac{n_i(n_i-1)}{2} - \mu n_i \right) . \tag{5.4}$$

The many-body ground-state is the state of minimal energy of $\mathcal{H}_{\mathrm{BH}}$. No exact solution for this many-body ground state is known in general, and we have to resort to either numerical approaches, or to approximate calculations. In $d = 1$, density-matrix renormalization-group techniques (DMRG) provide a very efficient numerical approach to low-energy properties, but DMRG becomes problematic in dimensions $d \geq 2$ (see, however, Alba, Haque, and Läuchli (2013) for a DMRG study of the entanglement spectrum in the ground state of the Bose-Hubbard model on cylindrical geometries). In the following, we describe a semi-classical approach valid across the whole phase diagram in $d = 2, 3$, which consists of 1) finding the mean-field ground state (Section 5.2); and 2) building an effective quadratic Hamiltonian for quantum fluctuations around the mean-field solution (the so-called *slave-boson* approach, Section 5.3).

5.2 Mean-field phase diagram: the Gutzwiller approach

5.2.1 Mean-field Hamiltonian

The Gutzwiller mean-field (MF) approach to bosonic systems amounts to neglecting correlations between different sites. This is usually a good approximation as long

as the correlations are small in comparison to the average values. Considering two operators A and B, we may write

$$AB = A\langle B\rangle + \langle A\rangle B - \langle A\rangle\langle B\rangle + \underbrace{[A - \langle A\rangle]\,[B - \langle B\rangle]}_{\text{neglected at the MF level}} , \tag{5.5}$$

where we may neglect the correlation term if

$$\langle [A - \langle A\rangle]\,[B - \langle B\rangle]\rangle \ll \langle A\rangle\langle B\rangle . \tag{5.6}$$

This is equivalent to the following approximation

$$\langle AB\rangle \approx \langle A\rangle\langle B\rangle . \tag{5.7}$$

The MF approach to the BH Hamiltonian of Eq. (5.4) consists in neglecting all correlations among different lattice sites, while the local part of the Hamiltonian (containing the interaction term and the chemical potential term) is treated exactly. Introducing the notation

$$\phi_i = \langle b_i\rangle , \tag{5.8}$$

the kinetic part of $\mathcal{H}_{\rm BH}$ is then approximated as

$$\mathcal{H}_{\rm kin}^{\rm MF} = -\sum_{i,j} t_{ij}(\phi_j b_i^\dagger + \phi_i^* b_j - \phi_i^*\phi_j) \tag{5.9}$$

$$= -\sum_i \left(\sum_j t_{ij}\phi_j b_i^\dagger + \text{h.c.}\right) + \sum_{i,j} t_{ij}\phi_i^*\phi_j \tag{5.10}$$

where we used the fact that $t_{ij} = t_{ji}^*$. Finally, we see that, at the mean-field level of approximation, the BH Hamiltonian is a sum of local Hamiltonians

$$\mathcal{H}_{\rm BH}^{\rm MF} = \sum_i \left(b_i^\dagger \sum_j (-t_{ij}\phi_j) + \text{h.c.} + \frac{U}{2} n_i(n_i - 1) - \mu n_i \right) + \sum_{i,j} t_{ij}\phi_i^*\phi_j . \tag{5.11}$$

The MF ground state is then found by minimizing the energy of $\mathcal{H}_{\rm BH}^{\rm MF}$. This must be done self-consistently, since the MF Hamiltonian depends itself implicitly on the MF ground state through $\phi_i = \langle b_i\rangle$. As the Hamiltonian $\mathcal{H}_{\rm BH}^{\rm MF}$ is a sum of local terms, its ground state is a product state

$$|\Psi_{\rm MF}\rangle = \otimes_i |\psi_0\rangle_i . \tag{5.12}$$

The Hilbert space on site i is generated by the Fock states $|n\rangle_i$, corresponding to n bosons on site i: $b_i|n\rangle_i = \sqrt{n}|n-1\rangle_i$. In this basis, the local states may be written as

$$|\psi_0\rangle_i = \sum_{n\geq 0} c_n(i)|n\rangle_i \tag{5.13}$$

where $c_n(i)$ are complex numbers. For numerical purposes, we impose a maximal number of bosons per site $n_{\max} \gg \langle n \rangle$, which must be chosen much larger than the average density in order to keep the truncation error as small as possible. In practice, if the average density is around one boson per site, $n_{\max} = 5 - 6$ is sufficient. Normalization of $|\psi\rangle_i$ imposes that $\sum_{n=0}^{n_{\max}} |c_n(i)|^2 = 1$.

Finding the MF ground state amounts to minimize the MF variational energy

$$E_{\mathrm{MF}} = \langle \Psi_{\mathrm{MF}} | \mathcal{H}_{\mathrm{BH}} | \Psi_{\mathrm{MF}} \rangle = \langle \Psi_{\mathrm{MF}} | \mathcal{H}_{\mathrm{BH}}^{\mathrm{MF}} | \Psi_{\mathrm{MF}} \rangle \, , \tag{5.14}$$

which is a quartic function of the $c_n(i)$ coefficients. Such a minimization is formally equivalent to finding the self-consistent ground states of the local Hamiltonians

$$\mathcal{H}_i^{\mathrm{MF}} = - \left[\left(\sum_j (t_{ij} \phi_j \right) b_i^\dagger + \mathrm{h.c.} \right] + \frac{U}{2} n_i (n_i - 1) - \mu n_i \, , \tag{5.15}$$

whose expression depends in turn on the ground state via the ϕ_j coefficients.

Iterative algorithm. A practical way to find the MF ground state is to make use of an iterative algorithm:

0) choose randomly the coefficients $c_n(i)$ on each site i;

1) calculate

$$\phi_i = \langle b_i \rangle = \sum_n c_{n-1}(i)^* \sqrt{n} c_n(i) \tag{5.16}$$

on every site and form the MF Hamiltonian, Eq. (5.15);

2) find the ground state of the MF Hamiltonian on every site;

and iterate 1) and 2) up to convergence, by using the ground state found at 2) as the input to calculate ϕ_i in 1). One can devise many variants of this algorithm. For instance, it may be more convenient to perform "local updates" on the MF trial ground state instead of the "global update" we have described, namely, to update the parameters ϕ_i of step 1 after each calculation of the ground state (step 2) on a given site, before moving to step 2 on a neighboring site. In general, it is always wiser to try several ways to iterate the procedure, and to repeat the iterative process by starting from different initial states at step 0). A strong dependence on the initial state of the ground state after convergence may be caused by frustration, inducing metastable states. This possibility has been reported in the presence of long-range interactions between the bosons, see for instance the devoted chapter in the book of Lewenstein, Sanpera, and Ahufinger (2012). In our case, this phenomenology does not occur.

Simplified procedure for homogeneous systems. We shall be mainly concerned with homogeneous systems. In this case, we may considerably simplify the minimization procedure by assuming from step 0) that the MF ground state is translationally invariant

$$\forall i \; c_n(i) = c_n \; . \tag{5.17}$$

As a consequence, assuming that t_{ij} allows hopping to neighboring sites only with a hopping amplitude t, and denoting z the number of neighbors ($= 2d$ in a square or cubic lattice, d being the dimension), the local MF Hamiltonian on site i is

$$\mathcal{H}_i^{\mathrm{MF}} = -(zt\phi b_i^\dagger + \mathrm{h.c.}) + \frac{U}{2} n_i(n_i - 1) - \mu n_i + zt|\phi|^2 \; , \tag{5.18}$$

with $\phi = \langle b_i \rangle$. The minimization procedure, [steps 0), 1), 2)], can thus be performed self-consistently on a single site.

5.2.2 Signature of condensation

Condensation manifests itself in a nonzero condensed fraction. This criterion is equivalent to the presence of so-called off-diagonal long-range order (Penrose and Onsager, 1956; Yang, 1962; Anderson, 1966)

$$\langle b_i^\dagger b_j \rangle \underset{|i-j| \to \infty}{\approx} \phi_i^* \phi_j \neq 0 \tag{5.19}$$

where ϕ_i is the so-called "macroscopic wavefunction". At the MF level of approximation, this is equivalent to the simple criterion

$$\phi \neq 0 \; . \tag{5.20}$$

On the other hand, the Mott-insulating phase corresponds to a MF ground state with an integer number of bosons per site: $|\psi\rangle = |n\rangle$, for which $\langle b \rangle$ is zero. At the MF level of approximation, the average value of the bosonic field $\phi = \langle b \rangle$ thus plays the role of an order parameter for the superfluid-to-insulator phase transition.

5.2.3 Phase diagram

The ground-state phase diagram of the BH model, obtained by the procedure we have described[1], is plotted on Fig 5.1. It contains a superfluid (SF) region, where $\phi \neq 0$, and where the number of particles on each site fluctuates; and Mott-insulating (MI) lobes of integer density, where the number of particles at each site is fixed, and where $\phi = 0$. If

[1] In fact, the boundaries of the phase diagram at the mean-field level can be determined exactly, see Section 7.1.

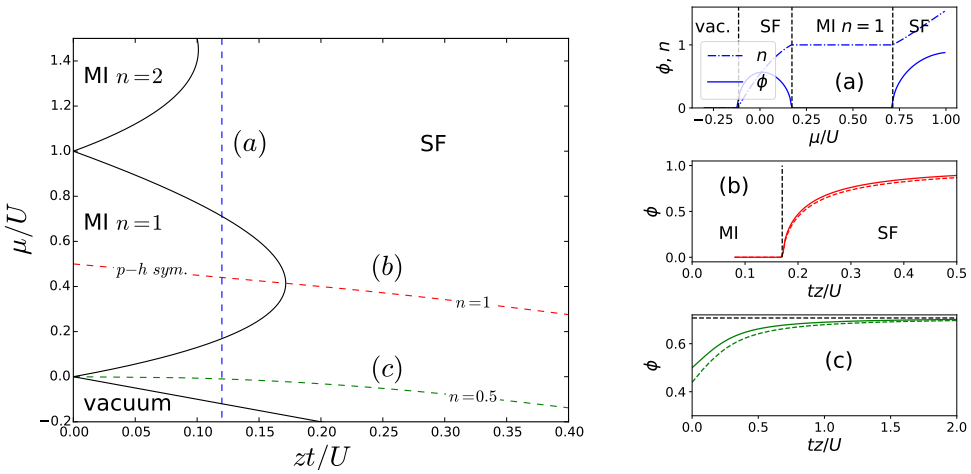

Figure 5.1: Left: Mean-field phase diagram of the Bose-Hubbard model. Outside the lobes, the phase is superfluid (SF), while inside the lobes, the phase is a Mott-insulator (MI). Dashed lines denoted (a), (b), and (c) indicate the lines along which the SF order parameter ϕ is plotted on panels (a), (b), and (c). (a) Density (dashed-dotted line) and SF order parameter ϕ (solid line) along the line $tz/U = 0.12$. (b) SF order parameter along the line of density $n = 1$. Solid line: MF prediction. Dashed lines: MF prediction renormalized by quantum fluctuations calculated within the slave-boson approach in $d = 2$ (see Section 5.3). (c) SF order parameter along the line of density $n = 0.5$. Same symbols as in panel (a). The horizontal dashed line indicates $\phi = \sqrt{0.5}$, corresponding to a coherent state of density $n = 0.5$.

$\mu < \epsilon_{\min}$, where $\epsilon_{\min}$ is the minimal single-particle energy (the minimal eigenvalue of the matrix $-t_{ij}$), the system is empty of particles. Here, on the square or cubic lattice, $\epsilon_{\boldsymbol{k}} = -2t \sum_{a=1}^{d} \cos k_a$, so that $\epsilon_{\min} = \epsilon_0 = -zt$ with $z = 2d$. So for $\mu < -zt$, the system is in the vacuum. As shown on Fig. 5.1(a,b), the SF order parameter ϕ vanishes continuously at the SF / MI phase transition, indicating that the transition is of second order. The MF approximation predicts the same type of transition along the critical line. Nonetheless, the transitions at the tips of the lobes (going beyond the MF approximation), which occur at fixed density, are predicted to belong to a different universality class than at a generic point of the phase boundary (Fisher et al., 1989). The generic transition is accompanied with a change of density, as shown on Fig. 5.1(a) (solid line). On the other hand, if the density is fixed at some noninteger value, the system is always superfluid. This is shown on Fig. 5.1(c), where we plot ϕ for a density of $n = 1/2$. In the limit of weak interactions, $t/U \to \infty$, the mean-field ground state is a coherent state, $|\psi\rangle \propto \exp\left(-\phi b^\dagger\right)|0\rangle$, with $|\phi^2| = \langle n \rangle$. In the opposite (hardcore) limit $t/U \to 0$, the system may be mapped to a XY spin-1/2 model, and the mean-field ground state is a factorized state of $s = 1/2$ spins, whose Bloch vectors

correspond to the orientation of classical spins minimizing the classical limit ($s \to \infty$) of the Hamiltonian. For $n = 1/2$, this classical ground state is a spin-1/2 lying in the XY plane, for instance $\psi = (|0\rangle + |1\rangle)/\sqrt{2}$, for which $\phi = 1/2$ (see Section 6.1). On Fig. 5.1(b,c), we have also plotted the SF order parameter $\langle b \rangle$ renormalized by quantum fluctuations, calculated within the slave-boson approximation described in the next section. We find that the quantum fluctuations always reduce the superfluid order, but are not strong enough to destroy it. As a consequence, the phase transition line within the slave-boson approach conicides with the MF solution. In contrast to these results, an exact calculation would show that the MI lobes are larger than predicted by the MF approximation, which underestimates the ability of quantum fluctuations to destabilize the SF phase.

5.3 Quantum fluctuations around the mean-field solution: the slave-boson approach

In this subsection, the so-called slave-boson (SB) approach is introduced in full generality. Although our focus is on the Bose-Hubbard model, the treatment applies to arbitrary bosonic and/or spin Hamiltonians: whenever the Gutzwiller mean-field (MF) is a good starting point, the SB approach represents a systematic way to introduce quantum fluctuations around the MF solution in the form of an effective quadratic Hamiltonian for bosonic quasiparticles. We then specify the general approach to the uniform Bose-Hubbard model; finally, the self-consistency of the SB approach across the whole phase diagram, including the critical points, is verified.

5.3.1 Slave-boson approach

Introduction. The MF approximation, although providing invaluable insight into the structure of the ground state, completely neglects correlations. In particular, it is impossible by construction to study the structure of entanglement within the MF approximation. It is however possible to add small quantum fluctuations around the MF solution, which enables us to access the entanglement content of the ground state at a minimal computational cost. The SB technique is an approximate, yet very convenient, method, because it incorporates quantum fluctuations as *gaussian* fluctuations, and therefore all the machinery of Wick's theorem may be applied. In essence, the SB technique is a semi-classical method, very similar to the Bogoliubov approach to weakly interacting bosons (Pitaevskii and Stringari, 2003), to the Holstein-Primakoff approach to spin models (which may be applied in the hardcore limit of the Bose-Hubbard model, see Coletta, Laflorencie, and Mila (2012)), or to the so-called random

phase approximation which may be applied for $\phi \ll 1$ (Sengupta and Dupuis, 2005). In fact the slave-boson approach is completely equivalent to the above-mentioned semi-classical treatments in their respective domains of applicability. As the SB technique turns out to be more general that these similar approximation schemes, we shall not describe them, and focus on the SB technique only. We might however, in passing, mention the relationship between the results obtained within the slave-boson approximation, and the results obtained with these other methods. The SB approach (sometimes called "Schwinger bosons approach") is already known in the literature (Frésard, 1994; Altman and Auerbach, 2002; Dickerscheid et al., 2003; Altman et al., 2003; Huber et al., 2007; Pekker et al., 2012; Huerga, Dukelsky, and Scuseria, 2013), but had not been used previously to study the structure of entanglement.

SB approach: extending the physical Hilbert space. The SB approach is three-fold.

1) On each site i of the lattice, we attach to each state $|n\rangle_i$ a fictitious ("slave") bosonic particle of "flavor" n. This amounts to introduce a bosonic operator $\beta_{i,n}$ for each n, on every site i. These slave-boson (SB) operators satisfy the usual bosonic commutation relations, and SB operators associated to different flavors n or to different sites i commute

$$\left[\beta_{i,n}, \beta_{i',n'}\right] = 0 \tag{5.21}$$
$$\left[\beta_{i,n}, \beta^\dagger_{i',n'}\right] = \delta_{i,i'}\delta_{n,n'} \, . \tag{5.22}$$

Each site is equipped with fictitious Fock spaces generated by the application of $\beta^\dagger_{i,n}$'s operators on a fictitious vacuum state $|\emptyset\rangle$. The state $|n\rangle_i$ of the physical Fock space corresponds to the state containing exactly one slave-boson of flavor n

$$|n\rangle_i = \beta^\dagger_{i,n}|\emptyset\rangle \, . \tag{5.23}$$

Higher occupations of this slave-boson mode i, n are unphysical. An arbitrary state $|\psi\rangle_i$ of the local (physical) Hilbert space may be created out of the slave-boson vacuum in a similar manner

$$|\psi\rangle_i = \sum_n c_n(i)|n\rangle_i = \sum_n c_n(i)\beta^\dagger_{i,n}|\emptyset\rangle \tag{5.24}$$

The local SB Hilbert space contains many unphysical states. In fact, only those states which may be written as in Eq. (5.24) are physical. In order to restrict the accessible SB Hilbert space to those, and only those states which belong to the

physical Hilbert space, we must add the following constraint

$$\sum_n \beta^\dagger_{i,n}\beta_{i,n} = 1 \; \forall i \; . \tag{5.25}$$

In other words, the physical states are exactly those which contain one slave-boson per site, possibly delocalized over the different flavors.

2) The key physical idea is then to assume that the true ground state is very close to the MF ground state. In the SB language, this amounts to postulate that on each site the population of SB corresponding to the MF flavor

$$\gamma^\dagger_{i,0} = \sum_n U_{n,0}(i)\beta^\dagger_{i,n} \tag{5.26}$$

is very close to one. Populations of flavors orthogonal to the MF one may thus be treated as perturbations.

To formulate this idea, we first rotate the local basis $|n\rangle_i$ to the basis which diagonalizes the MF Hamiltonian, Eq. (5.15) (in general, the rotation is site-dependent, although in our case it turns out to be the same on every site):

$$\mathcal{H}_i^{\rm MF} = U(i)E(i)U(i)^\dagger \tag{5.27}$$

where $E(i) = \mathrm{diag}(\epsilon_0(i), \ldots \epsilon_{n_{\max}}(i))$ in increasing order, where $n_{\max}$ is the maximal number of physical bosons per site. The MF ground state corresponds to $\epsilon_0(i)$. The matrix $U(i)$ defines a local rotation to a new family of SB operators, denoted $\gamma_{i,\alpha}$

$$\gamma^\dagger_{i,\alpha} = \sum_n U_{n,\alpha}(i)\beta^\dagger_{i,n} \; . \tag{5.28}$$

The eigenstate of $\mathcal{H}_i^{\rm MF}$ of energy $\epsilon_\alpha(i)$ is created out of the SB vacuum by applying the SB operator $\gamma^\dagger_{i,\alpha}$. In terms of the γ's operators, the constraint of Eq. (5.25) takes the same form

$$\sum_\alpha \gamma^\dagger_{i,\alpha}\gamma_{i,\alpha} = 1 \; \forall i \; . \tag{5.29}$$

If the system remains close to the MF ground state, we may say that

$$\gamma^\dagger_{i,0}\gamma_{i,0} \;\; = \;\; 1 - s_i \tag{5.30}$$

$$s_i = \sum_{\alpha\geq 1} \gamma^\dagger_{i,\alpha}\gamma_{i,\alpha} \;\; \ll \;\; 1 \tag{5.31}$$

and therefore, when restricted to act on the true ground state

$$\gamma_{i,0}, \;\; \gamma^\dagger_{i,0} = 1 + O(\gamma^2_{\alpha>0}) \; . \tag{5.32}$$

where $O(\gamma^2_{\alpha>0})$ denotes terms of order two or higher in the operators $\gamma^{(\dagger)}_{i,\alpha}$ for $\alpha > 0$.

3) We then re-write the Bose-Hubbard Hamiltonian in terms of the SB γ's operators, use Eq. (5.30) to express $\gamma_{i,0}^{(\dagger)}$ in terms of the $\gamma_{i,\alpha\neq 0}^{(\dagger)}$ operators, and develop the Hamiltonian up to quadratic order in the $\gamma_{i,\alpha>0}^{(\dagger)}$ operators. At order 0, we recover the MF energy function. The order-1 term vanishes if the MF ground state is a minimum of the MF variational energy. The order-2 term describes the quantum dynamics of the slave-bosons, corresponding to weak perturbations to the MF containing the entanglement structure we are looking for. Being quadratic in the SB operators, the effective Hamiltonian can finally be diagonalized by a Bogoliubov transformation.

We now explain in more details the step 3).

Expression of an arbitrary operator in terms of the SB operators. We need to express operators acting on site i (in our case, $b_i^{(\dagger)}$ and n_i) in terms of the SB operators. Considering an arbitrary local operator $\hat{\mathcal{O}}_i$, it may be written as

$$\hat{\mathcal{O}}_i = \sum_{n,n'} {}_i\langle n|\hat{\mathcal{O}}_i|n'\rangle_i \beta_{i,n}^\dagger \beta_{i,n'} \tag{5.33}$$

$$= \boldsymbol{\beta}_i{}^\dagger \mathcal{O}_i \boldsymbol{\beta}_i \tag{5.34}$$

where we have introduced the vector notation

$$\boldsymbol{\beta}_i = (\beta_{i,0}, \ldots, \beta_{i,n_{\max}})^T \tag{5.35}$$

and where $\mathcal{O}_i$ is the matrix

$$(\mathcal{O}_i)_{nn'} = {}_i\langle n|\hat{\mathcal{O}}_i|n'\rangle_i \, . \tag{5.36}$$

Since we are working with the γ's operators, we shall use the form

$$\hat{\mathcal{O}}_i = \boldsymbol{\gamma}_i{}^\dagger \tilde{\mathcal{O}}_i \boldsymbol{\gamma}_i \tag{5.37}$$

where

$$\boldsymbol{\gamma}_i = U(i)^\dagger \boldsymbol{\beta}_i \tag{5.38}$$

$$\tilde{\mathcal{O}}_i = U(i)^\dagger \mathcal{O}_i U(i) \tag{5.39}$$

with $U(i)$ defined by Eq. (5.27). We then isolate the contribution of $\gamma_{i,0}^{(\dagger)}$, and use $\gamma_{i,0}^\dagger \gamma_{i,0} = 1 - \sum_{\alpha>0} \gamma_{i,\alpha}^\dagger \gamma_{i,\alpha}$.

$$\hat{\mathcal{O}}_i = (\tilde{\mathcal{O}}_i)_{00} \left(1 - \sum_{\alpha>0} \gamma_{i,\alpha}^\dagger \gamma_{i,\alpha}\right) + \sum_{\alpha>0} (\tilde{\mathcal{O}}_i)_{\alpha 0} \gamma_{i,\alpha}^\dagger \gamma_{i,0} + \sum_{\alpha>0} (\tilde{\mathcal{O}}_i)_{0\alpha} \gamma_{i,0}^\dagger \gamma_{i,\alpha}$$
$$+ \sum_{\alpha,\beta>0} (\tilde{\mathcal{O}}_i)_{\alpha,\beta} \gamma_{i,\alpha}^\dagger \gamma_{i,\beta} \, . \tag{5.40}$$

If the constraint (5.25) is exactly preserved, this last expression is exact. Then, we keep terms up to second order in the $\gamma^{(\dagger)}_{\alpha>0}$ operators. At this level of approximation, we may replace $\gamma^{(\dagger)}_{i,0}$ by 1, since they are already multiplied by terms of order 1. By doing so, one is neglecting terms of order 3 or higher. We finally obtain

$$\begin{aligned}\hat{\mathcal{O}}_i &= (\tilde{\mathcal{O}}_i)_{00} + \sum_{\alpha>0}\left[(\tilde{\mathcal{O}}_i)_{\alpha 0}\gamma^\dagger_{i,\alpha} + (\tilde{\mathcal{O}}_i)_{0\alpha}\gamma_{i,\alpha}\right] \\ &\quad + \sum_{\alpha,\beta>0}\left[(\tilde{\mathcal{O}}_i)_{\alpha,\beta} - \delta_{\alpha,\beta}(\tilde{\mathcal{O}}_i)_{00}\right]\gamma^\dagger_{i,\alpha}\gamma_{i,\beta} \\ &\quad + O(\gamma^3_{\alpha>0})\ . \end{aligned} \tag{5.41}$$

The average value of $\hat{\mathcal{O}}_i$ will then contain a 0^{th}-order term corresponding to the expectation value on the MF ground state $(\tilde{\mathcal{O}}_i)_{00} = {}_i\langle\psi_0|\hat{\mathcal{O}}_i|\psi_0\rangle_i$, with $|\psi_0\rangle_i$ the MF ground state on site i. The higher-order terms describe therefore the fluctuations around the MF solution.

Onsite term and kinetic term of the Bose-Hubbard Hamiltonian. The onsite term of the Bose-Hubbard Hamiltonian, Eq. (5.4), containing both the onsite interaction term and the chemical potential term, is of this form, with $\hat{\mathcal{O}}_i = \mathcal{H}_{i,\text{loc}} = Un_i(n_i-1)/2 - \mu n_i$.

The kinetic part, on the other hand, contains products of local operators

$$b^\dagger_i b_j = \boldsymbol{\gamma}_i{}^\dagger \tilde{b}^\dagger_i \boldsymbol{\gamma}_i \boldsymbol{\gamma}_j{}^\dagger \tilde{b}_j \boldsymbol{\gamma}_j\ . \tag{5.42}$$

The 0^{th}-order term is

$$\begin{aligned} b^\dagger_i b_j &\underset{\text{order 0}}{=} (\tilde{b}^\dagger_i)_{00}(\tilde{b}_j)_{00} \\ &= \phi^*_i\phi_j\ , \end{aligned} \tag{5.43}$$

with $\phi_i = \langle b_i\rangle_{\text{MF}}$ where the average is taken in the MF ground state. The order-1 term is

$$\begin{aligned} b^\dagger_i b_j \underset{\text{order 1}}{=} \sum_{\alpha>0}\Big[&\phi^*_i(\tilde{b}_j)_{0\alpha}\gamma_{j,\alpha} + \phi_j(\tilde{b}^\dagger_i)_{0\alpha}\gamma_{i,\alpha} \\ &+ \phi^*_i(\tilde{b}_j)_{\alpha 0}\gamma^\dagger_{j,\alpha} + \phi_j(\tilde{b}^\dagger_i)_{\alpha 0}\gamma^\dagger_{i,\alpha}\Big]\ . \end{aligned} \tag{5.44}$$

The order-2 term contains products of the order-0 term of one operator, with the order-2 term of the other operator, plus the product of order-1 terms for both operators.

$$\begin{aligned} b^\dagger_i b_j \underset{\text{order 2}}{=} \sum_{\alpha,\beta>0}\Big\{&\left[\phi^*_i(\tilde{b}_j)_{\alpha\beta} - \phi^*_i\phi_j\delta_{\alpha,\beta}\right]\gamma^\dagger_{j,\alpha}\gamma_{j,\beta} + \left[\phi_j(\tilde{b}^\dagger_i)_{\alpha\beta} - \phi^*_i\phi_j\delta_{\alpha,\beta}\right]\gamma^\dagger_{i,\alpha}\gamma_{i,\beta} \\ &+ \left[(\tilde{b}^\dagger_i)_{\alpha 0}\gamma^\dagger_{i,\alpha} + (\tilde{b}^\dagger_i)_{0\alpha}\gamma_{i,\alpha}\right]\left[(\tilde{b}_j)_{\beta 0}\gamma^\dagger_{j,\beta} + (\tilde{b}_j)_{0\beta}\gamma_{j,\beta}\right]\Big\}\ . \end{aligned} \tag{5.45}$$

Order-0 contribution: the MF ground-state energy. Now, collecting contributions from both the onsite term and the kinetic term, we see that the order-0 contribution to the BH Hamiltonian

$$\mathcal{H}_{\rm BH}^{(0)} = -\sum_{i,j} t_{ij}\phi_i^*\phi_j + \sum_i {}_i\langle\psi_0|\mathcal{H}_{i,\rm loc}|\psi_0\rangle_i \tag{5.46}$$

is just the energy of the MF ground state, Eq. (5.11). Recalling the definition of the MF Hamiltonian on site i, Eq. (5.15)

$$\mathcal{H}_i^{\rm MF} = -\sum_j (t_{ij}\phi_j b_i^\dagger + \text{h.c.}) + \frac{U}{2} n_i(n_i-1) - \mu n_i \,, \tag{5.47}$$

this may also be rewritten as

$$\mathcal{H}_{\rm BH}^{(0)} = \sum_i {}_i\langle\psi_0|\mathcal{H}_i^{\rm MF}|\psi_0\rangle_i + \sum_{i,j} t_{ij}\phi_i^*\phi_j \,. \tag{5.48}$$

The MF approximation may then just be viewed as the 0^{th} order approximation for the slave-bosons.

Vanishing of the order-1 term. The order 1 contribution to the BH Hamiltonian is

$$\mathcal{H}_{\rm BH}^{(1)} = \sum_i \sum_{\alpha>0} \left[(\widetilde{\mathcal{H}}_{i,\rm loc})_{0\alpha} - \sum_j t_{ij}\phi_j(\tilde{b}_i^\dagger)_{0\alpha} - \sum_j t_{ji}\phi_j^*(\tilde{b}_i)_{0\alpha} \right] \gamma_{i,\alpha} + \text{h.c.} \tag{5.49}$$

The matrix element between the brackets is

$$(\widetilde{\mathcal{H}}_{i,\rm loc})_{0\alpha} - \sum_j t_{ij}\phi_j(\tilde{b}_i^\dagger)_{0\alpha} - \sum_j t_{ji}\phi_j^*(\tilde{b}_i)_{0\alpha} = {}_i\langle\psi_0|\mathcal{H}_i^{\rm MF}|\psi_\alpha\rangle_i = 0 \tag{5.50}$$

where $|\psi_\alpha\rangle_i$ is the eigenstate of $\mathcal{H}_i^{\rm MF}$ associated to the eigenvalue $\epsilon_\alpha(i)$. This matrix element vanishes, since the states $|\psi_\alpha\rangle_i$ are orthogonal to each other. This represents a useful numerical check that the MF ground state has been found. One thus has

$$\mathcal{H}_{\rm BH}^{(1)} = 0 \,. \tag{5.51}$$

Quadratic Bose-Hubbard Hamiltonian in terms of the SB operators. Finally, the contributions of order 2 to the BH Hamiltonian contain three terms: a local (onsite) term, a "hopping" term, and a "pair" term

$$\mathcal{H}_{\rm BH}^{(2)} = \mathcal{H}_{\rm BH,local}^{(2)} + \mathcal{H}_{\rm BH,hopping}^{(2)} + \mathcal{H}_{\rm BH,pair}^{(2)} \,. \tag{5.52}$$

The local term is diagonal in the i and α indices

$$\begin{aligned}\mathcal{H}^{(2)}_{\mathrm{BH,local}} &= \sum_i \sum_{\alpha,\beta>0} \big[{}_i\langle\psi_\alpha|\mathcal{H}_i^{\mathrm{MF}}|\psi_\beta\rangle_i \\ &\quad - {}_i\langle\psi_0|\mathcal{H}_i^{\mathrm{MF}}|\psi_0\rangle_i\, \delta_{\alpha,\beta}\big]\, \gamma^\dagger_{i,\alpha}\gamma_{i,\beta} \qquad (5.53)\\ &= \sum_i \sum_{\alpha>0} [\epsilon_\alpha(i) - \epsilon_0(i)]\gamma^\dagger_{i,\alpha}\gamma_{i,\alpha}\,, \qquad (5.54)\end{aligned}$$

and represents local deviations from the MF energy $\epsilon_0(i)$ due to the occupation of modes orthogonal to the MF.

The hopping term is[2]

$$\begin{aligned}\mathcal{H}^{(2)}_{\mathrm{BH,hopping}} &= -\sum_{i,j} t_{ij} \sum_{\alpha,\beta>0} \Big[(\tilde{b}_i^\dagger)_{\alpha 0}(\tilde{b}_j)_{0\beta}\gamma^\dagger_{i,\alpha}\gamma_{j,\beta} + (\tilde{b}_i^\dagger)_{0\alpha}(\tilde{b}_j)_{\beta 0}\gamma^\dagger_{j,\beta}\gamma_{i,\alpha}\Big] \\ &= \sum_{i,j}\sum_{\alpha,\beta>0} \gamma^\dagger_{i,\alpha}\gamma_{j,\beta}\mathcal{A}^{(1)}_{i\alpha,j\beta} \qquad (5.55)\end{aligned}$$

where we introduced the matrix $\mathcal{A}^{(1)}$ with matrix elements

$$\mathcal{A}^{(1)}_{i\alpha,j\beta} = -t_{ij}(\tilde{b}_i^\dagger)_{\alpha 0}(\tilde{b}_j)_{0\beta} - t_{ji}(\tilde{b}_i)_{\alpha 0}(\tilde{b}_j^\dagger)_{0\beta} \qquad (5.56)$$

which is hermitian (*i.e.* it satisfies $\mathcal{A}^{(1)}_{j\beta,i\alpha} = (\mathcal{A}^{(1)}_{i\alpha,j\beta})^*$). The hopping Hamiltonian $\mathcal{H}^{(2)}_{\mathrm{BH,hopping}}$ describes processes where a slave-bosonic particle is destroyed in the mode β on site j (operator $\gamma_{j\beta}$), sent to the "MF condensate" on site j by the operator $b_j^{(\dagger)}$ (matrix element $(\tilde{b}_j)_{0\beta}$ or $(\tilde{b}_j^\dagger)_{0\beta}$), and created again at site i in the SB mode α (operator $\gamma^\dagger_{i,\alpha}$) out of the "MF condensate" on site i (matrix element $(\tilde{b}_i^\dagger)_{\alpha 0}$ or $(\tilde{b}_i)_{\alpha 0}$). These processes have an overall amplitude t_{ij} or t_{ji}, and a phase may be acquired through both t_{ij} and the matrix elements of b's operators which are in general complex numbers.

The pair term is

$$\begin{aligned}\mathcal{H}^{(2)}_{\mathrm{BH,pair}} &= -\sum_{i,j} t_{ij} \sum_{\alpha,\beta>0} \Big[(\tilde{b}_i^\dagger)_{\alpha 0}(\tilde{b}_j)_{\beta 0}\gamma^\dagger_{i,\alpha}\gamma^\dagger_{j,\beta} + (\tilde{b}_i^\dagger)_{0\alpha}(\tilde{b}_j)_{0\beta}\gamma_{i,\alpha}\gamma_{j,\beta}\Big] \\ &= \frac{1}{2}\sum_{i,j}\sum_{\alpha,\beta>0} \big[\gamma_{i,\alpha}\gamma_{j,\beta}\mathcal{B}_{i\alpha,j\beta} + \mathrm{h.c.}\big] \qquad (5.57)\end{aligned}$$

where we introduced the matrix $\mathcal{B}$ with matrix elements

$$\mathcal{B}_{i\alpha,j\beta} = -t_{ij}(\tilde{b}_i^\dagger)_{0\alpha}(\tilde{b}_j)_{0\beta} - t_{ji}(\tilde{b}_j^\dagger)_{0\beta}(\tilde{b}_i)_{0\alpha} \qquad (5.58)$$

which is symmetric ($\mathcal{B}_{i\alpha,j\beta} = \mathcal{B}_{j\beta,i\alpha}$). This pair Hamiltonian describes processes where two SB particles are extracted out of the MF condensate (operator $\gamma^\dagger_{i\alpha}\gamma^\dagger_{j\beta}$), or are simultaneously destroyed and then recreated into the MF condensate (operator $\gamma_{i\alpha}\gamma_{j\beta}$), with amplitudes given by the matrix elements of $\mathcal{B}$.

[2] Note that $i \neq j$, so that $\gamma^{(\dagger)}$ operators related to i and j commute with each other; a term with $i = j$ would have to be incorporated in the local part of the Hamiltonian.

Discussion. The approach we have described is very general. Although our focus is ultimately the homogeneous Bose-Hubbard model, it is straightforward to implement similar calculations with arbitrary hopping amplitudes (possibly complex, representing gauge fields), to include spin degrees of freedom for the bosons, and to consider inhomogeneities in the system. Indeed, our derivation of the quadratic Hamiltonian did not make use of the specific form of the onsite part of the Hamiltonian (we only introduced the matrix elements of the onsite Hamiltonian between the eigenstates of the MF Hamiltonian, but this is completely general), and the hopping part of the Hamiltonian may be replaced by a sum of terms of the form $\sum_{ij} J_{ij} A_i B_j$ with J_{ij} an arbitrary complex number, and A_i and B_j arbitrary operators on sites i and j without changing anything to the derivation of the quadratic Hamiltonian. Furthermore, a time-dependent version of the slave-boson technique may also be derived, but shall not be discussed here. The generalization to a cluster-slave-boson approach, based on a cluster-mean-field rather than on the simple mean-field Ansatz we have used, is also straightforward to implement (Huerga, Dukelsky, and Scuseria, 2013): what we have called "sites" i and j in our derivation are only labels which may be related to an arbitrary subset of the actual sites of the lattice.

Bogoliubov diagonalization of the quadratic SB Hamiltonian for the homogeneous BH model. The last step is to diagonalize the quadratic Hamiltonian $\mathcal{H}^{(2)}_{\mathrm{BH}}$ via a Bogoliubov transformation (Blaizot and Ripka, 1986). In our case, since the system is homogeneous, and since no spontaneous breaking of the translational invariance occurs, all the parameters are site-independent. It is thus more convenient to Fourier-transform the SB operators before the diagonalization. Furthermore, the matrix elements of $\mathcal{A}$ and $\mathcal{B}$ may always be chosen as real numbers. This basically amounts to a choice of a real ϕ. In this case, the MF Hamiltonian is a real symmetric matrix in the basis $|n\rangle$, so that its eigenstates $|\psi_\alpha\rangle$ have only real coefficients in the same basis. Hence, the matrix elements of b and $b^\dagger$ between these states are real numbers. Recall that we are working on a square lattice in $2d$, or a cubic lattice in $3d$. We introduce

$$\gamma_{\boldsymbol{k},\alpha} = \frac{1}{\sqrt{V}} \sum_i e^{-i\boldsymbol{k}\cdot\boldsymbol{r}_i} \gamma_{i,\alpha} \tag{5.59}$$

in terms of which the local term is just

$$\mathcal{H}^{(2)}_{\mathrm{BH,local}} = \sum_{\boldsymbol{k}} \sum_{\alpha>0} (\epsilon_\alpha - \epsilon_0) \gamma^\dagger_{\boldsymbol{k},\alpha} \gamma_{\boldsymbol{k},\alpha} \tag{5.60}$$

while the hopping term is

$$\mathcal{H}^{(2)}_{\mathrm{BH,hopping}} = \sum_{\boldsymbol{k}} \sum_{\alpha,\beta>0} (A^{(1)}_{\boldsymbol{k}})_{\alpha\beta} \gamma^\dagger_{\boldsymbol{k},\alpha} \gamma_{\boldsymbol{k},\beta} \tag{5.61}$$

where

$$(A^{(1)}_{\boldsymbol{k}})_{\alpha\beta} = -t_{\boldsymbol{k}} \left[(\tilde{b})_{0\alpha}(\tilde{b})_{0\beta} + (\tilde{b})_{\beta 0}(\tilde{b})_{\alpha 0} \right] \tag{5.62}$$

with $t_{\boldsymbol{k}} = \sum_j t_{ij} e^{-i\boldsymbol{k}\cdot(\boldsymbol{r}_i - \boldsymbol{r}_j)} = -2t \sum_{a=1}^{d} \cos k_a$. Finally, the pair term is

$$\mathcal{H}^{(2)}_{\mathrm{BH,pair}} = \frac{1}{2} \sum_{\boldsymbol{k}} \sum_{\alpha,\beta>0} (B_{\boldsymbol{k}})_{\alpha\beta} \gamma_{-\boldsymbol{k},\alpha} \gamma_{\boldsymbol{k},\beta} + \mathrm{h.c.} \tag{5.63}$$

where

$$(B_{\boldsymbol{k}})_{\alpha\beta} = -t_{\boldsymbol{k}} \left[(\tilde{b})_{\alpha 0}(\tilde{b})_{0\beta} + (\tilde{b})_{\beta 0}(\tilde{b})_{0\alpha} \right] . \tag{5.64}$$

It will be convenient to use the vectorial notation $\boldsymbol{\gamma}_{\boldsymbol{k}} = (\gamma_{\boldsymbol{k},1}, \ldots \gamma_{\boldsymbol{k},n_{\max}})^T$[3]. Putting everything together, we finally obtain

$$\mathcal{H}^{(2)}_{\mathrm{BH}} = \frac{1}{2} \sum_{\boldsymbol{k}} (\boldsymbol{\gamma}^{\dagger}_{\boldsymbol{k}}, \boldsymbol{\gamma}_{-\boldsymbol{k}}) \begin{pmatrix} A_{\boldsymbol{k}} & B_{\boldsymbol{k}} \\ B_{\boldsymbol{k}} & A_{\boldsymbol{k}} \end{pmatrix} \begin{pmatrix} \boldsymbol{\gamma}_{\boldsymbol{k}} \\ \boldsymbol{\gamma}^{\dagger}_{-\boldsymbol{k}} \end{pmatrix} - \frac{1}{2} \sum_{\boldsymbol{k}} \mathrm{Tr} A_{\boldsymbol{k}} \tag{5.65}$$

with $A_{\boldsymbol{k}} = A^{(1)}_{\boldsymbol{k}} + \mathrm{diag}(\epsilon_\alpha - \epsilon_0)$. The final step in order to put the quadratic Hamiltonian $\mathcal{H}^{(2)}_{\mathrm{BH}}$ in a diagonal form is to diagonalize the matrices (Blaizot and Ripka, 1986)

$$\mathcal{M}_{\boldsymbol{k}} = \eta \begin{pmatrix} A_{\boldsymbol{k}} & B_{\boldsymbol{k}} \\ B_{\boldsymbol{k}} & A_{\boldsymbol{k}} \end{pmatrix} \tag{5.66}$$

$$= P_{\boldsymbol{k}} \begin{pmatrix} \Omega_{\boldsymbol{k}} & 0 \\ 0 & -\Omega_{\boldsymbol{k}} \end{pmatrix} P^{-1}_{\boldsymbol{k}} \tag{5.67}$$

where $\eta = \begin{pmatrix} \mathbb{1} & 0 \\ 0 & -\mathbb{1} \end{pmatrix}$ and $\Omega_{\boldsymbol{k}} = \mathrm{diag}(\omega_{\boldsymbol{k},\alpha})$. $\omega_{k,\alpha}$ are the eigenfrequencies of the system. The diagonalization is generally performed numerically given the potentially large number of SB flavors retained in the calculation. The matrix P satisfies $P^{-1} = \eta P^{\dagger} \eta$ (Blaizot and Ripka, 1986). The Bogoliubov rotation

$$\begin{pmatrix} \boldsymbol{\gamma}_{\boldsymbol{k}} \\ \boldsymbol{\gamma}^{\dagger}_{-\boldsymbol{k}} \end{pmatrix} = P_{\boldsymbol{k}} \begin{pmatrix} \boldsymbol{\lambda}_{\boldsymbol{k}} \\ \boldsymbol{\lambda}^{\dagger}_{-\boldsymbol{k}} \end{pmatrix} \tag{5.68}$$

preserves the bosonic commutation relations (Blaizot and Ripka, 1986), and this last transformation finally leads us to the diagonal form

$$\mathcal{H}^{(2)}_{\mathrm{BH}} = \sum_{\boldsymbol{k}} \sum_{\alpha=1}^{n_{\max}} \omega_{\boldsymbol{k},\alpha} \lambda^{\dagger}_{\boldsymbol{k},\alpha} \lambda_{\boldsymbol{k},\alpha} - \frac{1}{2} \sum_{\boldsymbol{k}} \mathrm{Tr}(A_{\boldsymbol{k}} - \Omega_{\boldsymbol{k}}) . \tag{5.69}$$

[3] Note that the $\alpha = 0$ mode is not present any more. It is indirectly present through the dependency of the matrices A and B on the MF ground state. Its status is somewhat analogous to the condensate mode in the Bogoliubov approximation: its serves as a "reservoir" for the SB particles.

The slave-boson ground state is the vacuum of the $\lambda_{\boldsymbol{k},\alpha}$ operators, which differs from the vacuum of the γ's operators (namely the MF ground state) because of the mixture of γ and $\gamma^\dagger$ involved in the Bogoliubov rotation, and the ground-state energy is lowered, with respect to the MF contribution $\mathcal{H}^{(0)}_{\rm BH}$, by an amount $\frac{1}{2}\sum_{\boldsymbol{k}} \mathrm{Tr}(A_{\boldsymbol{k}} - \Omega_{\boldsymbol{k}})$.

5.3.2 Self-consistency of the SB approach and correlation functions.

Self-consistency criterion. The approximation we have made relies on the hypothesis that the SB population of modes orthogonal to the MF state remain small

$$\sum_{\alpha>0} \langle \gamma^\dagger_{i,\alpha}\gamma_{i,\alpha}\rangle \ll 1 \;\forall i \;. \tag{5.70}$$

In the case of a homogeneous system, this is equivalent to

$$s = \frac{1}{V}\sum_{\boldsymbol{k}}\sum_{\alpha>0} \langle \gamma^\dagger_{\boldsymbol{k},\alpha}\gamma_{\boldsymbol{k},\alpha}\rangle \ll 1 \;. \tag{5.71}$$

One thus has to calculate $\langle \gamma^\dagger_{\boldsymbol{k},\alpha}\gamma_{\boldsymbol{k},\alpha}\rangle$ in the ground-state of the BH Hamiltonian, at the SB level of approximation.

Correlation matrices. More generally, we shall be interested in correlation functions of various observables, which are completely characterized by the correlation matrices

$$C_{\alpha,\alpha'}(\boldsymbol{k}) = \langle \gamma^\dagger_{\boldsymbol{k},\alpha}\gamma_{\boldsymbol{k},\alpha'}\rangle \tag{5.72}$$

$$F_{\alpha,\alpha'}(\boldsymbol{k}) = \langle \gamma_{\boldsymbol{k},\alpha}\gamma_{-\boldsymbol{k},\alpha'}\rangle \;, \tag{5.73}$$

since the SB ground-state of the BH Hamiltonian is a gaussian state, for which Wick's theorem applies (Blaizot and Ripka, 1986). A convenient way to obtain these correlation matrices is to consider the following matrix

$$\mathcal{C}(\boldsymbol{k}) = \left\langle \begin{pmatrix} \boldsymbol{\gamma}_{\boldsymbol{k}} \\ \boldsymbol{\gamma}^\dagger_{-\boldsymbol{k}} \end{pmatrix} \begin{pmatrix} \boldsymbol{\gamma}^\dagger_{\boldsymbol{k}} & \boldsymbol{\gamma}_{-\boldsymbol{k}} \end{pmatrix} \right\rangle \tag{5.74}$$

$$= P_{\boldsymbol{k}} \left\langle \begin{pmatrix} \boldsymbol{\lambda}_{\boldsymbol{k}} \\ \boldsymbol{\lambda}^\dagger_{-\boldsymbol{k}} \end{pmatrix} \begin{pmatrix} \boldsymbol{\lambda}^\dagger_{\boldsymbol{k}} & \boldsymbol{\lambda}_{-\boldsymbol{k}} \end{pmatrix} \right\rangle P^\dagger_{\boldsymbol{k}} \tag{5.75}$$

$$= P_{\boldsymbol{k}} \begin{pmatrix} \mathrm{diag}(1+n_{\boldsymbol{k},\alpha}) & 0 \\ 0 & \mathrm{diag}(n_{\boldsymbol{k},\alpha}) \end{pmatrix} P^\dagger_{\boldsymbol{k}} \;. \tag{5.76}$$

where

$$n_{\boldsymbol{k},\alpha} = \frac{1}{e^{\beta\omega_{\boldsymbol{k},\alpha}} - 1} \tag{5.77}$$

if we are considering a thermal state at temperature $T = 1/\beta$. In the ground state, one simply has $n_{\boldsymbol{k},\alpha} = 0$[4]. Since the matrix $P_{\boldsymbol{k}}$ has the form (Blaizot and Ripka, 1986)

$$P_{\boldsymbol{k}} = \begin{pmatrix} U_{\boldsymbol{k}} & V_{\boldsymbol{k}}^* \\ V_{\boldsymbol{k}} & U_{\boldsymbol{k}}^* \end{pmatrix} , \tag{5.78}$$

we obtain that

$$\mathcal{C}(\boldsymbol{k}) = \begin{pmatrix} \mathbb{1} + C(\boldsymbol{k}) & F(\boldsymbol{k}) \\ F(\boldsymbol{k})^\dagger & C(-\boldsymbol{k}) \end{pmatrix} \tag{5.79}$$

$$= \begin{pmatrix} U_{\boldsymbol{k}} U_{\boldsymbol{k}}^\dagger & U_{\boldsymbol{k}} V_{\boldsymbol{k}}^\dagger \\ V_{\boldsymbol{k}} U_{\boldsymbol{k}}^\dagger & V_{\boldsymbol{k}} V_{\boldsymbol{k}}^\dagger \end{pmatrix} \tag{5.80}$$

where we used that $\langle \gamma_{\boldsymbol{k},\alpha} \gamma_{-\boldsymbol{k},\alpha'} \rangle^* = \langle \gamma^\dagger_{-\boldsymbol{k},\alpha} \gamma^\dagger_{\boldsymbol{k},\alpha'} \rangle$. Note also that

$$U_{\boldsymbol{k}} U_{\boldsymbol{k}}^\dagger = \mathbb{1} + V_{\boldsymbol{k}} V_{\boldsymbol{k}}^\dagger \tag{5.81}$$

and that we have the symmetry $\boldsymbol{k} \leftrightarrow -\boldsymbol{k}$. In particular, we see immediately that the stability criterion for the SB approximation is

$$s = \frac{1}{V} \sum_{\boldsymbol{k}} \mathrm{Tr}(V_{\boldsymbol{k}} V_{\boldsymbol{k}}^\dagger) \ll 1 . \tag{5.82}$$

If s is very small, the MF ground state is an excellent approximation to the true ground state, and calculations within the SB approach are expected to be in quantitative agreement with exact calculations. If s exceeds 10%, quantum corrections the MF solution are not so small, and we expect a stronger departure of the SB predictions from the exact results.

Self-consistency across the phase diagram of the BH model. On the left panel of Fig. 5.2 we have plotted the value of s across the zero-temperature phase diagram of the $2d$ BH Hamiltonian. The first observation is that the SB approximation is self-consistent over nearly all the phase diagram. The maximum value of s is ≈ 0.11, and is found near the O(2) point, namely at the phase transition occurring at integer

[4] A subtlety occurs for zero-energy modes. In fact, the Bogoliubov transformation requires $\omega > 0$ (Blaizot and Ripka, 1986). This situation is problematic in the gapless SF phase. Unless otherwise stated, we always remove the contribution of the zero energy mode(s) from our calculations. As the neglected contribution is microscopic (stemming from a single mode), this does not alter the reliability of our predictions in the thermodynamic limit, but may have significant impact on finite size systems, especially regarding the spatial structure of entanglement (Frérot and Roscilde, 2015). An alternative procedure is to introduce a very small gap, scaling to zero in the thermodynamic limit, by adding a term of the form $-h \sum_i (b_i + b_i^\dagger)$ to the Hamiltonian, with $h \to 0$ when increasing the system size. We shall come back to this issue in Section 6.1.

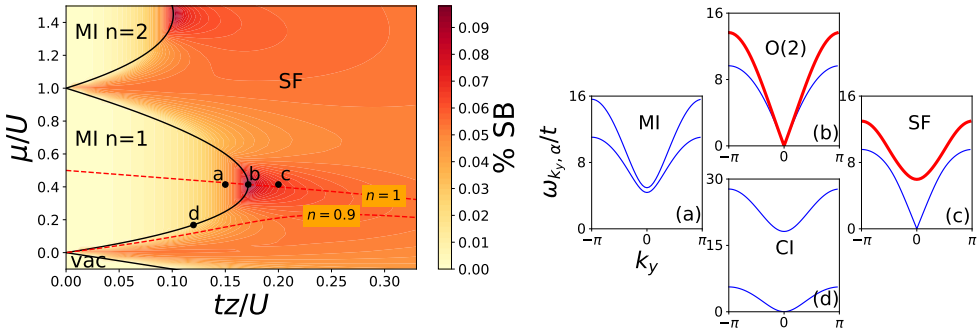

Figure 5.2: Left: Slave-boson population (orthogonal to the MF state) in the SB ground-state of the $2d$ Bose-Hubbard model. In the Mott-insulating phases (MI), the population of SB is around $2-3\%$, while in the superfluid phase (SF), it is around $5-6\%$. The maximal population is found at the tip of the MI lobes. For instance, at the b point, corresponding to the phase transition at unit filling $n=1$, the population is slightly below 11%. In $3d$, the topography is similar, with a maximum value of about 4% at the same point. Strong SB populations indicate that quantum fluctuations are large. Interestingly, entanglement entropy exhibits a very similar behavior (see Fig. 7.3). a, b, c and d mark the points where the excitation spectrum is plotted on the right panel. Right: Excitation spectrum from the SB approach at $k_x=0$. Only the two lowest branches are shown. (a) $tz/U=0.15$, $\mu/U=\sqrt{2}-1$; (b) $tz/U=3-2\sqrt{2}$, $\mu/U=\sqrt{2}-1$; (c) $tz/U=0.2$, $\mu/U=\sqrt{2}-1$ and (d) $tz/U=0.12$, $\mu/U=0.168$. The thick red line marks the amplitude mode in the SF phase.

density ($n=1$)[5]. For comparison, in $3d$, the SB population has a maximal value of ≈ 0.04 at the same point. This result is in itself a validation of the MF theory, which represents a rather good approximation throughout the phase diagram. In fact, MF theory only breaks down in the very vicinity of the O(2) points: the universality class of the phase transition at the O(2) points is that of the $(d+1)$-XY model, which is not captured by a gaussian theory such as the SB approximation. In contrast, the generic transition is described by a gaussian theory, so that the SB predictions are reliable everywhere in the phase diagram, except in the very vicinity of the O(2) points — with the caveat that the actual phase-transition line is a shifted with respect to the MF prediction. MF theory by itself does not provide any self-consistency check, and the first virtue of the SB approach is to provide such a self-consistent validation.

Limitations of the SB approximation. The limitation of the SB approximation stems from the fact that the constraint of having exactly one SB particle per site, Eq. (5.25), is only approximately accounted for. The self-consistency of the SB

[5] The term O(2) characterizing this point comes from the fact that the low-energy effective field-theory describing the phase transition is a O(N=2) model.

approach is a necessary, yet not sufficient condition for having an accurate description of the system. Ultimately, the validity of the SB approach relies on the comparison of certain of its physical predictions with exact calculations (see, for instance, Coletta, Laflorencie, and Mila (2012) for a comparison with quantum Monte Carlo calculations in the hardcore limit, showing a remarkably good accuracy of the SB approach), or with experiments (see Endres et al. (2012) for a comparison between the SB prediction and experiments concerning the spectrum of amplitude fluctuations of the order parameter across the SF-MF phase transition, demonstrating also quantitative agreement). In general, we expect that the SB approach is "semi-quantitative".

Physical content of the SB approach. A crucial observation of Fig. 5.2 is that the O(2) points are clearly singled out as the points where quantum fluctuations have the strongest effect on the structure of the ground state — in fact, they are so strong that they induce a failure of the gaussian theory to capture the critical exponents of the phase transition. In contrast, the generic (or commensurate-incommensurate, CI) transition occurring at any other point of the phase-transition line does not exhibit strong quantum fluctuations. In fact, the critical point of the generic transition is, strictly speaking, still in the MI phase. When leaving the MI lobe by increasing μ, one can picture the ground state as a Mott insulator, to which a very dilute gas of bosons has been added. These bosons condense and form a very dilute superfluid, inducing very weak quantum fluctuations (in this case, the quantum fluctuations are mostly due to the Mott insulator itself). When leaving the MI lobe by decreasing μ, the picture is the same, but one is adding very few holes instead of particles. The generic transition is thus not induced by quantum fluctuations, but rather by the fact that adding or removing a few particles to a Mott-insulator immediately leads to a very dilute superfluid. In essence, it is not different from the "phase transition" from the vacuum to a very dilute superfluid of a few bosons.

In contrast to the generic transition, the O(2) transition occurring at fixed, integer density, is much richer. Here, increasing the ratio tz/U at fixed density from the MI phase, one is effectively increasing the virtual particle-hole pair fluctuations in the MI by increasing the role of the kinetic energy term in the Hamiltonian, and at some critical ratio, the particle-hole fluctuations become so large that the bosons become delocalized over the whole lattice to form a superfluid. When approached from the SF phase, the picture is better formulated in terms of the fluctuations of the SF order parameter ϕ. Recalling that ϕ is a complex number, we notice that it fluctuates both in phase and in amplitude. The phase fluctuations are always gapless and correspond to the well-known Goldstone mode of this continuous symmetry-broken phase. Deep

in the SF, this is the sound mode described by Bogoliubov theory. But the gapped *amplitude* fluctuations of the order parameter, absent from Bogoliubov theory, soften when approaching the O(2) transition, and are gapless at the O(2) point (at the SB level of approximation). These amplitude fluctuations of the order parameter form an additional source of quantum fluctuations, and are responsible for a richer structure of entanglement in the vicinity of the O(2) points (see Chapter 7). On the right panel of Fig. 5.2, we have plotted the excitation spectrum at various representative points of the phase diagram: in the gapped MI phase (panel a), in the gapless SF phase (c), at the CI generic transition (d) and at the O(2) point (b).

5.3.3 Discussion

Although the SB approach can incorporate an arbitrary number of modes orthogonal to the MF to describe quantum fluctuations, in several regions of the phase diagram we can give an accurate, and physically simpler description of the structure of fluctuations, by restricting us to a limited number of SB flavors.

Hardcore limit. In the limit of infinite interaction $U/t \to \infty$, but imposing a non-integer filling fraction $\bar{n}$, the system is in a SF regime. In this hardcore limit, if $n_0 < \bar{n} < n_0 + 1$ with n_0 an integer, only occupations with n_0 or $n_0 + 1$ bosons are allowed. One may then keep only one SB flavor in addition to the MF. This regime is further explored in Chapter 6.

Weak-interaction limit. In the limit of a dilute and/or weakly interacting superfluid $\bar{n}U/t \ll 1$, the system is accurately described by Bogoliubov theory. The MF is close to a coherent state $|\psi_0\rangle \propto e^{-\phi b^\dagger}|0\rangle$, and we may keep only one mode orthogonal to the MF, describing collective fluctuations of the phase, the other branches being very high in energy. This regime is very similar, regarding the structure of quantum correlations in the ground-state, to the hardcore limit and is also explored in Chapter 6.

Mott insulator. In the Mott insulator of density n, the MF ground state is $|\psi_0\rangle_{\mathrm{MI}} = |n\rangle$. In this case, the only modes connected to the MF state by the MF Hamiltonian contain $n \pm 1$ bosons. We can thus keep only two SB flavors, describing particle and holes fluctuations in the MI. Other branches do not contribute to the low-energy dynamics, and in particular, to entanglement (Section 7.1).

5.4 Reduced-density matrix for bosonic gaussian states

In this section we provide the technical details related to the calculation of the entanglement Hamiltonian from the correlation matrix, and to the definition of the entanglement contour for bosonic gaussian states.

5.4.1 Reduced density-matrix and entanglement spectrum within the SB approximation

Since, within the SB approximation, the ground state is a gaussian state, we can use Wick's theorem to reconstruct the reduced density matrix of any subset of sites through the knowledge of the two-point correlators only. Considering a subset of sites $i \in A$, as for the free fermion case studied in Section 4, the validity of Wick's theorem implies that the reduced density matrix of A takes the form of the exponential of a quadratic Hamiltonian for the SB degrees of freedom in A

$$\rho_A \propto \exp(-\mathcal{H}_{\text{ent}}) \tag{5.83}$$

$$\mathcal{H}_{\text{ent}} = \sum_{i,j\in A}\sum_{\alpha,\alpha'>0}\left\{\mathcal{A}_{i\alpha,j\beta}\gamma^\dagger_{i\alpha}\gamma_{j,\beta} + \frac{1}{2}\left(\mathcal{B}_{i\alpha,j\beta}\gamma_{i\alpha}\gamma_{j,\beta} + \text{h.c.}\right)\right\} \tag{5.84}$$

where $\mathcal{A}^\dagger = \mathcal{A}$ and $\mathcal{B}^T = \mathcal{B}$. Indices α, α' denote the SB flavors. As for the free fermion case, the matrices $\mathcal{A}$ and $\mathcal{B}$ can be reconstructed from the one-body correlation matrix for degrees of freedom within the subsystem A. If

$$\mathcal{M} = \eta\begin{pmatrix}\mathcal{A} & \mathcal{B}\\ \mathcal{B}^* & \mathcal{A}^*\end{pmatrix} = P\begin{pmatrix}\Omega & 0\\ 0 & -\Omega\end{pmatrix}P^{-1}\,, \tag{5.85}$$

we know that $P^{-1} = \eta P^\dagger \eta$ (Blaizot and Ripka, 1986), and that, if $\mathcal{C}_A$ is the correlation matrix for A degrees of freedom

$$\mathcal{C}_A = \begin{pmatrix}\mathbb{1} + C_A^* & F_A\\ F_A^\dagger & C_A\end{pmatrix}\,, \tag{5.86}$$

with $(C_A)_{i\alpha,j\beta} = \langle\gamma^\dagger_{i\alpha}\gamma_{j\beta}\rangle$ and $(F_A)_{i\alpha,j\beta} = \langle\gamma_{i\alpha}\gamma_{j\beta}\rangle$ for $i,j \in A$ and $\alpha,\beta > 0$, then (as $\mathcal{C}_A$ is hermitian)

$$\mathcal{C}_A = P\begin{pmatrix}1+N & 0\\ 0 & N\end{pmatrix}P^\dagger\,. \tag{5.87}$$

Multiplying on the right by η, and using the fact that $P^\dagger\eta = \eta P^{-1}$, we conclude that

$$\mathcal{C}_A\eta = P\begin{pmatrix}1+N & 0\\ 0 & -N\end{pmatrix}P^{-1} \tag{5.88}$$

where $N = (\exp \Omega - 1)^{-1} = \mathrm{diag}(n_1, \dots n_p, \dots)$. What we have to do is then to diagonalize the matrix $\mathcal{C}_A \eta$. Its negative eigenvalues $-n_p$ are related to the (one-body) eigenvalues of $\mathcal{H}_{\mathrm{ent}}$ (the one-body entanglement spectrum ω_p) by

$$n_p = \frac{1}{e^{\omega_p} - 1} \tag{5.89}$$

$$\omega_p = \ln\left(\frac{1}{n_p} + 1\right) , \tag{5.90}$$

while the matrix

$$P = \begin{pmatrix} U & V^* \\ V & U^* \end{pmatrix} \tag{5.91}$$

contains the associated entanglement eigenmodes

$$\boldsymbol{\lambda}^{\mathrm{ent}} = U^\dagger \boldsymbol{\gamma} - V^\dagger \boldsymbol{\gamma}^\dagger \tag{5.92}$$

where we introduced the vector $\boldsymbol{\gamma} = (\gamma_{i\alpha})_{i \in A, \alpha > 0}$. As for the $2d$ free-fermion case, Section 4.3, we are often going to consider a region A consisting of a cylinder cut out of a torus. In this case, we can use the translational invariance of A along the direction parallel to the cut. Denoting $\boldsymbol{k}_\parallel$ the wavevector in this direction, the correlation matrix $\mathcal{C}_A$ is block diagonal with respect to $\boldsymbol{k}_\parallel$, and the diagonalization can be performed in each sector $\boldsymbol{k}_\parallel$ successively. Then, the entanglement modes are labeled by two indices $(\boldsymbol{k}_\parallel, p)$ where the index p expresses 1) the modes in the direction perpendicular to the cut; and 2) the different SB flavors. If the width of the cylinder A in the direction perpendicular to the cut is l, and if $n_{\max}$ SB flavors are retained (in addition to the MF state which has been "condensed" during the SB construction), then p runs over $l \times n_{\max}$ values.

5.4.2 Entanglement contour for bosonic gaussian states

Beyond the free fermion case first discussed by Chen and Vidal (2014), the definition of the entanglement contour is still an open question. We are not aware of results concerning entanglement contours beyond quadratic models; and even for quadratic bosonic Hamiltonians, the question is delicate, since only two studies have been reported in the literature dealing with this problem (Frérot and Roscilde, 2015; Coser, De Nobili, and Tonni, 2017).

Mode decomposition of entanglement entropy. Similarly to the case of fermions, the entanglement entropy for bosonic gaussian states takes the form a thermal entropy for a fictitious system of free bosons

$$S = \sum_p s_{\mathrm{Bose}}(n_p) \tag{5.93}$$

and s_{Bose} is the entropy of a bosonic mode containing n_p bosons in average

$$s_{\mathrm{Bose}}(n) = (1+n)\ln(1+n) - n\ln n\,. \tag{5.94}$$

Mode decomposition of the entanglement contour. It is then natural to seek a decomposition of S as

$$S = \sum_{i\in A} \mathcal{C}_s(i) \tag{5.95}$$

where

$$\mathcal{C}_s(i) = \sum_p w_p(i) s(n_p) \tag{5.96}$$

is the entanglement contour, weighting the contribution of site i to the entanglement entropy shared by A and its complement, and $w_p(i)$ is weighting the contribution of site i to the entanglement entropy stemming from the mode p. In order to recover the entanglement entropy when summing the contours over the sites i in A, we impose that

$$\sum_{i\in A} w_p(i) = 1\ \forall p\,. \tag{5.97}$$

Definition of the weights entering in the mode decomposition of the contours. The remaining question is then how to define the weights $w_p(i)$. They must obviously be related to the spatial structure of the modes contained in the matrix P of Eq. (5.91), but there is not a unique way to do so. In our paper, we proposed the following definition[6]

$$w_p(i) = |U_{ip}|^2 - |V_{ip}|^2 \tag{5.98}$$

directly inspired by the physical concept of local density of states, adapted to the entanglement Hamiltonian [see the corresponding section in Frérot and Roscilde (2015)]. Although the normalization condition Eq. (5.97) is automatically satisfied due to the η-orthogonality of the matrix P (namely, the fact that $P\eta P^\dagger \eta = \mathbb{1}$), it is *a priori* not obvious that $\mathcal{C}_s(i) \geq 0$ holds. Indeed, each $w_p(i)$ may happen to be negative. However, we have never encountered such situations where $\mathcal{C}_s(i) < 0$, which would be physically problematic. Nonetheless, in face of this problem, Coser, De Nobili, and Tonni (2017) have proposed an alternative definition of the entanglement contour.

We shall explain the idea of Coser, De Nobili, and Tonni (2017) in the simplified framework where the correlation matrices $C_{ij} = \langle b_i^\dagger b_j\rangle$ and $F_{ij} = \langle b_i b_j\rangle$ are real, which is the case in the slave-boson approach to the Bose-Hubbard model, and refer

[6] In order to simplify the notations, we suppose that indices i are related to a single site, and a single SB flavor. In the case of several flavors, on simply has to sum the contributions stemming from the different flavors on site i: $w_p(i) = \sum_{\alpha=1}^{n_{\max}} w_p(i,\alpha)$.

the reader to the original paper for the general case. The canonical transformation to the normal modes can be expressed in terms of the correlators of the quadratures (q, p) instead of the bosonic operators $(b, b^\dagger)$. They are related by

$$\left\{\begin{array}{rcl} b & = & \frac{q+ip}{\sqrt{2}} \\ b^\dagger & = & \frac{q-ip}{\sqrt{2}} \end{array}\right. \Longleftrightarrow \left\{\begin{array}{rcl} q & = & \frac{b+b^\dagger}{\sqrt{2}} \\ p & = & \frac{b-b^\dagger}{i\sqrt{2}} \end{array}\right. . \tag{5.99}$$

One can then verify that the correlation matrices are related by

$$\left\{\begin{array}{rcl} \langle q_i p_j\rangle & = & \Im \underbrace{\langle b_i^\dagger b_j\rangle}_{C_{ij}} + \Im \underbrace{\langle b_i b_j\rangle}_{F_{ij}} + i\frac{\delta_{ij}}{2} \\ \langle q_i q_j\rangle & = & \Re\langle b_i^\dagger b_j\rangle + \Re\langle b_i b_j\rangle + \frac{\delta_{ij}}{2} \\ \langle p_i p_j\rangle & = & \Re\langle b_i^\dagger b_j\rangle - \Re\langle b_i b_j\rangle + \frac{\delta_{ij}}{2} \end{array}\right. . \tag{5.100}$$

Apart from the term $i/2$ in the diagonal of $\langle q_i p_j\rangle$, stemming solely from the commutation relation $[q_i, p_j] = i\delta_{ij}$, the correlators for the q and p quadratures are real[7]. Defining $\boldsymbol{r} = (q_1, \dots q_N, p_1, \dots p_N)^T$, the diagonalization of the entanglement Hamiltonian $\mathcal{H}$ then amounts to find a canonical transformation W bringing the matrix $\Gamma = \Re\langle \boldsymbol{r}\boldsymbol{r}^T\rangle$ into a diagonal form. Using the fact that C and F are real matrices, so that $\Re\langle q_i p_j\rangle = 0$, we obtain

$$\left\{\begin{array}{rcl} \mathcal{H} & = & \sum_{\alpha=1}^N \omega_\alpha \frac{Q_\alpha^2 + P_\alpha^2}{2} + \text{const.} \\ \Gamma & = & W \begin{pmatrix} \Lambda & 0 \\ 0 & \Lambda \end{pmatrix} W^T \end{array}\right. \tag{5.101}$$

where $\Lambda = \mathrm{diag}(\lambda_1, \dots, \lambda_N)$, with $\lambda_\alpha = \frac{1}{2} + (\exp \omega_\alpha - 1)^{-1}$ and

$$\begin{pmatrix} \boldsymbol{q} \\ \boldsymbol{p} \end{pmatrix} = W \begin{pmatrix} \boldsymbol{Q} \\ \boldsymbol{P} \end{pmatrix} \tag{5.102}$$

with $\boldsymbol{q} = (q_1, \dots, q_N)^T$, etc[8]. The canonical commutation relations for the quadratures q, p and Q, P are preserved if, and only if

$$W J W^T J = -\mathbb{1} \tag{5.103}$$

where $J = \begin{pmatrix} 0 & \mathbb{1} \\ -\mathbb{1} & 0 \end{pmatrix}$[9]. In particular, W is invertible of inverse $W^{-1} = -JW^T J$. Note that since W is in general not an orthogonal matrix, the decomposition of Eq.

[7] Obviously, $\Re C$ and $\Re F$ can be reconstructed from the correlators $\langle q_i q_j\rangle$ and $\langle p_i p_j\rangle$. On the other hand, since F (and hence $\Im F$) is symmetric, while C is hermitian (and hence $\Im C$ is antisymmetric), $\Im F$ and $\Im C$ are extracted as the symmetric and antisymmetric part of $\Re\langle q_i p_j\rangle$ respectively.

[8] Note the factor $1/2$ in the relation between λ_α and ω_α which corresponds to the zero-point motion of the oscillators.

[9] W is then called a symplectic matrix. The existence of such symplectic diagonalization of γ is guaranteed by Williamson's theorem, stating that any $2N \times 2N$ matrix M which is real, symmetric, and definite positive, can be decomposed as $M = W(D \oplus D)W^t$ where $D = \mathrm{diag}(d_1, \dots d_N)$, $d_i > 0$, and W symplectic and real. See the Appendix of Coser, De Nobili, and Tonni, 2017 for a constructive elementary proof of Williamson's theorem.

(5.101) dos not result from a standard diagonalization of γ. The question is then to construct the matrix W. In the particular case where C and F are real matrices, one sees that the matrix γ is block diagonal (since $\langle q_i p_j \rangle = i\delta_{ij}/2$, see. Eq. (5.100)). The canonical transformation W is then also block diagonal

$$W = \begin{pmatrix} X & 0 \\ 0 & Y \end{pmatrix} , \tag{5.104}$$

which means that the canonical transformation acts independently of the q and p quadratures[10]

$$\begin{cases} q &= XQ \\ p &= YP \\ Y^T &= X^{-1} \end{cases} , \tag{5.105}$$

and the matrix γ takes the form

$$\gamma = \begin{pmatrix} G & 0 \\ 0 & H \end{pmatrix} = \begin{pmatrix} X\Lambda X^T & 0 \\ 0 & Y\Lambda Y^T \end{pmatrix} . \tag{5.106}$$

Note again that since X is not an orthogonal matrix, this form does not result from the usual diagonalization of the matrices $G_{ij} = \langle q_i q_j \rangle$ (top left block), or $H_{ij} = \langle p_i p_j \rangle$ (bottom-right block). To perform the symplectic diagonalization, we remark instead that

$$GH = X\Lambda \underbrace{X^T Y}_{\mathbb{1}} \Lambda Y^T = X\Lambda^2 Y^T . \tag{5.107}$$

Since $Y^T = X^{-1}$, we can conclude that, whenever the correlation matrices C and F are real, the problem of bringing the correlation matrix γ (or, equivalently, the matrix $\mathcal{C}$, or also equivalently, the entanglement Hamiltonian) into a canonical form reduces to the problem of diagonalizing the matrix GH, where

$$\begin{cases} G &= C + F + \mathbb{1}/2 \\ H &= C - F + \mathbb{1}/2 \end{cases} . \tag{5.108}$$

The eigenvalues λ_α^2 of GH provide the entanglement spectrum through the relation

$$\lambda_\alpha = \frac{1}{2} + \frac{1}{e^{\omega_\alpha} - 1} \tag{5.109}$$

and the matrix X contains the eigenvectors. The matrices U and V bringing the bosonic modes $\boldsymbol{b}$ to the normal modes $\boldsymbol{\beta} = (\boldsymbol{Q} + i\boldsymbol{P})/\sqrt{2}$ according to

$$\boldsymbol{b} = U\boldsymbol{\beta} + V\boldsymbol{\beta}^\dagger \tag{5.110}$$

[10] In this case, the symplectic character of W is equivalent to $Y^T = X^{-1}$, as a direct evaluation of $-JW^T J$ shows.

are related to the matrices X and $Y = (X^T)^{-1}$ according to

$$\begin{cases} U &= \frac{X+Y}{2} \\ V &= \frac{X-Y}{2} \end{cases} . \tag{5.111}$$

In terms of the matrix X, our definition of the entanglement contour in Frérot and Roscilde (2015), Eq. (5.98), reads

$$w_\alpha(i) = X_{i\alpha}(X^{-1})_{\alpha i} . \tag{5.112}$$

As $X^{-1} \neq X^T$, $w_\alpha(i)$ may be negative. Recalling that X rotates the original "positions" q_i into the normal modes, see Eq. (5.105), we notice that, in addition to a mere rotation of the q_i's, X may involve some "squeezing" of the modes. Indeed, the singular value decomposition (SVD) of X

$$X = U_1 \Xi U_2 \tag{5.113}$$

with U_1 and U_2 orthogonal matrices, and $\Xi = \mathrm{diag}(e^{\xi_\alpha})$, shows that the squeezing part Ξ of the SVD is responsible for the non-orthogonality of X. This observation lead Coser, De Nobili, and Tonni (2017) to work with

$$\tilde{X} = U_1 U_2 \tag{5.114}$$

instead of X[11]. The matrix $\tilde{X}$ is then orthogonal, and the associated contour is

$$w_\alpha(i) = \tilde{X}^2_{i\alpha} \tag{5.115}$$

which is non-negative by construction. We will show that the two definitions for the entanglement contour lead to qualitatively similar insights: we observe that both definitions lead to a contour decaying when moving from the edges towards the bulk of A, and the decays exhibit a similar shape. Although there is *a priori* no reason to favor one or the other definition, we nonetheless find that the definition of Coser, De Nobili, and Tonni (2017) is in better agreement with the local thermodynamic hypothesis discussed in Section 3.3.3 on finite-size systems, supporting a related observation reported by Coser, De Nobili, and Tonni (2017) for the $1d$ harmonic chain.

5.5 Correlation functions in the SB approach

In the SB representation, a local observable $\mathcal{O}_i$ is expressed as in Eq. (5.41).

[11] It is equivalent to perform the polar decomposition (unique since X is invertible) $X = \tilde{X}P$ with P a symmetric definite positive matrix, and $\tilde{X}$ orthogonal.

Average value. Then, the average value of $\mathcal{O}_i$ is corrected, with respect to its MF value $(\tilde{\mathcal{O}}_i)_{00} = {}_i\langle\psi_0|\mathcal{O}_i|\psi_0\rangle_i$ by the nonzero population of SB modes orthogonal to the MF

$$\langle\mathcal{O}_i\rangle - (\tilde{\mathcal{O}}_i)_{00} = \sum_{\alpha,\beta>0}\left[(\tilde{\mathcal{O}}_i)_{\alpha,\beta} - \delta_{\alpha,\beta}(\tilde{\mathcal{O}}_i)_{00}\right]\langle\gamma^\dagger_{i,\alpha}\gamma_{i,\beta}\rangle\ . \tag{5.116}$$

Covariance. The covariance for two operators $\mathcal{O}_i$ and $\mathcal{O}_j$ at two different positions i and j can be obtained in a similar manner:

$$\langle\mathcal{O}_i\mathcal{O}_j\rangle - \langle\mathcal{O}_i\rangle\langle\mathcal{O}_j\rangle = \sum_{\alpha,\beta>0}\left\langle\left[(\tilde{\mathcal{O}}_i)_{\alpha 0}\gamma^\dagger_{i,\alpha} + (\tilde{\mathcal{O}}_i)_{0\alpha}\gamma_{i,\alpha}\right]\left[(\tilde{\mathcal{O}}_j)_{\beta 0}\gamma^\dagger_{j,\beta} + (\tilde{\mathcal{O}}_j)_{0\beta}\gamma_{j,\beta}\right]\right\rangle \tag{5.117}$$

where we neglected terms of order $(\gamma^{(\dagger)}_{\alpha>0})^3$ or higher, and used the fact that $\langle\gamma^{(\dagger)}_{i,\alpha>0}\rangle = 0$. Note that this holds only if the observables have nonzero matrix elements between different eigenstates of the MF Hamiltonian $(\tilde{\mathcal{O}}_i)_{\alpha 0} \neq 0$, etc. In particular, in the MI phase, the density n_i does not fulfill this condition. In this case, one must go to the next order in calculating the correlation function, and use Wick's theorem to express higher order correlators in terms of the two-body correlators. The corresponding formulas are given in the Appendix of Frérot and Roscilde (2016b).

Structure factor. If the system is translationnally invariant, it is convenient to introduce the structure factor $S(\boldsymbol{k})$ for the correlations of $\mathcal{O}$:

$$\langle\mathcal{O}_i\mathcal{O}_j\rangle - \langle\mathcal{O}_i\rangle\langle\mathcal{O}_j\rangle = \frac{1}{N}\sum_{\boldsymbol{k}} e^{i\boldsymbol{k}\cdot(\boldsymbol{r}_i-\boldsymbol{r}_j)}S(\boldsymbol{k}) \tag{5.118}$$

with

$$\begin{aligned} S(\boldsymbol{k}) \quad = \quad & \sum_{\alpha,\beta>0}\Big[(\tilde{\mathcal{O}}_i)_{\alpha 0}(\tilde{\mathcal{O}}_j)_{\beta 0}\langle\gamma^\dagger_{-\boldsymbol{k},\alpha}\gamma^\dagger_{\boldsymbol{k},\beta}\rangle + (\tilde{\mathcal{O}}_i)_{0\alpha}(\tilde{\mathcal{O}}_j)_{0\beta}\langle\gamma_{\boldsymbol{k},\alpha}\gamma_{-\boldsymbol{k},\beta}\rangle \\ & + (\tilde{\mathcal{O}}_i)_{\alpha 0}(\tilde{\mathcal{O}}_j)_{0\beta}\langle\gamma^\dagger_{-\boldsymbol{k},\alpha}\gamma_{-\boldsymbol{k},\beta}\rangle + (\tilde{\mathcal{O}}_i)_{0\alpha}(\tilde{\mathcal{O}}_j)_{\beta 0}\langle\gamma_{\boldsymbol{k},\alpha}\gamma^\dagger_{\boldsymbol{k},\beta}\rangle\Big] \end{aligned} \tag{5.119}$$

Chapter 6

Structure of entanglement in the bosonic superfluid

Introduction. This chapter is devoted to a study of the entanglement structure in the superfluid (SF) phase of the Bose-Hubbard (BH) Hamiltonian. To simplify the calculations and develop some understanding at the analytical level, we specify our attention to the limiting cases of infinite (or *hardcore*) interactions, and weak interactions. In subsection 6.1, we derive the quadratic Hamiltonian in the limit of hardcore interactions. In particular, the dispersion relation and the structure factor for the density correlations are obtained. The corresponding formulas in the Bogoliubov limit are also given. In subsection 6.2, we show that the entanglement contour exhibits a $1/r^d$ decay at large distance from the boundaries which appears to be completely universal throughout the SF phase, and we explain this result from a local thermodynamic perspective, based on the validity of the Bisognano-Wichmann theorem for Lorentz-invariant field theories. As the area law for entanglement entropy is strict in the bosonic SF, the short-distance decay of the contours actually dominates the scaling of entanglement entropy, and we show in Section 6.3 that this scaling is uniquely governed by the healing length. In subsection 6.4, we show that the density-fluctuations contour has a structure similar to the entanglement contour (exponential short-distance decay governed by the healing length, followed by a power-law decay at large distance). However, the density-fluctuations contour decays as $1/r$ at large distances, giving rise to a logarithmically violated area law for the particle-number variance in a subsystem. As for the entanglement contour, we demonstrate that the density contour at large distance follows from a local thermodynamic hypothesis, and show that the entanglement contour can be qualitatively reconstructed from the density contour via a thermodynamic relation between entropy and density fluctuations valid

at low temperature. Subsection 6.6 is finally devoted to the study of the entanglement spectrum and of the entanglement Hamiltonian in the SF phase, and several open issues are put forward.

6.1 The hardcore and Bogoliubov limits

6.1.1 Hardcore limit

We first focus on the hardcore limit, namely

$$U/t \to \infty \tag{6.1}$$

$$\bar{n} \text{ fixed} , \tag{6.2}$$

where the density $\bar{n} = \langle n \rangle$ is fixed between n_0 and $n_0 + 1$. On the phase diagram of Fig. 5.1, the hardcore limit coincides with the vertical axis $t/U = 0$. On the phase diagram, the system seems to be always in the MI phase, but this is an artifact of the representation in the $(t/U, \mu/U)$ plane: all lines of density between n_0 and $n_0 + 1$ collapse onto the single point $(t/U = 0, \mu/U = n_0)$ in the hardcore limit. Nonetheless, the density is still a function of the ratio t/μ. This situation is conceptually simple, since only occupations of n_0 or $n_0 + 1$ boson are allowed on each site. We may thus keep only two states to find the MF ground state, condense one of them, and describe the quantum fluctuations around the MF solution with a single SB flavor. We focus on the case $n_0 = 0$ for simplicity, but the following treatment is easily generalized to any n_0. In this case, since $n_i = 0$ or 1, the interaction term $Un(n-1)/2$ vanishes identically. The Hamiltonian then reduces to

$$\mathcal{H}_{\text{hardcore}} = -\sum_{ij} t_{ij} b_i^\dagger b_j - \mu \sum_i b_i^\dagger b_i \, . \tag{6.3}$$

Because of the hardcore constraint, $n_i \in \{0, 1\}$, $\mathcal{H}_{\text{hardcore}}$ is not a free Hamiltonian. Equivalently, the hardcore boson Hamiltonian can be mapped onto an XY spin model

$$\begin{cases} |0\rangle & \leftrightarrow & |\downarrow\rangle \\ |1\rangle & \leftrightarrow & |\uparrow\rangle \end{cases} . \tag{6.4}$$

In terms of the spin-1/2 operators

$$\begin{cases} S_j^x &=& (b_j^\dagger + b_j)/2 \\ S_j^y &=& (b_j^\dagger - b_j)/(2i) \\ S_j^z &=& b_j^\dagger b_j - 1/2 \\ \sigma_i^\alpha &=& 2 S_i^\alpha \end{cases} , \tag{6.5}$$

the Hamiltonian can be rewritten (we assume that t_{ij} is real)

$$\mathcal{H}_{\rm hardcore} = -\sum_{ij} t_{ij}(S_i^x S_j^x + S_i^y S_j^y) - \mu \sum_i (S_i^z + 1/2)\ . \tag{6.6}$$

In terms of the spin-1/2 operators, the hopping term is an exchange term, while the chemical potential is a magnetic field along z. The SB approach is then fully equivalent to the semi-classical approach of Holstein and Primakoff (1940), as described for instance in Coletta, Laflorencie, and Mila (2012).

Mean-field ground state in the hardcore limit. Since $\phi = \langle b_i \rangle$ is defined up to a global phase factor, we may assume that $\phi^* = \phi \geq 0$. Then, $\phi = \langle \sigma^+ \rangle = \langle \sigma^- \rangle = \frac{1}{2}\langle \sigma^x \rangle$. Considering only nearest-neighbor hopping in the matrix t_{ij}, the MF Hamiltonian takes the simple form

$$\begin{aligned} \mathcal{H}^{\rm MF}_{\rm hardcore} &= -tz\phi(b + b^\dagger) - \mu n + tz\phi^2 & (6.7)\\ &= -\vec{B}\cdot\vec{\sigma} - \mu/2 + tz\phi^2 & (6.8) \end{aligned}$$

with $\vec{B} = (tz\phi, 0, \mu/2)$ and $z = 2d$ on a hyper-cubic lattice in d dimensions. $\mathcal{H}^{\rm MF}_{\rm hardcore}$ has eigenvectors

$$\begin{aligned} |\psi_0\rangle &= \begin{pmatrix} \cos(\theta/2) \\ \sin(\theta/2) \end{pmatrix} & (6.9)\\ |\psi_1\rangle &= \begin{pmatrix} \sin(\theta/2) \\ -\cos(\theta/2) \end{pmatrix} & (6.10) \end{aligned}$$

in the basis $(|\uparrow\rangle, |\downarrow\rangle) = (|1\rangle, |0\rangle)$, with

$$\begin{cases} \tan\theta &= 2tz\phi/\mu \\ \phi &= (1/2)\sin\theta \end{cases}\ . \tag{6.11}$$

The respective eigenvalues are $\epsilon_{0/1} = \mp|\vec{B}| - \mu/2 + tz\phi^2$. From Eq. (6.11), one sees that either $\phi = \theta = 0$, or

$$\begin{cases} \cos\theta &= \mu/tz \\ \phi &= (1/2)\sqrt{1-(\mu/tz)^2} \end{cases}\ . \tag{6.12}$$

$\phi \neq 0$ is only possible if $|\mu/tz| \leq 1$, which is the situation considered in the following[1]. One also sees that the density $\bar{n} = (\langle \sigma^z \rangle + 1)/2 = \cos^2(\theta/2)$ is related to the chemical potential μ and to the superfluid order parameter ϕ according to

$$\begin{aligned} \bar{n} &= \frac{1}{2}\left(\frac{\mu}{tz} + 1\right) & (6.13)\\ \phi &= \sqrt{\bar{n}(1-\bar{n})}\ . & (6.14) \end{aligned}$$

[1] If $|\mu/tz| > 1$ in the hardcore limit, the ground state is either the vacuum ($\mu < -tz$), or in the product state containing exactly 1 boson per site ($\mu > tz$).

Slave-boson Hamiltonian and excitation spectrum in the hardcore limit. The quadratic SB Hamiltonian, see Eqs. (5.62), (5.64) and (5.65), is

$$\mathcal{H}^{(2)}_{\rm hardcore} = \frac{1}{2}\sum_{\boldsymbol{k}} \begin{pmatrix} \gamma^\dagger_{\boldsymbol{k}} & \gamma_{-\boldsymbol{k}} \end{pmatrix} \begin{pmatrix} A_{\boldsymbol{k}} & B_{\boldsymbol{k}} \\ B_{\boldsymbol{k}} & A_{\boldsymbol{k}} \end{pmatrix} \begin{pmatrix} \gamma_{\boldsymbol{k}} \\ \gamma^\dagger_{-\boldsymbol{k}} \end{pmatrix} - \sum_{\boldsymbol{k}} {\rm Tr} A_k/2 \tag{6.15}$$

where $\gamma_{\boldsymbol{k}} = V^{-1/2}\sum_j e^{-i\boldsymbol{k}\cdot\boldsymbol{r}_j}\gamma_j$, with γ_j the SB operator associated to the eigenstate $|\psi_1\rangle$ of the MF Hamiltonian. Since we have a single SB flavor, $A_{\boldsymbol{k}}$ and $B_{\boldsymbol{k}}$ are not matrices but simply numbers given by

$$\left\{ \begin{array}{rcl} A_{\boldsymbol{k}} &=& \epsilon_1 - \epsilon_0 - t_{\boldsymbol{k}}[(b_{01})^2 + (b_{10})^2] \\ B_{\boldsymbol{k}} &=& -t_k[2b_{01}b_{10}] \end{array} \right. . \tag{6.16}$$

One can evaluate $b_{01} = \langle\psi_0|\sigma^-|\psi_1\rangle = -\cos^2(\theta/2)$ and similarly $b_{10} = \sin^2(\theta/2)$. Note that $\epsilon_1 - \epsilon_0 = 2|\vec{B}| = 2\sqrt{(tz\phi)^2 + (\mu/2)^2} = tz$ in virtue of Eq. (6.12). Finally, we have[2]

$$\left\{ \begin{array}{rcl} A_{\boldsymbol{k}} &=& tz[1 - (\eta_{\boldsymbol{k}}/2)(1+\cos^2\theta)] \\ B_{\boldsymbol{k}} &=& tz(\eta_{\boldsymbol{k}}/2)\sin^2\theta \end{array} \right. \tag{6.17}$$

where we introduced $\eta_{\boldsymbol{k}} = t_{\boldsymbol{k}}/tz = (1/d)\sum_{i=1}^d \cos k_i$. The above Hamiltonian can be diagonalized by a canonical Bogoliubov transformation

$$b_{\boldsymbol{k}} = u_{\boldsymbol{k}}\beta_{\boldsymbol{k}} - v_{\boldsymbol{k}}\beta^\dagger_{-\boldsymbol{k}} \tag{6.18}$$

where $\beta_{\boldsymbol{k}}, \beta^\dagger_{\boldsymbol{k}}$ are bosonic operators destroying/creating Bogoliubov quasiparticles.

Requiring the above transformation to diagonalize $\mathcal{H}^{(2)}_{\rm hardcore}$ and to satisfy bosonic commutation relations for $\beta_{\boldsymbol{k}}, \beta^\dagger_{\boldsymbol{k}}$, leads us to the following expressions for the $u_{\boldsymbol{k}}$ and $v_{\boldsymbol{k}}$ coefficients:

$$u_{\boldsymbol{k}} = \frac{1}{\sqrt{2}}\left(\frac{A_{\boldsymbol{k}}}{\sqrt{A^2_{\boldsymbol{k}} - B^2_{\boldsymbol{k}}}} + 1\right)^{1/2} \tag{6.19}$$

$$v_{\boldsymbol{k}} = \frac{A_{\boldsymbol{k}}}{|A_{\boldsymbol{k}}|}\frac{1}{\sqrt{2}}\left(\frac{A_{\boldsymbol{k}}}{\sqrt{A^2_{\boldsymbol{k}} - B^2_{\boldsymbol{k}}}} - 1\right)^{1/2} \tag{6.20}$$

We also obtain the energy spectrum for the SB excitations

$$E_{\boldsymbol{k}} = \sqrt{A^2_{\boldsymbol{k}} - B^2_{\boldsymbol{k}}} \tag{6.21}$$

$$= tz\sqrt{(1-\eta_{\boldsymbol{k}})(1-\eta_{\boldsymbol{k}}\cos^2\theta)} \tag{6.22}$$

[2] We made use of the identities $\cos^4(\theta/2) + \sin^4(\theta/2) = (1+\cos^2\theta)/2$ and $\cos(\theta/2)\sin(\theta/2) = (1/2)\sin\theta$.

which is gapless at $\boldsymbol{k} = 0$. At small k, we may approximate $\eta_{\boldsymbol{k}} \approx 1 - k^2/2d$. Consequently, the spectrum at small k is linear

$$E_{\boldsymbol{k}} \approx \underbrace{t\sqrt{2d}|\sin\theta|}_{c} k \tag{6.23}$$

where c is the sound velocity. In terms of the density, the sound velocity is

$$c = 2t\sqrt{2d}\sqrt{\bar{n}(1-\bar{n})}\,. \tag{6.24}$$

Given the linear dispersion relation at small k, we anticipate that the gas of hardcore bosons displays an effective Lorentz invariance at low energy. It will thus be instructive to compare the prediction of the Bisognano-Wichmann theorem for the entanglement Hamiltonian, Eq. (3.37), with an explicit calculation for the lattice gas of hardcore bosons.

Density correlations in the hardcore limit. The structure factor for the density correlations is evaluated through Eq. (5.119). In the hardcore limit, the sum on $\alpha, \beta > 0$ reduces to a single term with $\alpha = \beta = 1$. One then has to evaluate the matrix elements of the density $n = S^z + 1/2$ between the MF states $|\psi_0\rangle$ and $|\psi_1\rangle$. Namely:

$$\tilde{n}_{01} = \tilde{n}_{10} = \frac{1}{2}\sin\theta\,. \tag{6.25}$$

The structure factor then reads

$$S(\boldsymbol{k}) = \frac{\sin^2\theta}{4}(2F_{\boldsymbol{k}} + 2C_{\boldsymbol{k}} + 1) \tag{6.26}$$

where $F_{\boldsymbol{k}} = \langle b_{\boldsymbol{k}} b_{-\boldsymbol{k}}\rangle$ and $C_{\boldsymbol{k}} = \langle b^\dagger_{\boldsymbol{k}} b_{\boldsymbol{k}}\rangle$. In terms of the coefficients $u_{\boldsymbol{k}}$ and $v_{\boldsymbol{k}}$ or the Bogoliubov transformation defined in Eq. (6.20), we have

$$F_{\boldsymbol{k}} = -u_{\boldsymbol{k}} v_{\boldsymbol{k}}(2n_{\boldsymbol{k}} + 1) \tag{6.27}$$

$$C_{\boldsymbol{k}} = u^2_{\boldsymbol{k}} n_{\boldsymbol{k}} + v^2_{\boldsymbol{k}}(1 + n_{\boldsymbol{k}}) \tag{6.28}$$

where $n_{\boldsymbol{k}} = [\exp(E_{\boldsymbol{k}}/T) - 1]^{-1}$ is the thermal population of the mode $\boldsymbol{k}$ ($= 0$ in the ground-state). Using the fact that $u^2_{\boldsymbol{k}} - v^2_{\boldsymbol{k}} = 1$, we can express the structure factor as

$$\begin{aligned} S(\boldsymbol{k}) &= \frac{\sin^2\theta}{4}\frac{A_{\boldsymbol{k}} - B_{\boldsymbol{k}}}{E_k}(2n_{\boldsymbol{k}} + 1) \\ &= \bar{n}(1-\bar{n})\frac{\epsilon_{\boldsymbol{k}}}{E_{\boldsymbol{k}}}(2n_{\boldsymbol{k}} + 1) \end{aligned} \tag{6.29}$$

where we introduced the free particle dispersion relation $\epsilon_{\boldsymbol{k}} = tz(1 - \eta_{\boldsymbol{k}})$, and we used the fact that $\bar{n}(1-\bar{n}) = \phi^2 = \sin^2(\theta)/4$.

6.1.2 The weak interaction limit

In the weakly interacting limit, the system also admits an accurate description in terms of a unique gapless mode of bosonic quasiparticles. This is the well-known Bogoliubov theory for the weakly interacting Bose gas (Pitaevskii and Stringari, 2003). In the SB approach, we recover the Bogoliubov limit when $U\bar{n}/t \ll 1$. In this limit, the MF ground state is a coherent state $|\psi_0\rangle \propto e^{\phi b^\dagger}|0\rangle$. The SB Hamiltonian then contains a gapless mode identical to the sound mode of Bogoliubov theory, and a family of highly gapped modes which play no role far from the phase transition to the Mott insulator. The effective Hamiltonian describing collective fluctuations of the SF order parameter takes the form of Eq. (6.15), with coefficients A_k and B_k given by

$$\left\{ \begin{array}{rcl} A_{\boldsymbol{k}} & = & \epsilon_{\boldsymbol{k}} + U\bar{n} \\ B_{\boldsymbol{k}} & = & U\bar{n} \end{array} \right. \tag{6.30}$$

where $\bar{n}$ is the density and $\epsilon_{\boldsymbol{k}} = tz(1-\eta_{\boldsymbol{k}})$. The structure factor[3] then takes a similar form as in the hardcore regime, Eq. (6.29),

$$S(\boldsymbol{k}) = \bar{n}\frac{\epsilon_{\boldsymbol{k}}}{E_{\boldsymbol{k}}}(2n_{\boldsymbol{k}}+1) \tag{6.31}$$

although with a different dispersion relation

$$E_{\boldsymbol{k}} = \sqrt{\epsilon_{\boldsymbol{k}}(\epsilon_{\boldsymbol{k}} + 2U\bar{n})}\,. \tag{6.32}$$

In particular, the dispersion relation at small k is also linear, $E_{\boldsymbol{k}} \approx ck$, with a sound velocity $c = t\sqrt{2U\bar{n}}$.

6.2 Universal entanglement structure in the SF phase

In this section, we show that the local thermodynamic hypothesis, together with the effective Lorentz invariance in the SF, predicts a universal behavior for the entanglement contour, and verify this prediction by an explicit calculation in $d = 2$ and $d = 3$.

6.2.1 Universal prediction for the entanglement contour

Strict area law in the bosonic superfluid. In contrast to the free fermion case discussed in Section 4, the gapless bosonic superfluid in $d \geq 2$ is known to obey a strict area law

$$S \sim l^{d-1} \tag{6.33}$$

[3] See for instance the Appendix of Frérot and Roscilde (2015) for the derivation of this expression.

where S is the entanglement entropy of a subsystem A whose linear size is l. In Frérot and Roscilde (2015), we have shown this result for the weakly interacting Bose gas within Bogoliubov theory. Similar results have been reported in the Heisenberg antiferromagnet by Song et al. (2011) via spin-wave theory and by (Hastings et al., 2010; Kallin et al., 2011; Humeniuk and Roscilde, 2012) via quantum Monte Carlo calculations. Field-theory calculations have also proved the area law of entanglement entropy for free bosonic fields (Casini and Huerta, 2009). The area law scaling in a gapless phase is *a priori* not obvious, since correlations decay as a power-law with distance: as for the free fermion case, one could have expected logarithmic corrections to the area law[4].

Decay of the entanglement contour. In Section 4, we showed that the logarithmic correction to the area law for free fermions originates from the very slow decay of the entanglement contour when moving into the bulk of A:

$$\mathcal{C}_s(i) \sim 1/r(i) \tag{6.34}$$

where $r(i)$ is the distance of site i to the A-B boundary. Integrating the contour over the region A then provides the $\ln l$ multiplicative correction to the area law. In a similar spirit, in Frérot and Roscilde (2015), we showed that the strict area law scaling for bosons can be explained by the observation that the entanglement contour decays as

$$\mathcal{C}_s(i) \sim 1/r(i)^d \tag{6.35}$$

in d dimensions. In agreement with the critical nature of the phase, the entanglement contour decays as a power-law with distance, but in an integrable manner as long as $d \geq 2$, justifying the strict area law.

In fact [and this represents the main novelty of the present chapter with respect to Frérot and Roscilde (2015)], the decay of the entanglement contour is partly explained by the Bisognano-Wichmann (BW) prediction, supplemented by the local equilibrium approximation (LEA) discussed in Section 3.3.3.

BW prediction. Indeed, considering that A is a half-infinite system $(x_1 > 0, x_2, \dots x_d)$, the BW theorem predicts that the entanglement Hamiltonian is the physical Hamilto-

[4] Note that we are not discussing here the logarithmic *additive* (and thus subdominant) correction to the area associated to the spontaneous breaking of a continuous symmetry in the thermodynamic limit (Metlitski and Grover, 2011), see the devoted chapter in the review of Laflorencie (2016) and references therein. We are only interested in developing a thermodynamic understanding for the dominant area term, and its dependency on the physical properties of the system under investigation.

nian modulated in space by the local entanglement temperature

$$T(\boldsymbol{r}) = \frac{c}{2\pi}\frac{1}{x_1} \,. \tag{6.36}$$

where c is the speed of light (in our case, c is the speed of sound in the superfluid).

Local equilibrium approximation. According to the LEA hypothesis, the entanglement entropy of A is then

$$S \approx \int_{\boldsymbol{r}\in A} d^d\boldsymbol{r}\ \underbrace{s[T(\boldsymbol{r})]}_{\mathcal{C}_s(\boldsymbol{r})} \tag{6.37}$$

where $s(T)$ is the thermal entropy evaluated at the local temperature $T(\boldsymbol{r})$. When the entropy is associated to free bosonic modes with a linear dispersion $E_{\boldsymbol{k}} = ck$, we have (in units where $k_B = \hbar = 1$)

$$s(T) = \int \frac{d^d\boldsymbol{k}}{(2\pi)^d} s_{\rm Bose}\left(\frac{1}{e^{ck/T}-1}\right) \tag{6.38}$$

where $s_{\rm Bose}$ is defined in Eq. (5.94). Making the change of variable $u = ck/T$ in the integral, we conclude that

$$s(T) = \left(\frac{T}{c}\right)^d \alpha_d \tag{6.39}$$

where α_d is some d-dependent constant which can be evaluated to[5]

$$\begin{aligned} \alpha_2 &= \frac{3\zeta(3)}{2\pi} \approx 0.574 \\ \alpha_3 &= \frac{2\pi^2}{45} \approx 0.439 \,. \end{aligned} \tag{6.42}$$

Universal entanglement contour. As a consequence, the BW + LET prediction that the entanglement contour should coincide with the local thermodynamic entropy is, for a semi-infinite subsystem:

$$\mathcal{C}_s(\boldsymbol{r}) = s[T(\boldsymbol{r})] = \frac{\alpha_d}{(2\pi x_1)^d} \,. \tag{6.43}$$

[5] The constant α_d can be evaluated as follows. We start from the energy per unit volume

$$u(T) = \int \frac{d^d\boldsymbol{k}}{(2\pi)^d}\frac{ck}{e^{ck/T}-1} = \frac{\Omega_d}{(2\pi)^d}\frac{T^{d+1}}{c^d} f_B(d) \tag{6.40}$$

where $f_B(d) = \int_0^\infty dx\ x^d/(e^x-1) = d!\,\zeta(d+1)$ with ζ the Riemann function, and Ω_d the solid angle: $\Omega_2 = 2\pi$ and $\Omega_3 = 4\pi$. We then use

$$s(T) = \int_0^T \frac{\partial u}{\partial T}\frac{dT}{T} = \left(\frac{T}{c}\right)^d \frac{d+1}{d}\frac{\Omega_d f_B(d)}{(2\pi)^d} \,. \tag{6.41}$$

Since $\zeta(3) = 1.20205\ldots$ and $\zeta(4) = \pi^4/90$, we conclude the expressions given in Eq. (6.42).

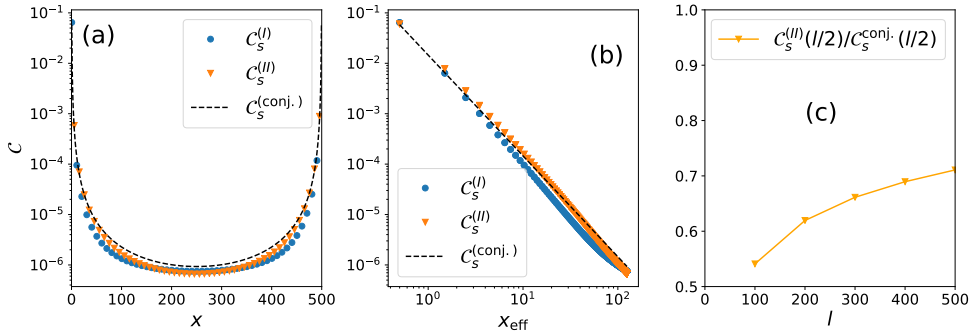

Figure 6.1: Entanglement contour for $2d$ hardcore bosons at half filling. A is a 500×500 cylinder cut out of a $10^4 \times 500$ torus. The mode at $\boldsymbol{k} = 0$ has been gapped with a small field $h = 1/500^2$, and the entanglement lowest mode removed (see the footnote 6). (a) Contour $\mathcal{C}_s^{(I)}$ (Frérot and Roscilde, 2015) (blue circles), contour $\mathcal{C}_s^{(II)}$ (Coser, De Nobili, and Tonni, 2017) (orange triangles), and BW + LET conjecture, Eq. (6.45) (black dashed line); see text for details. (b) Same as (a), but as a function of the effective distance x_{eff} defined in Eq. (6.46). (c) Ratio $\mathcal{C}_s^{(II)}/\mathcal{C}_s^{(\text{conj.})}$ at the center of A (namely at $x = l/2$).

This prediction nicely agrees with the $1/x_1^d$ decay of the entanglement contour for a system of gapless bosons we have reported in Frérot and Roscilde (2015). Furthermore, it predicts that the prefactor of the $1/x_1^d$ decay is universal, independent of the microscopic details of the Hamiltonian (such the sound velocity, the density and so on).

6.2.2 Numerical verification of the universal prediction

On Fig. 6.1 and 6.2, we show that the BW + LET conjecture contained in Eq. (6.43) is in reasonable agreement with the lattice calculation of the entanglement contour in $d = 2$ and $d = 3$ respectively[6].

[6] There are two main subtleties related to the calculation of the entanglement contour for bosons, discussed extensively in Frérot and Roscilde (2015). The first one is related to the treatment of the $\boldsymbol{k} = 0$ mode. Being of zero energy, it cannot be handled by the Bogoliubov transformation. If it is simply ignored in the calculations, the entanglement contour on a cylinder acquires a spurious alteration. A better procedure is to follow the prescription of Song et al. (2011) to gap it out by introducing a small term $-h(b_i + b_i^\dagger)$ into the Hamiltonian, slightly modifying the expressions for the MF ground state and the resulting quadratic SB Hamiltonian (the only difference, in the end, is that we must add a term $+h \sin\theta$ to $A_{\boldsymbol{k}}$ in Eq. (6.17)). The size-dependent field h should scale to zero as $1/V^2$ in the thermodynamic limit in order for the zero mode to contribute at most a constant to the momentum-space integrals of the kind $(1/V)\sum_{\boldsymbol{k}}(\cdots)/\omega_{\boldsymbol{k}}$ (see discussion in Frérot and Roscilde (2015)). The second subtlety comes from the fact that, on any accessible size, the entanglement contour is dominated by the contribution of a single entanglement mode — the entanglement mode of lowest energy, hence of highest weight — whose profile decays as $1/x$ instead of $1/x^d$. The contribution of this entanglement lowest mode to the contour should then be removed to properly study the thermodynamic limit (as it represents a microscopic contribution to the entanglement entropy). Unless otherwise stated, we follow this procedure

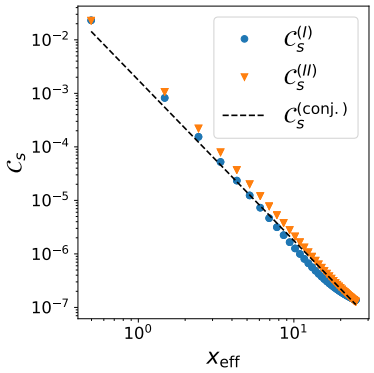

Figure 6.2: Entanglement contour for $3d$ hardcore bosons at half filling. A is a $100 \times 100 \times 100$ hyper-cylinder cut out of a $2000 \times 100 \times 100$ hyper-torus. Same treatment of the zero modes as for Fig. 6.1. Contour $\mathcal{C}_s^{(I)}$ (Frérot and Roscilde, 2015) (blue circles), contour $\mathcal{C}_s^{(II)}$ (Coser, De Nobili, and Tonni, 2017) (orange triangles), and BW + LET conjecture, Eq. (6.45) (black dashed line); see text for details. Contours are plotted as a function of the effective distance x_{eff} defined in Eq. (6.46).

Universal entanglement contour for a cylinder-in-a-torus geometry. The geometry we are considering is not the semi-infinite plane of the BW theorem. Instead, our subsystem A is a $l \times l^{d-1}$ (hyper-)cylinder cut out of a $L \times l^{d-1}$ (hyper-)torus. Namely, A contains sites $x = 1, \dots l$ in the first direction (denoted x), and all sites in the remaining $d-1$ dimensions where periodic boundary conditions are imposed. This geometry enables us to take advantage of the translational invariance along $d-1$ directions parallel to the cut, and to simplify the diagonalization of the correlation matrix, since the latter is block-diagonal with respect to the momentum $k_{\|}$. To approximate at best the thermodynamic limit, we take $L \gg l$ (in practice, we work with $L/l = 20$). Nonetheless, since A and B have now two boundaries in common, the conjecture of Eq. (6.43) must be adapted. In analogy with the result of conformal field theory (Wong et al., 2013), and with our findings on free fermions reported in Section 4, we conjecture that the local temperature is

$$T(x) = \frac{c}{2\pi}\left(\frac{1}{x-1/2} + \frac{1}{l-x+1/2}\right) , \tag{6.44}$$

namely the sum of the temperatures associated to the presence of each boundary. The term $1/2$ comes from the fact that the first boundary between A and B is between sites at $x = 0$ and $x = 1$, so at position $x = 1/2$, and similarly the second boundary

in our analyses of the entanglement contours for gapless bosons (namely, here, in the SF phase of the BH model). In a gapped phase (namely, here, in the MI phase), no such subtlety occurs and we can keep all the physical modes, without the need of gapping one of them out, and all the entanglement modes alike.

is at position $l + 1/2$. Then the conjecture for the entanglement contour is

$$\mathcal{C}_s^{(\text{conj.})}(\boldsymbol{r}) = \frac{\alpha_d}{(2\pi)^d} \left(\frac{1}{x - 1/2} + \frac{1}{l - x + 1/2} \right)^d . \tag{6.45}$$

An equivalent way to formulate this statement is to introduce the effective distance

$$\begin{aligned} x_{\text{eff}} &= \left(\frac{1}{x - 1/2} + \frac{1}{l - x + 1/2} \right)^{-1} \\ &= \frac{(x - 1/2)(l - x + 1/2)}{l} \end{aligned} \tag{6.46}$$

such that the conjectured entanglement contour is $\mathcal{C}_s^{(\text{conj.})}(\boldsymbol{r}) = \alpha_d/(2\pi x_{\text{eff}})^d$.

Discussion. On Fig. 6.1 and 6.2, we have calculated two proposed forms for the entanglement contour: the contour $\mathcal{C}_s^{(I)}$ proposed in our paper (Frérot and Roscilde, 2015), corresponding to Eq. (5.112) for the local weight $w_\alpha(i)$ associated to the entanglement mode α; and the contour $\mathcal{C}_s^{(II)}$ of Coser, De Nobili, and Tonni (2017), corresponding to Eq. (5.115) for $w_\alpha(i)$. The first, reassuring observation, is that both definitions give rise to a contour exhibiting a similar decay when moving towards the bulk of A [panel (a)]. The second observation is that the BW + LET conjecture of Eq. (6.45) is rather close to the lattice calculation [panel (b)]. Since the agreement is slightly better with for the contour $\mathcal{C}_s^{(II)}$ of Coser, De Nobili, and Tonni (2017), from now on, unless otherwise stated, we shall always use this definition of the entanglement contour. On panel (c), we show that on the sizes accessible to the calculation (here a 500×500 cylinder in a $10^4 \times 500$ torus), finite size effects are still manifest, and we may conjecture that the agreement between $\mathcal{C}_s^{(I)}$, $\mathcal{C}_s^{(II)}$ and $\mathcal{C}_s^{(\text{conj.})}$ increases for even larger sizes. Similar observations hold in $d = 3$, as illustrated on Fig. 6.2.

6.3 Entanglement structure and the healing length

6.3.1 Beyond of the field-theory prediction

Short-distance cutoff of the field-theory. In the previous section, we showed that the universal decay of the entanglement contour in the bulk of A is in good agreement with the Bisognano-Wichmann field theory prediction, according to which the entanglement Hamiltonian for a gapless bosonic superfluid is completely universal. Nonetheless, this prediction holds only *beyond a certain short distance cutoff*, that we denote ξ. The first, naive expectation is that ξ is just the lattice spacing. But if this were the case, then entanglement entropy would be almost constant throughout the SF phase, since the entanglement Hamiltonian would be almost constant, at least far from

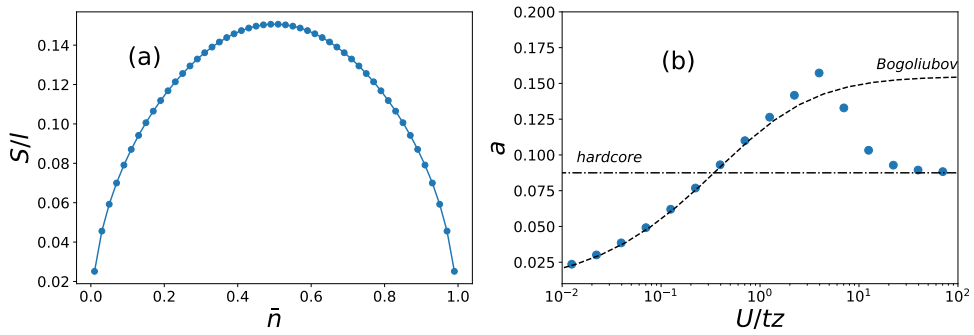

Figure 6.3: Entanglement entropy in the SF phase in two dimensions. (a) Entanglement entropy in the hardcore limit $U/tz = \infty$, as a function of the density $\bar{n}$. A is half of a $2l \times l$ torus with $l = 100$. (b) Entanglement entropy in the softcore (generic) regime, calculated within the SB approximation (circles), with $\bar{n} = 0.9$. a results from fits of the form $S = al + b \ln l + c$, with $l = 10, \dots 100$. The dashed line is the prediction of Bogoliubov theory, valid in weak interaction limit $U \ll tz$, and the dashed-dotted line the prediction in the hardcore limit $U \gg tz$. The SB calculation, valid throughout the SF phase, interpolates between these two limiting cases. The local maximum results from the proximity of a quantum critical point (namely the SF/MI phase transition at the O(2) point).

the O(2) points, where the description in terms of a unique gapless mode ceases to be correct. But this prediction is in complete contradiction with the observation. On Fig. 6.3, we have plotted the entanglement entropy in the hardcore regime varying the density between 0 and 1, and in the softcore regime varying interaction from very weak (Bogoliubov regime) to infinity (hardcore regime) at fixed density $\bar{n} = 0.9$. Clearly, entanglement entropy is very sensitive to the microscopic details, a sensitivity which is completely missed by the field-theory prediction. In fact, this dependency is largely explained by the existence of another microscopic length scale, independent of the lattice cutoff: the healing length of the condensate.

The healing length. The healing length ξ is the characteristic length beyond which the SF order parameter ϕ recovers its bulk value near a defect. In our case, it is also the characteristic length below which the Lorentz invariance, associated to the linear dispersion relation at small k, is not a good approximation. The healing length can be introduced as

$$\xi = \frac{1}{mc}\,, \tag{6.47}$$

where $m = (2t)^{-1}$ is the mass (in our case, the effective mass given by the curvature of the one-particle dispersion relation on the lattice $\epsilon_{\boldsymbol{k}} \approx tk^2 = k^2/2m$, and c is the speed of sound; restoring the units, the healing length would be $\xi = \hbar/mc$). In the

Bogoliubov and hardcore limits respectively, the speed of sound is $c_{\text{Bogo.}} = t\sqrt{2U\bar{n}}$ and $c_{\text{HC}} = 2t\sqrt{z\bar{n}(1-\bar{n})}$ with $z = 2d$. As a consequence, the healing length is (in units of the lattice spacing)

$$\xi_{\text{Bogo.}} = \sqrt{\frac{2t}{U\bar{n}}} \tag{6.48}$$

$$\xi_{\text{HC}} = \frac{1}{\sqrt{z\bar{n}(1-\bar{n})}} . \tag{6.49}$$

6.3.2 Non-universal entanglement contour at short distance

As we show on Fig. 6.4(a, b), it is only beyond ξ that the entanglement contours assume their universal value.

Exponential decay of the short-distance entanglement contour. As shown on panel (c, d) of the same Fig. 6.4, at distances smaller than ξ, on the other hand, the decay of the contour is exponential, with a decay length compatible with the healing length ξ

$$\mathcal{C}_s(x_{\text{eff}}) \approx \mathcal{C}_s(1/2)e^{-ax_{\text{eff}}/\xi} \tag{6.50}$$

with a some constant of order 1, and $\mathcal{C}_s(1/2)$ is the value of the contour at the boundary. Furthermore, as shown on Fig. 6.4(e), $\mathcal{C}_s(1/2)$ converges in the thermodynamic limit to

$$\mathcal{C}_s(1/2) \approx \frac{a'}{\xi^d} , \tag{6.51}$$

with a' a numerical factor which is weakly dependent on the model.

Short- and long-distance contributions of the contours to entanglement entropy. Finally, summing the universal, long-distance contribution and the non-universal, healing-length dominated, short-distance contribution to entanglement entropy, we conclude that

$$S = S_{\text{univ.}}(\xi) + S_{\text{short-dist.}}(\xi) . \tag{6.52}$$

Since the integration of the contour along the boundary provides a trivial $2l^{d-1}$ factor (recall that A has the shape of a cylinder immersed in a torus, hence it has two boundaries, each of area l^{d-1}), both terms on the r.h.s are proportional to $2l^{d-1}$, while the prefactor of the area-law stems from the integration of the contour when moving to the bulk of A. The universal contribution is

$$S_{\text{univ.}}(\xi) = 2l^{d-1}\int_{\xi}^{\infty} dr\, \frac{\alpha_d}{(2\pi r)^d} \tag{6.53}$$

$$= 2l^{d-1}\frac{\alpha_d}{(2\pi)^d(d-1)\xi^{d-1}} \tag{6.54}$$

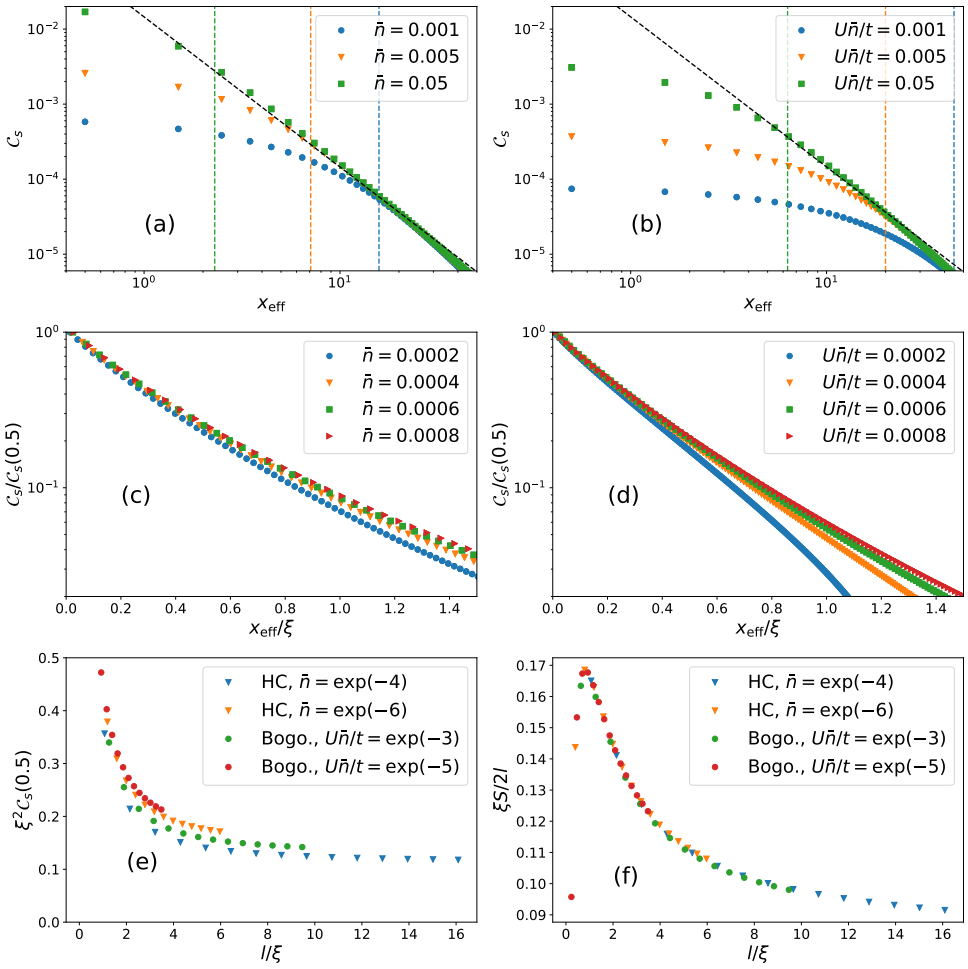

Figure 6.4: Spatial structure of entanglement in the SF phase in two dimensions. A is a $l \times l$ cylinder cut out of a $20l \times l$ torus. (a) Entanglement contour in the hardcore limit $U/tz = \infty$, for various densities $\bar{n}$ (for $l = 500$). Contours are plotted as a function of the effective distance x_{eff}, see Eq. (6.46). Vertical dashed lines indicate the cross-over to the universal regime occurring at $x \approx \xi = 1/\sqrt{z\bar{n}(1-\bar{n})}$. (b) Same as in (a), but in the Bogoliubov regime, varying the small parameter $U\bar{n}/t$. The healing ξ is $\sqrt{2t/U\bar{n}}$. (c) and (d): Entanglement contours are rescaled to the value at the boundary $\mathcal{C}_s(1/2)$, and plotted as a function of the rescaled position x/ξ. Note the logarithmic scale on the vertical axis, showing an exponential decay at short distance. (c) Hardcore limit and (d) Bogoliubov limit. (e) Value of the contour at the boundary, rescaled to $1/\xi^2$, as a function of l/ξ. Data are plotted on the same graph for both the hardcore limit (HC, triangles), and the Bogoliubov limit (Bogo., circles), showing that the behavior of the contour is uniquely controlled by the healing length ξ. (f) Entanglement entropy, rescaled to $2l/\xi$, as a function of l/ξ. In (e) and (f), instead of introducing a small gap into the spectrum, we have removed the mode at $\boldsymbol{k} = 0$, and we have kept the contribution from the lowest entanglement mode, since it complicates the analysis of the structure of entanglement only in the bulk of A. For comparison, the curve similar to (f) presented in Frérot and Roscilde (2015) was without the contribution from the lowest entanglement mode, and for a different aspect ratio.

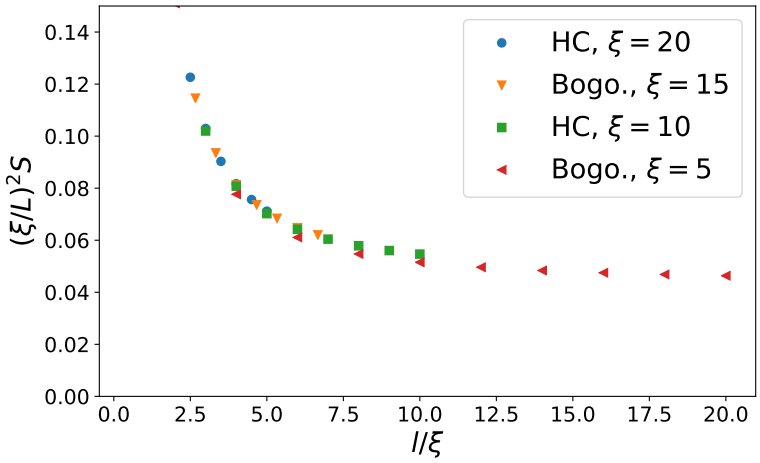

Figure 6.5: Scaling of entanglement entropy in the SF regime, in $d = 3$. Subsystem A is a $l \times l \times l$ hyper-cylinder (periodic along the y and z directions), immersed in a $20l \times l \times l$ hyper-torus, for $l = 10, \ldots 100$. Entanglement entropy (rescaled to $(l/\xi)^2$)) as a function of l/ξ, for various values of the healing length, for either the hardcore limit (HC) or the Bogoliubov limit (Bogo.).

with α_d the constant calculated in Eq. (6.42), and the short-distance contribution is

$$S_{\text{short-dist.}}(\xi) = 2l^{d-1} \frac{a'}{\xi^d} \int_0^\infty dr\, e^{-ar/\xi} \tag{6.55}$$

$$= 2l^{d-1} \frac{a'}{a\xi^{d-1}} . \tag{6.56}$$

Area-law prefactor of entanglement entropy. Overall, we find that both terms give a similar contribution to the prefactor of the area law, so that the entanglement entropy behaves simply as

$$S = b \left(\frac{l}{\xi} \right)^{d-1} . \tag{6.57}$$

In the cylinder-in-a-torus geometry,

$$b = \frac{2\alpha_2}{(2\pi)^2} + \frac{2a'}{a} \tag{6.58}$$

contains a first universal term and a second one which, despite being non-universal, shows only a weak dependence on the specific model [Fig. 6.4(e)]. On Fig. 6.4(f), we have plotted $\xi S/(2l)$ as a function of l/ξ in $d = 2$ in both the hardcore and the Bogoliubov limits. The collapse of the various data onto a single curve further confirms the validity of the arguments presented in this section. Finally, the validity of the scaling Ansatz is further demonstrated on Fig. 6.5 for $d = 3$.

6.4 Contour of density correlations in the SF phase

The density correlations in the SF phase have the same structure in both the Bogoliubov and the hardcore regimes. In this section, we are going to show that the contour of density fluctuations, $\mathcal{C}_n$, introduced in Section 3.3.3, enables one to extract the local entanglement temperature of the Bisognano-Wichmann theorem, Eq. (6.44). In order to do so, we are going to

1. calculate the density contour at large distance for the cylinder-in-a-torus geometry;
2. calculate the variance $\langle \delta^2 N \rangle(T)$ of the number of particles in a system containing V sites at thermal equilibrium;
3. show that at large distance, the density contour is
$$\mathcal{C}_n(\boldsymbol{r}) \approx \frac{\langle \delta^2 N \rangle[T(\boldsymbol{r})])}{V} \tag{6.59}$$
with
$$T(\boldsymbol{r}) = \frac{c}{2\pi}\left(\frac{1}{x-1/2} + \frac{1}{l-x+1/2}\right) , \tag{6.60}$$
c being the sound velocity, and x the position in the direction perpendicular to the cut between A and B (hence moving towards the bulk of A).

6.4.1 Expression of the structure factor

To unify the notations, we first remark that the prefactor $\bar{n}(1-\bar{n})$ of the structure factor in the hardcore regime, Eq. (6.29), and $\bar{n}$ in the Bogoliubov regime, Eq. (6.31), are just the onsite variance of the number of particles, as predicted by the MF Ansatz. In the hardcore regime, we can have only 0 or 1 particle, so that the variance of n is just $\langle \delta^2 n \rangle_{\mathrm{MF}} = \bar{n}(1-\bar{n})$ with $\bar{n}$ the average of n. In the Bogoliubov regime, the MF Ansatz is a coherent state, and coherent states have purely poissonnian fluctuations with $\langle \delta^2 n \rangle_{\mathrm{MF}} = \langle n^2 \rangle - \langle n \rangle^2 = \bar{n}$. In both the hardcore and the Bogoliubov limit, the structure factor for the density correlations takes the form
$$\frac{S(\boldsymbol{k})}{\langle \delta^2 n \rangle_{\mathrm{MF}}} = \frac{\epsilon_{\boldsymbol{k}}}{E_{\boldsymbol{k}}}(2n_{\boldsymbol{k}}+1) \tag{6.61}$$
Since we are interested in the behavior of the correlations at long distance (namely at small k), we introduce an effective mass $m = (2t)^{-1}$ such that the free-particle dispersion relation on the lattice is
$$\epsilon_{\boldsymbol{k}} \approx \frac{k^2}{2m} . \tag{6.62}$$
On the other hand, at small k the spectrum is linear, $E_{\boldsymbol{k}} \approx ck$.

Structure factor in the ground state. At $T = 0$ (so that $n_k = 0$), the structure factor at small k is then

$$\frac{S(\boldsymbol{k})}{\langle \delta^2 n \rangle_{\rm MF}} \approx \frac{k}{2mc} \ . \tag{6.63}$$

To develop a thermodynamic understanding of the structure of entanglement entropy, we will relate the contour of density fluctuations to the thermal behavior of $\langle \delta^2 N \rangle$, the variance of the total number of particles.

Thermal variance of the number of particles. We have $\langle \delta^2 N \rangle = S(\boldsymbol{k} = 0)/V$. Since the spectrum is gapless at $k \to 0$, we may replace $2n_{\boldsymbol{k}} + 1$ by $2k_B T/E_{\boldsymbol{k}}$ at small $\boldsymbol{k}$. We thus see that the structure factor has a finite limit at $k \to 0$, given by

$$\frac{S(\boldsymbol{k} = 0)}{\langle \delta^2 n \rangle_{\rm MF}} = \frac{\langle \delta^2 N \rangle}{V \langle \delta^2 n \rangle_{\rm MF}} = \frac{k_B T}{mc^2} \ . \tag{6.64}$$

6.4.2 Density fluctuations contour

General expression. The density-fluctuations contour is

$$\begin{aligned} \mathcal{C}_n(\boldsymbol{r}) &= \sum_{\boldsymbol{r}' \in A} \langle \delta n(\boldsymbol{r}) \delta n(\boldsymbol{r}') \rangle & (6.65) \\ &= \frac{1}{V} \sum_{\boldsymbol{r}' \in A} \sum_{\boldsymbol{k}} e^{-i\boldsymbol{k}\cdot(\boldsymbol{r}'-\boldsymbol{r})} S(\boldsymbol{k}) & (6.66) \\ &= \frac{1}{V} \sum_{\boldsymbol{k}} T_A(\boldsymbol{k}) S(\boldsymbol{k}) e^{i\boldsymbol{k}\cdot\boldsymbol{r}} & (6.67) \end{aligned}$$

where we have introduced the form factor

$$T_A(\boldsymbol{k}) = \sum_{\boldsymbol{r}' \in A} e^{-i\boldsymbol{k}\cdot\boldsymbol{r}'} \ . \tag{6.68}$$

Expression on a half-(hyper)-torus. We assume that A has the shape of a (hyper)-cylinder, containing sites $1, \dots l$ in the first direction, of total size L, and all sites in the remaining $d-1$ directions, of sizes $l_2, \dots l_d$, where periodic boundary conditions are imposed. As a consequence, the form factor is

$$T_A(\boldsymbol{k}) = l_2 \delta_{k_2,0} \cdots l_d \delta_{k_d,0} \frac{1 - e^{-ik_1 l}}{1 - e^{-ik_1}} e^{-ik_1} \ , \tag{6.69}$$

so that the density-fluctuations contour is, factorizing $e^{ik_1(1-l)/2}$ on the r.h.s

$$\mathcal{C}_n(\boldsymbol{r}) = \frac{1}{L} \sum_{k_1} S(k_1, 0, \dots 0) \frac{\sin(k_1 l/2)}{\sin(k_1/2)} e^{ik_1(x_1 - 1/2 - l/2)} \ . \tag{6.70}$$

In the thermodynamic limit of large L, we can replace the sum over the Brillouin zone by an integral. Furthermore, in the limit of large l, the factor $\sin(k_1 l/2)/\sin(k_1/2)$ is strongly peaked near $k_1 = 0$. We may thus replace $\sin(k_1/2)$ by $k_1/2$. Finally, in this regime, the structure factor can be approximated by Eq. (6.63). Hence we obtain the following expression, valid in the thermodynamic limit

$$\frac{\mathcal{C}_n(\boldsymbol{r})}{\langle\delta^2 n\rangle_{\rm MF}} \approx \int_0^{2\pi} \frac{dq}{2\pi}\,\frac{1}{mc}\sin(ql/2)e^{iq(x_1-1/2-l/2)}\,. \tag{6.71}$$

Replacing $\sin(ql/2)$ by $(e^{-iql/2}-e^{iql/2})/(2i)$ and integrating between 0 and 2π, we finally obtain

$$\frac{\mathcal{C}_n(\boldsymbol{r})}{\langle\delta^2 n\rangle_{\rm MF}} \approx \frac{1}{2\pi mc}\left(\frac{1}{x_1-1/2}+\frac{1}{l+1/2-x_1}\right)\,. \tag{6.72}$$

This expression is manifestly equal to the thermal variance $k_B T/(mc^2)$, evaluated at the local temperature given by Eq. (6.44).

In terms of the effective distance $x_{\rm eff}$ introduced in Eq. (6.46), the density contour reads

$$\frac{\mathcal{C}_n(\boldsymbol{r})}{\langle\delta^2 n\rangle_{\rm MF}} \approx \frac{\xi}{2\pi x_{\rm eff}}\,, \tag{6.73}$$

an expression showing that, apart from the prefactor $\langle\delta^2 n\rangle_{\rm MF}$, the large distance decay of the density contour is uniquely controlled by the healing length $\xi = (mc)^{-1}$.

Short- and long-distance structure of the density-fluctuations contour. As illustrated on Fig. 6.6(a) in $d = 2$, this scaling is perfectly reproduced by an exact calculation at distances larger than the healing length: as for the entanglement contour, the density-fluctuations contour exhibits an exponential decay $\exp(-ax/\xi)$ at short distance, controlled by the healing length, followed by an algebraic decay as $1/x$ at long distance.

Scaling of the particle-number variance in a subsystem. In contrast to the entanglement contour, however, the $1/x$ tail is not integrable, and dominates the scaling of the particle-number variance $\langle\delta^2 N\rangle$ in a subsystem. Indeed, we can predict that the asymptotic scaling of $\langle\delta^2 N\rangle$ is

$$\frac{\langle\delta^2 N\rangle}{\langle\delta^2 n\rangle_{\rm MF}} = \frac{\sum_{\boldsymbol{r}\in A}\mathcal{C}_n(\boldsymbol{r})}{\langle\delta^2 n\rangle_{\rm MF}} \approx 2l^{d-1}\frac{\xi}{2\pi}\int_\xi^l \frac{dx}{x} = \frac{\xi}{\pi}l^{d-1}\ln(l/\xi)\,. \tag{6.74}$$

As shown on Fig. 6.6(b) for $d = 2$, and 6.6(c) for $d = 3$, this scaling forms allows a perfect collapse of the data for various values of the healing length, in both the hardcore and Bogoliubov regimes.

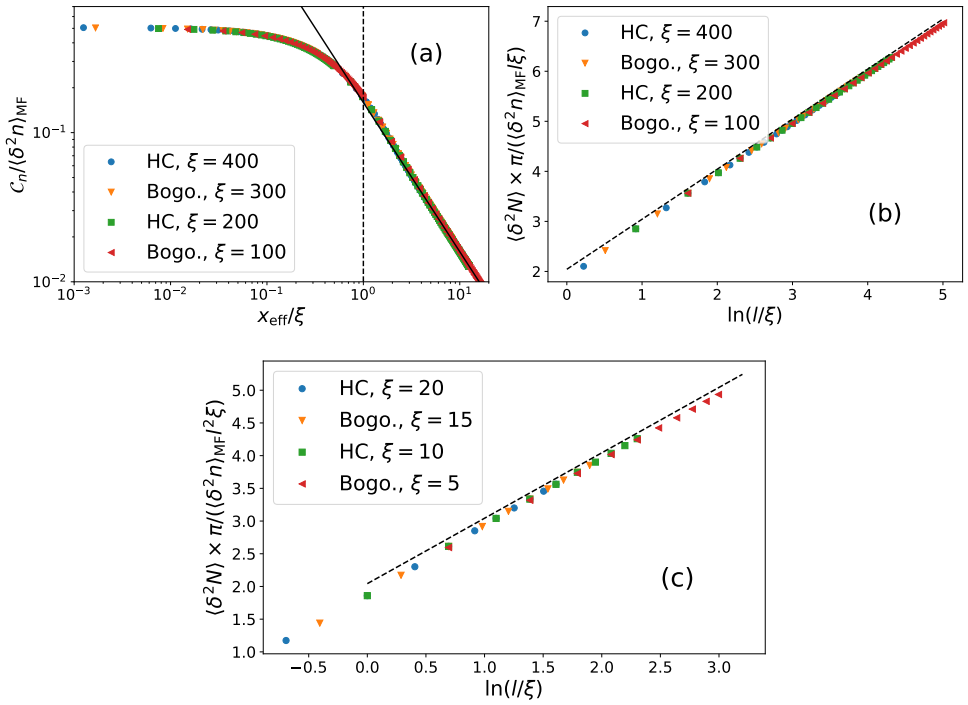

Figure 6.6: Density contour in the SF phase. A is a $l \times l$ cylinder in a $l \times 20l$ torus. (a) Density contour rescaled to the MF variance of the density $\langle\delta^2 n\rangle_{\rm MF}$, as a function of the effective distance $x_{\rm eff}$ defined in Eq. (6.46), rescaled to the healing length ξ. Data are shown for various values of the healing length (related to the microscopic parameters of the Hamiltonian by Eq. (6.49)), for either the hardcore limit (HC) or the Bogoliubov limit (Bogo.). The vertical dashed line indicates the cross-over from exponential to power-law decay at $x_{\rm eff} \approx \xi$, and the black solid line is the theoretical prediction $\xi/(2\pi x_{\rm eff})$ (see text). $l = 10^4$. (b) Scaling of the particle-number variance $\langle\delta^2 N\rangle$ in a subsystem, rescaled to $l\xi\langle\delta^2 n\rangle_{\rm MF}/\pi$, as a function of $\ln(l/\pi)$. The dashed line indicates a slope 1, and $l = 500, 1000, \ldots 15000$. (c) Particle-number variance in A in $d = 3$ dimensions, rescaled to $l^2\xi\langle\delta^2 n\rangle_{\rm MF}/\pi$, as a function of $\ln(l/\xi)$. The dashed line indicates a slope of 1. Same geometry and symbols as in Fig. 6.5.

6.5 Discussion

Summary of the results obtained for the contours in the bosonic superfluid. We have found that the entanglement contour and the density-fluctuations contour display a similar behavior: an exponential short-range decay controlled by the healing length, followed by an algebraic decay at distances larger than the healing length. They differ in the exponent of the algebraic decay: $1/x$ for the density contour, and $1/x^d$ for the entanglement contour. We have been able to interpret this difference in terms of a local temperature, theoretically predicted to decay as $c/(2\pi x_{\rm eff})$ for Lorentz invariant field theories, with c the sound velocity and $x_{\rm eff}$ the (effective) distance to the boundary of the subsystem A[7]. In particular, we have shown that the prefactor of the algebraic decay of the contours can be predicted by a local equilibrium hypothesis, according to which the contour takes the value of the associated thermodynamic quantity, evaluated at the local temperature:

$$\mathcal{C}_s(\boldsymbol{r}) \approx s[T(\boldsymbol{r})] = \alpha_d \left(\frac{T(\boldsymbol{r})}{c}\right)^d = \frac{\alpha_d}{(2\pi x_{\rm eff})^d} \tag{6.75}$$

$$\mathcal{C}_n(\boldsymbol{r}) \approx \frac{\langle\delta^2 N\rangle[T(\boldsymbol{r})]}{V} = \langle\delta^2 n\rangle_{\rm MF}\frac{T(\boldsymbol{r})}{mc^2} = \frac{\langle\delta^2 n\rangle_{\rm MF}}{2\pi}\frac{\xi}{x_{\rm eff}}\,. \tag{6.76}$$

These expressions, valid only for distances larger than the healing length, show in particular that the decay of the entanglement contour is universal (α_d is a d-dependent constant that we have determined exactly, see the discussion around Eq. (6.42)).

Thermodynamic relation among the contours. We have not discussed the validity of the thermodynamic point of view at distances shorter than the healing length, because we cannot rely on the prediction of field theory in this regime. However, we see that, if correct, the LET hypothesis implies that the entanglement contour and density-fluctuations contour are related by

$$\mathcal{C}_s = \alpha_d \left(\frac{\mathcal{C}_n}{\xi\langle\delta^2 n\rangle_{\rm MF}}\right)^d\,. \tag{6.77}$$

This expression is a simple consequence of Eqs. (6.75) and (6.76), without any assumption on the specific value of the local temperature — provided that it is sufficiently small, so that the expressions $s(T) = \alpha_d(T/c)^d$ and $\langle\delta^2 N\rangle/V = \langle\delta^2 n\rangle_{\rm MF}T/(mc^2)$

[7] strictly speaking, the Bisognano-Wichmann (BW) theorem has only been demonstrated for A being a half-infinite system. However, for systems having conformal invariance in addition to Lorentz invariance, the BW theorem has been extended to cylindrical subsystems (Wong et al., 2013), where the local temperature behaves exactly as $c/(2\pi x_{\rm eff})$, with $x_{\rm eff}$ given by Eq. (6.46) (in its continuum version, namely without the factors $1/2$). This is also our conclusion, and we may conjecture that Lorentz invariance alone is sufficient for the validity of the Ansatz on a cylindrical subsystem.

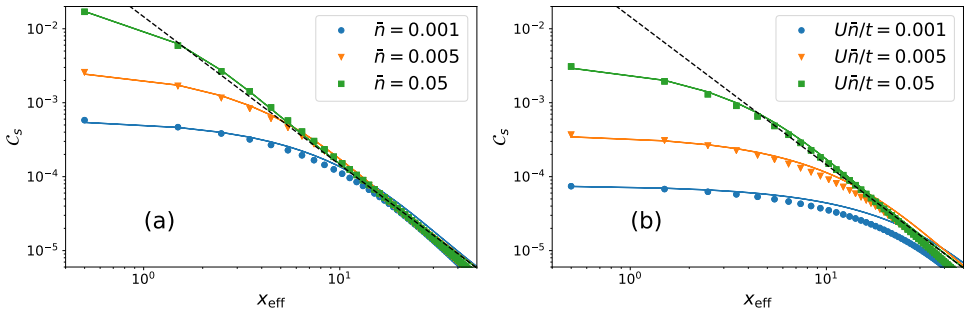

Figure 6.7: Reconstruction of the entanglement contour from the density-fluctuations contour. Data from Fig. 6.4. (a) Hardcore limit and (b) Bogoliubov limit. The solid lines show $\mathcal{C}_s = 0.574 \left(\frac{\mathcal{C}_n}{\xi \langle \delta^2 n \rangle_{\rm MF}} \right)^2$, where $\mathcal{C}_n$ is the density contour.

are valid. Fig. 6.7 shows that Eq. (6.77) is well reproduced at large distances, modulo the finite-size effects which prevent us from observing the expected universal behaviors of the contours. Remarkably, the prediction of Eq. (6.77) is found to apply quantitatively also to the short-range regime $x_{\rm eff} \lesssim \xi$.

Conclusion. As for free fermions in Section 4, we are thus led to the remarkable conclusion that the entanglement contour can be reconstructed from the density-fluctuations contour through Eq. (6.77), which is a thermodynamic relation between entropy and density fluctuations. This conclusion holds with the caveat that we are only concerned with the approximate behavior of entanglement. In fact, a detailed calculation shows that the area-law prefactor for entanglement entropy, resulting from the integration of the contour, can only be predicted within about 10% with this method. In particular, the investigation of subdominant corrections to entanglement entropy (mostly logarithmic terms or constant terms) seems out of reach.

6.6 Entanglement Hamiltonian in the SF phase

In the previous sections, we have investigated the structure of entanglement from the point of view of the contours, which proved to be invaluable tools to relate the area law of entanglement entropy (EE) to the spatial structure of correlations in the system. A complementary approach to the same question is to investigate the structure of the entanglement Hamiltonian. Even though the local thermodynamic picture developed in the previous section strongly suggests that the Ansatz of the Bisognano-Wichmann theorem, Eq. (3.37), is a good approximation to the entanglement Hamiltonian at distances larger than the healing length ξ, we have not verified it directly. In

particular, we have not discussed the structure of the entanglement spectrum, and the possibility to obtain it as the physical spectrum of the same model with energy scales (interaction strength, external potentials, hopping terms) modulated in space by the local temperature extracted from, *e.g.*, the density-fluctuations contour. This is not necessarily a trivial statement: for instance the $2d$ free fermion gas (see Section 4.3) was an example where the local thermodynamic picture is correct, but where the entanglement Hamiltonian is not at all the physical Hamiltonian modulated in space by a local temperature. However we could understand why, and the fact that the $2d$ free fermion gas is *not* Lorentz invariant at low energy was a crucial ingredient of our understanding. Here, in contrast, the $d \geq 2$ bosonic superfluid *is* Lorentz invariant at distance larger than ξ, and we should find that the entanglement spectrum is very well approximated by the spectrum of a physical Hamiltonian modulated in space by the entanglement temperature. We first discuss the structure of the entanglement spectrum, and then discuss the issues about the entanglement Hamiltonian.

6.6.1 Entanglement spectrum in the SF phase

Just like the EE can be decomposed as a sum of local contributions, $S = \sum_{i \in A} \mathcal{C}_s(i)$, it can also be expressed as a sum of contributions stemming from the different modes which diagonalize the entanglement Hamiltonian, $S = \sum_\alpha s_\alpha$. In our case, since we are considering a quadratic approximation to the Bose-Hubbard Hamiltonian, the modes α are single-particle bosonic modes, so that $s_\alpha = s_{\mathrm{Bose}}(n_\alpha)$ is just the thermal entropy corresponding to the occupation $n_\alpha = 1/[\exp(\epsilon_\alpha) - 1]$ of the mode α.

The EE is thus the thermal entropy, evaluated at temperature 1, of a fictitious system whose (dimensionless) density of states is associated with the (dimensionless) entanglement energies ϵ_α, the single-particle eigenvalues of the entanglement Hamiltonian. Anticipating the area law of EE, we expect that this entanglement density of states scales as l^{d-1}, so that in the thermodynamic limit

$$S = l^{d-1} \int_0^\infty d\epsilon \; \rho(\epsilon) s(\epsilon) \tag{6.78}$$

where $\rho(\epsilon)$ takes some well-defined value in the thermodynamic limit. The area law prefactor is then directly controlled by the entanglement density of states. Based on the results of the previous sections, we anticipate that the density of states is uniquely controlled by the healing length. For the sake of simplicity, we consider a cylinder-in-a-torus geometry, with subsystem A consisting of a $l \times l^{d-1}$ (hyper)-cylinder, periodic along the last $d-1$ directions, cut out of a $L \times l^d$ torus with $L \gg l$ (in practice, we work with $L = 20l$). As already remarked in Section 5.4, this geometry considerably simplifies the analysis, for the periodicity of A along $d-1$ directions allows us to

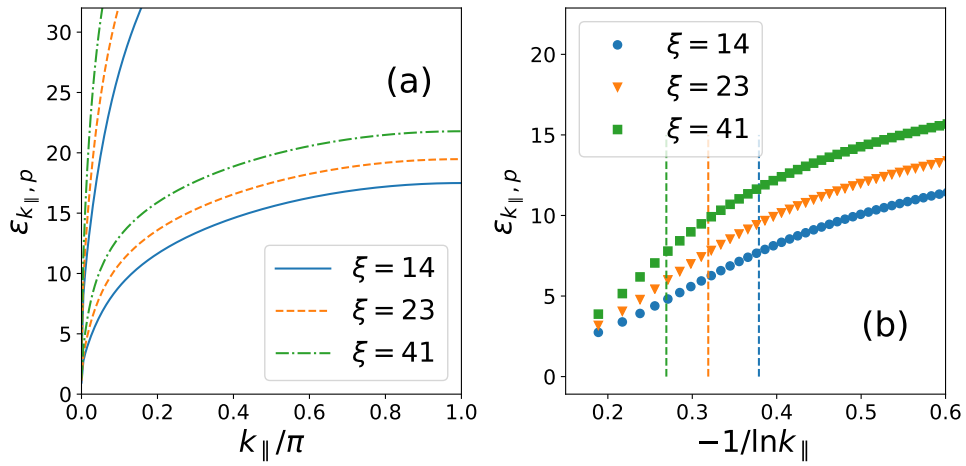

Figure 6.8: Entanglement dispersion relation in the SF phase in two dimensions (Bogoliubov regime). A is a $l \times l$ cylinder in a $20l \times l$ torus with $l = 400$. Due to the symmetry $k_\parallel \leftrightarrow -k_\parallel$, only positive values of $k_\parallel$ are shown. (a) Entanglement spectrum as a function of $k_\parallel$. Only the two lowest branches are shown. Although it is not visible on the figure, each branch contains two almost degenerate modes, related to the presence of two boundaries for A. (b) Lowest branch of (a), plotted as a function of $-1/\ln k_\parallel$, showing a dispersion relation of the form $\epsilon_{k_\parallel,1} \propto -1/\ln k_\parallel$ at small $k_\parallel$. Vertical dashed lines indicate a cross-over from this regime to a different, sub-linear behavior at $k_\parallel \gtrsim 1/\xi$.

organize the entanglement spectrum into bands, indexed by the momentum $\boldsymbol{k}_\parallel$ in the $d-1$ directions parallel to the cut. Equivalently, the entanglement Hamiltonian is a sum over different sectors of $\boldsymbol{k}_\parallel$ which are decoupled from each other:

$$\mathcal{H}_{\text{ent}} = \sum_{\boldsymbol{k}_\parallel} \sum_{p=1}^{l} \epsilon_{\boldsymbol{k}_\parallel,p} \gamma^\dagger_{\boldsymbol{k}_\parallel,p} \gamma_{\boldsymbol{k}_\parallel,p} \tag{6.79}$$

where p labels the dynamics in the direction perpendicular to the cut. In the thermodynamic limit, the EE may then be expressed as

$$S = l^{d-1} \int \frac{d^{d-1}\boldsymbol{k}_\parallel}{(2\pi)^{d-1}} s_{\boldsymbol{k}_\parallel} \tag{6.80}$$

$$s_{\boldsymbol{k}_\parallel} = \sum_{p=1}^{\infty} s(\epsilon_{\boldsymbol{k}_\parallel,p}) \tag{6.81}$$

where, anticipating the convergence of the sum over p (guaranteed by the fact that the area law is strict in $d \geq 2$), we have pushed the upper bound of summation to ∞. On Fig. 6.8, we have plotted the entanglement spectrum in the Bogoliubov regime for various values of the healing length $\xi = \sqrt{2t/U\bar{n}}$ in two dimensions. As the physical

spectrum, the entanglement spectrum is gapless at $k_\parallel = 0$. However, the entanglement dispersion relation is not linear, but rather *logarithmic* at small $k_\parallel$

$$\epsilon_{k_\parallel,\alpha} \sim \frac{1}{\ln(1/k_\parallel)} \,. \tag{6.82}$$

Furthermore, as shown on Fig. 6.8(b), the entanglement dispersion relation becomes steeper when $\xi \to \infty$. This behavior is at variance with the physical spectrum, since the sound velocity is $c = \hbar/(m\xi)$, and goes to zero when $\xi \to \infty$. However, this behavior is not a surprise, in view of the fact that $S \sim (l/\xi)^{d-1}$: when ξ increases, the EE decreases, and accordingly, the entanglement energies become larger, so that at a fixed temperature $T = 1$, the thermal entropy associated to the entanglement spectrum, which equals the EE, becomes smaller. It is neither immediate to infer the scaling behavior of the EE $S \sim (l/\xi)^{d-1}$ from the scaling behavior of the entanglement spectrum at small $k_\parallel$ proposed in Eq. (6.82), nor to identify in the entanglement spectrum a universal contribution to the EE, somewhat similar to the contribution stemming from the entanglement contour at distances larger than the healing length. We leave these questions open to future studies. Finally, we note that the logarithmic dispersion relation of the entanglement spectrum, Eq. (6.82) has been predicted by Metlitski and Grover (2011) and Swingle (2013). In particular, Swingle (2013) has shown that this dispersion relation is that of the Ansatz entanglement Hamiltonian of the Bisognano-Wichmann theorem, Eq. (3.37).

6.6.2 An Ansatz for the entanglement Hamiltonian

In this section, we propose an Ansatz for the entanglement Hamiltonian, and discuss some open issues related to the validation of this Ansatz within the slave-boson approach.

Ambitious strategy. We propose (similarly to Section 3.3.2)

$$\mathcal{H}_{\rm ent} = \sum_{i\in A} \beta_i \mathcal{H}_{\rm loc}(i) - t \sum_{i \text{ n.n } j} \beta_{ij} b_i^\dagger b_j \tag{6.83}$$

where the second sum runs over nearest-neighbors, and with $\mathcal{H}_{\rm loc}(i) = U n_i(n_i - 1)/2 - \mu n_i$ and

$$\beta_{ij} = \frac{\beta_i + \beta_j}{2} \,. \tag{6.84}$$

The local inverse temperature $\beta_i = 1/T_i$ is extracted from the density contour $\mathcal{C}_n$ in the ground state from the relation of Eq. (6.77), valid in the deep SF phase (hardcore limit or Bogoliubov limit)

$$T_i = \mathcal{C}_n(i) \frac{mc^2}{\langle \delta^2 n \rangle_{\rm MF}} \tag{6.85}$$

where $m = (2t)^{-1}$ is the effective mass on the lattice and c the speed of sound. $\langle \delta^2 n \rangle_{\rm MF}$ is the onsite variance of the number of particles at the mean-field (MF) level of approximation (if $\bar{n}$ is the average density, $\langle \delta^2 n \rangle_{\rm MF} = \bar{n}$ in the Bogoliubov limit where the MF ground state is a coherent state, and $\langle \delta^2 n \rangle_{\rm MF} = \bar{n}(1-\bar{n})$ in the hardcore limit, see Section 6.1). This expression for T_i is valid only in the deep SF phase, while in general, the function $\langle \delta^2 N \rangle(T)$ at thermal equilibrium has to be inverted in order to extract T_i from $\mathcal{C}_n(i)$, see Section 3.3.2. A basic test for the validity of the Ansatz is to compare its spectrum with the entanglement spectrum.

In order to do so within the slave-boson approach, the first step is to find the MF ground state (see Section 5.2). Owing to the presence of boundaries and to the spatial modulation associated to T_i, the MF ground state is *a priori* not translationally invariant. On the other hand, since the Ansatz is supposed to mimic the properties of a system which *is* translationally invariant (being extracted as a subsystem of a uniform ground state), we expect that the effects of the boundaries and of the local temperature somehow cancel each other to give rise to a state which is (almost) translationally invariant. This is precisely what we observed for free fermions in Section 4.2, see Fig. 4.3. In particular, we emphasized the subtle point that the entanglement Hamiltonian should give rise to the same thermodynamic expectation values as those calculated on the ground state when such thermal averages are evaluated at a dimensionless temperature of 1.

Limitations of the SB approach to study the Ansatz Hamiltonian at temperature 1. For free fermions, figure 4.3 clearly showed that, *e.g*, the density in the ground state of the entanglement Hamiltonian is not at all translationally invariant. This subtlety turns into a technical issue in the case of bosons treated within the slave-boson (SB) approach: being in essence a low-energy approach, there is no guarantee that it can accurately capture the properties of the Ansatz Hamiltonian at temperature 1. In fact, as shown on Fig. 6.9, the mean-field ground state of the Hamiltonian of Eq. (6.83) is not homogeneous. Although the spatial modulation of the energy scale partly compensates the effect of the boundaries on the SF order parameter, this compensation is not perfect. Surprisingly, we also note that the purely parabolic profile

$$\beta_x \propto x_{\rm eff} = \frac{(x-1/2)(L-x+1/2)}{L}\,, \tag{6.86}$$

expected to be correct only for $x \gtrsim \xi$, compensates better the effect of boundaries than the local temperature extracted from the density contour through Eq. (6.85). We observe that adding quantum and thermal fluctuations through the SB approach to the MF solution only leads to a decrease of ϕ everywhere, and does not produces

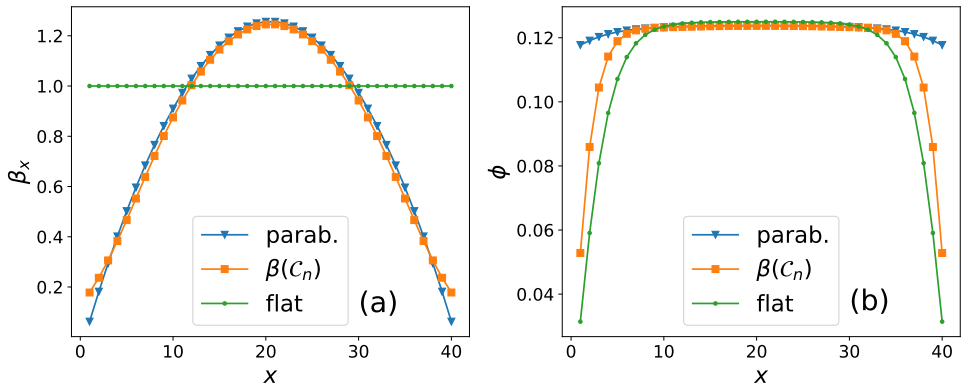

Figure 6.9: Superfluid order parameter in the ground-state of the Ansatz Hamiltonian of Eq. (6.83). Hardcore limit of the BH model, $\xi = 4$. (a) Inverse local energy scale β_x in a 40×40 cylinder. Blue triangles: parabolic profile $\beta_x = (2\pi/c)(x - 0.5)(L - x + 0.5)/L$; yellow squares: β_x extracted from the density contour through Eq. (6.85); green dots: flat profile $\beta_x = 1$. (b) Corresponding profile of the SF order parameter ϕ in the MF ground state. For a flat profile of β, ϕ is suppressed in a shell of width ξ near the boundaries. This suppression is partly compensated by a parabolic profile of β.

the expected uniform profile of $\langle b \rangle$. Furthermore, the spectrum of excitations around MF solution presents only qualitative similarities with the entanglement spectrum. In particular, we are not able to reproduce the logarithmic dispersion relation at small $k_{\|}$ shown on Fig. 6.8.

Alternative, less ambitious strategy. A possible alternative strategy to reproduce the properties of the entanglement Hamiltonian could be to start directly from the slave-boson Hamiltonian (and not from the Bose-Hubbard Hamiltonian), and modulate its parameters in space by the local temperature. This procedure, although lacking of direct physical motivation, would probably provide a better Ansatz for the entanglement Hamiltonian within the SB framework. We postpone a more in-depth study of this option to a future work.

Chapter 7

Entanglement across the superfluid / Mott-insulator phase transition

Introduction. In this chapter, largely based on Frérot and Roscilde (2016a), we study the structure of entanglement in the Mott-insulating phase of the Bose-Hubbard model (subsection 7.1), and its reorganization across the phase transition to a superfluid at the O(2) point, namely when increasing the ratio t/U of kinetic to potential energy at fixed, commensurate density (subsection 7.2). In the following we shall first discuss the entanglement structure in the Mott-insulating phase, and the applicability of the local-temperature Ansatz for the entanglement Hamiltonian. Then we will move on to discuss the O(2) transition. The closing of the MI gap at the O(2) transition has for consequence an increased low-energy density of state for quantum fluctuations in the ground state, as manifest in the entanglement spectrum (Fig. 7.2), and entanglement entropy is found to exhibit a sharp singularity at the O(2) points (Fig. 7.3). On the SF side of the transition, a similar singularity is found as a consequence of the softening of amplitude fluctuations of the SF order parameter, going gapless at the transition. A gaussian field theory prediction for the critical scaling of the singularity on the MI side (Metlitski, Fuertes, and Sachdev, 2009; Calabrese and Cardy, 2004) is found in quantitative agreement with our results. We shall conclude by discussing the difficulties related to the understanding of the entanglement singularity via the contours and their relations.

7.1 Entanglement structure in the Mott-insulating phase

7.1.1 Quadratic SB Hamiltonian in the MI phase

Mean-field solution. In the MI phase, the MF ground state $|n_0\rangle$ is an eigenstate of n, the operator counting the number of particles on a site: $n|n_0\rangle = n_0|n_0\rangle$, where the integer n_0 is the density in the MI phase. The SF order parameter $\phi = \langle n_0|b|n_0\rangle$ vanishes, so that the MF Hamiltonian defined in Eq. (5.15) is readily diagonalized in the $|n\rangle$ basis:

$$\mathcal{H}_{\rm MF}|n\rangle = \epsilon_n|n\rangle \tag{7.1}$$

$$\epsilon_n = Un(n-1)/2 - \mu n\ . \tag{7.2}$$

In particular, the γ's operators that destroy particles in the eigenstates of the MF Hamiltonian are simply the original β's operators of the SB construction.

Quadratic Hamiltonian. In order to build the quadratic SB Hamiltonian describing quantum fluctuations around the MF solution, we need to evaluate the matrix elements of b connecting the MF ground state to the other eigenstates of the MF Hamiltonian. Here, we immediately see that the only non-zero matrix elements are between $|n_0\rangle$ and $|n_0 \pm 1\rangle$. This implies that the matrices $A^{(1)}_{\boldsymbol{k}}$ and $B_{\boldsymbol{k}}$ defined in Eqs. (5.62) and (5.64) have no matrix elements involving states with $|n - n_0| \geq 2$. For those states, the only nonzero terms in the quadratic Hamiltonian come from the diagonal part $\mathcal{H}^{(2)}_{\rm BH,local} = \sum_{n\neq n_0}\sum_{\boldsymbol{k}}(\epsilon_n - \epsilon_{n_0})\beta^\dagger_{\boldsymbol{k},n}\beta_{\boldsymbol{k},n}$. They thus form flat bands, completely decoupled from the MF state and from the states with $n = n_0 \pm 1$, and do not contribute to quantum fluctuations in the ground-state. In order to simplify the notations, we denote $\beta_{\boldsymbol{k},n_0\pm1} \equiv \beta_{\boldsymbol{k},\pm}$. Restricting ourselves to these two families of modes, the matrices $A_{\boldsymbol{k}}$ and $B_{\boldsymbol{k}}$ are then 2×2 matrices. Using the fact that $\epsilon_{n+1} - \epsilon_n = nU - \mu$, and evaluating the matrix elements of b between n_0 and $n_0 \pm 1$, we find that

$$A_{\boldsymbol{k}} = \begin{pmatrix} a_{\boldsymbol{k},+} & 0 \\ 0 & a_{\boldsymbol{k},-} \end{pmatrix} \tag{7.3}$$

$$B_{\boldsymbol{k}} = \begin{pmatrix} 0 & b_{\boldsymbol{k}} \\ b_{\boldsymbol{k}} & 0 \end{pmatrix}\ , \tag{7.4}$$

with $a_{\boldsymbol{k},+} = n_0U - \mu - t_{\boldsymbol{k}}(n_0+1)$, $a_{\boldsymbol{k},-} = \mu - U(n_0-1) - t_{\boldsymbol{k}}n_0$ and $b_{\boldsymbol{k}} = -t_{\boldsymbol{k}}\sqrt{n_0(n_0+1)}$. We have introduced $t_{\boldsymbol{k}} = 2t\sum_{i=1}^d \cos k_i$. In particular, we remark

that the quadratic Hamiltonian takes the block-diagonal form

$$\mathcal{H}^{(2)}_{\rm MI} = \frac{1}{2}\sum_{\boldsymbol{k},\epsilon=\pm} \begin{pmatrix} \beta^\dagger_{\boldsymbol{k},\epsilon} & \beta_{-\boldsymbol{k},-\epsilon} \end{pmatrix} \begin{pmatrix} a_{\boldsymbol{k},\epsilon} & b_{\boldsymbol{k}} \\ b_{\boldsymbol{k}} & a_{\boldsymbol{k},-\epsilon} \end{pmatrix} \begin{pmatrix} \beta_{\boldsymbol{k},\epsilon} \\ \beta^\dagger_{-\boldsymbol{k},-\epsilon} \end{pmatrix} . \tag{7.5}$$

To perform the Bogoliubov rotation bringing $\mathcal{H}^{(2)}_{\rm MI}$ into a diagonal form, it is convenient to write $a_{\boldsymbol{k},\pm} = (a_{\boldsymbol{k},+} + a_{\boldsymbol{k},-})/2 \pm (a_{\boldsymbol{k},+} - a_{\boldsymbol{k},-})/2$, and rewrite the Hamiltonian as

$$\begin{aligned} \mathcal{H}^{(2)}_{\rm MI} &= \sum_{\boldsymbol{k}} \frac{a_{\boldsymbol{k},+} - a_{\boldsymbol{k},-}}{2} (\beta^\dagger_{\boldsymbol{k},+}\beta_{\boldsymbol{k},+} - \beta^\dagger_{\boldsymbol{k},-}\beta_{\boldsymbol{k},-}) + \\ &\quad \frac{1}{2}\sum_{\boldsymbol{k},\epsilon=\pm} \begin{pmatrix} \beta^\dagger_{\boldsymbol{k},\epsilon} & \beta_{-\boldsymbol{k},-\epsilon} \end{pmatrix} \begin{pmatrix} \frac{a_{\boldsymbol{k},+}+a_{\boldsymbol{k},-}}{2} & b_{\boldsymbol{k}} \\ b_{\boldsymbol{k}} & \frac{a_{\boldsymbol{k},+}+a_{\boldsymbol{k},-}}{2} \end{pmatrix} \begin{pmatrix} \beta_{\boldsymbol{k},\epsilon} \\ \beta^\dagger_{-\boldsymbol{k},-\epsilon} \end{pmatrix} \end{aligned} \tag{7.6}$$

The Bogoliubov rotation which diagonalizes the Hamiltonian is thus

$$\lambda_{\boldsymbol{k},\pm} = u_{\boldsymbol{k}}\beta_{\boldsymbol{k},\pm} - v_{\boldsymbol{k}}\beta^\dagger_{-\boldsymbol{k},\mp} \tag{7.7}$$

where the coefficients $u_{\boldsymbol{k}}$ and $v_{\boldsymbol{k}}$ are given by

$$v_{\boldsymbol{k}} = \frac{a_{\boldsymbol{k},+} + a_{\boldsymbol{k},-}}{|a_{\boldsymbol{k},+} + a_{\boldsymbol{k},-}|} \frac{1}{\sqrt{2}} \left(\frac{a_{\boldsymbol{k},+} + a_{\boldsymbol{k},-}}{2\omega_{\boldsymbol{k}}} - 1 \right)^{1/2} \tag{7.8}$$

$$u_{\boldsymbol{k}} = \sqrt{1 + v^2_{\boldsymbol{k}}} \tag{7.9}$$

with $\omega_{\boldsymbol{k}} = \sqrt{(a_{\boldsymbol{k},+} + a_{\boldsymbol{k},-})^2/4 - b^2_{\boldsymbol{k}}} = (1/2)\sqrt{t^2_{\boldsymbol{k}} - 2Ut_{\boldsymbol{k}}(2n_0+1) + U^2}$. Putting everything together, we finally obtain

$$\mathcal{H}^{(2)}_{\rm MI} = \sum_{\boldsymbol{k},\epsilon=\pm} \lambda^\dagger_{\boldsymbol{k},\epsilon}\lambda_{\boldsymbol{k},\epsilon} \left[-\epsilon(t_{\boldsymbol{k}}/2 + \delta\mu) + \omega_{\boldsymbol{k}}\right] \tag{7.10}$$

where we have dropped a constant term and introduced $\delta\mu = \mu - U(n_0 - 1/2)$. The spectrum at two representative points of the MI phase is plotted on Fig. 5.2(a, d).

Physical interpretation of the quadratic SB Hamiltonian. Several points are worth mentioning concerning the structure of the SB ground state in the MI phase.

First, we note that the action of $\lambda^\dagger_{\boldsymbol{k},\pm}$ ($(\lambda_{\boldsymbol{k},\pm})$ creates locally states with $n_0 \pm 1$ ($n_0 \mp 1$) particles, so that $\lambda^\dagger_{\boldsymbol{k},\pm}\lambda_{\boldsymbol{k},\pm}$ leaves the total number of particles unchanged. The total number of particles is thus conserved by the SB Hamiltonian, and in particular, the ground state renormalized by quantum fluctuations is an eigenstate of the total number of particles, like the MF ground state. However, it contains particle-hole fluctuations, implying that the number of particles on each site can fluctuate.

A second observation is that the ground state is independent of the chemical potential μ in the MI phase. This comes from the fact that the coefficients $u_{\boldsymbol{k}}$ and $v_{\boldsymbol{k}}$

of the Bogoliubov transformation are independent of μ. The physical reason for this is clear: changing μ does not affect the number of particles as long as we stay in the MI phase, and the properties of the ground state only depend on the number of particles and on the ratio t/U. While the particle and hole excitations have an energy which depends on μ, the ground state is only sensitive to the sum of them, $2\omega_{\boldsymbol{k}}$, since at the level of quantum fluctuations, they can only occur as combined particle-hole pairs.

Thirdly, since the $u_{\boldsymbol{k}}$ and $v_{\boldsymbol{k}}$ coefficients of the Bogoliubov rotation are identical for $\lambda_{\boldsymbol{k},+}$ and $\lambda_{\boldsymbol{k},-}$, these two families of modes give exactly the same contribution to the entanglement entropy of a subsystem, and the entanglement spectrum is exactly twice degenerate.

Finally, the boundaries of the MI phase at the SB level of approximation can be determined by the equations $t_0/2 + \delta\mu = \pm\omega_0$[1]. By doing so, one finds a phase boundary exactly at the location predicted by the MF criterium $\phi = 0$. In particular, the O(2) points at the extremity of the MI lobes are located along the particle-hole symmetry line defined by the equality of the particle and hole gaps, namely at $\mu/U = n_0 - (1+g)/2$ with $g = 2dt/U$, and at the value of g for which both gaps vanish, namely $g_c = 2n_0 + 1 - 2\sqrt{n_0(n_0+1)} \approx 0.1716$ for $n_0 = 1$.

7.1.2 Spatial structure of entanglement in the MI phase

Energy of particle-hole fluctuations. The spectrum of the particle-plus-hole fluctuations in the MI phase at small k is

$$\begin{aligned} 2\omega_{\boldsymbol{k}} &= \sqrt{t_{\boldsymbol{k}} - 2Ut_{\boldsymbol{k}}(2n_0+1) + U^2} && (7.11)\\ &\approx \sqrt{\Delta^2 + k^2c^2} && (7.12)\\ &\approx \Delta + \frac{k^2}{2m} && (7.13) \end{aligned}$$

where we introduced the gap Δ, and the speed of sound c given by

$$(\Delta/U)^2 = 2(\omega_0/U)^2 = 1 + g^2 - 2g(2n_0+1) = (g_c - g)(1/g_c - g) \quad (7.14)$$

$$(c/U)^2 = (g/d)(2n_0 + 1 - g)\,. \quad (7.15)$$

Close to $g = g_c$, and focusing on $n_0 = 1$, these expressions are approximately given by

$$(\Delta/U)^2 = 4\sqrt{2}(g - g_c) \quad ; \quad (c/U)^2 = \frac{g_c 2\sqrt{2}}{d} \quad (7.16)$$

The mass m is related to the gap by $\Delta = mc^2$.

[1] This condition corresponds to the criterium of thermodynamical stability of the SB approach in the MI phase, requiring non-negative energies in the quadratic Hamiltonian of Eq. (7.10).

Correlation length. The particle-hole gap induces a finite correlation length

$$\xi = b\frac{c}{\Delta} = b\sqrt{\frac{g(3-g)}{d(1+g^2-6g)}} \approx b[2d(1-g/g_c)]^{-1/2} \tag{7.17}$$

where we focus on the first MI lobe with $n_0 = 1$. b is some constant of order 1 which we have determined by fitting the density-density correlations according to

$$\langle \delta n_i \delta n_j \rangle = a\frac{e^{-|\boldsymbol{r}_i - \boldsymbol{r}_j|/\xi}}{|\boldsymbol{r}_i - \boldsymbol{r}_j|^{d+1}} , \tag{7.18}$$

an expression valid close to the O(2) point. By doing so, we found $b \approx 0.5$ in $d = 2$.

Spatial structure of the entanglement contour. We can expect that both the entanglement and density contours are exponentially decaying at distances larger than ξ. At distances smaller than ξ, we expect to observe the universal prediction for the entanglement contour, Eq. (6.45). A natural prediction for the entanglement contour is then

$$\mathcal{C}_s(\boldsymbol{r}) = 2\alpha_d \frac{e^{-x/\xi}}{(2\pi x)^d} \tag{7.19}$$

where x is the distance to the boundary of subsystem A. Note that in the limit $\xi \to \infty$, there is a factor 2 with respect to the SF phase discussed in the previous sections. The origin of this factor 2 is the presence of *two* modes becoming gapless at the O(2) point, where the correlation length diverges. As a consequence, exactly at the O(2) point the universal part of the entanglement contour is twice that of a single Lorentz-invariant mode [see Fig. 7.1(a)]. This prediction holds only within the SB approximation, which breaks down precisely at the O(2) point by predicting incorrect critical exponents for the phase transition[2]. However, in view of the moderate renormalization of the MF ground state by quantum fluctuations at the O(2) point we expect this prediction to be at least qualitatively valid. As shown on Fig. 7.1(a), both the entanglement contour and the density contour exhibit a short-range power-law decay followed by an exponential decay controlled by the correlation length ξ. We observe that the entanglement contour in the "cylinder-in-a-torus" geometry is well approximated by the expression

$$\mathcal{C}_s(\boldsymbol{r}) = 2\alpha_d \left(\frac{e^{-x'/\xi}}{(2\pi x')^d} + \frac{e^{-(l-x')/\xi}}{[2\pi(l-x')]^d} \right) \tag{7.20}$$

where $x' = x - 1/2$ if A contains the sites at position $x = 1, \ldots l$. Surprisingly, we note that when $\xi \to \infty$, this expression does not simply extrapolates to the expression

[2] Indeed, the SB approach being a gaussian theory, the phase transition is predicted to belong to the gaussian universality class, and not to the $d+1$-dimensional XY class it actually belongs to.

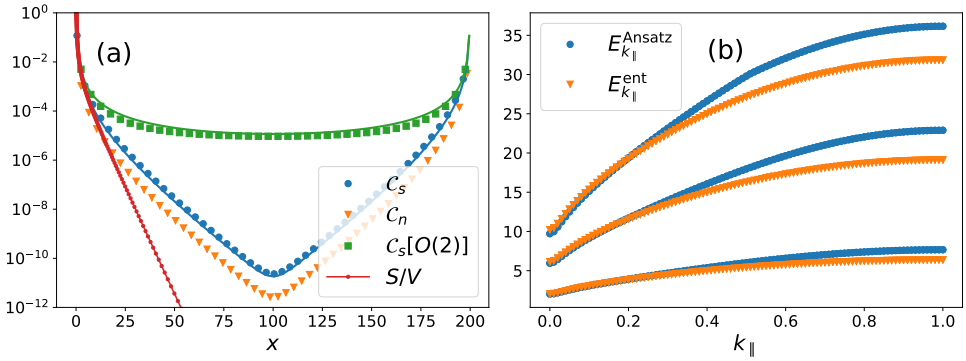

Figure 7.1: Structure of entanglement in the MI phase in two dimensions. $g/g_c = 0.999$ ($\xi \approx 16$), and A is a $l \times l$ cylinder cut out of a $l \times 20l$ torus for $l = 200$. (a) Entanglement (blue circles) and density (orange triangles) contours. The solid blue line is the expression of Eq. (7.20), and the red dots show S/V as a function of $c/(2\pi x)$. The x-axis is the distance to the left boundary ($= i - 0.5$ if the first site is at $i = 1$). Also shown is the entanglement contour at $g = g_c$ (green squares), and the universal prediction $2\alpha_d/(2\pi x_{\text{eff}})^2$ (solid green line, see text). (b) Entanglement spectrum (orange triangles) and spectrum of the Ansatz Hamiltonian of Eq. (6.83) with $\beta_i = (2\pi/c)(i-0.5)(l-i+0.5)/l$ (blue circles). Only the lowest branches are shown, and the spectra are plotted as a function of the momentum $k_\parallel$ in the direction parallel to the $A-B$ boundary. Although it is not visible on the plot, each dot contains in fact 4 modes: a double degeneracy is exact (related to the particle/hole symmetry, exact in the ground state), and a double quasi-degeneracy is related to the presence of two boundaries, almost perfectly decoupled if l is large compared to the correlation length ξ. Note also that modes at $k_\parallel < 0$ are not shown ($E_{-k_\parallel} = E_{k_\parallel}$).

of Eq. (6.45). An alternative expression such as

$$\mathcal{C}_s(\boldsymbol{r}) = \alpha_d \frac{e^{-x'/\xi} + e^{-(l-x')/\xi}}{(2\pi x_{\text{eff}})^d} \tag{7.21}$$

would do so, but is found in worse agreement with the contour in the bulk of A. However, as shown on Fig. 7.1(a), exactly at the O(2) point, the contour is compatible with the prediction of Eq. (7.21) (with $\xi = \infty$, so that the numerator provides the factor of 2 stemming from the presence of two modes going gapless at the O(2) point). We anticipate that the formula (7.20) has to be modified to correctly account for the fate of the contours in the very vicinity of the O(2) point, to correctly extrapolate to the universal result when $\xi \to \infty$.

Thermal entropy. In order to compare the entanglement contour with the thermal entropy evaluated at the local entanglement temperature, we have calculated the thermal entropy in the Mott-insulating phase. In order to do so, to take into account

the fact that the ground state is only sensitive to the particle-plus-hole gap, we have considered the entropy of a fictitious system of free bosonic particles with dispersion relation $2\omega_{\boldsymbol{k}}$. We have fitted the this entropy to

$$S(T)/V \approx \alpha_d \left[\left(\frac{T}{c} \right)^d + b' \left(\frac{\Delta}{c} \right)^d \right] e^{-\Delta/T} \, . \tag{7.22}$$

We have verified the validity of this scaling behavior in $d = 2$ varying the ratio t/U and found $b' \approx 0.17$. To take into account the fact that the entanglement spectrum contains the contribution from two degenerate modes, on Fig. 7.1(a) we have plotted twice this entropy as a function of the local temperature $T = c/(2\pi x)$, predicted by the Bisognano-Wichmann theorem. This formula generalizes the gapless behavior $S(T)/V = \alpha_d (T/c)^d$ to the gapped case.

Prediction of the correlation length from the local equilibrium hypothesis. In particular, we see that the hypothesis of a local entanglement temperature $T = c/(2\pi x)$ implies an exponential decay of the entanglement contour at large distance

$$\mathcal{C}_s^{\text{conj.}}(x) = s(c/2\pi x) \sim e^{-2\pi\Delta x/c} \, . \tag{7.23}$$

Furthermore, this relation predicts that the correlation length ξ should be

$$\xi^{\text{conj.}} = \frac{c}{2\pi\Delta} \, . \tag{7.24}$$

Unfortunately, as shown on Fig. 7.1(a), this does not correspond to the correct result $\xi \approx 0.5 c/\Delta$ found from fitting the density-density correlations, and which governs the spatial decay of the contours.

This seemingly negative result shows that either the local equilibrium hypothesis is not valid, or that the local temperature is not $c/(2\pi x)$ (or both). Note, however, that Fig. 7.1(a) shows that the hypothesis of a local temperature of $c/(2\pi x)$ is in very good agreement with the entanglement contour at distances shorter than ξ (namely the length scale below which the system looks like a superfluid).

Entanglement spectrum *vs.* spectrum of the Ansatz Hamiltonian. In the MI phase, since the order parameter vanishes uniformly, the local temperature Ansatz for the entanglement Hamiltonian is easier to verify. Indeed, the issues mentioned in Section 6.6 for the SF phase, and relative to the precise behavior of the SF order parameter in the vicinity of the boundaries, are not present. On Fig. 7.1(b), we have plotted both the entanglement spectrum and the spectrum of the Ansatz Hamiltonian with a local inverse temperature

$$\beta(x) = \frac{2\pi}{c} \frac{(x - 1/2)(l - x + 1/2)}{l} \, , \tag{7.25}$$

as calculated within the SB approximation.

We observe that the spectrum of the Ansatz entanglement Hamiltonian has a dependence on μ which is not acceptable in the MI phase, but which is cancelled by considering pairs of eigenenergies associated with particle-hole excitations. We therefore postulate that the entanglement spectrum is obtained from the Ansatz as the spectrum of particle-hole excitations. The relatively good agreement shown in Fig. 7.1(b) justifies this choice a posteriori.

Discussion. The good agreement between the entanglement spectrum and the spectrum of the Ansatz Hamiltonian with an entanglement temperature given by the field-theory prediction seems to point to a failure of the local equilibrium hypothesis. A more in-depth study of the contours in the vicinity of the O(2) point is necessary to clarify this issue.

7.2 The MI / SF phase transition

7.2.1 Introduction

In this section, we investigate the reorganization of the structure of entanglement across the phase transition between the MI and the SF occurring at the O(2) point (namely at fixed integer density, here set to $n_0 = 1$ for simplicity). As the generic transition which occurs when adding or removing a few particles to a MI is not induced by quantum fluctuations, we shall not discuss it in details. In essence, on the SF side of the generic transition, the structure of entanglement is that of a very dilute SF coexisting with a MI background. The difference with the usual SF is that the vacuum is here nontrivial, but contributes also to entanglement. In addition to the gapless mode, whose contribution to entanglement has the structure that we have discussed in the SF phase, the underlying MI contributes in the form of a gapped mode, affecting the entanglement contours at short distance.

In contrast, the O(2) transition offers a different situation. As is already clear on Fig. 5.2, where we have plotted the SB population in states orthogonal to the MF ground state across the phase diagram, the O(2) points are singled out as the points were the quantum fluctuations are the strongest.

Approaching the transition from the MI side. When approached from the MI phase, the fluctuations are particle-hole pairs, confined within a distance $\sim \xi$. When a subsystem of size smaller than ξ is examined, it is practically indistinguishable from a SF. From the perspective of the contours, they exhibit the characteristic power-law

decay of the SF phase, and the entanglement contour is universal at distances $x \ll \xi$. Approaching the transition by increasing the ratio $g = tz/U$ of kinetic to potential energy ($z = 2d$ is the number of nearest neighbors on a cubic lattice in d dimensions), the particle-hole gap $\Delta/c \sim \sqrt{g_c - g}$ closes, and the correlation length diverges ($\xi \sim c/\Delta$), so that the particle-hole pairs become deconfined.

The O(2) point at the SB level of approximation. At the SB level of approximation, the O(2) point is described by two gapless modes of a free bosonic theory, so that, following the arguments presented in Section 6.2, we expect that the entanglement contour becomes fully universal. One may wonder about the role of the healing length, which was shown in Section 6.2 to control the short-distance behavior of the contours in the gapless phase. The healing length is given by $\xi_h = 1/(mc)$ with $m = 1/(2t)$ and $c = U\sqrt{g_c(3 - g_c)/d}$ at the O(2) point. The healing length is then approximately given by $\xi_h = \sqrt{\frac{g_c}{d(3-g_c)}}$ near the O(2) point, of order 0.1 in $d = 2, 3$, which is completely negligible.

Note that we have this picture only thanks to the quantum fluctuations incorporated in the SB approach. The MF ground state on the MI side remains unchanged up to the very O(2) point (at $g_c = 3 - 2\sqrt{2}$ for $n_0 = 1$).

On the SF side. Continuing to increase g above g_c, the SF order parameter acquires continuously a nonzero value ($\phi \propto \sqrt{g - g_c}$), and long-range order is truly established. From the perspective of fluctuations, on the SF side of the O(2) transition they are better understood as phase and amplitude fluctuations of the order parameter (sometimes respectively called "transverse" and "longitudinal" fluctuations, or "Goldstone" and "Higgs" modes by analogy with high energy physics). The phase fluctuations are gapless in the whole SF phase, and their consequences for entanglement have been extensively discussed in Section 6 in the limiting case of infinite interactions (hardcore limit), and weak interactions (Bogoliubov limit). On the other hand, the amplitude fluctuations are gapped ($\Delta_H/c \sim \sqrt{g - g_c}$).

7.2.2 Entanglement spectrum vs. physical spectrum on the SF side of the O(2) transition

The softening of the particle-hole fluctuations on the MI side of the transition, and of the amplitude fluctuations of the order parameter on the SF side, are responsible for a singular contribution to entanglement entropy. This is manifest when comparing the physical spectrum (PS) and the entanglement spectrum (ES) across the transition. On Fig. 7.2, we have plotted the ES and PS as a function of the momentum $k_{\|}$

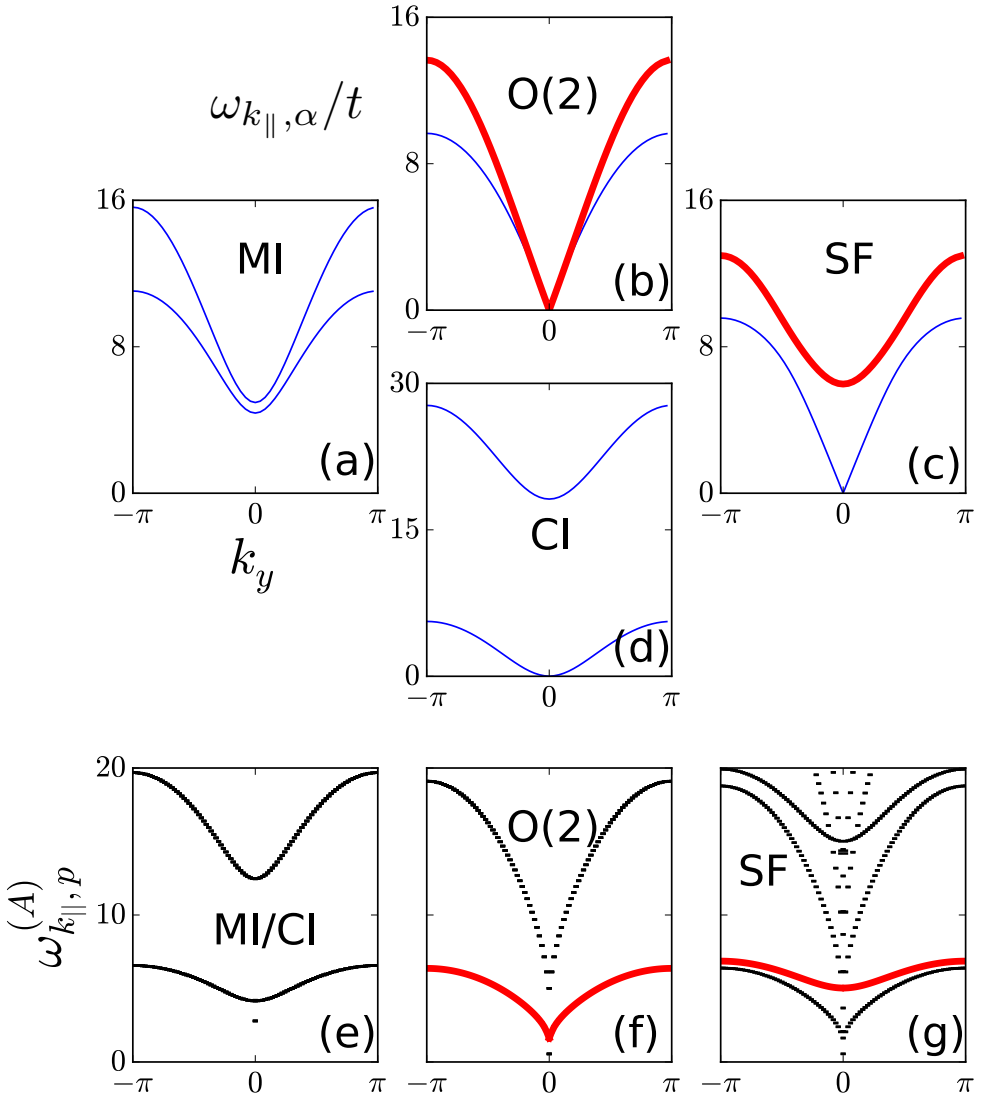

Figure 7.2: Physical spectrum *v.s.* entanglement spectrum in two dimensions. *Upper panels*.– Physical spectrum at $k_x = 0$ (the spectra were already shown on Fig. 5.2; they are reproduced here to be compared with the entanglement spectra on the lower panels). Only the two lowest branches are shown. (a) $tz/U = 0.15$, $\mu/U = \sqrt{2} - 1$; (b) $tz/U = 3 - 2\sqrt{2}$, $\mu/U = \sqrt{2} - 1$; (c) $tz/U = 0.2$, $\mu/U = \sqrt{2} - 1$ and (d) $tz/U = 0.12$, $\mu/U = 0.168$. *Lower panels*.– Entanglement spectrum against the wave vector $k_{||}$ parallel to the $A - B$ boundary. Only the lowest branches are shown. In the SF (MI) phase, each branch is actually two-fold (four-fold) degenerate. (e), (f), (g) correspond to the same parameters as (a), (b), (c) respectively. In all the panels, the thick red line marks the amplitude mode in the physical spectrum and in the entanglement spectrum.

parallel to the $A-B$ boundary. In particular, the O(2) point is singled out as the only point of the phase diagram where exactly *two* modes are gapless in both the ES and PS[3]. This shows that the softening of the fluctuation modes in the critical region is indeed responsible for an *enhanced entanglement density of states* at low entanglement energy. Since entanglement entropy is the thermal entropy (evaluated at temperature 1) for fictitious bosonic quasiparticles whose dispersion relation is the entanglement spectrum, this in turn is responsible for a singularity of entanglement entropy at the O(2) point.

To further illustrate this point, on Fig. 7.3(h) we have plotted the entanglement "Higgs" and "Goldstone" gaps for the phase and amplitude fluctuations respectively (in the SF phase). In the MI phase, they are just the particle-hole gap in the entanglement spectrum. In striking analogy with the physical spectrum, the "Higgs" gap vanishes as $\sqrt{|g-g_c|}$ at the transition[4]. On Fig. 7.3(i), we show that the region where the Higgs entanglement gap is smaller than 1, corresponding to a noticeable population of this mode at a temperature of order 1, is precisely the region where the cusp in entanglement entropy may be observed. Finally, on Fig. 7.3(j), we have represented in false colors the entanglement entropy of a 50×50 cylinder cut out of a 50×100 torus above the phase diagram in the vicinity of the O(2) point (denoted 'b' on the figure). Clearly, this figure is very similar to Fig. 5.2, which represented the renormalization of the MF ground state by quantum fluctuations. In particular, the entanglement entropy has a cusp singularity at the O(2) point, while the cusp is rounded off at the generic transition. Note also that entanglement entropy is independent of μ in the MI phase, a consequence of the fact that the ground state itself is independent of μ.

7.2.3 Critical scaling of entanglement entropy

Entanglement entropy obeys a strict area law across all the phase diagram, including at the critical points. In particular, it can be fitted to the following form

$$S = aL_A^{d-1} + b\ln L_A + c\,. \tag{7.26}$$

The t/U-dependence of the area-law coefficient a and of the logarithm coefficient b are predicted in a robust manner by the SB approach[5], and plotted in Fig. 7.4(a). In

[3] Actually, in the ES, all modes are always (nearly) two-fold degenerate, but this generic quasi-degeneracy is trivial and stems simply from the presence of two boundaries between A and B in the geometry chosen for our calculations.

[4] There is also a finite-size gap for the entanglement Goldstone mode in the SF phase, $\Delta_G \sim L_A^{-(d-1)/2}$. This scaling may be related to the logarithmic contribution $[(d-1)/2]\log L_A$ to entanglement entropy, characteristic of a phase breaking spontaneously a continuous symmetry (Metlitski and Grover, 2011). See Frérot and Roscilde (2015) for a more in-depth discussion.

[5] By robust, here we mean that the coefficients are independent of the details of the regularization scheme of the zero mode in the SB approach. The ability of the SB approach to reproduce the log term

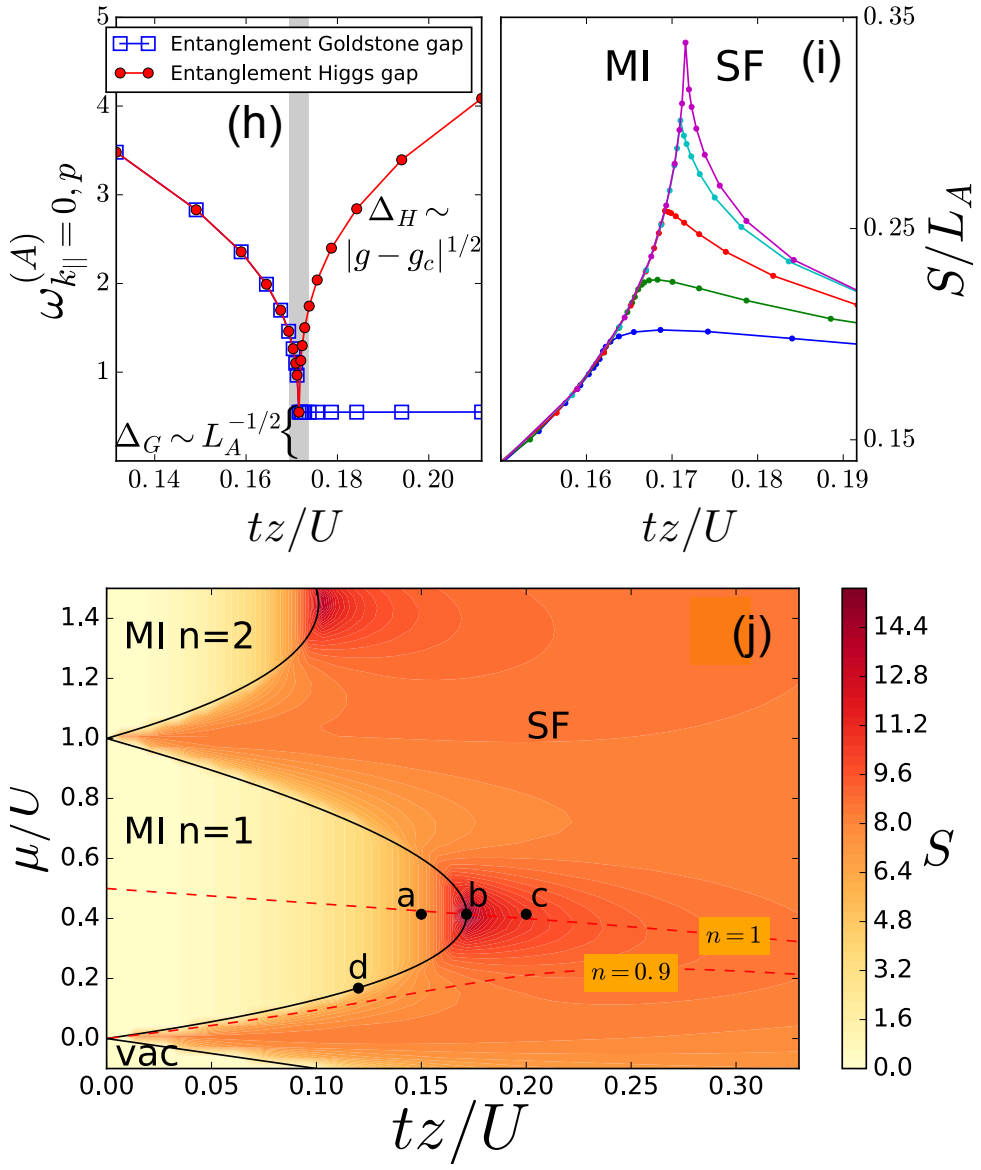

Figure 7.3: (h) Entanglement gaps across the SF-MI transition of the $2d$ Bose-Hubbard model. Region A corresponds to half of a $L_A \times 2L_A$ torus ($L_A = 100$). The shaded area marks the region in which $\Delta_{\mathrm{H}} \lesssim 1$. In the SF phase, the entanglement spectrum exhibits a finite-size gap $\Delta_G \sim L_A^{-1/2}$. (i) EE across the SF-MI phase transition for $\mu/U = 0.3, 0.329, 0.357, 0.386$ and $\sqrt{2} - 1$ from bottom to top. Shaded area as in (h), and $L_A = 50$ (j) EE across the phase diagram of the $2d$ Bose-Hubbard model ($L_A = 50$). a, b, c and d mark the points where the spectra are evaluated in Fig. 7.2. Dashed lines correspond to constant density $n = 1$ and $n = 0.9$, and $z = 4$.

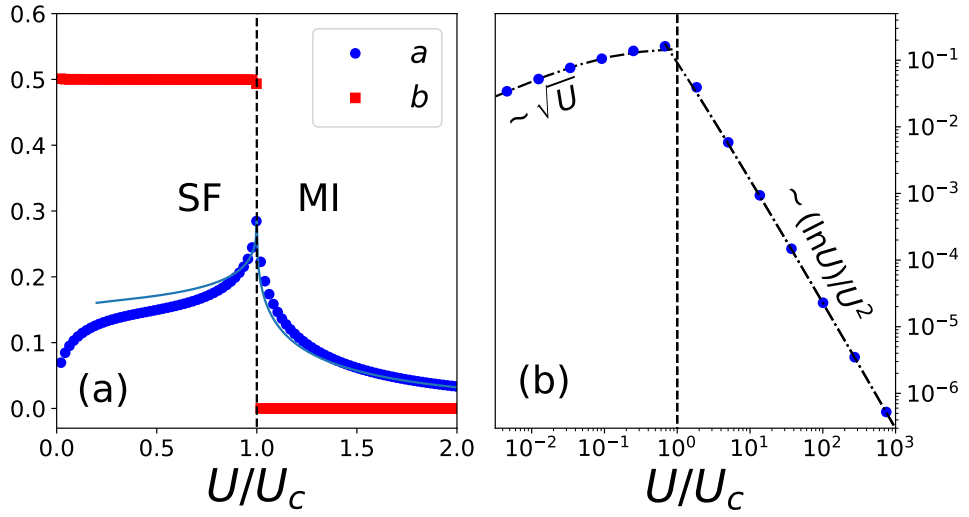

Figure 7.4: (a) a and b coefficients of EE scaling across the $2d$ SF-MI transition at $n = 1$, extracted from a fit on $L_A \times 2L_A$ half toruses with $10 \leq L_A \leq 100$. The thin blue line shows $a = 2a_1$ in the MI and $a = a_0 + a_1$ in the SF, where a_0 and a_1 are defined in Eqs. (7.33) and (7.34) respectively; (b) Area-law coefficient a on a log-log scale. Shown are the predictions of Bogoliubov theory for small U, and the large-U prediction of Alba, Haque, and Läuchli (2013) (dash-dotted line).

particular the coefficient a exhibits the above-mentioned cusp singularity associated with the gapless Higgs entanglement mode. Our approach allows us to predict as well the behavior of the area-law coefficient away from the transition. As shown in Fig. 7.4(b), $a \sim \sqrt{U}$ for small U, consistent with the prediction of Bogoliubov theory (see Section 6.1) and with the fact that the area law term disappears in a perfect condensate (Ding and Yang, 2009); for large U deep in the insulating phase the coefficient is instead found to decrease as $\ln U/U^2$, in complete agreement with the analytical and numerical calculations of Alba, Haque, and Läuchli (2013) (see also Fig. 6.3 for the calculation of a at non-integer filling, namely $\bar{n} = 0.9$.

Universal logarithmic contribution to entanglement entropy. On the other hand, the coefficient b of the logarithmic term takes the universal value $(d-1)/2$ throughout the superfluid phase, and jumps to zero at the phase transition [Fig. 7.4(a)]. This is perfectly consistent with the prediction of Metlitski and Grover (2011) of a universal

relies on the prescription (Song et al., 2011) of introducing a gap Δ in the SB spectrum, scaling as $\Delta = hL^{-d}$ in the same way as the lowest excitation of the Anderson tower of states (Frérot and Roscilde, 2015); the precise value of the b coefficient is found to be robust to the choice of the h prefactor. On the other hand, the c coefficient may depend strongly on the choice of h (Luitz et al., 2015), and its prediction is therefore not reliable. See the supplementary material of (Frérot and Roscilde, 2016a) for a more detailed discussion.

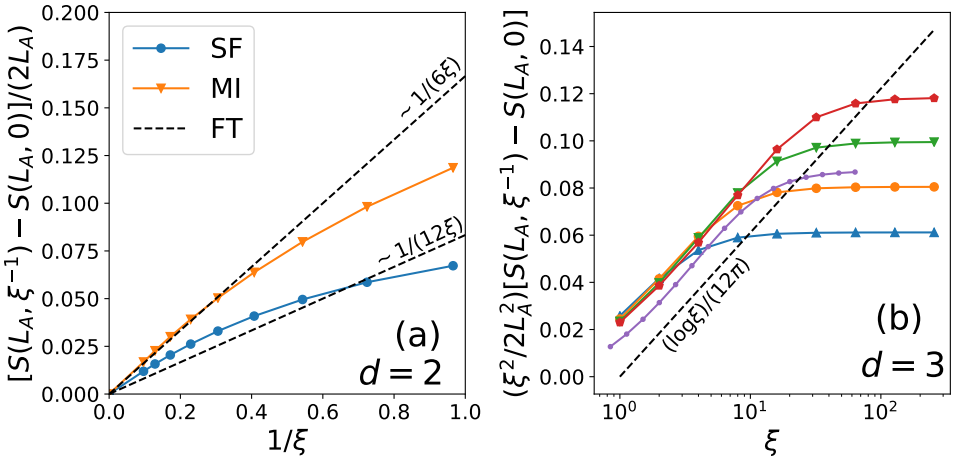

Figure 7.5: Critical scaling of the singular contribution to entanglement entropy at the O(2) point. A is half of a (hyper)-torus of dimension $L_A^{d-1} \times 2L_A$. (a) In $d = 2$, $[S(L_A, \xi^{-1}) - S(L_A, 0)]/(2L_A)$ as a function of $1/\xi$. Dashed black line shows the field theory prediction $1/(6\xi)$ of Eq. (7.29) on the MI side of the transition. $L_A = 100$. (b) In $d = 3$, $(\xi^2/2L_A^2)[S(L_A, \xi^{-1}) - S(L_A, 0)]$ as a function of $\log \xi$, showing the logarithmic correction predicted by Eq. (7.30) when $L_A < \xi$. Large symbols correspond to the MI side for $L_A = 8, 16, 32, 64$ (from bottom to top), and the purple dots correspond to the SF side ($L_A = 20$). The black dashed line indicated a slope $1/(12\pi)$, in compliance with Eq. (7.30). On the SF side, there is no prediction from field theory, but we see that the singularity behaves in a qualitatively (and even quantitatively in $d = 3$) similar manner than on the MI side.

logarithmic term $N_G(d-1)/2 \ln L_A$ in a phase breaking spontaneously a continuous symmetry (here the SF phase which breaks the U(1) symmetry), and stemming from the number of Goldstone modes N_G (=1 in the case at hand).

Field-theory prediction on the MI side of the O(2) transition. Traditionally the generic and O(2) transitions are distinguished via the different critical exponents manifested by the order parameter, its susceptibility and the correlation length (Fisher et al., 1989). In fact, the entanglement entropy is also sensitive to the critical behavior of the correlation length: indeed the area-law coefficient on the MI side of the O(2) transition is predicted (Metlitski, Fuertes, and Sachdev, 2009; Calabrese and Cardy, 2004) to manifest the singular behavior (up to logarithmic corrections in $d = 3$)

$$\frac{S}{\mathcal{A}} = a_0(g) - \frac{a_1}{\xi^{d-1}} \tag{7.27}$$

where $a_0(g)$ is a smooth function of g, and $a_1 > 0$. $\mathcal{A} = 2L_A^{d-1}$ is the area of the $A - B$ boundary. Since $a_0(g)$ varies smoothly in the vicinity of $g = g_c$, it may be

considered constant in the critical region. ξ is the correlation length, related to g in the vicinity of the critical point by $\xi \sim c/\Delta$, see Eq. (7.17). In fact, the prediction (7.27) of Metlitski, Fuertes, and Sachdev (2009) is only valid below the upper critical dimension $d_c = 3$. An explicit prediction for the coefficient a_1 is obtained from the Eq. (6.6) of Calabrese and Cardy (2004), namely :

$$S_{\text{sing}}/\mathcal{A} = S/\mathcal{A} - a_0 = -\frac{N}{12}\int \frac{\mathrm{d}^{d-1}k_{||}}{(2\pi)^{d-1}} \log \frac{k_{||}^2 + \xi^{-2}}{k_{||}^2 + a^{-2}} \,, \tag{7.28}$$

where the integration runs over the $d-1$ spatial dimensions of the boundary, and a is the lattice spacing. The singular part comes from the large ξ terms resulting from the integration, namely

$$S_{\text{sing}}/\mathcal{A} = -\frac{N}{12\xi} \quad (d=2) \tag{7.29}$$

$$S_{\text{sing}}/\mathcal{A} = -\frac{N}{24\pi}\xi^{-2}\log\xi \quad (d=3), \tag{7.30}$$

so that a logarithmic correction to Eq. (7.27) appears in $d = 3$. As shown on Fig. 7.5, this prediction agrees very well with our calculations on the MI side of the transition both in $d = 2$ (panel a) and $d = 3$ (panel b). A similar behavior has been reported in previous studies by Singh, Melko, and Oitmaa (2012) and Helmes and Wessel (2014).

Discussion of the field-theory prediction. It is important to stress that Eq. (7.27), as obtained by the field-theory calculation of Metlitski, Fuertes, and Sachdev (2009), applies only to the insulating side of the transition and, within the Gaussian approximation, it predicts quantitatively the a_1 coefficient of our calculations. Yet it does *not* predict the entanglement cusp observed at the O(2) transition. The existence of this cusp on the superfluid side is dominated by the presence of the amplitude mode going gapless both in the physical and in the entanglement spectrum. This suggests that the entanglement entropy reveals the divergence of the elusive correlation length $\xi_H \sim c/\Delta_H$ of longitudinal fluctuations (Kardar, 2007), which is proportional to the inverse mass of the amplitude mode [see Fig. 7.3(h)], but which is challenging to extract from any microscopic observable of the original model. On the SF side of the transition, the behavior of the singular contribution to entanglement entropy is similar to the behavior on the MI side. In $d = 2$, the prefactor of $1/\xi$ is slightly smaller than that on the MI side [Fig. 7.5(a)], while in $d = 3$, the prefactor of $(\log\xi)/\xi^2$ is the same as on the MI side [Fig. 7.5(b)].

7.2.4 Entanglement contours at the O(2) transition.

It would be interesting to understand the singular behavior predicted by Eqs. (7.29) and (7.30) from the perspective of the entanglement contours. Unfortunately, this is

not possible in a straightforward manner. Indeed, we have already discussed (see Fig. 7.1) that the following approximation

$$\mathcal{C}_s(i) \approx 2\frac{\alpha_d}{[2\pi(i-1/2)]^d} e^{-a'\frac{i-1/2}{\xi}} \tag{7.31}$$

qualitatively captures the behavior of the entanglement contour in the MI phase (we place ourselves directly in thermodynamic limit, so that the second boundary between A and B is pushed to infinity). Fig. 7.1(a) only showed the data in $d = 2$, but we have observed that similar results holds in $d = 3$. We also know that this prediction is valid at the O(2) point where the entanglement contour is universal. However, if this approximation were correct up to the critical point, a prediction for the prefactor of the area law would then be

$$a = a_0 - a_1(\xi) \tag{7.32}$$

$$a_0 = \sum_{i=1}^{\infty} \frac{2\alpha_d}{[2\pi(i-1/2)]^d} \tag{7.33}$$

$$a_1(\xi) = \sum_{i=1}^{\infty} \frac{2\alpha_d}{[2\pi(i-1/2)]^d} \left(1 - e^{-a'\frac{i-1/2}{\xi}}\right) . \tag{7.34}$$

Unfortunately, this prediction is incompatible with the field theory calculation (and thus with the actual lattice calculation which agrees with it). For instance, a scaling analysis of $a_1(\xi)$ would show that a logarithmic correction is predicted in $d = 2$, while in $d = 3$ we would predict $a_1(\xi) \sim 1/\xi$, in contradiction with Eq. (7.30). Nonetheless, as shown on Fig. 7.4(a) in $d = 2$, this conjecture still qualitatively describes the behavior of a when traversing the critical point. But obviously, something is missing in Eq. (7.31) to capture correctly the singularity of entanglement entropy at the critical point, something which must be related to the precise way in which the contour decays in the bulk of A. Indeed, we have observed that Eq. (7.31) works well only at distances $i \lesssim \xi$ to the boundary, and that the agreement with the exact calculation worsens at $i > \xi$ when approaching the critical point. We leave open to future studies the possibility to understand quantitatively the singular contribution to entanglement entropy from the perspective of the contours. Another related question that we leave open, is the possibility to understand the singularity through the local equilibrium hypothesis for the entanglement Hamiltonian. This would include on both sides of the transition a detailed study of the density contours, of the entanglement contours, and of the corresponding thermal quantities — namely thermal entropy and thermal variance of the number of particles.

7.3 Conclusion on the local entanglement thermodynamics

This second part of the thesis has been devoted to a *local entanglement thermodynamics* (LET) approach to the structure of entanglement in many-body ground states. In its strongest form, this hypothesis proposes an Ansatz for the entanglement Hamiltonian of an extended subsystem in the form of the physical Hamiltonian modulated in space by a local entanglement temperature, and supplements this Ansatz with a local equilibrium approximation. The local thermodynamics perspective has appeared to be valid at least as a useful heuristic viewpoint on the structure of entanglement in many-body ground states, and often as a tool for semi-quantitative predictions of entanglement features. The main motivation behind the LET hypothesis is to build a consistent physical explanation of the area laws and of their possible violation reported in a variety of situations. As such, the LET hypothesis is justified in all the situations we have encountered in this chapter. While a quantitative understanding is still missing in some cases (especially the bosonic superfluid-insulator transition), the LET hypothesis is always found to predict correctly the scaling behavior of entanglement entropy.

If correct as a general principle, the LET hypothesis has the remarkable consequence that the rough structure of entanglement can be reconstructed indirectly from the knowledge 1) of correlation functions in the ground state; and 2) of the thermal behavior of entropy and fluctuations. In other words, the study of quantum correlations (in the physical sense) is, in its own right, as interesting as the study of entanglement *per se*, for the two are bridged by thermodynamic relations. This conclusion is important when moving away from ground states (as we will do in the last part of this manuscript), for we know how to generalize the concept of quantum correlations to finite temperature (Part I), but not the concept of entanglement entropy in a physically transparent manner.

Part III

Inspecting quantum criticality and nonzero temperatures

La pureté est horreur de la vie, haine de l'homme, passion morbide du néant. Un corps chimiquement *pur* a subi un traitement barbare pour parvenir à cet état absolument contre nature. L'homme chevauché par le démon de la pureté sème la ruine et la mort autour de lui. Purification religieuse, épuration politique, sauvegarde de la pureté de la race, nombreuses sont les variations sur ce thème atroce, mais toutes débouchent avec monotonie sur des crimes sans nombre dont l'instrument privilégié est le feu, symbole de pureté et symbole de l'enfer.

Michel Tournier

Summary of Part III. The third part of the manuscript is dedicated to the study of quantum fluctuations and quantum correlations at finite temperature.

In Chapter 8, we introduce the basic concepts on the example of a one-dimensional lattice gas of free fermions. The quantum and thermal contributions to the structure factor are discussed, together with the corresponding spatial structure of quantum and thermal correlations. We also discuss the area-law scaling for quantum fluctuations of a conserved quantity in a subsystem (here, the number of particles), as opposed to the volume-law scaling of total fluctuations, and to the volume-law scaling of both quantum and thermal fluctuations for non-conserved quantities.

Chapter 9 discusses general aspects of quantum correlations in the vicinity of phase transitions. In particular, the scaling of the (quantum and thermal) fluctuations of the order parameter in the vicinity of a quantum critical point are established. We propose to define the quantum critical region in terms of the scaling behavior of quantum fluctuations. We also propose a simple gaussian field-theory model which captures the essence of the (non-divergent) behavior of quantum fluctuations when crossing a thermal critical point.

In Chapter 10, we focus on the Ising model in a transverse field with infinite-range ferromagnetic interactions (also known as the Lipkin-Meshkov-Glick model), which presents a characteristic phase diagram for the study of quantum vs. thermal criticality. This example allows us to illustrate the general scaling laws derived in Chapter 9 through direct microscopic calculations. We show in particular that the quantum fluctuations of the order parameter (the collective spin component S^z which is involved in the ferromagnetic Ising interaction) diverge at the quantum critical point, and that this divergency is fully accompanied by the "squeezing" of S^y fluctuations, perpendicular to both the order parameter and the transverse field (along x). Since squeezing implies augmented precision on the a priori knowledge of an observable in quantum mechanics, this is a first example suggesting the potential use of quantum critical states for metrological purposes (specifically, interferometric schemes).

In Chapter 11, which closes the manuscript, we investigate the opposite limit of a $d = 1$ quantum Ising chain with nearest-neighbor interactions. This model offers the opportunity to enrich our understanding of quantum vs. thermal criticality by discussing the spatial structure of quantum vs. thermal fluctuations. In particular, quantum and thermal fluctuations show a complete separation of scales in the thermal critical region, while they have the same scaling behavior in the quantum critical region (although quantum fluctuations are at least one order of magnitude weaker than thermal ones). Finally, we show that the divergence of coherent fluctuations at the quantum critical point is not accompanied by a consequent squeezing of S^y

fluctuations, which leaves open the question about the potential use of these states for interferometric purposes.

Chapter 8

Basic aspects: free fermions

Introduction. In this chapter, we explore coherent fluctuations and the correlations between them in a simple system of non-interacting fermions. We consider a tight-binding Hamiltonian on a $d = 1$ lattice

$$\mathcal{H} = -\sum_{i=1}^{L} c_i^\dagger (t c_{i+1} + t c_{i-1} + \mu c_i) \tag{8.1}$$

in the grand-canonical ensemble, where the chemical potential μ fixes the average density. The system is thermalized at temperature T. t is the hopping amplitude setting the energy scale, and we consider periodic boundary conditions ($L + 1 \equiv 1$). Free fermions in dimension $d \geq 2$ show similar features as in $d = 1$ regarding the spatial structure of correlations discussed in the present chapter. $\mathcal{H}$ is diagonalized by Fourier transform

$$\mathcal{H} = \sum_k \epsilon_k c_k^\dagger c_k \tag{8.2}$$

with $\epsilon_k = -2t \cos k - \mu$, and $c_k = L^{-1/2} \sum_j e^{-ikr_j} c_j$.

8.1 Total, thermal and quantum structure factors

8.1.1 Total structure factor

We shall focus on the correlations among the most elementary local observables, namely the local densities n_i (as the local fields c_i are not proper observables). We aim at separating quantum and thermal contributions to these correlations (see Section 2.2). As we are considering non-interacting particles, correlation effects stem solely from Pauli principle. Naively, we thus expect that a reliable separation of total correlations

into a classical and a quantum contribution identifies all correlations as purely quantum ones. Though excessively simplistic, this expectation turns out to be partly justified.

Total correlations are defined as the covariance of density fluctuations on different sites (see Section 2.2). With the notation $\delta\mathcal{O} = \mathcal{O} - \langle\mathcal{O}\rangle$

$$\begin{aligned}
\langle\delta n_i \delta n_j\rangle &= \langle c_i^\dagger c_i c_j^\dagger c_j\rangle - \langle c_i^\dagger c_i\rangle\langle c_j^\dagger c_j\rangle && (8.3)\\
&\underset{\text{(Wick)}}{=} \langle c_i^\dagger c_j\rangle\langle c_i c_j^\dagger\rangle && (8.4)\\
&= \frac{1}{L^2}\sum_{k_1,k_2} e^{i(k_2-k_1)(r_i-r_j)} f_{k_1}(1-f_{k_2}) && (8.5)\\
&= \frac{1}{L}\sum_{k} e^{ik(r_i-r_j)} \underbrace{\frac{1}{L}\sum_{q} f_q(1-f_{k+q})}_{S_k^{\text{tot}}} && (8.6)
\end{aligned}$$

where the structure factor S_k^{tot} has been defined on the last line. We have introduced the Fermi factors $f_k = 1/(e^{\beta\epsilon_k}+1)$, with $\beta = (k_B T)^{-1}$, and used Wick's theorem (Blaizot and Ripka, 1986) plus particle-number conservation to factorize the order-4 correlators in terms of order-2 correlators.

8.1.2 Thermal and quantum structure factor

The thermal structure factor is defined as

$$S_k^{\text{T}} = k_B T \chi(k) \tag{8.7}$$

where

$$\chi(k) = \left.\frac{\partial\langle N_k\rangle}{\partial h_{-k}}\right|_{h_{-k}=0} \tag{8.8}$$

is the static susceptibility. We introduced the Fourier-component of the density profile $N_k = L^{-1/2}\sum_j e^{ikr_j} n_j$. The thermal structure factor can be expressed in terms of imaginary-time correlations (Section 1.7) as

$$S_k^{\text{T}} = \int_0^\beta \frac{d\tau}{\beta}\langle\delta N_k(\tau)\delta N_{-k}(0)\rangle \tag{8.9}$$

where $\mathcal{O}(\tau) = e^{\tau\mathcal{H}}\mathcal{O}e^{-\tau\mathcal{H}}$. The discrepancy between total and thermal covariances stems from the possible non-trivial dynamics of $N_k(\tau)$ in imaginary time if $[N_k, \mathcal{H}] \neq$

0. We have

$$\begin{aligned}
\langle \delta N_k(\tau)\delta N_{-k}(0)\rangle &= \frac{1}{L}\sum_{i,j} e^{ik(r_i-r_j)}\langle \delta n_i(\tau)\delta n_j(0)\rangle && (8.10)\\
&= \frac{1}{L}\sum_{i,j} e^{ik(r_i-r_j)}\Big[\langle c_i^\dagger(\tau)c_i(\tau)c_j^\dagger(0)c_j(0)\rangle - \\
&\quad \langle c_i^\dagger(\tau)c_i(\tau)\rangle\langle c_j^\dagger(0)c_j(0)\rangle\Big] && (8.11)\\
&= \frac{1}{L}\sum_{i,j} e^{ik(r_i-r_j)}\langle c_i^\dagger(\tau)c_j(0)\rangle\langle c_i(\tau)c_j^\dagger(0)\rangle && (8.12)\\
&= \frac{1}{L}\sum_{i,j} e^{ik(r_i-r_j)}\frac{1}{L^2}\sum_{k_1,k_2}\Big[\\
&\quad e^{i(k_2-k_1)(r_i-r_j)}e^{\tau(\epsilon_{k_1}-\epsilon_{k_2})}f_{k_1}(1-f_{k_2})\Big] && (8.13)\\
&= \frac{1}{L}\sum_{q} f_q(1-f_{k+q})e^{\tau(\epsilon_q-\epsilon_{k+q})}\,. && (8.14)
\end{aligned}$$

We have used that $c_k(\tau) = e^{-\tau\epsilon_k}c_k$ and $c_k^\dagger(\tau) = e^{\tau\epsilon_k}c_k^\dagger$. Integrating over τ, we find that

$$S_k^{\mathrm{T}} = \frac{1}{L}\sum_q f_q(1-f_{k+q})\frac{e^{\beta(\epsilon_q-\epsilon_{k+q})}-1}{\beta(\epsilon_q-\epsilon_{k+q})}\,, \tag{8.15}$$

In particular, we see that for $k = 0$, corresponding to the total number of particles (conserved by $\mathcal{H}$)

$$S_{k=0}^{\mathrm{T}} = S_{k=0}^{\mathrm{tot}}\,. \tag{8.16}$$

For $k \neq 0$, the thermal contribution from any other $k \neq 0$ does not exhaust the total fluctuations, due to the decay of $\langle \delta N_k(\tau)\delta N_{-k}(0)\rangle$ as a function of τ [Fig. 8.1(a)]

$$S_{k\neq 0}^{\mathrm{T}} < S_{k\neq 0}^{\mathrm{tot}}\,. \tag{8.17}$$

We thus define the quantum structure factor as

$$S_k^{\mathrm{Q}} = S_k^{\mathrm{tot}} - S_k^{\mathrm{T}}\,. \tag{8.18}$$

Thermal and quantum covariance. The thermal (quantum) covariance is

$$\langle \delta n_i \delta n_j\rangle_{\mathrm{T(Q)}} = \frac{1}{L}\sum_k e^{ik(r_i-r_j)}S_k^{\mathrm{T(Q)}}\,. \tag{8.19}$$

8.1.3 Temperature dependence of the structure factors

In Fig. 8.1, we explore the amplitude of fluctuations as a function of wavevector k and of temperature T. Fig. 8.1(a) presents the imaginary-time correlations

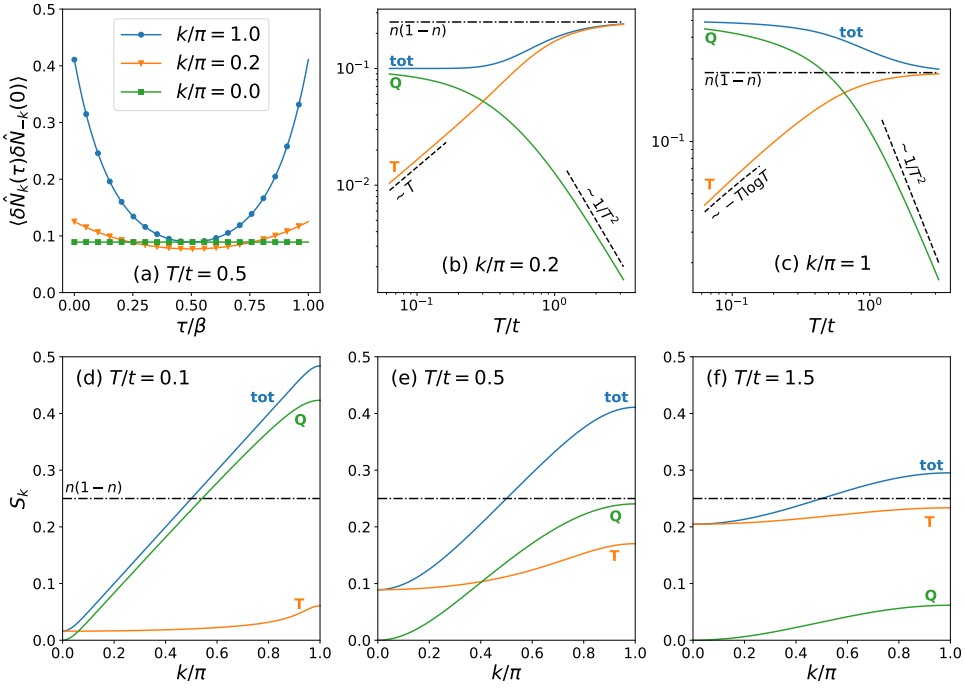

Figure 8.1: Quantum and thermal structure factors for free fermions in $d = 1$ at half filling ($n = 1/2$). (a) Correlations in imaginary time of the fluctuations at wavevector k, for $T/t = 0.5$. $N_{k=0}(\tau) = N_{k=0}(0)$, so that correlations in imaginary time are constant. At a generic $k \neq 0$, instead, the correlation function is maximal at $\tau = 0$ (corresponding to total fluctuations), and decays in imaginary time under the effect of quantum fluctuations. Being symmetric with respect to $\tau = \beta/2$, the correlation function then increases again up to the initial value. (b) Fluctuations at $k/\pi = 0.2$ as a function of the temperature. At low temperature, the thermal variance increases linearly with T and coincides with the total variance for $T \gg t$ (where it attains the shot-noise limit $n(1-n)$ with n the density). The quantum variance (QV) is observed to monotonically decrease with T, and scales as $1/T^2$ at large temperature. (c) Same as in (b) but for $k = \pi$. The $k = \pi$ quantum fluctuations are so strong that the *total* fluctuations are found to *decrease* with the temperature, in complete contradiction with classical intuition. At low temperature, the thermal variance increases as $T\log(1/T)$ because of the divergence of $\chi^{\rm stat}(\pi) \sim \log(1/T)$. (d) Total, quantum and thermal structure factors as a function of wavevector k at $T/t = 0.1$. Quantum fluctuations represent the dominant contribution to the total structure factor at almost all wavevectors, and cause it to exceed the shot-noise limit for $k \geq \pi/2$ (this behavior is observed at all temperatures, see panels (e) and (f)). (e) and (f): Same as in (d) but at a temperature $T/t = 0.5$ and 1.5 respectively. At high temperature, the quantum structure factor vanishes, while the thermal structure factor converges towards the shot-noise limit.

$\langle \delta N_k(\tau)\delta N_{-k}(0)\rangle$ at $k=0$, $k=\pi/5$ and $k=\pi$ as a function of τ/β, showing that correlations are symmetric with respect to $\tau=\beta/2$[1] and, except at $k=0$, decay in imaginary time. The total structure factor is the $\tau=0$ value of this correlation function, $S_k^{\rm tot}=\langle \delta N_k(0)\delta N_{-k}(0)\rangle$, and the decay as a function of τ is a consequence of quantum fluctuations. On Fig. 8.1(b, c) we show the variation of the total, quantum and thermal structure factor at $k=\pi/5$ (panel b) and $k=\pi$ (panel c) as a function of temperature. At high temperature, the quantum variance (QV) decreases to zero as $1/T^2$[2], and the total ($\approx$ thermal) variance saturates to the shot-noise limit $n(1-n)$, with $n=\langle n_i\rangle$ the average density, corresponding to uncorrelated fluctuations on every lattice site. The monotonic decrease of the QV as a function of temperature is a generic feature: though it is not a mathematical necessity[3], thermal agitation is generally expected to destroy coherence. On the contrary, the thermal variance is monotonically increasing with the temperature. This behavior is also expected to be generic, unless a phase transition is crossed, which is not the case here. In general, the thermal variance is expected to grow linearly with T at low temperature ($\langle\delta^2\mathcal{O}\rangle_{\rm T}=k_BT\chi_{\mathcal{O}}$) if the susceptibility $\chi_{\mathcal{O}}$ has a finite value at $T=0$. This linear behavior is observed for free

[1] In general, if $\mathcal{O}$ is an hermitian operator, the property $\langle\delta\mathcal{O}(\tau)\delta\mathcal{O}(0)\rangle=\langle\delta\mathcal{O}(\beta-\tau)\delta\mathcal{O}(0)\rangle$ holds:

$$\frac{1}{Z}\mathrm{Tr}\left(e^{-\beta\mathcal{H}}e^{\tau\mathcal{H}}\mathcal{O}e^{-\tau\mathcal{H}}\mathcal{O}\right)=\frac{1}{Z}\mathrm{Tr}\left(e^{-\beta\mathcal{H}}e^{(\beta-\tau)\mathcal{H}}\mathcal{O}e^{-(\beta-\tau)\mathcal{H}}\mathcal{O}\right) \tag{8.20}$$

using the invariance of the trace under cyclic permutations.

[2] We can prove that the decrease of the QV at high temperature is at least as fast as $1/T^2=\beta^2$. At high temperature, we may expand

$$\mathcal{O}(\tau)=e^{\tau\mathcal{H}}\mathcal{O}e^{-\tau\mathcal{H}}=\mathcal{O}+\tau[\mathcal{H},\mathcal{O}]+O(\tau^2)\,. \tag{8.21}$$

Hence

$$\langle\mathcal{O}^2\rangle-\langle\mathcal{O}(\tau)\mathcal{O}(0)\rangle=\tau(\langle\mathcal{H}\mathcal{O}^2\rangle-\langle\mathcal{O}\mathcal{H}\mathcal{O}\rangle)+O(\tau^2)\,. \tag{8.22}$$

We then use the fact that

$$\rho=\frac{1}{Z}e^{-\beta\mathcal{H}}=\frac{1}{Z}(1-\beta\mathcal{H})+O(\beta^2)\,, \tag{8.23}$$

so that finally

$$\langle\mathcal{O}^2\rangle-\langle\mathcal{O}(\tau)\mathcal{O}(0)\rangle=O(\beta\tau)\,. \tag{8.24}$$

Integrating over τ, we find that

$$\langle\delta^2\mathcal{O}\rangle_Q = \int_0^\beta\frac{d\tau}{\beta}[\langle\mathcal{O}^2\rangle-\langle\mathcal{O}(\tau)\mathcal{O}(0)\rangle] \tag{8.25}$$

$$= \int_0^\beta\frac{d\tau}{\beta}O(\beta\tau)=O(\beta^2)\,. \tag{8.26}$$

[3] The convexity of the QV with respect to the density matrix, see Section 1.5, does not imply that the QV decreases upon increasing the temperature. Convexity only implies that the QV of $\mathcal{O}$ in a thermal state is smaller than the average variance of $\mathcal{O}$ in the eigenstates of the Hamiltonian, and not that it is smaller than the variance of $\mathcal{O}$ in, say, the ground state (GS). If energy states slightly above the GS have a much larger variance of $\mathcal{O}$ than in the GS, one can expect that the QV increases at low temperature. This behavior is however not observed in general.

fermions at half filling, apart at $k = \pi$ where $\chi(\pi) \sim \log(1/T)$[4]. The total variance, being the sum of a decreasing and of an increasing function of T, cannot be predicted to display any specific behavior, and indeed, we observe that *e.g.* at $k = \pi/5$, quantum fluctuations are rather weak, and the total structure factor monotonically increases to the shot-noise limit (panel b), while at $k = \pi$, quantum fluctuations are so strong that the *total* fluctuations *monotonically decrease* with temperature, in complete contradiction with our classical intuition (panel c). The strong quantum fluctuations at $k = \pi$ are a consequence of strong anti-correlations of the density between neighboring sites at half filling.

Fig. 8.1(d,e,f) shows the total, quantum and thermal structure factors as a function of k for $T/t = 0.1$ (panel a), 0.5 (panel b) and 1.5 (panel c). The first observation, in compliance with our expectation and with the results presented on panels (b) and (c), is that, upon increasing the temperature, the quantum structure factor is decreasing, while the total and thermal structure factors get closer to the shot-noise limit $n(1-n)$. The second observation, that we already made, is that the quantum structure factor always vanishes at $k = 0$, corresponding to the fact that the particle number is conserved in the whole system: there is no coherence in the density matrix between states with different numbers of particles.

8.2 Spatial structure of density correlations

At different sites, density fluctuations are always anticorrelated: $\mathcal{C}_{\rm tot} = \langle \delta n_i \delta n_j \rangle = -|\langle c_i^\dagger c_j \rangle|^2 \leq 0$, and, within an envelope decreasing as $e^{-r_{ij}/\xi(T)}$ ($\xi(T)$ is the T-dependent correlation length), oscillate at a spatial frequency $2k_F$, with k_F the Fermi wave-vector ($2k_F = \pi$ at half-filling). Thermal correlations $\mathcal{C}_{\rm T} = \langle \delta n_i \delta n_j \rangle_{\rm T} = k_B T \partial \langle n_j \rangle / \partial \mu_i$ have a similar structure, but oscillate in sign (this behavior is related to the Friedel oscillations of the density in the vicinity of an impurity, as illustrated on Fig. 4.3). Quantum correlations $\mathcal{C}_{\rm Q}$, which are the difference between the two, have also the same structure but are found to be always negative, as total correlations. Furthermore, at distances larger than the correlation length, we observe that the oscillations of thermal correlations almost perfectly compensate the oscillations of total correlations, so that quantum correlations show almost no oscillations at all. These findings are illustrated on Fig. 8.2. On the same figure, for comparison, we have also plotted the density correlations associated to the quantum Fisher information

[4] This behavior may be checked by evaluating the static susceptibility $\chi(\pi)$ in Eq. (**??**).

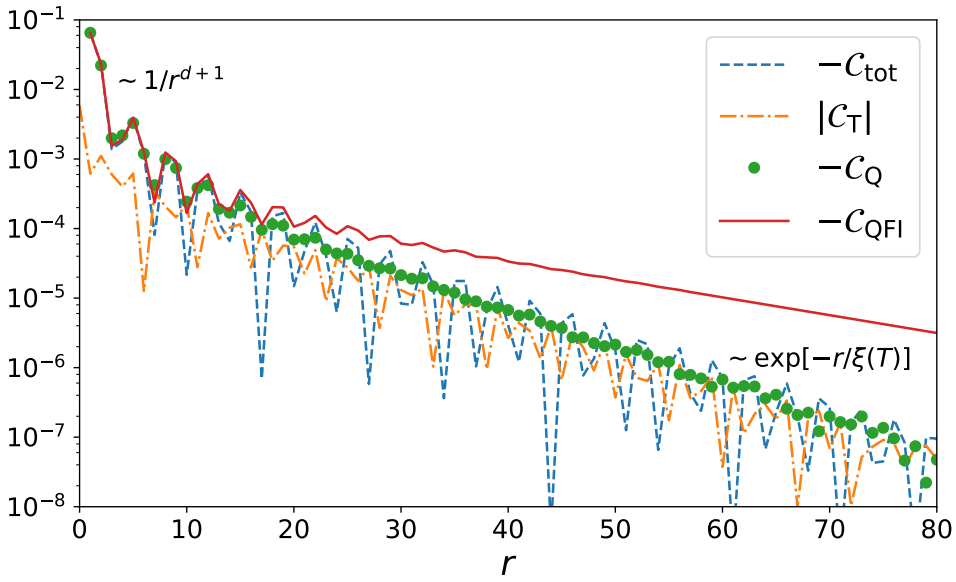

Figure 8.2: Density correlations for $d = 1$ free fermions, for $\mu/t = -1.2$ ($k_F \approx 0.3\pi$) and $T/t = 0.03$. Total covariance $\mathcal{C}_{\rm tot}$ (dashed blue line), thermal covariance $\mathcal{C}_{\rm T}$ (dashed-dotted orange line), quantum covariance $\mathcal{C}_{\rm Q}$ (green dots) and the QFI covariance $\mathcal{C}_{\rm QFI}$ (red solid line) are plotted as a function of the spatial separation r between the two sites. At distances shorter than the correlation length $\xi \sim t/T$, all correlations are mostly coherent, and decay as $1/r^{d+1}$ in d spatial dimensions, and at distances larger than ξ, they decay exponentially. The correlation length for the QFI covariance is twice larger than the usual correlation length.

(QFI, see Section 1.4.2), which we call "QFI covariance", given by

$$\mathcal{C}_{\rm QFI}(r) = \frac{1}{L}\sum_k e^{-ikr} S_k^{\rm QFI}/4 \tag{8.27}$$

$$S_k^{\rm QFI}/4 = \frac{1}{L}\sum_q f_q(1-f_{k+q})\tanh^2[\beta(E_q - E_{k+q})/2] \tag{8.28}$$

$$= \frac{1}{4}{\rm QFI}(N_k)\ , \tag{8.29}$$

where ${\rm QFI}(N_k)$ is the quantum Fisher information of N_k.

At distances shorter than the correlation length, thermal effects are negligible, and all correlations have a coherent nature: $\mathcal{C}_{\rm tot} \approx \mathcal{C}_{\rm QFI} \approx \mathcal{C}_{\rm Q}$ (these are exact equalities at $T = 0$). Remarkably, at distances larger than ξ, only the quantum covariance $\mathcal{C}_{\rm Q}$ follows the exponential decay of the total covariance, while the QFI covariance decay exponentially also, but with a correlation length twice as large. This result is rather unexpected, for it implies that certain form of quantum correlations (as quantified by the QFI covariance), may exceed by far the total correlations for the

same observable. Yet we remark that 2ξ is the correlation length for the decay of the first-order correlation function $\langle c_i^\dagger c_j \rangle$, and therefore the range of the QFI covariance does not exceed the range of all correlations in the system. It remains surprising that quantum correlations related to the density show sensitivity to the correlations of the field; something which, parenthetically, only shows up at $T > 0$. Nonetheless, we shall further remark in Chapter 11 that the QFI covariance exhibits a systematically slower decay than the quantum covariance, suggesting a certain ambiguity on the actual range of quantum correlations.

Finally, we emphasize that, in the context of parameter estimation (Pezzè and Smerzi, 2014), the QFI covariance is the proper quantifier of the metrological usefulness of the state, and is interesting to study from that perspective.

8.3 Area-law scaling of the local QV of the number of particles

We now turn our attention on bipartite fluctuations, namely the fluctuations on subsystems of observables which are conserved globally — we focus here on the particle number. Such fluctuations in the ground state are tightly linked to entanglement in the case of free fermions, as discussed in Chapter 3, and their scaling with subsystem size exhibits a logarithmically violated area law. When moving to finite temperatures, the link between entanglement and fluctuations breaks down, as fluctuations acquire a thermal contribution which has no relationship to entanglement — yet, we can continue quantifying quantum fluctuations with the quantum variance. It is remarkable to observe that, in spite of the volume-law scaling of total fluctuations at finite temperature, the quantum variance of the subsystem particle number obeys an area law (Frérot and Roscilde, 2016b)

$$\langle \delta^2 N_A \rangle_Q \sim L_A^{d-1} \tag{8.30}$$

Here $N_A = \sum_{i \in A} n_i$ counts the number of particles in a subsystem A, whose linear size is L_A. This area-law scaling can be seen as the finite-temperature counterpart of the (log-violated) area-law scaling of particle-number fluctuations in the ground state, itself being a manifestation of the scaling of entanglement entropy S_A. And indeed, as shown on Fig. 8.3 for free fermions in $d = 2$, we observe that the thermodynamic relation $(\pi^2/3)\langle \delta^2 N_A \rangle \approx S_A$ between fluctuations and entanglement entropy in the ground state, translates at finite temperature into a similar relation between the QV of N_A and (half of) the mutual information

$$I(A:B)/2 \approx \frac{\pi^2}{3} \langle \delta^2 N_A \rangle_Q \tag{8.31}$$

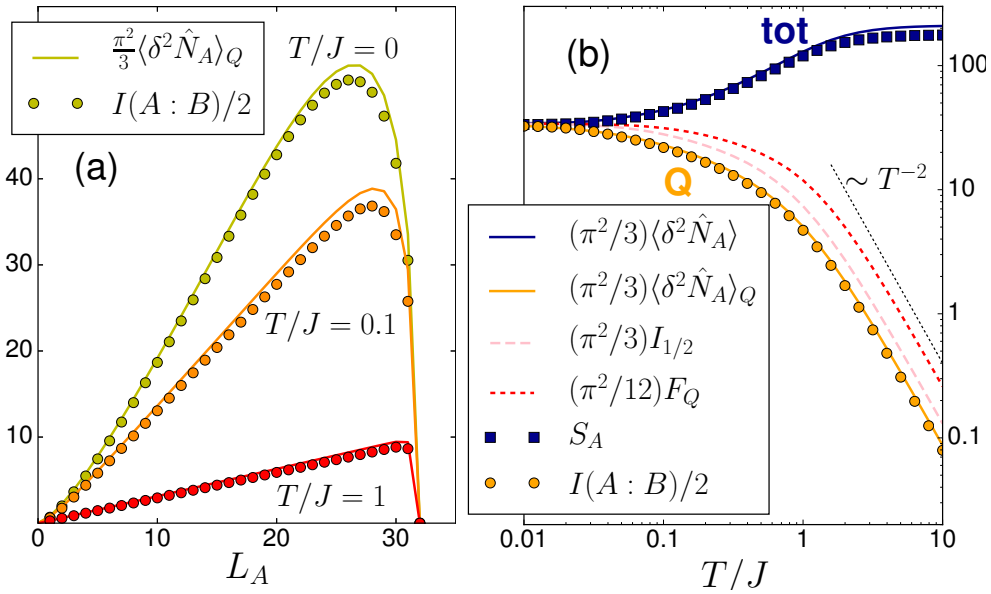

Figure 8.3: Quantum correlations vs. quantum mutual information. (a) Scaling of the quantum variance of bipartite particle-number fluctuations and of the quantum mutual information in a system of free fermions on a $L \times L$ square lattice ($L = 32$) at half filling for three different temperatures (J is the hopping amplitude); (b) temperature dependence of the same two quantities, along with the total entropy S_A, the total fluctuations $\langle\delta^2 N_A\rangle$, the Wigner-Yanase skew information $I_{1/2}(N_A, \rho)$, and the quantum Fisher information $F_Q(N_A; \rho)$, for an A square region with linear size $L_A = L/2$. The T^{-2} decay of the mutual information at high temperature has been proven rigorously for free fermions in Bernigau, Kastoryano, and Eisert (2015), and it is proven for the quantum variance, skew information and quantum Fisher information in App. F of Frérot and Roscilde (2016b), from which this figure is reproduced.

where the mutual information $I(A:B) = S_A + S_B - S_{AB}$ (B is the complement of A in the total system) is a measure of total correlations between A and B, and reduces to (twice) the entanglement entropy in the ground state where $S_A = S_B$ and $S_{AB} = 0$ (see Section 3.2). As the mutual information does not in principle isolate quantum from thermal correlations, but accounts for all of them together, this relation further confirms that essentially all correlations in a noninteracting system stem from quantum effects. Furthermore, as shown on Fig. 8.3(b), only the QV is related by Eq. (8.31) to the mutual information, while the QFI (divided by 4, is also equal to the variance in the ground state), is about three times larger (see the Appendix F of Frérot and Roscilde (2016b) for a calculation of the QV and of the QFI at large T).

Chapter 9

Generalities on quantum criticality

Introduction. In this chapter, we present general aspects of quantum fluctuations in the vicinity of a second-order phase transition. Approaching a *thermal* (*i.e.* finite-temperature) critical transition, the fluctuations of the order parameter $\mathcal{O}$ diverge according to

$$\langle \delta^2 \mathcal{O} \rangle_{\rm tot} \sim t^{-\gamma_{\rm T}} \tag{9.1}$$

with $t = |T - T_c|/T_c$ and $\gamma_{\rm T}$ a (thermal) critical exponent. t is the distance to the critical temperature T_c, expressed in dimensionless units. In Section 1.9, we showed that this critical behavior of the fluctuations of the order parameter is entirely due to the thermal contribution. Indeed, it was shown that the quantum variance (QV) of $\mathcal{O}$ acquires a singular part scaling according to

$$\langle \delta^2 \mathcal{O} \rangle_Q^{\rm sing} \sim t^{2\nu_{\rm T}(z_{\rm T}+\eta_{\rm T}/2-1)} \tag{9.2}$$

where $\nu_{\rm T}$ is the critical exponent of the correlation length ($\xi \sim t^{-\nu_{\rm T}}$), and $z_{\rm T}$ the dynamical critical exponent (Hohenberg and Halperin, 1977; Collins, 1989; Täuber, 2014; Kamenev, 2011). As all the values for $z_{\rm T}$ reported in the literature satisfy the condition $z_{\rm T} > 1$, and as $\nu_{\rm T}, \eta_{\rm T} \geq 0$, we concluded that this singular part for the QV of the order parameter *vanishes* at the critical point, so that the divergence of $\langle \delta^2 \mathcal{O} \rangle_{\rm tot}$ stems entirely from the divergence of the thermal variance

$$\langle \delta^2 \mathcal{O} \rangle_{\rm tot} \approx \langle \delta^2 \mathcal{O} \rangle_{\rm T} = k_B T \chi \sim t^{-\gamma_{\rm T}} \ . \tag{9.3}$$

Obviously, the situation must be completely different in the vicinity of a *quantum* critical point, where the phase transition is driven by quantum fluctuations. In Section

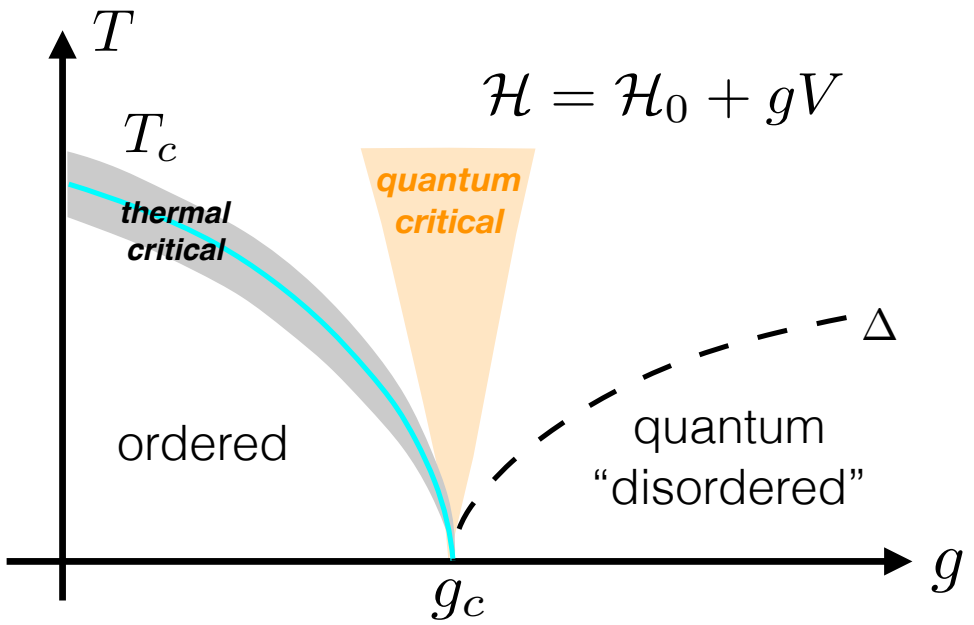

Figure 9.1: Quantum critical region. Schematic representation of the phase diagram of a Hamiltonian $\mathcal{H}_0$ having a low-temperature ordered phase, and a high-temperature disordered phase. The application of a perturbation gV which does not commute with $\mathcal{H}_0$ induces quantum fluctuations which ultimately destabilize the ordered phase beyond a critical value $g \geq g_c$, even at $T = 0$. On the disordered side $g \geq g_c$, an energy gap Δ opens. At finite temperature above the quantum critical point $(g = g_c, T = 0)$, the scaling of fluctuations is controlled by the critical exponents of the quantum phase transition in the so-called "quantum critical region" (orange shaded area). These exponents are in general different from the critical exponents of the finite-temperature phase transition, which govern the scaling of fluctuations in the thermal critical region (grey shaded area).

9.1, we present the generic phase diagram of a system possessing both thermal and quantum phase transitions, having in mind the quantum Ising model explicitly studied in Chapters 10 and 11. We briefly comment on the novel insights into the so-called "quantum critical region" provided by our approach in Section 9.2. Section 9.3 is devoted to general scaling predictions (including finite-size scaling) for thermal and quantum fluctuations both in the vicinity of a thermal and of a quantum critical point, while Section 9.4 illustrates the dichotomy between thermal and quantum fluctuations at a thermal phase transition in the simple case of a gaussian field theory.

9.1 Representative phase diagram

On Fig. 9.1, we show the typical phase diagram of a system possessing a thermal critical trajectory terminating at a quantum critical point (Sachdev, 2001). The general form of the Hamiltonian describing such a system is

$$\mathcal{H} = \mathcal{H}_0 + gV \tag{9.4}$$

where $\mathcal{H}_0$ has a low-temperature ordered phase, and a high-temperature disordered phase. gV is a term which does not commute with $\mathcal{H}_0$. As in Chapters 10 and 11 we shall discuss in details the quantum Ising model in a transverse field, corresponding to the Hamiltonian

$$\mathcal{H}_{\rm TFIM} = -\sum_{i,j} J_{ij} S_i^z S_j^z - B \sum_i S_i^x \ , \tag{9.5}$$

the Fig. 9.1 can be seen as the phase diagram of $\mathcal{H}_{\rm TFIM}$, but is not restricted to this example (Sachdev, 2001). In this case, S_i^α is the α component of spin $s = 1/2$ particles localized at the nodes i of a generic lattice. $J_{ij} \geq 0$ are coupling constants favoring ferromagnetic alignment of the spins along the z axis, while B is a transverse-field term favoring a magnetization along the x axis.

When $[V, \mathcal{H}_0]$, the term gV induces quantum fluctuations of the order parameter which destabilize the ordered phase for $g \geq g_c$. In the vicinity of the thermal critical trajectory $T \approx T_c(g) > 0$, the scaling of fluctuations is governed by the critical exponents of the classical field theory, describing the long-wavelength properties close to the transition (Sachdev, 2001). The universality class of the transition is the same as for $g = 0$. Physically, this is a consequence of the fact that the critical behavior of fluctuations is entirely carried by thermal fluctuations, while quantum fluctuations do not diverge, as we argued in Section 1.9. They merely "renormalize" the parameters of the classical field theory, and the region at $g < g_c$ is often described as a "renormalized classical" regime (Sachdev, 2001).

9.2 The quantum critical region

The situation is completely different in the vicinity of the quantum critical point (QCP) $(g = g_c, T = 0)$. At $T = 0$, thermal fluctuations are absent, and the critical behavior is entirely carried by quantum fluctuations. At $T > 0$ above $g = g_c$, on the other hand, the situation is much richer (Sachdev, 2001). In this so-called *quantum critical region*, both quantum and thermal fluctuations are of equal importance to understand the scaling of fluctuations. The notion of quantum fluctuations / correlations we have developed in Chapters 1 and 2 thus appears especially suited to disentangle

thermal and quantum effects in this quantum critical region. In particular, the quantum critical region is usually defined as the finite-temperature region where the scaling of fluctuations is governed by the critical exponents of the *quantum* phase transition, as opposed to the critical exponents of the *thermal* phase transition. In the specific case of the Ising model, the universality class of the *quantum* critical point is that of the $(d+1)$-dimensional *classical* Ising model (Sachdev, 2001). However, in practice, if focusing on *total* fluctuations, this region may be very difficult to identify, for the proximity of the thermal critical trajectory may "pollute" the scaling behavior associated to the quantum critical point. If instead one focuses on *quantum* fluctuations, the discussion is much simpler: as quantum fluctuations diverge *only* at the quantum critical point, it is more convenient and natural to define the quantum critical region as the region where the scaling of *quantum* fluctuations is governed by the critical exponents of the QCP.

The redefinition of the quantum critical region in terms of the scaling behavior of quantum fluctuations is one of the main conceptual improvements associated to the present work in the context of quantum statistical mechanics.

9.3 Scaling of thermal and quantum fluctuations

In this section, we briefly review the scaling behavior of critical fluctuations in the vicinity of a second-order phase transition, namely the scaling of the variance $\langle \delta^2 \mathcal{O} \rangle$ of the order parameter. This includes a discussion of the finite-size scaling behavior (namely the scaling of fluctuations with the size L of the system, or with the number $N = L^d$ of sites for a lattice model in d spatial dimensions). We already showed in Section 1.9 that the quantum variance of the order parameter $\langle \delta^2 \mathcal{O} \rangle_Q$ does not diverge at a thermal phase transition. We first review the finite-size scaling of $\langle \delta^2 \mathcal{O} \rangle$ at a thermal phase transition (Section 9.3.1), and then of both $\langle \delta^2 \mathcal{O} \rangle_Q$ and $\langle \delta^2 \mathcal{O} \rangle_{\mathrm{T}} = k_B T \chi$ at a quantum phase transition, and in particular in the quantum critical region (Section 9.3.2).

9.3.1 Thermal critical scaling

Approaching the thermal phase transition, the scaling behavior of $\langle \delta^2 \mathcal{O} \rangle$ is the same as for the static susceptibility χ of the order parameter. On a system of finite size L,

the scaling theory (Täuber, 2014) predicts the following behavior

$$\langle \delta^2 \mathcal{O} \rangle / N \sim \chi / N \sim t^{-\gamma_{\mathrm{T}}} f(\xi/L) \tag{9.6}$$

$$\sim L^{\gamma_{\mathrm{T}}/\nu_{\mathrm{T}}} g(L t^{\nu_{\mathrm{T}}}) \tag{9.7}$$

$$\sim N^{(2-\eta_{\mathrm{T}})/d} g'(N t^{\nu_{\mathrm{T}} d}) \,, \tag{9.8}$$

where f is a scaling function of ξ/L. $\xi \sim t^{-\nu_{\mathrm{T}}}$ is the correlation length governing the large-distance decay of the correlation function

$$\langle \delta \mathcal{O}_i \delta \mathcal{O}_j \rangle \sim \frac{e^{-|r_i - r_j|/\xi}}{|r_i - r_j|^{d-2+\eta_{\mathrm{T}}}} \,, \tag{9.9}$$

with η_{T} the exponent characterizing the power-law decay of the correlation function at the critical point ($\xi = \infty$). In Eq. (9.7), we introduced $g(x) = x^{-\gamma_{\mathrm{T}}\nu_{\mathrm{T}}} f(1/x)$, and in Eq. (9.8) $g'(x) = g(x^d)$ with d the number of spatial dimension ($N = L^d$). We also used the relation $\gamma_{\mathrm{T}}/\nu_{\mathrm{T}} = 2 - \eta_{\mathrm{T}}$ (Täuber, 2014). These scaling forms show that 1) in the limit $N \to \infty$, we have $\langle \delta^2 \mathcal{O} \rangle / N \sim t^{-\gamma_{\mathrm{T}}}$; and 2) at $T = T_c$, the variance of the order parameter diverges with the system size as $\langle \delta^2 \mathcal{O} \rangle \sim N^{1+(2-\eta_{\mathrm{T}})/d}$.

9.3.2 Quantum critical scaling

Scaling of the thermal variance. The scaling laws of the previous section apply also to the static susceptibility of the order parameter χ at $T = 0$, where now $\delta = |g - g_c|/g_c$ replaces $t = |T - T_c|/T_c$

$$\chi / L^d \sim \delta^{-\gamma} f(L \delta^{\nu}) \tag{9.10}$$

and where the exponents refer to the universality class of the *quantum* critical point (for the sake of clarity, the critical exponents for the thermal phase transition are denoted with a subscript "T", and the exponents for the quantum phase transition without substript). At finite temperature, this scaling behavior is modified into

$$\chi \sim \delta^{-\gamma} f(L \delta^{\nu}, T/\Delta) \tag{9.11}$$

where Δ is the energy gap for $g > g_c$, and a characteristic energy scale for $g < g_c$. This characteristic energy may be a gap, or the critical temperature for the thermal phase transition. The energy gap closes at the critical point with the scaling behavior $\Delta \sim \xi^{-z} \sim \delta^{\nu z}$, where z is a (quantum) dynamical critical exponent[1]. Note that the

[1] The quantum dynamical exponent z bears no relation to the dynamical exponent z_T of the thermal phase transition.

exponent η, characterizing the decay of the order-parameter correlations close to the QCP, is now defined by

$$\langle \delta\mathcal{O}_i \delta\mathcal{O}_j \rangle \sim \frac{e^{-|r_i - r_j|/\xi}}{|r_i - r_j|^{d+z-2+\eta}} \,. \tag{9.12}$$

This definition is related to the fact that, according to the field theory describing the critical behavior, the d real-space dimensions of the system are embedded in a higher-dimensional space with an effective number $d + z$ of dimensions (Sachdev, 2001).

To predict the scaling behavior of thermal fluctuations at finite temperature along the critical trajectory $t = 0$, we proceed to the following manipulations

$$\begin{aligned} \langle \delta^2 \mathcal{O} \rangle_{\mathrm{T}} / L^d = k_B T \chi / L^d &\sim T \delta^{-\nu} f(L\delta^{\nu}, T\delta^{-\nu z}) \\ &\sim T^{1-\gamma/(\nu z)} (T\delta^{-\nu z})^{\gamma/\nu z} f(L\delta^{\nu}, T\delta^{-\nu z}) \\ &\sim T^{1-\gamma/(\nu z)} g(\delta^{\nu z}/T, TL^z) \,. \end{aligned} \tag{9.13}$$

This shows that at $\delta = 0$ and $L^z \gg 1/T$, the thermal variance diverges according to $\langle \delta^2 \mathcal{O} \rangle_{\mathrm{T}} / L^d \sim T^{1-\gamma/(\nu z)} \sim T^{1-(2-\eta)/z}$. In particular, in the thermodynamic limit, the thermal variance does not scale to zero when approaching $T = 0$ provided $2 - \eta \geq z$. For the Ising model, $z = 1$ and $\eta < 1$ so that this condition is satisfied. This counter-intuitive behavior is a specificity of the quantum critical region, where thermal and quantum fluctuations diverge with the same critical exponents, as we now show.

Scaling of the quantum variance. In fact, we can show that the quantum variance of the order parameter has the same scaling as the thermal variance (and hence, obviously, as the total variance) in the quantum critical region. In order to do so, we resort to the expression of the quantum variance in terms of the dynamical susceptibility (see Section 1.7)

$$\mathcal{C}_f = \int_0^{\infty} \frac{d\omega}{\pi} h_f^Q(\omega/T) \chi''(\omega) \,. \tag{9.14}$$

We have set $\hbar = 1$. Here $\mathcal{C}_f$ can be the quantum variance, or any one of the measures of coherence introduced in Section 1.5.2. In particular, it applies also to the quantum Fisher information, for which a similar scaling analysis has been given in Hauke et al. (2016). h_f^Q is a quantum filter which is linear for $\omega \ll T$, and goes to 1 for $\omega \gg T$. As discussed in Section 1.9, we can formulate a scaling hypothesis for the dynamical susceptibility (Täuber, 2014; Collins, 1989; Sachdev and Ye, 1992)

$$\chi''(\omega) = \chi f(\omega/T, T/\Delta, L\delta^{\nu}) \,. \tag{9.15}$$

Contrary to thermal phase transition, we do not need to introduce a new critical exponent to characterize the dynamics. In quantum mechanics, energy scales (Δ, T) are sufficient to determine a characteristic frequency $(\omega_c = \Delta/\hbar, T/\hbar)$. Combining Eqs. (9.14) and (9.15), we obtain

$$\begin{aligned} \mathcal{C}_f &= \chi \int_0^\infty \frac{d\omega}{\pi} h_f^Q(\omega/T) f(\omega/T, T/\Delta, L\delta^\nu) && (9.16) \\ &= \chi T g(T/\Delta, L\delta^\nu) && (9.17) \end{aligned}$$

where

$$g(T/\Delta, Lt^\nu) = \int_0^\infty \frac{dx}{\pi} h_f^Q(x) f(x, T/\Delta, L\delta^\nu) \, . \tag{9.18}$$

We can reshape this expression to predict the scaling behavior at $T = 0$:

$$\mathcal{C}_f/L^d \sim \delta^{\nu z - \gamma} h_1(T/\Delta, L\delta^\nu) \, , \tag{9.19}$$

showing that for $L \gg 1/\delta^\nu$ and $T \ll \Delta \sim \delta^{\nu z}$, the quantum fluctuations scale as $\mathcal{C}_f/L^d \sim \delta^{\nu z - \gamma}$. A more convenient form to analyse the scaling along the critical trajectory $\delta = 0$ is

$$\mathcal{C}_f/L^d \sim T^{1-\gamma/(\nu z)} h_2(\delta^{\nu z}/T, L^z T) \, . \tag{9.20}$$

This shows that the quantum variance diverges along the critical trajectory with the same exponent $T^{1-\gamma/(\nu z)}$ as the thermal variance, see Eq. (9.13). This observation supports the common picture according to which, in the quantum critical region, quantum and thermal fluctuations are equally important (Sachdev, 2001). Finally, we can also reshape this expression to study the finite-size scaling at the critical point

$$\mathcal{C}_f/L^d \sim L^{\gamma/\nu - z} h_3(\delta^\nu L, L^z T) \, . \tag{9.21}$$

Using $\gamma/\nu = 2 - \eta$, and setting $\delta = 0$ and $T = 0$, we obtain

$$\mathcal{C}_f \sim L^{d+2-\eta-z} \sim N^{1+(2-\eta-z)/d} \, . \tag{9.22}$$

9.3.3 Quantum coherence volume

From the scaling behavior of $\mathcal{C}_f$ at the QCP, we can define a "quantum coherence volume" (see also Hauke et al. (2016))

$$N_Q = \frac{\mathcal{C}_f}{N} \sim N^{(2-\eta-z)/d} \, . \tag{9.23}$$

Indeed, as $\mathcal{C}_f/N$ is the integral of the quantum covariance between a point and the rest of the system, N_Q characterizes the effective number of particles whose fluctuations are quantum-mechanically correlated. In fact, focusing on the quantum

Fisher information(QFI) ($\mathcal{C}_f(\mathcal{O}) = F_Q(\mathcal{O})$, with $\mathcal{O} = \sum_{i=1}^N \mathcal{O}_i$ is sum of local observables whose spectrum is rescaled in order to fall into the interval $[-1/2, 1/2]$), N_Q is a "multi-particle entanglement witness", in the sense of the k-producibility criterium (Hyllus et al., 2012; Pezzè and Smerzi, 2014; Tóth, 2012). A many-body pure state ψ is said to be k-producible if it can be written as a product state

$$|\psi_{\text{k-prod}}\rangle = |\psi_1\rangle \otimes \cdots \otimes |\psi_p\rangle \tag{9.24}$$

where the states ψ_j involves at most k particles. A mixed state ρ is said to be k-producible if it is a mixture of k-producible pure states

$$\rho_{k\text{-prod}} = \sum_i p_i |\psi^{(i)}_{k\text{-prod}}\rangle\langle\psi^{(i)}_{k\text{-prod}}| \, . \tag{9.25}$$

Using the convexity of the QFI with respect to ρ, the fact that the QFI is upper-bounded by four times the variance, and that the variance itself is upper-bounded when $\mathcal{O}$ has a bounded spectrum (the upper bound is attained for equal-weight superpositions of extremal eigenstates of $\mathcal{O}$), it is straightforward to show that (Hyllus et al., 2012; Pezzè and Smerzi, 2014; Tóth, 2012)[2]

$$N_Q = F_Q(\mathcal{O}, \rho_{k\text{-prod}})/N \leq k \, . \tag{9.28}$$

The divergence of N_Q at a quantum critical point if $z + \eta \leq 2$ (which is the case of the Ising model where $z = 1$ and $\eta < 1$), thus signals the presence of entanglement extending over the whole system. More importantly, it signals the potentiality of many-body states produced as thermal states in the vicinity of certain QCP for metrological purposes. Indeed, the fact the $N_Q \geq 1$ is necessary and sufficient for quantum-correlated states to be useful in interferometric frameworks (Pezzè and Smerzi, 2014; Pezzè et al., 2016). We shall have a more in-depth discussion of this observation for the Ising model in Sections 10.5 and 11.5

[2] Using the convexity of the QFI and the fact that F_Q equals four times the variance in a pure state

$$F_Q(\mathcal{O}, \rho_{k\text{-prod}}) \leq 4 \sum_i p_i \langle\psi^{(i)}_{k\text{-prod}}|\mathcal{O}^2|\psi^{(i)}_{k\text{-prod}}\rangle \, . \tag{9.26}$$

Then, in a k-producible pure state, the variance of $\mathcal{O} = \sum_{i=1}^N$ is the sum of uncorrelated fluctuations on the different clusters, whose maximal size is k. There are at most $\lfloor N/k \rfloor$ clusters of size k, and the last cluster is of size $N - k\lfloor N/k \rfloor$. On a cluster of size k, the variance is at most $(k/2)^2$, corresponding to an equal weight superposition of the extreme eigenvectors of $\sum_{i=1}^k \mathcal{O}_i$, whose spectrum is contained in $[-k/2, k/2]$. We thus conclude that

$$F_Q(\mathcal{O}, \rho_{k\text{-prod}}) \leq \lfloor N/k \rfloor k^2 + (N - k\lfloor N/k \rfloor)^2 \leq Nk \, . \tag{9.27}$$

As this proof relies solely on the fact that the QFI is convex in ρ, and that it is upper-bounded by (four times) the variance, it immediately applies to all the measures of coherence introduced in Section 1.5.2, and in particular, to the quantum variance (Malpetti and Roscilde, 2016).

9.4 Gaussian field theory for a thermal phase transition

The scaling predictions of the previous section apply to all universality classes for equilibrium phase transitions. More insight into the structure of quantum and thermal fluctuations in the vicinity of a *thermal* phase transition can be gained by studying a simple field theory model describing critical fluctuations. The purpose of this section is to provide a simple calculation of the structure factor for thermal and quantum fluctuations across a thermal phase transition, within a gaussian field theory. In particular, we will show that the correlation length $\xi_{\rm T}$ for thermal (and total) fluctuations diverges as $1/\sqrt{t}$ (as expected from the $\nu_{\rm T} = 1/2$ exponent of the gaussian theory), while the quantum correlation length ξ_Q remains finite. This matches the results from quantum Monte Carlo simulations presented in Malpetti and Roscilde (2016) for the $d = 2$ Ising model in a transverse field, and the exact results in $d = 1$ presented in Chapter 11.

9.4.1 Quantum O(N) model

In the following we consider the quantum O(N) model (or the quantum version of the Landau-Ginzburg-Wilson theory) for $N = 1$, namely a paradigmatic quantum field theory for the study of quantum and thermal phase transitions. Its partition function takes the form

$$Z = {\rm Tr}[e^{-\beta\mathcal{H}}] \tag{9.29}$$

$$= \int \mathcal{D}[\phi] e^{-S[\phi]} \tag{9.30}$$

where the Boltzmann weight for a field configuration $\phi(\boldsymbol{r},\tau)$ is given by

$$S[\phi] = \frac{1}{2}\int_0^\beta d\tau \int d^d\boldsymbol{r} \left\{ c^2|\nabla\phi|^2 + b^2(\partial_\tau\phi)^2 + r\phi^2 + \frac{u}{2}\phi^4 \right\} . \tag{9.31}$$

$S[\phi]$ is also called the "euclidean action". $\phi(\boldsymbol{r},\tau)$ is the field describing the real-space structure and imaginary-time dynamics of the order parameter, and it is periodic in τ with period β. While ϕ can generally be an N-component vector, for simplicity we shall consider the case $N = 1$, namely ϕ corresponds to the coarse-grained magnetization along z of a model having the same symmetries as those of the Ising model [Eq. (9.5)]. The imaginary-time dimension of length β is irrelevant to describe the scaling of critical fluctuations at a thermal phase transition and is usually neglected, but it contains the structure of quantum fluctuations we are trying to understand, and in our treatment it must be kept even at finite temperature.

The field-theory action of Eq. (9.31) provides an accurate description of fluctuations provided the microscopic details of the model can be ignored, which is possible only if the correlation length is much larger than the microscopic length scales (the lattice spacing in the Ising model). It is thus valid only sufficiently close to the critical trajectory (in the grey-shaded area of Fig. 9.1).

The coefficient $r \propto T - T_c$ in Eq. (9.31) changes its sign at $T = T_c$. At $T > T_c$, the minimal free energy configuration is at $\phi = 0$, corresponding to the high-temperature disordered phase, while for $r < 0$ ($T < T_c$), the system orders. The coefficient $u > 0$ ensures the stability of the model for $r < 0$ by penalizing very large fluctuations of ϕ. The $c^2|\nabla\phi|^2$ term penalizes fast spatial variations of ϕ and favors spatial homogeneity of the order parameter. The $b^2(\partial_\tau\phi)^2$ term has the same effect, but for the imaginary-time dynamics.

9.4.2 Quadratic effective action

We can derive an effective action for the small fluctuations about the saddle-point solution of the action, namely the field configuration ϕ_0 such that

$$\left.\frac{\delta S}{\delta\phi(\boldsymbol{r})}\right|_{\phi=\phi_0} = 0 \, . \tag{9.32}$$

This corresponds to a uniform configuration, which coincides with the value of the order parameter in Landau theory. We then introduce the decomposition

$$\phi(\boldsymbol{r},\tau) = \phi_0 + \psi(\boldsymbol{r},\tau) \, . \tag{9.33}$$

Assuming $\psi \ll \phi_0$, and inserting this decomposition into Eq. (9.31), we obtain

$$S[\phi_0+\psi] = S_0[\phi_0] + S_1[\phi_0,\psi] + S_2[\phi_0,\psi] + O(\psi^3) \tag{9.34}$$

where $O(\psi^3)$ contains terms of order ψ^3 or higher. We have introduced

$$S_0[\phi_0] = \frac{V\beta}{2}(r\phi_0^2 + \frac{u}{2}\phi_0^4) \, , \tag{9.35}$$

corresponding to the free energy of the homogeneous configuration ϕ_0. The term

$$S_1[\phi_0,\psi] = (r\phi_0 + u\phi_0^3)\int_0^\beta d\tau \int d^d\boldsymbol{r}\psi(\boldsymbol{r},\tau) \tag{9.36}$$

vanishes if the minimal free energy is chosen for ϕ_0, corresponding to $\phi_0 = 0$ for $T > T_c$ (disordered phase) and $\phi_0 = \pm\sqrt{-r/u}$ for $T < T_c$ (ordered phase)[3]. Finally,

[3] Indeed $\partial_{\phi_0} S_0 = V\beta(r\phi_0 + u\phi_0^3)$. The minimal free energy configuration satisfies $\partial_{\phi_0} S_0 = 0$ and thus $S_1 = 0$. The condition $\partial^2_{\phi_0} S_0 > 0$ then selects $\phi_0 = 0$ for $r > 0$ and $\phi_0 = \pm\sqrt{-r/u}$ for $r < 0$.

the effective quadratic action is

$$S_2[\psi] = \frac{1}{2}\int_0^\beta d\tau \int d^d\boldsymbol{r} \ \left\{c^2|\nabla\psi|^2 + b^2(\partial_\tau\psi)^2 + m^2\psi^2\right\} \ , \tag{9.37}$$

where

$$\begin{cases} m^2 = r & (T > T_c) \ , \\ m^2 = 2|r| & (T < T_c) \ . \end{cases} \tag{9.38}$$

This effective action is readily diagonalized in Fourier space:

$$\psi(\boldsymbol{r},\tau) = \frac{1}{\sqrt{V}}\int \frac{d^d\boldsymbol{k}}{(2\pi)^d} e^{-i\boldsymbol{k}\cdot\boldsymbol{r}}\psi_{\boldsymbol{k}}(\tau) \ , \tag{9.39}$$

where V is the volume of the system. Given the periodicity in imaginary time, $\psi_{\boldsymbol{k}}(\tau)$ can also be expressed as a discrete Fourier series:

$$\psi_{\boldsymbol{k}}(\tau) = \sum_{n=-\infty}^{\infty} e^{i\omega_n\tau}\psi_{\boldsymbol{k}}(\omega_n) \tag{9.40}$$

where $\omega_n = 2\pi n/\beta$ (the so-called "Matsubara frequencies"). The fact that $\psi(\boldsymbol{r},\tau)$ is real imposes that $\psi_{\boldsymbol{k}}(\omega_n)^* = \psi_{-\boldsymbol{k}}(-\omega_n)$. In terms of the Fourier-transformed fields, we obtain

$$S_2[\psi] = \frac{\beta}{2}\sum_{n=-\infty}^{\infty}\int \frac{d^d\boldsymbol{k}}{(2\pi)^d}|\psi_{\boldsymbol{k}}(\omega_n)|^2(b^2\omega_n^2 + c^2k^2 + m^2) \ . \tag{9.41}$$

The effective action describes a collection of independent modes $\psi_{\boldsymbol{k}}(\omega_n)$ whose fluctuations are gaussian. In particular, we immediately see that the variance of $\psi_{\boldsymbol{k}}(\omega_n)$ is

$$\langle\delta^2\psi_{\boldsymbol{k}}(\omega_n)\rangle = \frac{T}{b^2\omega_n^2 + c^2k^2 + m^2} \equiv T\chi(\boldsymbol{k}, i\omega_n) \tag{9.42}$$

with $T = 1/\beta$ the temperature. We have introduced the dynamical susceptibility $\chi(\boldsymbol{k},\omega)$, here evaluated for imaginary frequencies $i\omega_n$ (Sachdev, 2001; Täuber, 2014).

9.4.3 Quantum and thermal structure factors

In Section 1.7, we showed that within the path-integral framework, thermal fluctuations are the fluctuations from path to path of the mean-value in imaginary time (the path centroid). At a given wavevector $\boldsymbol{k}$, this corresponds to the fluctuations of $\psi_{\boldsymbol{k}}(\omega_n = 0)$. We thus obtain the thermal structure factor

$$S_{\boldsymbol{k}}^{\mathrm{T}} = \frac{T}{c^2k^2 + m^2} \ . \tag{9.43}$$

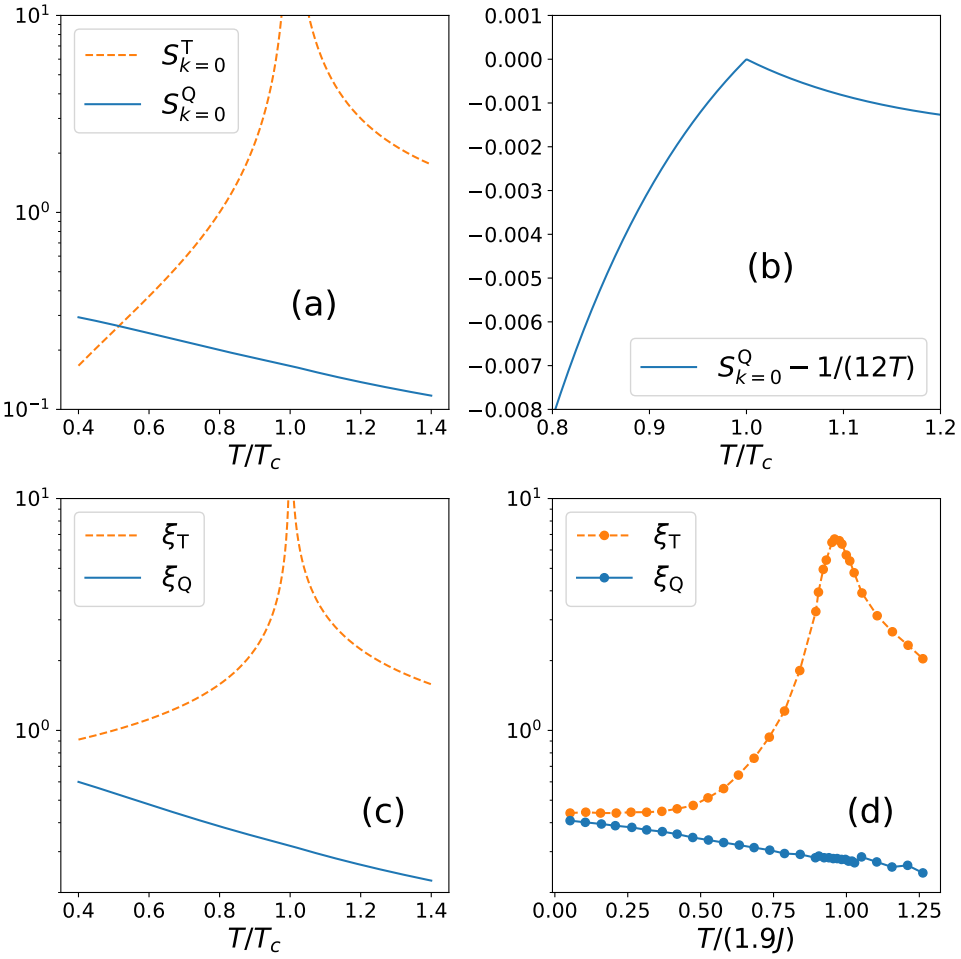

Figure 9.2: Quantum and thermal fluctuations at a thermal phase transition. (a) Quantum and thermal variance of the order parameter predicted by the gaussian field theory (Eqs. (9.43) and (9.50) with $b = c = 1$ and $r = T/T_c - 1$). The thermal variance diverges, while the QV has a barely visible cusp at the transition. (b) Singular part of the QV [see Eq. (9.51)]. (c) Quantum and thermal correlation length as predicted by the gaussian field theory [Eqs. (9.44) and (9.46)]. (d) ξ_{T} and ξ_Q calculated with quantum Monte Carlo for the $d = 2$ Ising model in a transverse field (namely the Hamiltonian of Eq. (9.5) with only nearest-neighbor couplings J on a square lattice, and a transverse field $B = 2J$; temperature in units of $1.9J$, so that that the maximum of ξ_{T} is for $T \approx 1$ in these rescaled units). System size 36×36 (ξ_{T} is not found to diverge at the transition because of finite-size effects). QMC results courtesy of T. Roscilde.

In this Lorentzian shape of the thermal structure factor, we immediately identify the thermal correlation length

$$\xi_{\mathrm{T}} = c/m = \begin{cases} c/\sqrt{r} & (T > T_c) \\ c/\sqrt{2|r|} & (T < T_c) \, . \end{cases} \tag{9.44}$$

The quantum fluctuations, on the other hand, correspond to the fluctuations in imaginary time with respect to the path centroid. These are the fluctuations at all the nonzero Matsubara frequencies. We thus obtain the quantum structure factor

$$S^{\mathrm{Q}}_{\boldsymbol{k}} = \sum_{n \neq 0} \frac{T}{b^2 \omega_n^2 + c^2 k^2 + m^2} \, . \tag{9.45}$$

The quantum structure factor being a sum of Lorentzians, its Fourier transform is a sum of exponentials. The long-distance behavior of the correlation function is governed by the slowest decay of these exponentials, corresponding to $\omega_1 = 2\pi T$. The quantum correlation function can thus be estimated as

$$\xi_{\mathrm{Q}} = \frac{c}{\sqrt{m^2 + (b 2\pi T)^2}} \, . \tag{9.46}$$

This demonstrates that the quantum correlation length remains finite at the critical point $m = 0$, and that it is a continuous function of the temperature. Its first derivative is however singular, since $m^2 = r$ above the critical point, while $m^2 = -2r$ below.

Note that the dynamical susceptibility is (Täuber, 2014)

$$\chi(\boldsymbol{k}, \omega + i0^+) = \frac{1}{c^2 k^2 + m^2 - b^2(\omega + i0^+)^2} \equiv \chi'(\boldsymbol{k}, \omega) + i\chi''(\boldsymbol{k}, \omega) \, . \tag{9.47}$$

Introducing

$$E_k = b^{-1}\sqrt{c^2 k^2 + m^2} \, , \tag{9.48}$$

the imaginary part of the dynamical susceptibility is

$$\chi''(\boldsymbol{k}, \omega > 0) = \frac{\pi}{2b^2 E_k} \delta(E_k - \omega) \tag{9.49}$$

and $\chi''(\boldsymbol{k}, -\omega) = -\chi''(\boldsymbol{k}, \omega)$. From this expression and from the expression of the QV as a function of the dynamical susceptibility [Eq. (9.14)], we see that the quantum structure factor is

$$S^{\mathrm{Q}}_{\boldsymbol{k}} = \frac{1}{2b^2 E_k} \left[\mathrm{cotanh}\left(\frac{E_k}{2T} \right) - \frac{2T}{E_k} \right] \, . \tag{9.50}$$

At $k = 0$ and close to the critical point, we obtain the following expression

$$S^{\mathrm{Q}}_{k=0} = \frac{1}{12 b^2 T} - \frac{m^2}{16 \times 45 b^4} + O[(m/b)^4] \, . \tag{9.51}$$

This result, illustrated on Fig. 9.2(a,b), shows that, similarly to the quantum coherence length $\xi_{\rm Q}$, the QV of the order parameter is nondivergent, but has a cusp at the critical point, the singular part being proportional to $m^2 \propto t = |T - T_c|/T_c$. The prediction of Eq. (9.51) is in agreement with the general prediction of Section 1.9, according to which the singular part of the QV is proportional to $t^{2\nu_T(z_{\rm T}+\eta_{\rm T}/2-1)}$. For the present case of a gaussian theory, $\nu_{\rm T} = 1/2$ and $\eta_{\rm T} = 0$. The agreement with Eq. (9.51) requires $z_{\rm T} = 2$, which is indeed the prediction of the dynamical scaling theory for a nonconserved order parameter, at the gaussian level of approximation (Hohenberg and Halperin, 1977; Täuber, 2014; Kamenev, 2011). An alternative interpretation is that, as the dispersion relation is linear at the critical point ($E_k \sim k^z$ with $z = 1$), the dynamical exponent is in fact $z_{\rm T} = 1$. Since $\eta_{\rm T} = 0$, given the discussion of Section 1.9, we could expect either a discontinuity of the QV (which is not observed), or a singularity proportional to $t^{2\nu_T(2z_{\rm T}+\eta_{\rm T}/2-1)} = t$, consistent with Eq. (9.51).

Our results are illustrated on Fig. 9.2, were the gaussian prediction for the correlation lengths $\xi_{\rm Q}$ and $\xi_{\rm T}$ (panel c) are contrasted with a numerical (quantum Monte Carlo) calculation for the $d = 2$ Ising model on a square lattice with nearest-neighbor interactions (panel d), showing that the qualitative trend predicted by the gaussian theory is well reproduced by a microscopic calculation.

Chapter 10

Ising model with infinite-range interactions

10.1 Introduction

Hamiltonian. This chapter is dedicated to a study of a mean-field-like version of the Ising model in a transverse field. We consider N spin-$1/2$ particles (we assume N even) interacting through the following Hamiltonian

$$\mathcal{H}/J = -\frac{1}{N}\sum_{i,j=1}^{N} S_i^z S_j^z - g\sum_{i=1}^{N} S_i^x \tag{10.1}$$

$$= -\frac{1}{N}(S^z)^2 - gS^x \tag{10.2}$$

where S_i^α for $\alpha = x, y, z$ are the spin$-1/2$ operators of the particle i. On the second line, we expressed $\mathcal{H}$ in terms of the collective spin operators $S^\alpha = \sum_{i=1}^N S_i^\alpha$. The coupling constant J sets the global energy scale, and g is a magnetic field along the x direction. The factor $1/N$ ensures the extensivity of the $(S^z)^2$ term when $N \to \infty$. This Hamiltonian (belonging to the family of so-called Lipkin-Meshkov-Glick (LMG) Hamiltonians), has infinite-range interactions, and can be seen as the $d \to \infty$ limit of the Ising model with nearest-neighbors interactions on a d-dimensional lattice.

Dicke states. As the Hamiltonian $\mathcal{H}$ conserves the total spin $\mathbf{S}^2$, it can be diagonalized in each sector of fixed $S = 0, 1, \ldots, N/2$. For a fixed S, the Hamiltonian takes the form of a $(2S+1) \times (2S+1)$ matrix, corresponding to the $2S+1$ values of the spin projection M along a given direction, here chosen along z. In other words, the Hamiltonian is block-diagonal in the basis of states $|S, M, \lambda\rangle$: all matrix elements between sectors of different S vanish. The states $|S, M, \lambda\rangle$ are often referred to as

the "Dicke states" in the atomic-physics literature (Arecchi et al., 1972). They are common eigenstates of the total angular momentum operator, and of its projection along the z axis: $\mathbf{S}^2|S,M,\lambda\rangle = S(S+1)|S,M,\lambda\rangle$ and $S^z|S,M,\lambda\rangle = M|S,M,\lambda\rangle$. The quantum numbers S, M do not generally specify the state fully, and further quantum numbers (λ) are necessary. The number of possible values of λ depends on $S = N/2 - p$ as

$$D(N/2-p) = \binom{N}{p} - \binom{N}{p-1} \tag{10.3}$$

for $p \geq 1$ and $D(N/2) = 1$ (Arecchi et al., 1972). One can verify that

$$\sum_{S=0}^{N/2} D(S) \times (2S+1) = 2^N \tag{10.4}$$

so that the Dicke states, including degeneracy, form a basis for the Hilbert space of an ensemble of N spin-$1/2$ particles.

Ground state. The ground state always lies in the $S = N/2$ sector, which is not degenerate. The $N+1$ states of the $S = N/2$ sector are generated by the successive application of $S^+ = \sum_{a=1}^{N}(S_a^x + iS_a^y)$ onto the state $|N/2,-N/2\rangle = \otimes_{i=1}^{N}|\downarrow_z\rangle_i$: $|N/2,-N/2+k\rangle \propto (S^+)^k|N/2,-N/2\rangle$. The state $|N/2,-N/2+k\rangle$ is the symmetric superposition of all states containing $N-k$ down spins and k up spins. If the model describes effective spins corresponding physically to indistinguishable two-level bosonic atoms, the symmetrization of the many-body wavefunction restricts the dynamics to this $S = N/2$ sector. In this case, $\mathcal{H}$ is also known as the "bosonic Josephson junction (BJJ) Hamiltonian" (Pezzè et al., 2016), because it can be derived as a boson-spin mapping of a bosonic gas with two spatial modes. As the ground state always lies in the $S = N/2$ sector, the ground-state physics of the LMG Hamiltonian and of the BJJ Hamiltonian are the same, but finite temperature properties are different. In particular, the BJJ Hamiltonian does not possess a finite-temperature phase transition. It is therefore important to keep all the sectors $S = N/2 - p$ with $p > 0$ to correctly capture the finite-temperature physics of the LMG Hamiltonian.

In the following, we first discuss the theoretical aspects underlying our understanding of the phase diagram of this model, and then discuss the critical behavior of the quantum and thermal fluctuations when approaching either the quantum critical point or a thermal one.

10.2 Phase diagram

Mean-field free energy. The phase diagram of $\mathcal{H}$, shown on Fig. 10.1, can be found by a mean-field (MF) argument (Das et al., 2006), which becomes exact in the limit $N \to \infty$ for a system with infinite-range interactions. Introducing $m = \langle S_i^z \rangle$, we can approximate the $S_i^z S_j^z$ term of Eq. (10.1) by $S_i^z S_j^z \approx S_i^z m + m S_j^z - m^2$. The MF Hamiltonian then reads

$$\mathcal{H}_{\rm MF}/J = -\sum_{i=1}^{N} \left(2m S_i^z + g S_i^x - m^2 \right) \ , \tag{10.5}$$

describing an ensemble of N uncorrelated $1/2$-spins, whose Hamiltonians are

$$\mathcal{H}_{\rm MF}^{(i)}/J = -\vec{B} \cdot \vec{\sigma_i} + m^2 \tag{10.6}$$

where $\vec{\sigma} = 2\vec{S_i}$ are the Pauli matrices, and $\vec{B} = (g/2, 0, m)$. The partition function at inverse temperature $\beta = (k_B T)^{-1}$ is readily obtained as $Z = e^{-\beta E_+} + e^{-\beta E_-}$ from the energies $E_\pm = Jm^2 \pm (J/2)\sqrt{g^2 + 4m^2}$. Finally, we obtain the mean-field free energy for the magnetization m along the z axis, $F = -\beta^{-1} \ln Z$

$$F(m) = Jm^2 - \frac{1}{\beta} \ln \left[2 \cosh \left(\frac{\beta J}{2} \sqrt{g^2 + 4m^2} \right) \right] \ . \tag{10.7}$$

Critical temperature. The critical temperature for the ferromagnetic (FM) / paramagnetic (PM) transition can be determined by analyzing the behavior of F at small m

$$F(m) = a + rm^2 + um^4 + O(m^6) \tag{10.8}$$

with the coefficients

$$\begin{aligned} a &= -\beta^{-1} \ln[2 \cosh(\beta J g/2)] \\ r &= (J/g)[g - \tanh(\beta J g/2)] \\ u &= (\beta J/4g)[2\beta J/g - \tanh(\beta J g/2)] \ . \end{aligned} \tag{10.9}$$

In particular, we see that if $g < 1$, the r coefficient is negative for a sufficiently small temperature, corresponding to $\tanh(\beta J g/2) \geq g$. This provides a finite-temperature phase transition at

$$\frac{T_c}{J} = \frac{g}{\ln\left(\frac{1+g}{1-g}\right)} \ . \tag{10.10}$$

For $g > 1$, or for $g < 1$ and $T > T_c$, the minimal free energy is at $m = 0$, corresponding to the PM phase. For $g < 1$ and $T < T_c$, the free energy F exhibits a double-well structure, with two symmetric minima at $m = \pm m_0$. The system spontaneously breaks the $z \leftrightarrow -z$ symmetry, and acquires a finite magnetization: this corresponds to the FM phase.

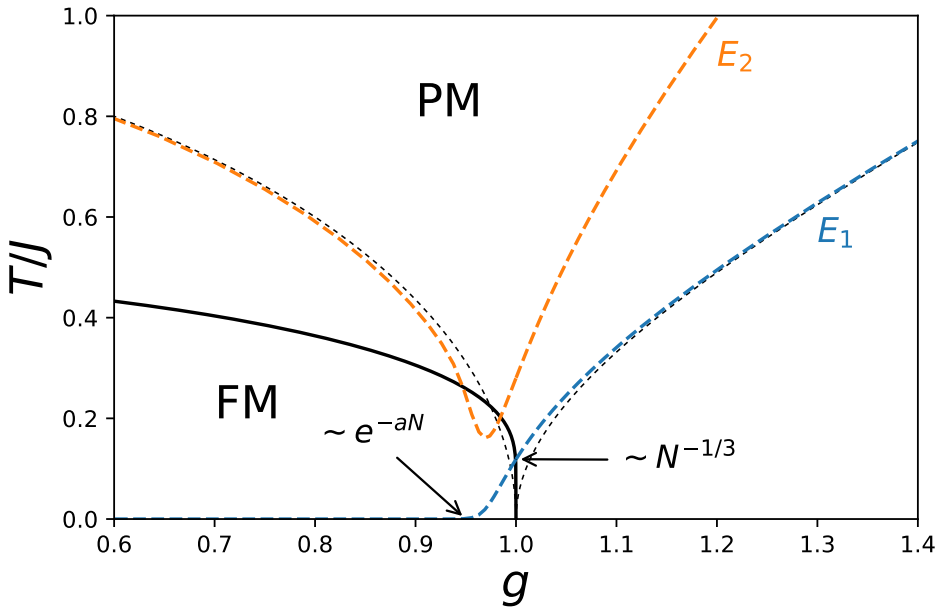

Figure 10.1: Phase diagram of the Ising model in a transverse field with infinite-range interactions. The solid black line is the critical temperature T_c predicted by Eq. (10.10). In the region $(g < 1, T < T_c)$, the system is in a ferromagnetic (FM) phase, and otherwise in a paramagnetic phase (PM). The dashed lines indicate the gap to the first (E_1, blue) and second (E_2, orange) excited states, as calculated by exact diagonalization for $N = 700$ spins. The thin dashed black lines are the prediction for the gap of a second order Holstein-Primakoff (HP) approximation [Eq. (10.17)]. In the FM phase, the HP prediction coincides with the gap to the second excited state, while the first excited state is quasi-degenerate with the ground state (the gap scales exponentially with N). The pair of quasi degenerate ground states represent the two possible orientations of the magnetization in the FM phase. Furthermore, there is a finite-size gap at $g = 1$ scaling as $N^{-1/3}$ (Dusuel and Vidal, 2004; Dusuel and Vidal, 2005). Deviations from the HP prediction are to be ascribed to finite-size effects.

Ferromagnetic and paramagnetic phase. The LMG model thus presents the two characteristic phases of the Ising model as a function of the temperature T and of the transverse field g: a high-T or high-g PM phase where $m = 0$, and a low-T and low-g FM phase where the $z \leftrightarrow -z$ symmetry is spontaneously broken. A second-order phase-transition line at $T = T_c(g)$, terminating at $T_c(g_c) = 0$ for the critical value $g_c = 1$ of the transverse field, separates the FM from the PM phase. At the phase transition, characterized by mean-field critical exponents, the variance of the collective spin component S^z becomes super-extensive. In particular, at the quantum critical point (QCP) $(T = 0, g = g_c)$, these fluctuations are of purely coherent origin, while at a thermal critical point $(g < g_c, T = T_c(g))$, the super-extensive scaling stems purely from thermal (and thus incoherent) fluctuations. This model, amenable to a simple exact diagonalization study, thus represents a testbed to study the crossover between thermal and quantum critical fluctuations in the vicinity of the QCP (compare Figs. 9.1 and 10.1).

10.3 Fluctuations in the ground state

10.3.1 Classical approximation

The fluctuations properties in the ground state are well-captured by a semi-classical Holstein-Primakoff (HP) approximation, valid for any value of g in the limit $N \to \infty$, but not at $g = 1$. The starting point of this approach is a classical approximation for the collective spin (Coletta, Laflorencie, and Mila, 2012; Das et al., 2006). The main assumption is that the collective spin operator $\vec{S}$ may, in a first approximation, be replaced by a classical magnetic moment of length $S = N/2$: $\vec{S} = S(\sin\theta, 0, \cos\theta)$. The y component of the collective spin vanishes since the Hamiltonian has a $y \leftrightarrow -y$ symmetry, and since there is no mechanism to break this symmetry, contrary to the z component, where the ferromagnetic interaction takes place. In terms of θ, the classical Hamiltonian is

$$E(\theta)/J = -\frac{S^2}{N}\cos^2\theta - gS\sin\theta\,. \tag{10.11}$$

The solution of $\partial_\theta E = 0$, $\partial_\theta^2 E \geq 0$ shows that the minimal energy is at $\theta = \pi/2$ for $g > 1$, and at $\sin\theta = g$ for $g < 1$, in agreement with the mean-field solution. In particular, the stability criterium $\partial_\theta^2 E \geq 0$ shows that the $\theta = \pi/2$ solution is unstable for $g < 1$ (it is a local maximum of E), while the two equivalent solutions θ and $\pi - \theta$ of $\sin\theta = g$ are absolute minima. For $g > 1$, $\theta = \pi/2$ provides the unique minimum of E. An expansion of E in the vicinity of $\theta = \pi/2$ in powers of $x = \theta - \pi/2$ gives

(recall that $S = N/2$)

$$\frac{2E}{JN} = -g + \frac{x^2}{2}(g-1) + \frac{x^4}{8} + O(x^6) \,. \tag{10.12}$$

This expression leads us to anticipate that at $g = 1$, where the potential is quartic in x, a harmonic treatment of the fluctuations around the classical ground state breaks down.

10.3.2 Semi-classical approximation

Holstein-Primakoff mapping. The HP approach, in its simplest form, precisely amounts to a harmonic treatment. It first consists of mapping the spin operators to bosonic operators encoding the quantum fluctuations around the classical solution (Coletta, Laflorencie, and Mila, 2012). In the FM phase, any one of the two solutions θ and $\pi - \theta$ may be chosen as the reference classical state. This yields

$$\begin{cases} S^z = \cos\theta[S - a^\dagger a] - \sin\theta\sqrt{S/2}(a + a^\dagger) + O(a^3) \\ S^y = \sqrt{S/2}(a - a^\dagger)/i + O(a^3) \\ S^x = \sin\theta[S - a^\dagger a] + \cos\theta\sqrt{S/2}(a + a^\dagger) + O(a^3) \end{cases} \tag{10.13}$$

where a and $a^\dagger$ are the HP bosonic operators satisfying $[a, a^\dagger] = 1$, and where the expressions are valid up to order $O((a^{(\dagger)})^3)$.

Quadratic effective Hamiltonian. The Hamiltonian is then expanded in terms of these HP operators, and terms up to order quadratic in the $a^{(\dagger)}$ are retained. The 0^{th} order term is simply the classical energy of Eq. (10.11), the linear term in the $a^{(\dagger)}$ vanishes if the classical ground state solution is chosen for θ, and the second-order term is a harmonic-oscillator Hamiltonian encoding the quantum fluctuations. In the paramagnetic and ferromagnetic phases respectively, this quadratic Hamiltonian reads

$$\mathcal{H}^{(2)}_{\text{PM}}/(Jg) = \frac{p^2}{2} + \frac{1}{2}(1 - 1/g)q^2 \tag{10.14}$$

$$\mathcal{H}^{(2)}_{\text{FM}}/J = \frac{p^2}{2} + \frac{1}{2}(1 - g^2)q^2 \,, \tag{10.15}$$

where $q = (a + a^\dagger)/\sqrt{2}$ and $p = (a - a^\dagger)/i\sqrt{2}$. In accordance with the classical analysis, the harmonic oscillator frequency vanishes at $g = 1$. In that case, a Hamiltonian quartic in the HP operators may then be derived, but it cannot be diagonalized analytically.

Self-consistency of the HP approach. The self-consistency of the HP approximation requires that the quantum fluctuations of the spin along the direction of $\vec{S}$ remain small compared to the mean value $N/2$. This condition is equivalent to $\langle a^\dagger a \rangle \ll S$, itself equivalent to $|g-1| \gg 1/N$[1]. This shows that in the limit $N \to \infty$ the approximation is valid all the way to, but strictly speaking not at, the critical point $g = 1$.

Gap above the ground state. An important prediction of the HP approach is the value of the gap above the ground state:

$$\Delta_{\rm PM} = Jg\sqrt{1-1/g} \tag{10.16}$$

$$\Delta_{\rm FM} = J\sqrt{1-g^2}\,. \tag{10.17}$$

The closing of the gap at the QCP $g = 1$ signals the breakdown of the second-order HP approximation.

Spin fluctuations in the ground state. Another important prediction of the HP approach is the variance of the various components of the collective spin. The results are summarized in Table 10.1, where we also included the finite-size-scaling behavior of the fluctuations and of the gap at the QCP. The finite-size-scaling of the fluctuations and of the gap at the QCP have been predicted theoretically by Dusuel and Vidal (2004) and Dusuel and Vidal (2005) using elaborate techniques involving the expansion of the Hamiltonian in terms of the HP operators at orders higher than quadratic, combined with renormalization group arguments. In passing, we notice that the Heisenberg inequality

$$\langle \delta^2 S^z \rangle \langle \delta^2 S^y \rangle \geq \frac{1}{4} \langle S^x \rangle^2 \tag{10.18}$$

is saturated both in the FM and in the PM phase (namely: it takes the form of an equality). This can be understood as the PM and FM ground states are ground states of the harmonic oscillator Hamiltonians [Eqs. (10.14) and (10.15) respectively], and as such states are of minimal uncertainty. At the QCP, we have verified that this property also holds within 3% for $N = 2000$. As it holds for any $g \neq 1$ in the limit $N \to \infty$, it is reasonable to conjecture that it also holds at the QCP.

[1] Indeed, we have (with $\omega^2 = 1 - 1/g$ if $g > 1$ and $\omega^2 = 1 - g^2$ if $g > 1$, so that $0 \leq \omega \leq 1$)

$$\begin{aligned} \langle a^\dagger a \rangle \ll S &\iff (\langle p^2 \rangle + \langle q^2 \rangle - 1)/2 \ll N/2 \\ &\iff \frac{1}{2\omega} + \frac{1}{2}\omega - 1 \ll N \iff \frac{1}{2\omega} \ll N \\ &\iff \omega^2 \gg 1/N^2 \iff |1-g| \gg 1/N^2\,. \end{aligned}$$

Scaling behavior at $T = 0$	FM ($g < 1$)	QCP ($g = 1$)	PM ($g > 1$)
$\langle S^x \rangle$	$\frac{N}{2} \sin\theta$	$\frac{N}{2}$	$\frac{N}{2}$
$\langle S^y \rangle$	0	0	0
$\langle S^z \rangle$	$\frac{N}{2} \cos\theta$	0	0
$\langle \delta^2 S^x \rangle$	$\frac{N}{4} \cos^2(\theta)(1-g^2)^{-1/2}$	$\sim N^{2/3}$	$O(1)$
$\langle \delta^2 S^y \rangle$	$\frac{N}{4}(1-g^2)^{1/2}$	$\sim N^{2/3}$	$\frac{N}{4}(1-1/g)^{1/2}$
$\langle \delta^2 S^z \rangle$	$\frac{N}{4} \sin^2(\theta)(1-g^2)^{-1/2}$	$\sim N^{4/3}$	$\frac{N}{4}(1-1/g)^{-1/2}$
gap Δ	$J\sqrt{1-g^2}$	$\sim N^{-1/3}$	$Jg\sqrt{1-1/g}$

Table 10.1: Scaling of the collective spin fluctuations and of the gap in the ground state of the Ising model with infinite-range interactions. In the FM phase ($g < 1$), the fluctuations are with respect to any one of the two ordered ground states such that $\sin\theta = g$, and the gap is for excitations above these two ground states. The scaling at the QCP has been analytically predicted by Dusuel and Vidal (2004) and Dusuel and Vidal (2005).

Finite-size vs. infinite-size ground state in the ferromagnetic phase. Finally, we emphasize that in the FM phase, the exact ground state on a finite-size system is a symmetric superposition of the two semi-classical solutions, and a naive calculation would give $\langle S^z \rangle = 0$ and $\langle \delta^2 S^z \rangle \sim N^2$ (Pezzè et al., 2016). This behavior is however an artifact of the ground state physics: the exact ground state is a Schrödinger's cat state separated from the antisymmetric superposition by a gap exponentially small in N. Any small perturbation (such as an infinitesimal magnetic field along z, exponentially small in the size of the system) will stabilize one of the two classical solutions, around which the HP approach is buit.

Gap above the ground state: Holstein-Primakoff approximation vs. exact finite-size calculation. As shown on Fig. 10.1, the gap calculated by the HP technique is in quantitative agreement with the exact calculation: it coincides with the gap to the first excited state in the PM phase, and to the gap between the pair of quasi-degenerate ground states and the first excited state above them. We have verified that any discrepancy between the exact gap and the HP prediction, visible on Fig. 10.1 for $N = 700$ spins, is a finite size effect. In particular, although the precursor of the phase transition (as characterized, for instance, by the value of g for which the gap is

minimal) appears for $g < 1$, it is progressively shifted towards $g = 1$ upon increasing N.

10.4 Quantum vs. thermal criticality

10.4.1 Total vs. quantum variance across the phase diagram

Expression of the QV and of the QFI. In order to extend the ground state study to finite temperatures, we rely on exact diagonalization. For a given observable we evaluated the quantum variance (QV) according to (see Section 1.7.4)

$$\langle \delta^2 \mathcal{O} \rangle_Q = \sum_{i,j} \left[p_i - \frac{p_i - p_j}{\ln(p_i/p_j)} \right] |\langle i|\mathcal{O}|j\rangle|^2 \tag{10.19}$$

and the quantum Fisher information (QFI) according to (Pezzè and Smerzi, 2014)

$$F_Q(\mathcal{O}) = \sum_{i,j} 2\frac{(p_i - p_j)^2}{p_i + p_j} |\langle i|\mathcal{O}|j\rangle|^2 \tag{10.20}$$

with $p_i = e^{-\beta E_i}/Z$, and $|i\rangle$ is the eigenstate of $\mathcal{H}$ of energy E_i. In practice, for $\mathcal{O} = S^z$ (or any other component of the collective spin), since matrix elements between different S sectors vanish, these expressions take the form

$$\langle \delta^2 S^z \rangle_Q = \frac{1}{Z} \sum_{S=0}^{N/2} D(S) \left[\sum_{i,j=1}^{2S+1} f_{ij}^{(S)} |\langle S, i|S^z|S, j\rangle|^2 \right] \tag{10.21}$$

where $f_{ij}^{(S)} = e^{-\beta E_i(S)} - (e^{-\beta E_i(S)} - e^{-\beta E_j(S)})/[\beta(E_j(S) - E_i(S))]$, and similarly for the QFI[2]. Here, $E_i(S)$ and $|S, i\rangle$ denote the energies and the eigenvectors of $\mathcal{H}$ in the S sector: $\mathcal{H}|S, i\rangle = E_i(S)|S, i\rangle$. $D(S)$ counts the degeneracy of each S sector and has been defined in Eq. (10.3). The average value of an observable $\mathcal{O}$ which conserves the total spin S (like any component of the collective spin does) is simply calculated as

$$\langle \mathcal{O} \rangle = \frac{1}{Z} \sum_{S=0}^{N/2} D(S) \left[\sum_{i=1}^{2S+1} \langle S, i|\mathcal{O}|S, i\rangle e^{-\beta E_i(S)} \right] . \tag{10.23}$$

The variance of $\mathcal{O}$ is obtained by $\langle \delta^2 \mathcal{O} \rangle = \langle \mathcal{O}^2 \rangle - \langle \mathcal{O} \rangle^2$.

[2] The numerical error using this formula for the QV can be large for closely spaced energies. If $|\beta(E_i - E_j)| \ll 1$, it is better to replace this expression by its Taylor expansion using

$$(e^{-\beta E_i} - e^{-\beta E_j})/[\beta(E_j - E_i)] = e^{-\beta E_i} \left(1 - \frac{\beta(E_j - E_i)}{2} + \frac{\beta^2 (E_j - E_i)^2}{6} - \cdots \right) . \tag{10.22}$$

For the QFI, there is no such instability in the numerical calculation.

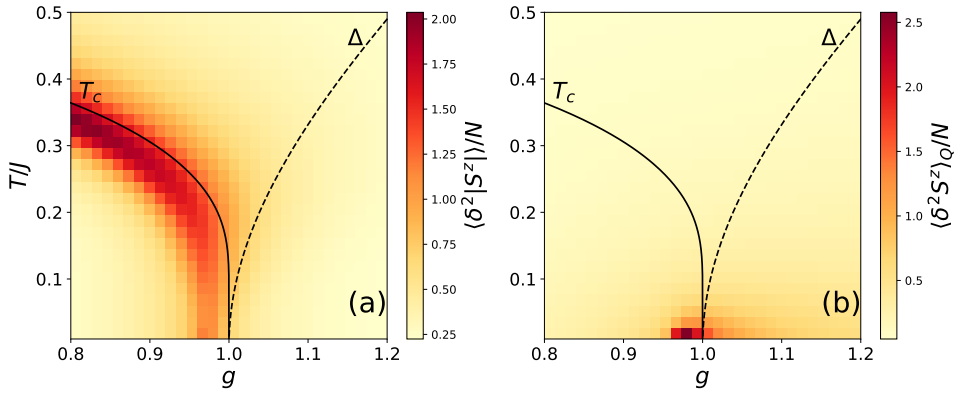

Figure 10.2: Total *vs.* quantum variance of S^z in the Ising model with infinite-range interactions. Exact diagonalization results with $N = 500$ spins. (a) Variance of $|S^z|$. At the thermal phase transitions, the variance of S^z is proportional to $N^{3/2}$ (see Fig. 10.3). (b) Quantum variance of S^z. In contrast to the total variance, the quantum variance is not critical at the thermal phase transitions, but only at the quantum critical point $(g = 1, T = 0)$, where $\langle\delta^2 S^z\rangle_Q \sim N^{4/3}$ (see Fig. 10.5). In (a) and (b), the solid line for $g < 1$ marks the critical temperature in the limit $N \to \infty$ predicted by Eq. (10.10), and the dashed line for $g > 1$ is the gap predicted by Eq. (10.17).

Total and quantum variance across the phase diagram. On Fig. 10.2, we have plotted the variance of $|S^z|$ (panel a) and the quantum variance of S^z above the phase diagram of the Ising model with infinite-range interactions for $N = 500$ spins. In the symmetry-breaking FM phase, the distribution of S^z is bimodal, so that $\langle\delta^2 S^z\rangle \sim N^2$. We thus consider the variance of $|S^z|$, which is singular only at the phase transition.

Fig. 10.2 shows that $\langle\delta^2|S^z|\rangle$ has a finite-temperature peak corresponding to the transition — interestingly, unlike what happens at most phase transitions, finite-size effects in the infinitely-connected model shift the peak of $\langle\delta^2|S^z|\rangle$ at temperatures below the value of T_c in the thermodynamic limit.

In the FM phase, there is no need to consider the quantum variance of $|S^z|$, since the fluctuations from one orientation of the magnetization to the opposite one are purely of incoherent origin, while coherent fluctuations are small fluctuations about a given orientation of the magnetization. Remarkably, Fig. 10.3(b) shows that the QV of S^z (the order parameter of the FM / PM transition), does not manifest any divergent bahavior at the thermal phase transition, in agreement with the general scaling considerations of Section 1.9. In fact, the QV seems to be completely smooth across the thermal phase transition, but a closer inspection reveals that the derivative of the quantum variance is singular (see below). In marked contrast with the behavior at thermal critical points, the QV diverges at the quantum critical point (QCP, at $g = 1$ and $T = 0$), and only there.

In the following, we analyze the behavior the quantum and thermal fluctuations at a thermal critical point (Section 10.4.2), in the paramagnetic phase for $g > 1$ (Section 10.4.3), and along the quantum critical trajectory $g = 1$ terminating on the QCP at $T = 0$ (Section 10.4.4). Our results are in agreement with the scaling considerations of Sections 1.9 and 9.3.

10.4.2 Quantum fluctuations do not diverge at a thermal critical point.

On Fig. 10.3, we analyze the scaling behavior of the (total) variance of $|S^z|$, of the QV of S^z, and of the QFI of S^z, across the thermal phase transition occurring at $g = 0.8$.

Total variance. The finite-size-scaling behavior of infinitely-connected systems has been investigated by Botet, Jullien, and Pfeuty (1982). In compliance with the scaling arguments of Section 9.3.1), the S^z fluctuations are predicted to obey the scaling form

$$\frac{\langle \delta^2 |S^z| \rangle}{N} = N^{(2-\eta_{\mathrm{T}})/d_c} g(N t^{\nu_{\mathrm{T}} d_c}) \, . \tag{10.24}$$

with $t = T/T_c - 1$ and g some scaling function. The exponents $\eta_{\mathrm{T}} = 0$ and $\nu_{\mathrm{T}} = 1/2$ are the mean-field critical exponents of the Ising model, and $d_c = 4$ is the upper critical dimension of the corresponding short-range model (Botet, Jullien, and Pfeuty, 1982).

This prediction complies well with our data. Indeed, as shown on panel (a), $\langle \delta^2 |S^z| \rangle / N$ diverges with N at $T = T_c$. Furthermore, on panel (b), we show the correctness of the following scaling Ansatz

$$\frac{\langle \delta^2 |S^z| \rangle}{N} = \sqrt{N} f(t\sqrt{N}) \tag{10.25}$$

with f some scaling function, in agreement with Eq. (10.24). T_c is given by Eq. (10.10). This proves that 1) $\langle \delta^2 |S^z| \rangle \approx N^{3/2} f(0)$ at $T = T_c$; and 2) $\langle \delta^2 |S^z| \rangle / N \approx f(1)/t$ for $N \to \infty$ and $T \neq T_0$.

QV and QFI. As shown on panels (c) and (e), neither the QV nor the QFI diverge at the critical point (given the inequalities $\langle \delta^2 \mathcal{O} \rangle_Q \leq F_Q(\mathcal{O})/4 \leq 3 \langle \delta^2 \mathcal{O} \rangle_Q$, see Section 1.8, if one of them diverges, the other one must also diverge). However, as we show on panels (d) and (f), their first derivative with respect to T is singular at the phase transition in the limit $N \to \infty$. We observe the following scaling behavior for the QFI at $T \to T_c^-$

$$\frac{1}{N} \frac{\partial F_Q}{\partial T} = f(t\sqrt{N}) \tag{10.26}$$

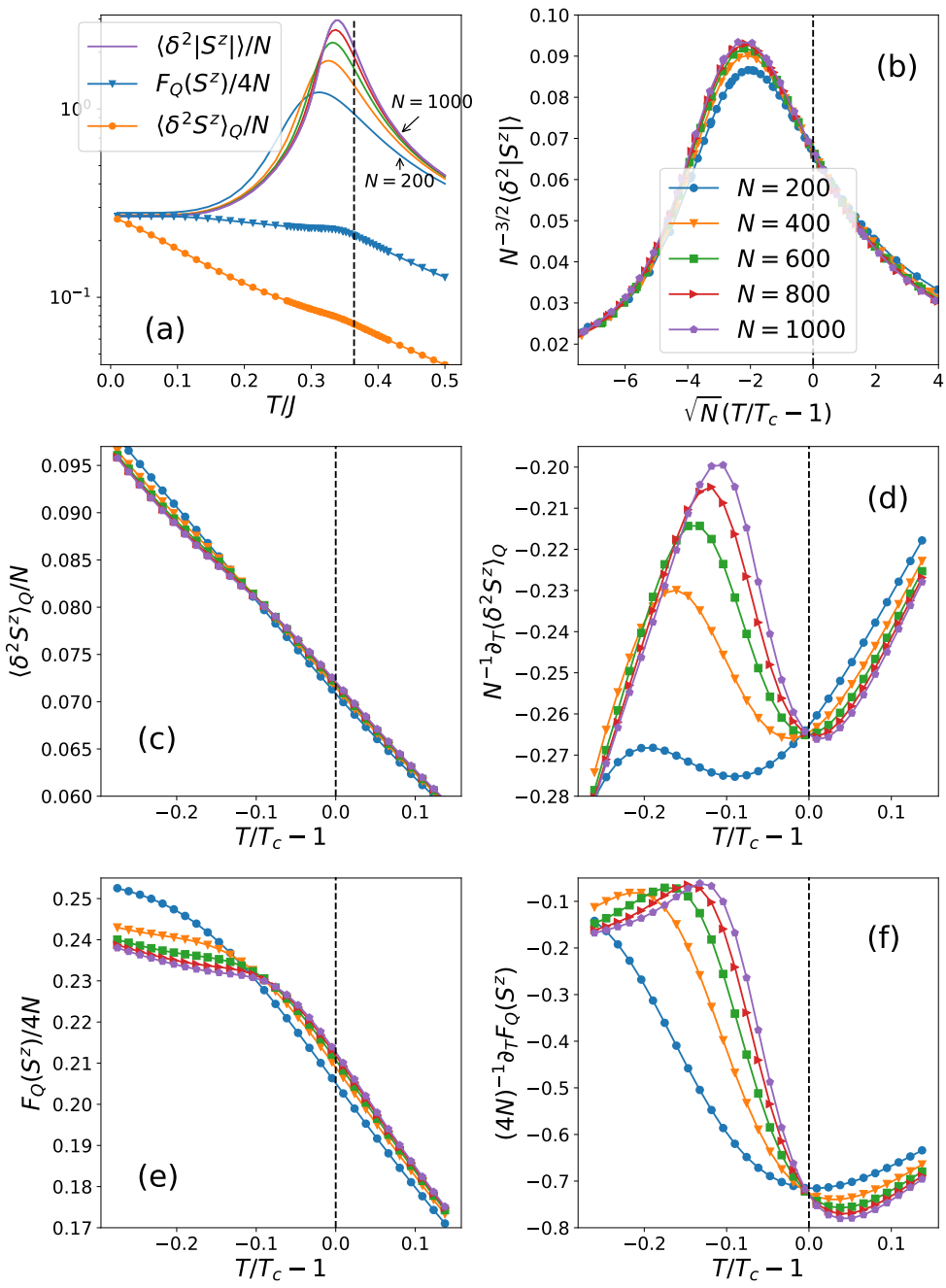

Figure 10.3: Scaling of total and quantum fluctuations at a thermal critical point of the infinite range Ising model ($g = 0.8$, $N = 200, 400, \ldots 1000$). (a) $\langle\delta^2|S^z|\rangle$ (solid lines), $F_Q(S^z)/4$ ($N = 1000$, blue triangles) and $\langle\delta^2 S^z\rangle_Q$ ($N = 1000$, orange circles), all per spin. The dashed black line indicates $T = T_c$ with T_c predicted in Eq. (10.10). (b) Same data for $\langle\delta^2|S^z|\rangle/N^{3/2}$ as a function of $(T/T_c - 1)\sqrt{N}$ (see text). (c) Quantum variance of S^z as a function of T and (d) its first derivative. (e) and (f): as (c) and (d) but for the QFI. Symbols in (c-f) are the same as in (b).

implying that the second derivative of F_Q/N with respect to T diverges as $\sqrt{N}$ at $T = T_c$. Extrapolating the data of panel (d) to $N \to \infty$, we also expect that the first derivative of the QV is singular at the transition in the thermodynamic limit, but we could not find a simple scaling Ansatz to explain the behavior of the QV. We also note that the singularity of the first derivative of the QV and the QFI with respect to the temperature at the thermal critical point is consistent with the gaussian field theory calculation of Section 9.4.

These results seem to be in contradiction with those presented by Hauke et al. (2016) where a similar calculation of the successive derivatives (up to the fifth) of the QFI across the transition lead the author to conclude the *absence* of any singularity (see Fig. 3b of Hauke et al. (2016)). Their conclusion is however incorrect, for the aforementioned authors only took into account the contributions from the $S = N/2$ sector of the collective spin in their calculation, being thus unable to describe the thermal phase transition.

10.4.3 Quantum and thermal fluctuations in the paramagnetic phase.

On Fig. 10.4, we have plotted the total, thermal and quantum variance of S^z, and the QFI in the paramagnetic phase ($g = 1.1$). Both on Fig. 10.4 and 10.3(a), we note that the QFI appears more robust to thermal effects than the QV, although both of them quantify the same physical property — the coherent fluctuations of S^z. Note that the QFI is always bounded between four and twelve times the QV (see Section 1.8).

10.4.4 Quantum and thermal fluctuations along the quantum critical trajectory.

As we showed in Section 9.3.2, both quantum and thermal fluctuations are predicted to scale in the same manner along the quantum critical trajectory $g = g_c$

$$\langle \delta^2 S^z \rangle_{\mathrm{tot,Q,T}} / N \sim T^{1-(2-\eta)/z} f_{\mathrm{tot,Q,T}}(N^{z/d} T) \, . \tag{10.27}$$

For the Ising model, $z = 1$ (Sachdev, 2001), and for the mean-field transition, $\eta = 0$. The dimension d for an infinite-range model is the upper critical dimension of the corresponding short-range model (Botet, Jullien, and Pfeuty, 1982), $d = 4 - z = 3$ for the Ising quantum critical point. We thus expect the scaling behavior

$$\langle \delta^2 S^z \rangle_{\mathrm{tot,Q,T}} / N \sim T^{-1} f_{\mathrm{tot,Q,T}}(N^{1/3} T) \, . \tag{10.28}$$

On Fig. 10.5 we analyse the validity of this scaling prediction, which turns out to be very difficult to confirm for the total fluctuations. We suspect that finite-size effects

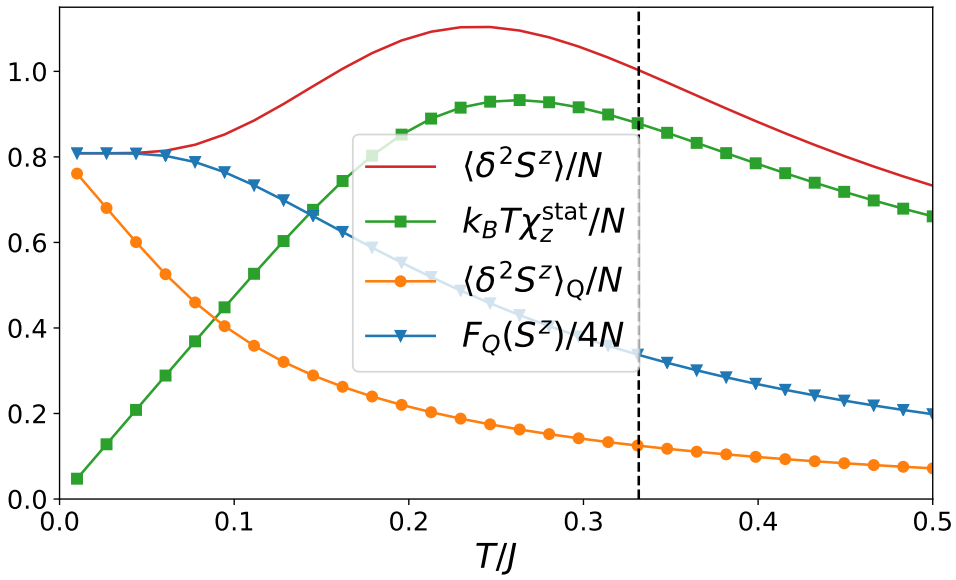

Figure 10.4: Total, quantum and thermal fluctuations in the paramagnetic phase of the Ising model with infinite-range interactions ($g = 1.1$, $N = 800$). The black vertical dashed line indicates the gap $\Delta/J = g\sqrt{1 - 1/g}$. The proximity of the QCP at $g = 1$ induces a non-monotonic behavior of the total fluctuations (solid red line), which increase upon lowering the temperature for $T \gtrsim \Delta$, and then crossover to the ground-state value.

are too strong for this infinite-range model to allow for the proper observation of the scaling regime. In fact, on a finite-size system, the critical trajectory $g = 1$ is still in the paramagnetic phase (see the phase diagram on Fig. 10.1), and the behavior of the total variance is similar to what we observed at $g = 1.1$ (Fig. 10.4). However, the scaling regime is clearly present for the *quantum* variance of the order parameter, which is much less affected by finite-size effects. On Fig. 10.5(a), we clearly see a divergence $\langle \delta^2 S^z \rangle_Q \sim 1/T$ starting for $T/J \lesssim 0.4$, and a cross-over to a finite, N-dependent ground-state value for $T/J \lesssim \Delta \sim N^{-1/3}$. The correctness of the Ansatz of Eq. (10.28) is further confirmed on panel (b), where we plotted $\langle \delta^2 S^z \rangle_Q \times T/(JN)$ against $N^{1/3}T/J$. The flat plateau corresponds to the scaling regime. On panel (b), we have also performed the same scaling analysis for the QFI for which the scaling regime is less clearly manifest, and the plateau resembles rather a broad shoulder. The scaling behavior of the QFI and of the QV must nonetheless be the same as a consequence of the inequality linking them (see Section 1.8).

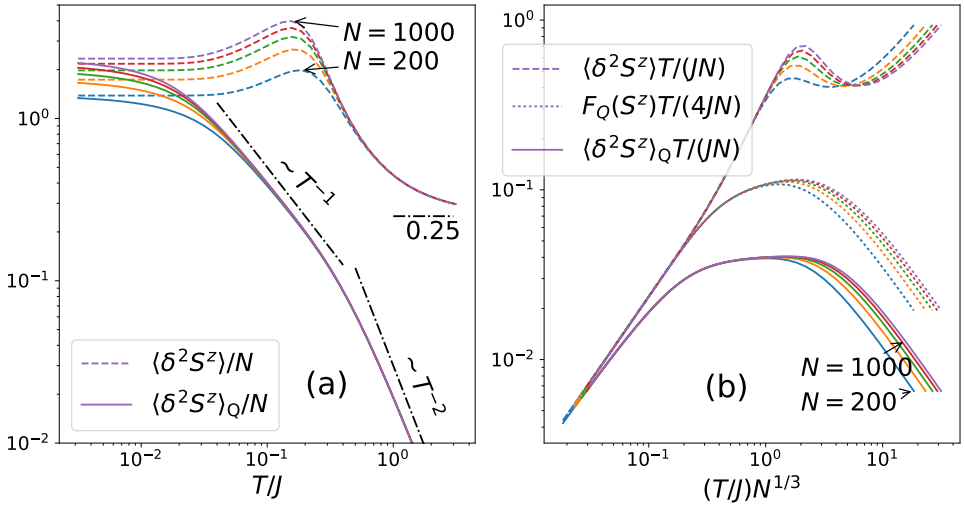

Figure 10.5: Scaling of fluctuations along the quantum critical trajectory $g = 1$ for the Ising model with infinite-range interactions. (a) Scaling of the total (dashed lines) and quantum (solid lines) variance of S^z for $N = 200, 400, \cdots 1000$. The scaling regime $\langle\delta^2 S^z\rangle_Q \sim 1/T$ is observed for the QV at $T/J \lesssim 0.4$, but is not visible for the total variance, presumably due to finite-size effects. At high temperature, the QV is proportional to $1/T^2$, while the total variance saturates to the shot-noise limit $\langle\delta^2 S_z\rangle \sim N/4$ of a completely mixed state of spin-1/2 particles. (b) Same data as in (a), but rescaled to $1/T$ and plotted as a function of $(T/J)N^{1/3}$. The QFI of S^z is also plotted. The collapse of the curves for various N signals the scaling regime.

10.4.5 Quantum critical region

Scaling along the quantum critical trajectory. At finite temperature, in the vicinity of the critical trajectory at $g = g_c$, the presence of the QCP is predicted to control the scaling behavior of fluctuations in an extended *quantum critical region* (Sachdev, 2001), see Fig. 9.1 and Section 9.2:

$$\langle\delta^2\mathcal{O}\rangle_{\mathrm{tot,Q,T}} \sim T^{1-(2-\eta)/z} f(E_c/T)\,. \tag{10.29}$$

E_c is an energy scale set by the gap on the PM side $g > g_c$, and by the critical temperature T_c on the FM side. Note that $E_c = 0$ for $g = g_c$, and conventionally, we choose $E_c = -T_c$ for $g < g_c$.

Critical scaling: total versus quantum fluctuations. The scaling exponents z and η are controlled by the QCP, and not by the exponents of the thermal phase transition occurring at T_c. As we argued in Section 9.2, this scaling behavior is difficult to observe when focusing on the *total* fluctuations — in fact, in Section 10.4.4, we were not able to confirm this scaling behavior along the critical trajectory, see Fig. 10.5.

This difficulty stems from the presence of the thermal phase transition which competes with the QCP to govern the scaling behavior of total fluctuations. Instead, focusing on *quantum* fluctuations is much more convenient, as they are very weakly affected by the thermal phase transition (see for instance Fig. 10.3). Indeed, the scaling behavior of quantum fluctuations (represented by the QV and the QFI) is clearly observed on Fig. 10.5.

Definition of the quantum critical region. More generally, as $E_c = 0$ for $g = g_c$, we can predict from Eq. (10.29) the existence of an extended region where $E_c/T \ll 1$ in which

$$\langle \delta^2 \mathcal{O} \rangle_Q T^{(2-\eta)/z-1} \approx \text{const.} \tag{10.30}$$

This last property is a natural definition for the quantum critical region. Equivalently, the QV may be replaced by the QFI, or any other measure of coherence introduced in Section 1.5.2, since they all have the same scaling behavior as a consequence of inequality (1.45). In our case, recall that $\eta = 0$ (gaussian model) and $z = 1$ (Ising universality class).

Description of the quantum critical region for the infinite-range Ising model. As shown on Fig. 10.6 where we have plotted the left hand side of Eq. (10.30) in the $(T/J, E_c/J)$ plane, for both the QV (panels b, e) and the QFI, (panels c, f), we clearly identify an extended plateau (or a broad maximum) for $T \gtrsim E_c$. In contrast, such a plateau is not clearly observed for the total fluctuations (panels a, d), strongly affected by the presence of the thermal phase transition (we do observe a small plateau, but it does not clearly correspond to an extended scaling region, see Fig. 10.5(b)).

Furthermore, according to Eq. (10.29), in the vicinity of the QCP we should observe a constant value $f(E_c/T)$ along straight lines $T = \text{const.} \times E_c$ in the $(T/J, E_c/J)$ plane. Interestingly, this structure is clearly present for the total fluctuations, especially on the PM side $g > g_c$ where the effect of the thermal phase transition is absent. For $g < g_c$, it is also visible well below T_c, although finite-size effects are important (the straight lines converge toward the precursor of the true phase transition, which occurs at $g_{c,\text{eff}}(N) < 1$).

Discussion. In conclusion, the separation of total fluctuations into a thermal and a quantum contribution allows for a refined analysis of the quantum critical region. In particular, we proposed to define this region in terms of the scaling behavior of quantum fluctuations, see Eq. (10.30), and showed, on the specific example of the Ising model with infinite-range interactions, that it can be unambiguously identified in this

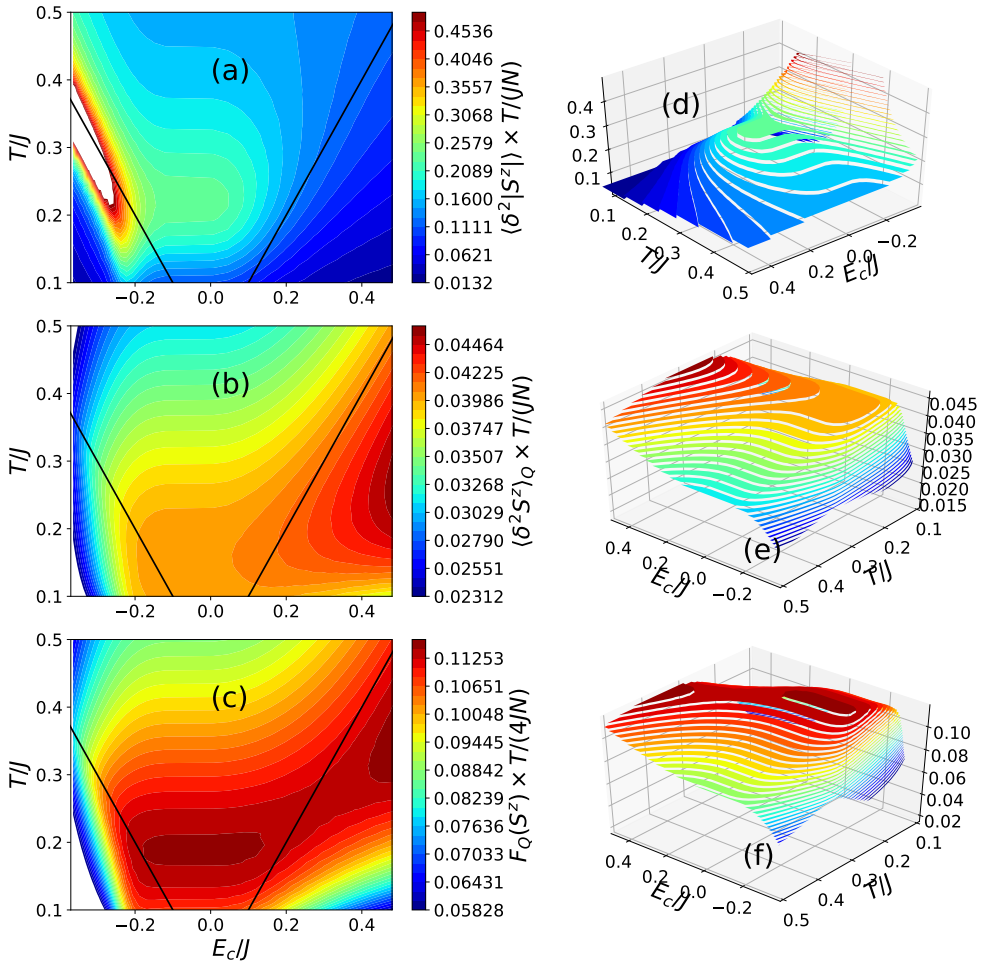

Figure 10.6: Quantum critical region for the Ising model with infinite-range interactions ($N = 1000$ spins). Panels (a), (b) and (c) show respectively the total fluctuations $\langle \delta^2 |S^z| \rangle$, the quantum variance $\langle \delta^2 S^z \rangle_Q$ and the QFI $F_Q(S^z)/4$ in the vicinity of the quantum critical region in the $(T/J, E_c/J)$ plane. All quantities are rescaled to the number of spins, and multiplied by T/J. The flat plateau for $T/J \leq 0.25$, $|E_c/J| \leq 0.2$ corresponds to the quantum critical region [see Eq. (10.30)]. On the abscissa, the energy scale E_c is the gap Δ for $g > 1$, and (minus) the critical temperature $-T_c$ for $g < 1$. Data below $T/J = 0.1$ are not shown because they are strongly affected by finite-size effects. The black lines indicate $T = |E_c|$. Panels (d), (e), (f) are the same data as (a), (b) and (c) respectively.

manner. In the following section, we explore the potential usefulness of the strongly coherent fluctuations present in the vicinity of the quantum critical point for quantum metrological purposes. We show in particular that the behavior of the quantum Fisher information is completely captured by the squeezing of S^y fluctuations.

10.5 Quantum critical squeezing

10.5.1 Spin squeezing and QFI

Quantum coherence volume. The divergence of coherent fluctuations in the vicinity of the QCP is the signature of a strong quantum cooperative behavior. In particular, we know that (see Hauke et al. (2016) and Section 9.3.2)

$$\frac{F_Q(S^z)}{N} = N_Q \sim N^{(2-\eta-z)/d} \tag{10.31}$$

is a lower bound to the size of entangled clusters of spins (as defined by the k-producibility criterium, see Tóth (2012), Hyllus et al. (2012) and Section 9.3.3), and can be qualified as a "quantum coherence volume", or "entanglement depth" following the terminology of Sørensen and Mølmer (2001). The Ising QCP is thus associated to a divergence of the quantum coherence volume for the z-component of the magnetization.

Metrology perspective. From the perspective of the metrological use of many-body states as input states for an interferometer (Pezzè et al., 2016), this implies an extreme sensitivity of the many-spin system to small variations of an external magnetic field along the z-axis. Indeed, if the system is placed in such external magnetic field $B\vec{e_z}$ during a time-interval t, it undergoes the unitary evolution $U = e^{-i\phi S^z}$ with $\phi = tB$, and this extreme sensitivity manifests itself in the possibility to determine the value of ϕ, after p independent measurements, with a minimal uncertainty given by the quantum Cramér-Rao bound (see Section 1.4.2)

$$(\Delta\phi_{\text{est}})^2 \geq \frac{1}{pF_Q} \sim \frac{1}{pN^{4/3}}\ , \tag{10.32}$$

beyond the standard quantum limit (SQL) $1/(pN)$ achievable with non-entangled spins (the existence of classical correlations among the spins is not helpful to increase the sensitivity of an interferometer beyond the SQL). However, the Cramér-Rao bound is a theoretical result, stemming from an optimization over all the possible measurements on the probe system. If the extreme sensitivity resides in too complicated observables, it may be impossible to exploit in practice. The very natural question is then the following one:

- Is there a simple way to take advantage of the diverging coherence volume close to a QCP for precision interferometric purposes?

Spin squeezing. The answer is positive, in the case under study of the Ising model with infinite-range interactions. The explanation is that the y-component of the collective spin — transverse to both the magnetization (along z) and the transverse field (along x) — has "squeezed" fluctuations at the QCP (squeezed with respect to the projection-noise limit $\langle \delta^2 S^y \rangle = N/4$ of N independent $s = 1/2$ spins)

$$\frac{\langle \delta^2 S^y \rangle}{N} \sim \frac{1}{N^{1/3}} \underset{N\to\infty}{\to} 0 \tag{10.33}$$

(see Table 10.1). The reason why squeezed fluctuations along y allow for a precise evaluation of a small magnetic field along z has been explained by Wineland et al. (1994). Preparing N spins in a collective squeezed state allows one to attain a precision $\Delta\phi_{\rm est}$ given by

$$\Delta\phi_{\rm est} = \frac{\sqrt{\langle \delta^2 S^y \rangle}}{\langle S^x \rangle} \equiv \frac{\xi_R}{\sqrt{N}} , \tag{10.34}$$

where we introduced the so-called *squeezing parameter* ξ_R (Wineland et al., 1994). This precision is below the projection-noise limit $1/\sqrt{N}$ whenever $\xi_R < 1$. The squeezing parameter is defined in such a way that for a coherent spin state $|\psi\rangle = \otimes_{i=1}^N |+_x\rangle_i$, for which $\langle S^x \rangle = N/2$ and $\langle \delta^2 S^y \rangle = N/4$, $\xi_R = 1$. The fluctuations of S^y are said to be squeezed if $\xi_R < 1$[3].

Spin squeezing and quantum Fisher information. Given the definition of the QFI, this quantity must be larger than $1/F_Q(S^z)$. The inequality (Pezzé and Smerzi, 2009)

$$\xi_R^2 \geq \frac{N}{F_Q(S^z)} \tag{10.36}$$

can be viewed as a special case of the Heisenberg-like inequality derived in Section 1.4.3

$$F_Q(A)\langle \delta^2 B \rangle \geq |\langle [A,B] \rangle|^2 \tag{10.37}$$

valid for arbitrary observables A and B. Indeed, taking $A = S^z$ and $B = S^y$, so that $[A,B] = -iS^x$, we obtain inequality (10.36). We already noted in Section 10.3 that inequality (10.36) is saturated in the ground-state (where it reduces to the usual

[3] More generally, the squeezing parameter is defined as (Wineland et al., 1994)

$$\xi_R = \sqrt{N} \frac{\min_{\vec{n}\perp\langle\vec{S}\rangle} \sqrt{\langle \delta^2 S^{\vec{n}} \rangle}}{|\langle \vec{S} \rangle|} , \tag{10.35}$$

where the minimum is over the directions $\vec{n}$ transverse to the mean spin direction $\langle \vec{S} \rangle$.

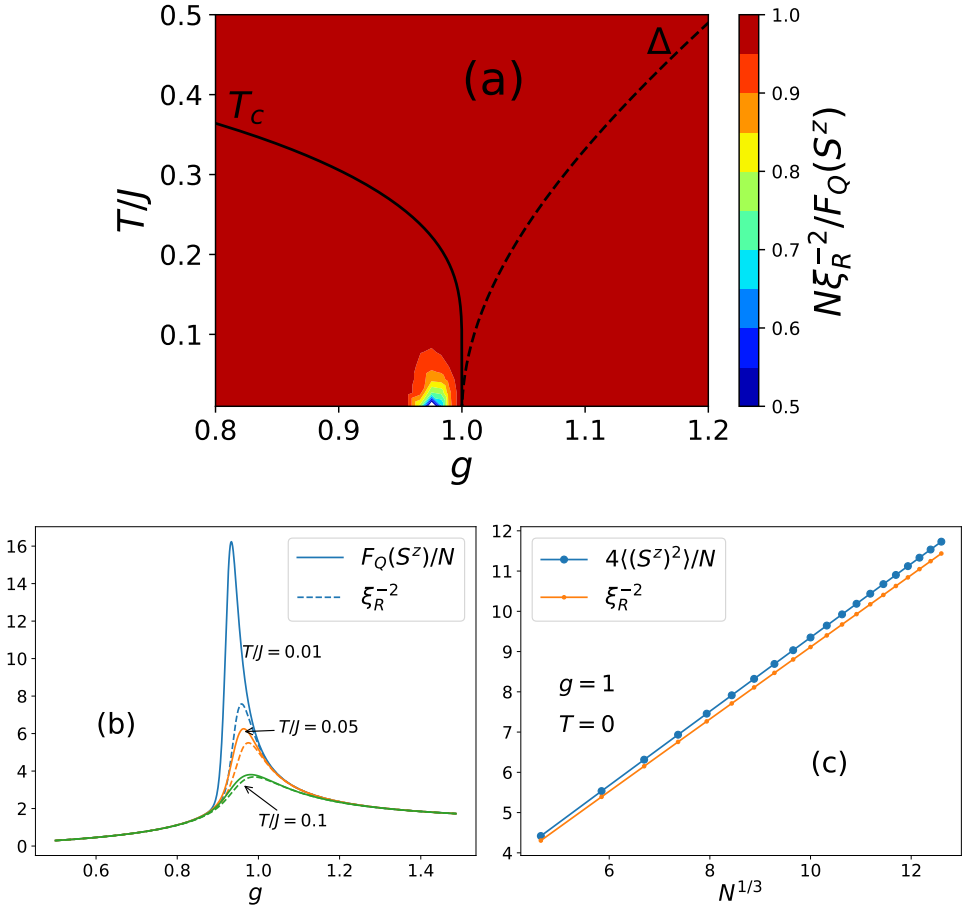

Figure 10.7: Spin squeezing versus QFI. (a) Squeezing parameter $\xi_R^{-2} = \langle S^x\rangle^2/(N\langle\delta^2 S^y\rangle)$ divided by the QFI per spin $F_Q(S^z)/N$ over the phase diagram of the Ising model with infinite-range interactions ($N = 1000$). (b) ξ_R^{-2} (dashed lines) and $F_Q(S^z)/N$ (solid lines) for $N = 200$ spins at $T/J = 0.01$ (blue), $T/J = 0.05$ (orange) and $T/J = 0.1$ (green). (c) ξ_R^{-2} and $F_Q(S^z)/N$ at the QCP $(g = 1, T = 0)$ for $N = 100, 200, \ldots, 2000$. Both diverge as $N^{1/3}$. Studying the ratio between them, we can conclude that the prefactors are equal with about 3% inaccuracy.

Heisenberg inequality, Eq. (10.18), since $F_Q(A) = 4\langle \delta^2 A \rangle$ for a pure state). Indeed, the HP mapping to an Harmonic oscillator Hamiltonian shows that for $N \to \infty$, the ground state is a minimal uncertainty state, saturating Heisenberg inequality. As illustrated on Fig. 10.7, it turns out that more generally

$$\frac{F_Q(S^z)}{N}\xi_R^2 \underset{N\to\infty}{\to} 1 \tag{10.38}$$

at any point of the phase diagram of the infinite-range Ising model, presumably including the QCP.

Hence, exploiting the squeezing of the fluctuations of S^y is the optimal way to benefit from the strong quantum correlations of the many-spin system for interferometric applications.

On Fig. 10.7(a), we have plotted the ratio

$$r = \frac{N}{\xi_R^2 F_Q(S^z)} = \frac{\langle S^x \rangle^2}{\langle \delta^2 S^y \rangle F_Q(S^z)} \leq 1 \tag{10.39}$$

across the phase diagram of the Ising model with infinite-range interactions for $N = 1000$ spins, showing that r is essentially constant equal to 1 everywhere, except in the vicinity of the quantum critical point where finite-size deviations are apparent. On panel (b), we have plotted $F_Q(S^z)/N$ and ξ_R^{-2} for different temperatures as a function of the transverse field g. The large increase of the QFI near the QCP is nicely reproduced by the squeezing. The difference observed between ξ_R^{-2} and $F_Q(S^z)/N$ is a finite-size effect. This is confirmed on panel (c) where both quantities are observed to diverge as $N^{1/3}$, with a prefactor equal within 3%. We may thus conjecture that in the limit $N \to \infty$, the ratio r goes to 1 including at the QCP.

10.5.2 Spin squeezing across the phase diagram

To conclude, we explicitly plot on Fig. 10.8 the squeezing parameter ξ_R^{-2} across the phase diagram for $N = 500$ spins, in the vicinity of the QCP. We clearly observe an extended region of robust squeezing $\xi_R < 1$, demonstrating the potential usefulness of an ensemble of spins thermalized in this parameter regime for precision interferometric measurements.

Adiabatic preparation of a spin-squeezed state. We can imagine an experimental realization of equilibrium states close to the QCP by 1) starting with a full polarized state $\otimes_{i=1}^N |+x\rangle_i$, corresponding to the ground state in an infinite transverse field $g \to \infty$; and 2) adiabatically decreasing g towards the critical point. The large gap in the PM phase should enable to implement a nearly-adiabatic preparation in a finite

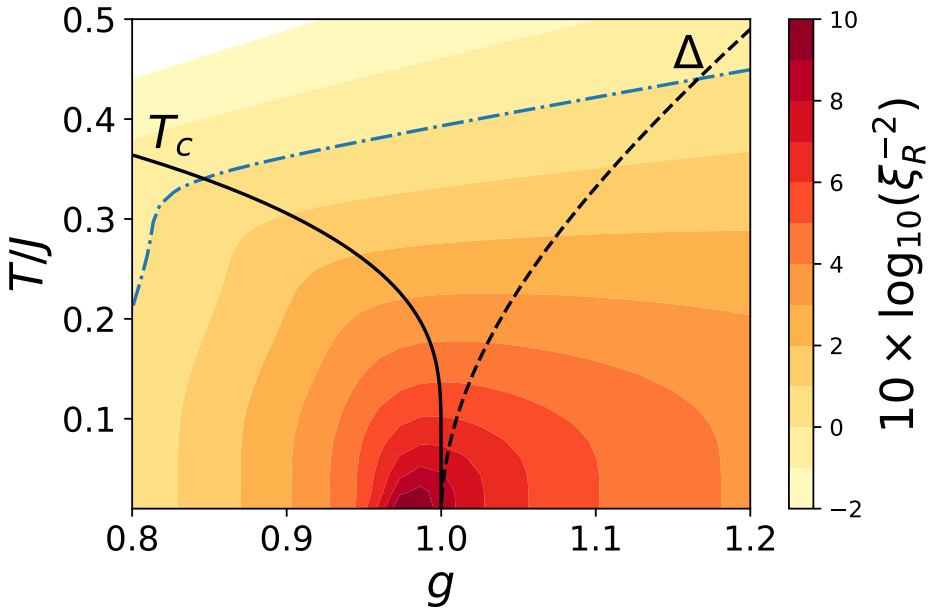

Figure 10.8: Spin squeezing across the phase diagram of the Ising model with infinite-range interactions ($N = 500$ spins). Following the convention of the metrology literature, the potential metrological gain exploiting spin squeezing is expressed as ξ_R^{-2} measured in decibels. The dashed-dotted blue line marks the limit below which $\xi_R < 1$, signaling the presence of metrologically useful entanglement among the spins. The solid line is the critical temperature T_c of the FM / PM transition, and the dashed line on the PM side is the gap Δ.

time. If the energy injected during the preparation remains small, the many-body state should then exhibit a squeezing $\xi_R < 1$ stable in time as long a external perturbations can be neglected. The same idea was proposed by Sørensen and Mølmer (2001).

An ideal platform for the realization of the infinite-range Ising model is offered by trapped ions, as recently shown by Islam et al. (2011) and Bohnet et al. (2016)

Chapter 11

Ising chain in a transverse field

11.1 Introduction

11.1.1 Summary of the results obtained for the infinite-range quantum Ising model

In Chapter 10, we investigated the critical behavior of a system of N spins interacting through infinite-range Ising ferromagnetic interactions, in the presence of a transverse field. We showed the existence of an extended region in the vicinity of the quantum critical point (QCP) characterized by a strongly coherent behavior, robust to finite-temperature effects.

Quantum critical scaling of quantum fluctuations at finite temperature. We proved that, in this *quantum critical region*, coherent fluctuations of the order parameter S^z — as quantified by the quantum variance (QV) or the quantum Fisher information (QFI) — scale with the temperature as (Hauke et al., 2016)

$$\langle \delta^2 S^z \rangle_Q, \; F_Q(S^z) \sim \frac{1}{T^{1-\eta}} \tag{11.1}$$

(see Section 9.3.2, where we set $z = 1$). η is the critical exponent governing the large-distance power-law decay of the correlation function at the QCP

$$\langle \delta S_i^z \delta S_j^z \rangle \sim \frac{1}{|r_i - r_j|^{d-1+\eta}} \, . \tag{11.2}$$

For the infinite-range model of Chapter 10, $\eta = 0$ (although correlations have no spatial structure at all for infinite-range interactions, η is consistently set to 0 for a system described by a gaussian field theory). We have been able to identify without ambiguity the quantum critical region where this scaling behavior is obeyed, a task more subtle (if ever possible) when focusing on total fluctuations.

Divergence of the quantum coherence volume at the quantum critical point. Furthermore, at the quantum critical point, both the QV and the QFI (which coincide respectively with the variance $\langle \delta^2 S^z \rangle$ and four times the variance at $T = 0$), diverge with the number of particles. We defined the coherence volume as

$$N_Q = \frac{F_Q(S^z)}{N} \sim \frac{\langle \delta^2 S^z \rangle_Q}{N} \sim N^{(1-\eta)/d} \, . \tag{11.3}$$

The number of spatial dimensions d of the system had to be replaced, for the infinite-range model of Chapter 10, by the upper critical dimension $d_c = 3$, and we found a divergence of the coherence volume $N_Q \sim N^{1/3}$.

Squeezing of fluctuations transverse to the order parameter. Finally, we showed that this strongly coherent behavior is completely captured by the squeezing of S^y fluctuations (Wineland et al., 1994)

$$\xi_R = \sqrt{N} \frac{\Delta S^y}{\langle S^x \rangle} \approx \sqrt{\frac{N}{F_Q(S^z)}} \sim N^{-1/6} \, , \tag{11.4}$$

where $\Delta S^y = \sqrt{\langle \delta^2 S^y \rangle}$. In other words, the sensitivity of the collective spin $\mathbf{S} = \sum_{i=1}^N \mathbf{S}_i$ to rotations around z, as ultimately quantified by the QFI, manifests itself in a transparent manner through the squeezing of S^y fluctuations. This may be seen as a consequence of the *gaussian* character of the fluctuations in this many-body system, including at the quantum critical point.

11.1.2 The quantum Ising chain

Hamiltonian of the quantum Ising chain. It is extremely insightful to contrast the results obtained in the limit of infinite-range interactions, with the behavior of a $d = 1$ system with short-range interactions. The model we focus on in the present chapter is the Ising chain in a transverse field, whose Hamiltonian reads

$$\mathcal{H} = -J \sum_{i=1}^{N-1} (\sigma_i^z \sigma_{i+1}^z + g \sigma_i^x) \, , \tag{11.5}$$

where σ_i^α ($\alpha = x, y, z$) are the Pauli matrices localized on a $1d$ chain. Open boundaries are assumed. $J > 0$ is the Ising interaction term favoring ferromagnetic ordering along z, while g is a transverse field (whose intensity is measured in units of J) favoring an alignment of the spins along x. A quantum phase transition occurs in the ground state at $g = g_c = 1$ (Sachdev, 2001). The schematic phase diagram is represented on Fig. 11.1.

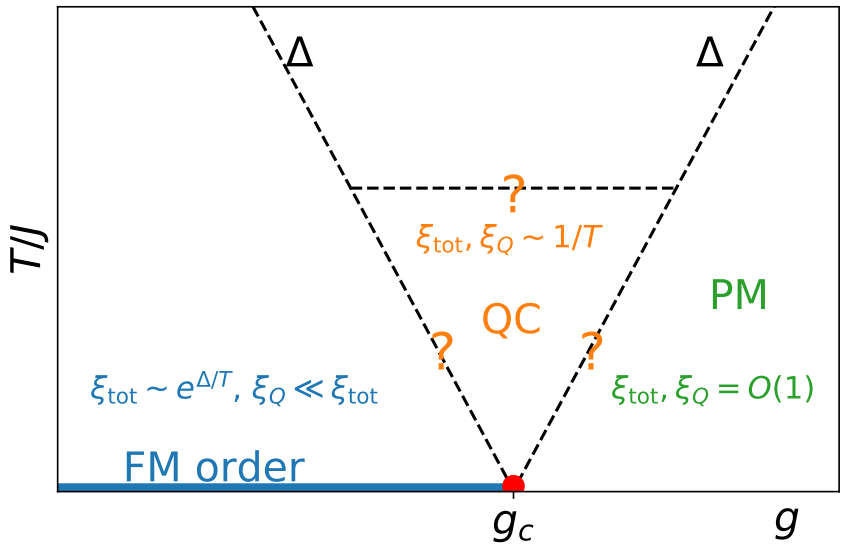

Figure 11.1: Phase diagram of the $d = 1$ Ising model in a transverse field. The system presents three regimes at low temperature: 1) a quasi-ferromagnetic (FM) phase at small g where the correlation length is proportional to $e^{\Delta/T}$, where $\Delta \propto |g - g_c|$ (FM order occurs only at $T = 0$). Quantum correlations merely renormalize the effective spin-length, and we find $\xi_Q \ll \xi$. 2) A paramagnetic (PM) phase at large g where spins preferentially align along the transverse field, and $\xi_{\rm tot} \gtrsim \xi_Q$ extends over a few lattice sites. 3) A quantum critical region for $T \gtrsim \Delta$, whose precise extension has to be determined, and where the scaling of fluctuations is governed by the exponents of the critical point $g = g_c$ (red dot). In the quantum critical region, both $\xi_{\rm tot}$ and ξ_Q are proportional to $1/T$.

Divergence of the quantum coherence volume at the QCP. Within the family of Ising models ($d = 1, 2, \ldots \infty$), the Ising chain represents the opposite limit to the infinite-range model studied in Chapter 10, which may be viewed as the $d \to \infty$ limit of this family of models. In a $d = 1$ system, fluctuations effects are expected to be stronger — indeed, they are so strong that the critical temperature for the ferromagnetic (FM) / paramagnetic (PM) phase transition is pushed down to $T_c = 0$: FM order exists only in the ground state for $g < g_c$. For instance, Eq. (11.3) predicts that the coherence volume diverges at the critical point as (Hauke et al., 2016)

$$N_Q \sim N^{3/4}\,, \tag{11.6}$$

($\eta = 1/4$ in Eq. (11.3) at the $d = 1$ Ising QCP) almost saturating the so-called Heisenberg limit $N_Q = N$[1].

[1] Necessarily, $N_Q = F_Q(S^z)/N \leq N$. This constraint follows from the inequality $F_Q(S^z) \leq 4\langle \delta^2 S^z \rangle$. The variance of S^z is maximal for an equal weight superposition of $\otimes_{i=1}^N |\uparrow_z\rangle$ and $\otimes_{i=1}^N |\downarrow_z\rangle$,

Thermal vs. quantum correlation length. Furthermore, the $d = 1$ Ising model represents a paradigmatic situation where the spatial structure of quantum correlations can be revealed, and contrasted with that of total correlations. For instance, while we gave general arguments within a gaussian field theory in Section 9.4 supporting a complete separation of scales for thermal and quantum fluctuations close to a thermal phase transition, we have not provided any evidence of such a behavior through explicit microscopic calculations [such calculations have been reported by Malpetti and Roscilde (2016) and Malpetti (2016); see Fig. 9.2(d)]. The divergence of the *quantum correlation length* ξ_Q (Malpetti and Roscilde, 2016) expected in the vicinity of the quantum critical point (Sachdev, 2001)

$$\xi_{\rm tot},\ \xi_Q \sim \frac{1}{T^{1/z}} \tag{11.7}$$

drives in turn the divergence of the coherence volume N_Q (although the behavior of N_Q is also sensitive to the algebraic decay of the correlation function at distances $\ll \xi_Q$, as indicated by the exponent η in Eq. (11.3)). The characterization of ξ_Q in the different phases of the Ising model (and, more generally, of the spatial structure of quantum correlations $\langle \delta S_i^z \delta S_j^z \rangle_Q$) thus represents a complementary, more microscopic understanding, of the scaling behavior of the quantum variance and of the quantum Fisher information.

Last, but not least, the Ising chain is a unique example of an exactly solvable model (Pfeuty, 1970) presenting a non-trivial quantum critical point (Sachdev, 2001), and which is moreover relevant for experiments, *e.g.* in quantum magnetism (Kinross et al., 2014) and atomic physics (Kim et al., 2011).

11.2 Technical aspects

In this section, we present the main technical aspects underlying the calculation of the correlations for the quantum Ising chain.

11.2.1 Jordan-Wigner mapping and Bogoliubov transformation

Jordan-Wigner mapping to fermions. The first step is to map the spin operators to fermionic operators through a Jordan-Wigner transformation (Lieb, Schultz, and

for which the variance of S^z is $N^2/4$.

Mattis, 1961; Pfeuty, 1970)

$$\begin{aligned}\sigma_i^x &= 1 - 2c_i^\dagger c_i \\ \sigma_i^y &= -i\left[\prod_{j=1}^{i-1}\sigma_j^x\right](c_i - c_i^\dagger) \\ \sigma_i^z &= -\left[\prod_{j=1}^{i-1}\sigma_j^x\right](c_i + c_i^\dagger)\,. \end{aligned} \tag{11.8}$$

where the operators $c_i^{(\dagger)}$ obey the fermionic anti-commutation relations $\{c_i, c_j\} = 0$ and $\left\{c_i, c_j^\dagger\right\} = \delta_{ij}$. In terms of the $c_i^{(\dagger)}$ operators, the Ising Hamiltonian of Eq. (11.5) takes the form of a quadratic Hamiltonian

$$\mathcal{H} = -J\sum_{i=1}^{N-1}(c_i^\dagger c_{i+1} + c_{i+1}^\dagger c_i + c_i^\dagger c_{i+1}^\dagger + c_{i+1}c_i - 2gc_i^\dagger c_i + g)\,, \tag{11.9}$$

which can be diagonalized by a Bogoliubov transformation.

Bogoliubov diagonalization. Introducing the symmetric $2N \times 2N$ matrix

$$\mathcal{L} = \begin{pmatrix} A & B \\ -B & -A \end{pmatrix} \tag{11.10}$$

with $A_{ij} = 2Jg\delta_{ij} - J(\delta_{j,i+1} + \delta_{j,i-1})$ and $B_{ij} = -J(\delta_{j,i+1} - \delta_{j,i-1})$, the Hamiltonian reads

$$\mathcal{H} = \frac{1}{2}\begin{pmatrix}\boldsymbol{c}^\dagger & \boldsymbol{c}\end{pmatrix}\mathcal{L}\begin{pmatrix}\boldsymbol{c} \\ \boldsymbol{c}^\dagger\end{pmatrix} + \text{const.}\,, \tag{11.11}$$

where $\boldsymbol{c} = (c_1, \ldots, c_N)^T$. As B is antisymmetric while A is symmetric, $\mathcal{L}$ is a symmetric matrix which can be diagonalized by a unitary transformation (Blaizot and Ripka, 1986)

$$\mathcal{L}\begin{pmatrix}\boldsymbol{c} \\ \boldsymbol{c}^\dagger\end{pmatrix} = U[E \oplus (-E)]U^\dagger\,, \tag{11.12}$$

where $E = \text{diag}(E_1, \ldots E_N)$. This finally brings the Hamiltonian into a diagonal form

$$\mathcal{H} = \sum_{\alpha=1}^{N} f_\alpha^\dagger f_\alpha E_\alpha + \text{const.} \tag{11.13}$$

where

$$\begin{pmatrix}\boldsymbol{c} \\ \boldsymbol{c}^\dagger\end{pmatrix} = U\begin{pmatrix}\boldsymbol{f} \\ \boldsymbol{f}^\dagger\end{pmatrix} \tag{11.14}$$

As we cannot deal exactly with periodic boundary conditions on a finite chain (Lieb, Schultz, and Mattis, 1961), we have worked with an open chain.

Spectrum in the infinite-size limit. In the thermodynamic limit, boundary conditions are irrelevant and the excitation spectrum for the free fermions is

$$E_k = 2J\sqrt{1+g^2-2g\cos k} \tag{11.15}$$

where k is the wavevector. The spectrum has a gap at $k=0$

$$\Delta = 2J|1-g| \tag{11.16}$$

which vanishes linearly when approaching the critical point $g=1$. Although in the fermionic picture the system seems to always possess well-defined quasiparticles, these quasiparticles are not related to local observables, and cannot be probed by conventional spectroscopic approaches (such as neutron scattering) which couple to local spin observables. It is only in the limit $g \gg 1$ and $g \ll 1$ that the fermionic quasiparticles can be approximated in terms of the spin degrees of freedom.

11.2.2 Fermionic correlations

Given the quadratic nature of the fermion Hamiltonian, the density-matrix of the system $\rho = e^{-\beta\mathcal{H}}/Z$ obeys Wick's theorem at any temperature $T=\beta^{-1}$. As a consequence, all correlations for the spin degrees of freedom can be expressed as combinations of the fundamental correlators for the fermions

$$\mathcal{C}(t) = \left\langle \begin{pmatrix} \boldsymbol{c}(t) \\ \boldsymbol{c}^\dagger(t) \end{pmatrix} \begin{pmatrix} \boldsymbol{c}^\dagger(0) & \boldsymbol{c}(0) \end{pmatrix} \right\rangle \tag{11.17}$$

where $\mathcal{O}(t) = e^{i\mathcal{H}t}\mathcal{O}e^{-i\mathcal{H}t}$. These correlators are themselves obtained via the Bogoliubov transformation U from the correlators of the f operators:

$$\mathcal{C}(t) = U \begin{pmatrix} \frac{e^{-itE}}{1+e^{-\beta E}} & 0 \\ 0 & \frac{e^{itE}}{1+e^{\beta E}} \end{pmatrix} U^\dagger \,, \tag{11.18}$$

where we used that $f_\alpha(t) = e^{-itE_\alpha} f_\alpha$ and $\langle f_\alpha^\dagger f_\alpha \rangle = [1+e^{\beta E_\alpha}]^{-1}$ (all other correlators for the $f_\alpha^{(\dagger)}$ vanish). Note that the expression for $\mathcal{C}(t)$ is valid both for real times t and imaginary times $\tau = it$.

In practice, it is more convenient to work with the following ("Majorana") operators

$$\phi_i^\pm = c_i \pm c_i^\dagger \tag{11.19}$$

whose correlations are readily obtained from the correlation matrix $\mathcal{C}(t)$. These operators anti-commute on different sites, and onsite, satisfy $(\phi_i^\pm)^2 = \pm 1$ and $\{\phi_i^+, \phi_i^-\} = 0$.

11.2.3 Spin correlations

XX correlations. From the Jordan-Wigner mapping of Eq. (11.8), correlations for σ_i^x are just the density correlations for the fermions:

$$\langle \delta\sigma_i^x(t)\delta\sigma_j^x(t)\rangle = 4\langle \delta n_i(t)\delta n_j(t)\rangle \tag{11.20}$$

where $n_i = c_i^\dagger c_i$. These correlations will not be necessary in our subsequent analyses. We shall only need the average magnetization which reads (note that $\sigma_i^x = 1 - 2n_i = \phi_i^+\phi_i^-$)

$$\langle S^x\rangle = \frac{1}{2}\sum_{i=1}^{N}\langle \phi_i^+\phi_i^-\rangle \ . \tag{11.21}$$

ZZ correlations. We have

$$\sigma_i^z = -\left[\prod_{j=1}^{i-1}\phi_j^+\phi_j^-\right]\phi_i^+ \ . \tag{11.22}$$

Obviously, being a product of an odd number of fermionic operators, the average value of σ_i^z vanishes. On the other hand, the correlation function takes the form

$$\langle \sigma_i^z(t)\sigma_j^z(0)\rangle = \left\langle \left[\prod_{k=1}^{i-1}\phi_k^+(t)\phi_k^-(t)\right]\phi_i^+(t)\left[\prod_{l=1}^{j-1}\phi_l^+\phi_l^-\right]\phi_j^+\right\rangle \ . \tag{11.23}$$

For equal-time correlators ($t = 0$), some simplifications are possible. Indeed equal-time correlations read

$$\langle \sigma_i^z\sigma_j^z\rangle_{\rm tot} = \left\langle \phi_i^-\left[\prod_{l=i+1}^{j-1}\phi_l^+\phi_l^-\right]\phi_j^+\right\rangle \ . \tag{11.24}$$

Although the mapping to fermions reduces the problem to that of free particles, the simple two-body correlations for the original spins are thus expressed in general as a $2(i+j-1) \approx N$-body correlator. According to Wick's theorem for fermionic operators (Blaizot and Ripka, 1986), this correlator can be expressed as a Pfaffian:

$$\langle a_1 a_2 \ldots a_{2n}\rangle = \mathrm{Pf}(A) \tag{11.25}$$

where $A_{ij} = \langle a_i a_j\rangle$ is an antisymmetric matrix. The Pfaffian of a $2n \times 2n$ antisymmetric matrix is

$$\mathrm{Pf}(A) = \frac{1}{2^n n!}\sum_{\mathcal{P}\in S_{2n}}\mathrm{sign}(\mathcal{P})\prod_{i=1}^{n}A_{\mathcal{P}(2i-1),\mathcal{P}(2i)} \ , \tag{11.26}$$

where the sum runs over the $(2n)!$ permutations of the $2n$ indices, and $\mathrm{sign}(\mathcal{P})$ is the sign of the permutation (namely the parity of the number of pair-wise exchanges of indices which compose $\mathcal{P}$). Wimmer (2012) has published a package to efficiently compute such Pfaffians numerically, which we used in its Python implementation.

YY correlations. Given that

$$\sigma_i^y = -i \left[\prod_{j=1}^{i-1} \phi_j^+ \phi_j^- \right] \phi_i^- \ , \tag{11.27}$$

the calculation of the correlations for the y component of the spins goes along the same line as for the zz correlations. For the yy correlations, we shall only need the equal-time (total) correlations, which simplify to

$$\langle \sigma_i^y \sigma_j^y \rangle_{\rm tot} = - \left\langle \phi_i^+ \left[\prod_{l=i+1}^{j-1} \phi_l^+ \phi_l^- \right] \phi_j^- \right\rangle \ . \tag{11.28}$$

11.2.4 Quantum correlations and QFI

Quantum covariance. The quantum covariance is obtained by subtracting the thermal covariance from the total one (see Section 2.2). We focus on the splitting between thermal and quantum correlations for the zz correlations, but what follows is immediately generalizable to all spin components. The thermal covariance is

$$\langle \sigma_i^z \sigma_j^z \rangle_{\rm T} = \frac{1}{\beta} \int_0^\beta d\tau \ \langle \sigma_i^z(\tau) \sigma_j^z(0) \rangle \ , \tag{11.29}$$

namely the averaged imaginary-time correlations ($\sigma_i(\tau) = e^{\tau \mathcal{H}} \sigma_i^z e^{\tau \mathcal{H}}$) (Malpetti and Roscilde, 2016), see Section 2.2. The quantum covariance is thus

$$\langle \sigma_i^z \sigma_j^z \rangle_Q = \langle \sigma_i^z \sigma_j^z \rangle_{\rm tot} - \langle \sigma_i^z \sigma_j^z \rangle_{\rm T} \ . \tag{11.30}$$

We obtain the structure factors by Fourier transform

$$S_k^{\rm tot,Q,T} = \frac{1}{4N} \sum_{i,j=1}^{N} e^{ik(r_i - r_j)} \langle \sigma_i^z \sigma_j^z \rangle_{\rm tot,Q,T} \tag{11.31}$$

(the factor $1/4$ is present because $S_i^z = \sigma_i^z/2$).

Quantum Fisher information. The calculation of the QFI is more demanding. Indeed, we have to resort to its expression in terms of the dynamical susceptibility (Hauke et al., 2016), see Section 1.6

$$F_Q(S_k^z) = (4/\pi) \int_0^\infty d\omega \ \chi''(k,\omega) \tanh(\beta\omega/2) \ . \tag{11.32}$$

Although we mainly focus on $k = 0$, we shall consider also the QFI for the fluctuations of $S_k^z = \sum_{r=1}^N e^{ikr} S_r^z$, expressing the sensitivity of the state to unitary transformations induced by a magnetic field varying in space at wavevector k, and oriented along the z

axis. The dynamical susceptibility $\chi''(k,\omega)$ is obtained from the dynamical structure factor via the fluctuation-dissipation theorem (Callen and Welton, 1951; Forster, 1995)

$$\chi''(k,\omega) = \frac{1-e^{-\beta\omega}}{2} S(k,\omega) \; . \tag{11.33}$$

To obtain the dynamical structure factor, we first introduce the Fourier transform of the real-time spin-spin correlations

$$4S_{ij}(\omega) = \int_{-\infty}^{\infty} dt \; e^{i\omega t} \langle \sigma_i^z(t)\sigma_j^z(0)\rangle \; . \tag{11.34}$$

Given the symmetries of the problem, one can show that $\langle \sigma_i^z(t)\sigma_j^z(0)\rangle = \langle \sigma_i^z(-t)\sigma_j^z(0)\rangle^* = \langle \sigma_j^z(t)\sigma_i^z(0)\rangle$[2]. This property allows one to simplify the expression of $S_{ij}(\omega)$ to

$$4S_{ij}(\omega) = 2\int_0^{\infty} dt \; \left\{ \cos(\omega t)\Re[\langle \sigma_i^z(t)\sigma_j^z(0)\rangle] - \sin(\omega t)\Im[\langle \sigma_i^z(t)\sigma_j^z(0)\rangle] \right\} \; . \tag{11.35}$$

The dynamical structure factor is then obtained after a spatial Fourier transform

$$S(k,\omega) = \frac{1}{N}\sum_{i,j=1}^{N} e^{ik(r_j-r_i)} S_{ij}(\omega) \; . \tag{11.36}$$

Given that, numerically, we worked with a discretized time, and given the rich behavior of the real-time correlation functions (as opposed to the imaginary-time correlations which show a simple monotonous decay, symmetric with respect to $\tau = \beta/2$), the final accuracy on the QFI is not obvious to control. We have verified that our precision on $\chi''(k,\omega)$ was sufficient to reconstruct the quantum structure factor with a relative accuracy of less than 10^{-2} through (see Section 1.7)

$$S_k^Q = \int_0^{\infty} \frac{d\omega}{\pi} \, h_{\rm QV}(\beta\omega) \, \chi''(k,\omega) \tag{11.37}$$

with

$$h_{\rm QV}(x) = \coth(x/2) - \frac{2}{x} \; , \tag{11.38}$$

in comparison with a direct calculation through Eq. (11.29), (11.30) and (11.31).

Quantum Fisher information matrix. Alternatively to the QFI of S^z fluctuations at different wavevectors k, we can directly study the spatial structure of quantum correlations contributing to the QFI by calculating the so-called "quantum-Fisher-information matrix", or, as we already renamed it in Chapter 8, the "quantum Fisher information covariance". The latter is defined as

$$\langle S_i^z S_j^z\rangle_{\rm QFI} = (4/\pi)\int_0^{\infty} d\omega \; \frac{1-e^{-\beta\omega}}{2} \tanh(\beta\omega/2) S_{ij}(\omega) \; . \tag{11.39}$$

[2] To prove this, one can calculate the average by inserting a basis of eigenstates of the Hamiltonian between $\sigma_i^z(t)$ and $\sigma_j^z(0)$, and use the fact that the matrix elements of σ_i^z are real.

$F_Q(S^z_k)$ can then be obtained from $\langle S^z_i S^z_j \rangle_{\rm QFI}$ by a spatial Fourier transform. This QFI covariance, already discussed in Chapter 8 in the context of free fermions, has a similar status to the quantum covariance: its spatial structure (typically an exponential decay at large distance) provides a microscopic understanding of the scaling behavior of the QFI, governed by a "QFI correlation length", denoted $\xi_{\rm QFI}$, to be compared to the quantum correlation length ξ_Q, governing the spatial decay of the quantum covariance (Malpetti and Roscilde, 2016), and to the usual, total correlation length $\xi_{\rm tot}$ governing the spatial decay of the usual, total covariance.

11.3 Spatial structure of quantum correlations away from the critical region

In this section, we study the spatial structure of correlations, and discuss the behavior of the correlation length for the total covariance ($\xi_{\rm tot}$), the quantum covariance (ξ_Q) and the QFI covariance ($\xi_{\rm QFI}$). The quantum critical region is studied in details in the next section. In the present section, we focus on $g < 1$, where the system orders ferromagnetically at $T = 0$, and on $g > 1$, where FM order never develops, and the system remains in a (quantum) PM phase down to $T = 0$. This quantum PM phase for the $d = 1$ Ising chain has properties very similar to the one described for the infinite-range Ising model in Chapter 10.

11.3.1 Ferromagnetic phase ($g < 1$)

Total fluctuations. For $g < 1$, the system develops true long-range order only at $T = 0$. However, as the correlation length $\xi_{\rm tot}$ diverges exponentially (Sachdev, 2001)

$$\xi_{\rm tot} \sim e^{\Delta/T} \tag{11.40}$$

finite-size systems appear effectively ordered at temperatures much smaller than the gap (*i.e.* for T such that $\xi_{\rm tot} \gtrsim N$, or $T \lesssim \Delta/\log N$). In fact, this divergence of the correlation length signals a thermal phase transition at a critical temperature $T = 0$. In essence, the phase diagram of the $d = 1$ Ising model has thus the topology of the generic phase diagram of 9.1, where the ordered FM phase has collapsed onto the segment $(T = 0, g < 1)$. The Ising model in $d = 1$ (like in any dimension) has two quasi-degenerate ground states for $g < g_c$ (the gap between them is exponentially small in N), corresponding to the symmetric and anti-symmetric superpositions of symmetry-breaking configurations, where all the spins order along $\pm z$. The divergence of $\xi_{\rm tot}$ signals that the system is effectively frozen in one of these configurations at sufficiently low temperature (strictly speaking, only at $T \to 0$ for $N = \infty$).

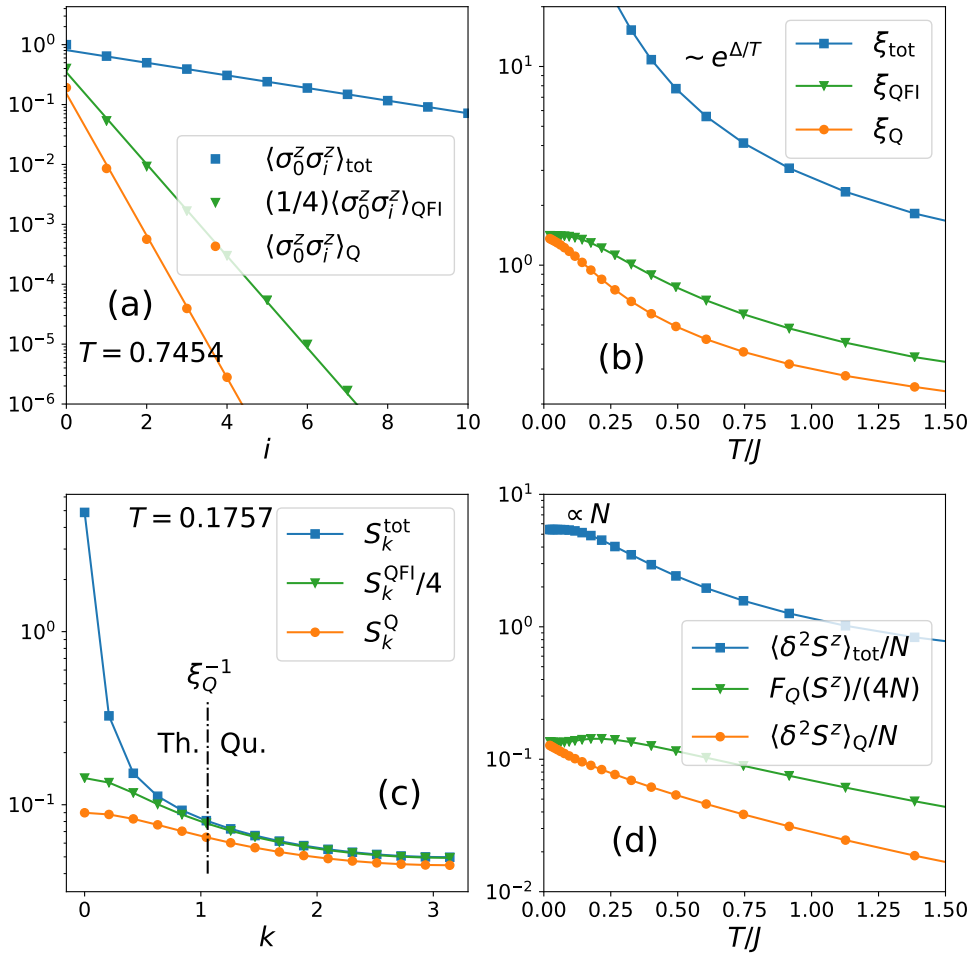

Figure 11.2: Structure of correlations in the FM region ($g = 0.8$, so that $\Delta/J = 0.4$, and $N = 30$). (a) Total, quantum and QFI covariance of σ^z between the first spin of the chain and the $i^{\rm th}$ spin ($T = 0.7454$). Solid lines are fit of the form $\langle\delta\sigma_0^z\delta\sigma_i^z\rangle = ae^{-i/\xi}$. The corresponding correlation lengths ξ are plotted on panel (b) as a function of temperature. (c) Structure factors at $T = 0.1757$. The vertical dashed-dotted black line indicates $k\xi_Q = 1$, separating quantum-dominated fluctuations ($k\xi_Q > 1$) from thermal-dominated fluctuations ($k\xi_Q < 1$). (d) $k = 0$ fluctuations as a function of temperature. The total structure factor diverges as $e^{\Delta/T}$ at low temperature, and saturates to $\propto N$ on a finite-size system, while quantum fluctuations are not critical.

Quantum fluctuations. Quantum fluctuations of S^z, on the other hand, represent the quantum uncertainty of the orientation of the magnetization: even if the spins order preferentially along, say $+z$, they continue to fluctuate quantum-mechanically down to $T = 0$ under the effect of the transverse field. But in contrast to thermal fluctuations, for $g < 1$ these quantum fluctuations are correlated only at short distances, $\xi_Q \ll \xi_{\rm tot}$ and are never strong enough to reverse the orientation of S^z. This scenario is the generic one expected near a thermal phase transition (see Chapter 9) and was observed for the Ising model with infinite-range interactions (Chapter 10). We thus expect that, as opposed to total fluctuations, quantum fluctuations do not exhibit any divergent behavior at low temperature.

Illustration for $g = 0.8$. Figure 11.2 illustrates this scenario. Panels (a) and (b) show a complete separation of scales for thermal and quantum fluctuations (as quantified by the quantum covariance or the QFI covariance): both decay exponentially (panel a), but $\xi_{\rm tot}$ diverges exponentially upon lowering the temperature (panel b), while ξ_Q and $\xi_{\rm QFI}$ smoothly increase towards their ground-state value $\xi(T = 0) \sim 1/\Delta$. We observe that $\xi_{\rm QFI}$ is about twice as large as ξ_Q for $T \gtrsim \Delta$, similar to our findings for free fermions (Chapter 8). For $T \ll \Delta$, quantum correlations take their ground state value, and they have the effect of lowering the value of the magnetization in the ground state (Sachdev, 2001) with respect to $\langle S^z \rangle = N/2$ found for the classical Ising chain (namely for $g = 0$). Even though this is not shown in Fig. 11.2(b), on a finite-size system even $\xi_{\rm tot}$ will eventually come down to a finite value when $T \to 0$, coinciding with the value of both ξ_Q and $\xi_{\rm QFI}$.

As expected, the behavior of the correlation lengths reflects in the integrated correlation functions (the structure factors) as illustrated on Fig. 11.2(c,d). On panel (c), we clearly see that at distances $x < \xi_Q$ ($k\xi_Q > 1$), the structure of fluctuations is dominated by quantum effects, while thermal fluctuations dominate for $x > \xi_Q$ ($k\xi_Q < 1$). The splitting between thermal and quantum fluctuations as proposed in this manuscript hence allow for a direct inspection of the length scales over which quantum and thermal effects are respectively dominant, without a priori knowledge of the detailed dynamics of the system. Finally, on panel (d), we have plotted the evolution of the $k = 0$ structure factors (*i.e.* the total variance, the QV and the QFI of S^z per spin). The observed behavior is very similar to that of the correlation lengths (panel b): the total variance diverges exponentially (and quickly saturate to $\langle \delta^2 S^z \rangle \sim N^2$ due to strong finite-size effects), while quantum fluctuations smoothly saturate their ground-state value.

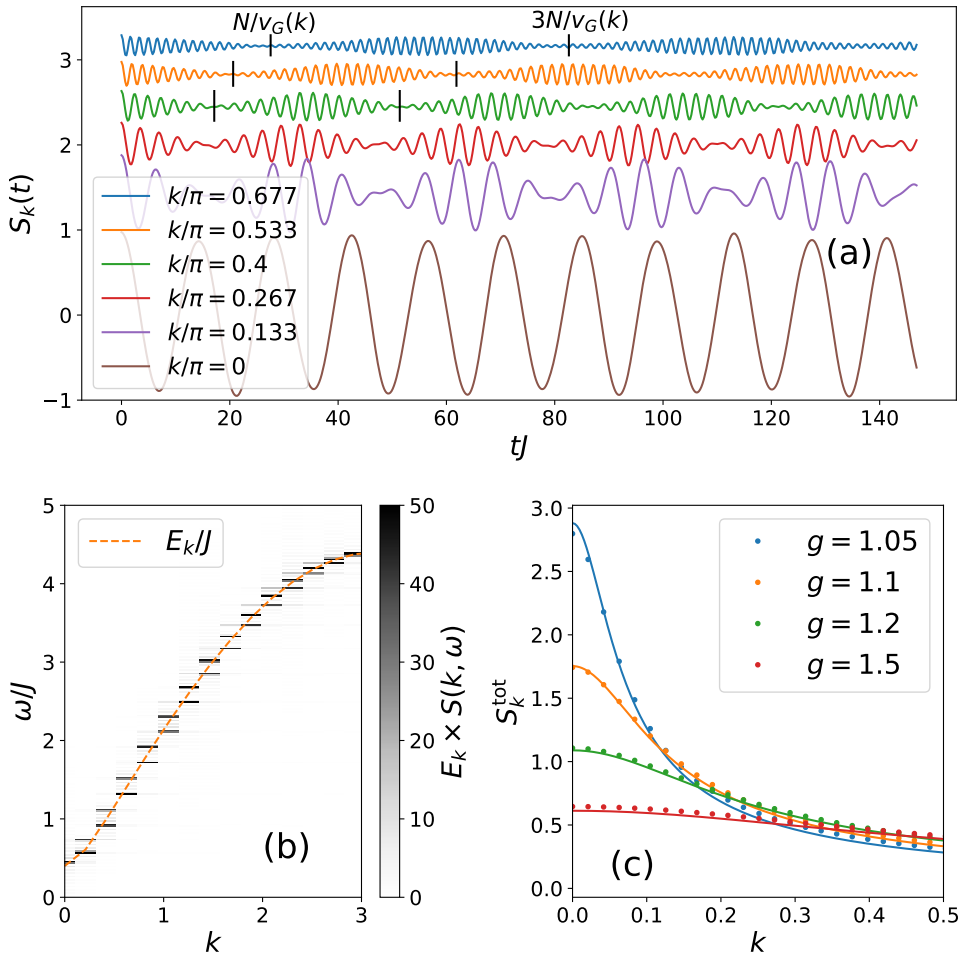

Figure 11.3: Dynamical correlations in the paramagnetic phase ($g > 1$). (a) Real-time dynamics of the fluctuations at wavevector k ($S_k(t)$ is defined in Eq. (11.43)). Data for different values of k are shifted by an amount $\sqrt{k}$ for a better visibility. The small vertical black lines indicate $t_1 = N/\partial_k E_k$ and $t_2 = 3t_1$. Calculation for $N = 30$, $g = 1.2$, $T = 0.012$, up to time $tJ = 147$ with 640 time steps. (b) Frequency spectrum of the data of (a), showing a resonance at $\omega = E_k$, consisting of two peaks separated by $\Delta\omega \propto 1/N$ (see text). The dashed orange line is the excitation spectrum in the limit $N \to \infty$ given by Eq. (11.15). (c) Static structure factor for $N = 300$ and $T = 0.02$. Solid lines are the prediction of Eq. (11.44).

11.3.2 Quantum paramagnetic phase ($g > 1$)

Dynamical structure factor. For $g > 1$, FM order never develops even at $T = 0$, but the system has a finite magnetic susceptibility with respect to the application of a field along the z axis (hence the term "paramagnet"). Spins are preferentially aligned along $+x$ (the orientation of the transverse field), and the system possesses

well-defined quasiparticles, consisting of spin-flips along $-x$. These quasiparticles manifest themselves as resonances at $\omega = E_k$ [given in Eq. (11.15)] in the dynamical structure factor for $S^z S^z$ correlations, predicted via quantum field theory to take the form (for $g \to 1^+$ and $k \to 0$) (Sachdev, 2001)

$$S(k,\omega) \approx \frac{c(\Delta/J)^{1/4}}{2E_k} \frac{1/\tau_\phi}{(\omega - E_k)^2 + (1/\tau_\phi)^2} \,. \tag{11.41}$$

$c = 2\sqrt{g}$ is defined through $E_k \approx \Delta + (ck)^2/(2\Delta)$ (E_k is given in Eq. (11.15)), and the amplitude of the resonance is known analytically (Sachdev, 2001). The quasiparticle picture breaks down when approaching the critical point where $\Delta \to 0$. In principle, this expression for the dynamical structure factor is valid only for $c|k| \ll \sqrt{\Delta T}$ (Sachdev, 2001).

The phase coherence time $\tau_\phi \sim e^{\Delta/T}$, responsible for a thermal broadening of the resonance, is essentially infinite for $T \ll \Delta$, and the Lorentzian peak can be approximated by a delta function

$$S(k,\omega) \approx \frac{c(\Delta/J)^{1/4}}{2E_k} \pi \delta(\omega - E_k) \,. \tag{11.42}$$

Real-time dynamics. Equivalently, the real-time dynamics of the structure factor exhibits undamped oscillations at a single frequency

$$S_k(t) = \frac{1}{4N} \sum_{i,j=1}^{N} e^{ik(r_i - r_j)} \langle \sigma_i^z(t) \sigma_j^z(0) \rangle \approx \frac{c(\Delta/J)^{1/4}}{4E_k} e^{iE_k t} \,. \tag{11.43}$$

As illustrated on Fig. 11.3(a), on a finite-size system (here $N = 30$), this perfectly coherent oscillation is modulated on a much longer period $T(k)$. This period turns out to coincide with the time needed for a quasiparticle at wavevector k, propagating ballistically at a velocity $v_G(k) = \partial_k E_k$, to travel twice across the chain: $T(k) = 2N/v_G(k)$. In the limit $N \to \infty$, this period becomes infinite, and only the frequency $\omega = E_k$ remains. On Fig. 11.3(b), we have plotted the frequency spectrum of $S_k(t)$ (namely the dynamical structure factor $S(k,\omega)$). Due to the low modulation at a frequency $2\pi/T(k)$, each $\omega = E_k$ peak is split into two components, separated by a frequency $\Delta\omega \propto 1/N$, so that a single peak is recovered in the thermodynamic limit. Note that as $S(k,\omega) \propto 1/E_k$ [see Eq. (11.42)] we have multiplied $S(k,\omega)$ by E_k to have a nearly uniform contrast on the figure.

Static structure factor. As a further validation of the prediction of Eq. (11.42) for the dynamical structure factor in the PM phase, and especially of the prediction for

the amplitude of the resonance, we have tested the corresponding prediction for the static structure factor

$$S_k^{\rm tot} = S_k(t=0) \approx \frac{c(\Delta/J)^{1/4}}{4E_k} \tag{11.44}$$

against an exact calculation on a chain of $N = 300$ spins, at $T = 0.02$, for various values of the transverse field g. The comparison is shown on Fig. 11.3(c), and the agreement is quite good at small k (note that for $g = 1.05$, finite-size effects are visible at $k = 0$, as expected close to the critical point).

Quantum versus total correlations. In the PM phase, quantum and thermal correlations have the same qualitative structure: all of them decay exponentially, as illustrated on Fig. 11.4(a). The correlation lengths, extracted from this exponential decay and plotted on Fig. 11.4(b), are of the same order of magnitude, with

$$\xi_Q < \xi_{\rm QFI} < \xi_{\rm tot} \ . \tag{11.45}$$

For $T \ll \Delta$, the correlation lengths are governed by the gap, so that $\xi = O(c/\Delta)$ (Sachdev, 2001). For $T \gg \Delta$, on the other hand, $\xi \sim 1/\sqrt{T}$, corresponding to the de Broglie wavelength of free particles. This exponential decay is equivalently understood from the Lorentzian shape of the corresponding structure factors at small k, plotted on Fig. 11.4(c).

Similarly to the FM phase, we observe that the structure of fluctuations is governed by the quantum contribution for $k\xi_Q > 1$, and by the thermal contribution for $k\xi_Q < 1$. For $T < \Delta$, the $k = 0$ structure factor (panel d) almost saturates its ground-state value, which is proportional to $\Delta^{-3/4}$, in agreement with Eq. (11.44). For $T \gg \Delta$, total fluctuations attain the shot-noise limit $\langle \delta^2 S^z \rangle = N/4$, while quantum fluctuations decrease proportionally to $1/T^2$. Interestingly, for intermediate values of T, the scaling behavior of both the QFI and the QV seems to cross-over to an intermediate power-law regime, somehow anticipating the $1/T^{1-\eta}$ divergence along the critical trajectory $g = 1$ (see discussion in Sec. 11.4.3).

11.4 Quantum critical scaling at $T > 0$

11.4.1 Field-theory prediction

At the quantum critical point $(g = 1, T = 0)$, the long-distance / low-frequency properties of the quantum Ising chain are captured by a field theory describing the fluctuations of the magnetization density $\phi(x, \tau)$ in space (x) and in imaginary time (τ) (Sachdev, 2001). This field theory (the $1 + 1$-dimensional quantum O(1) model) has

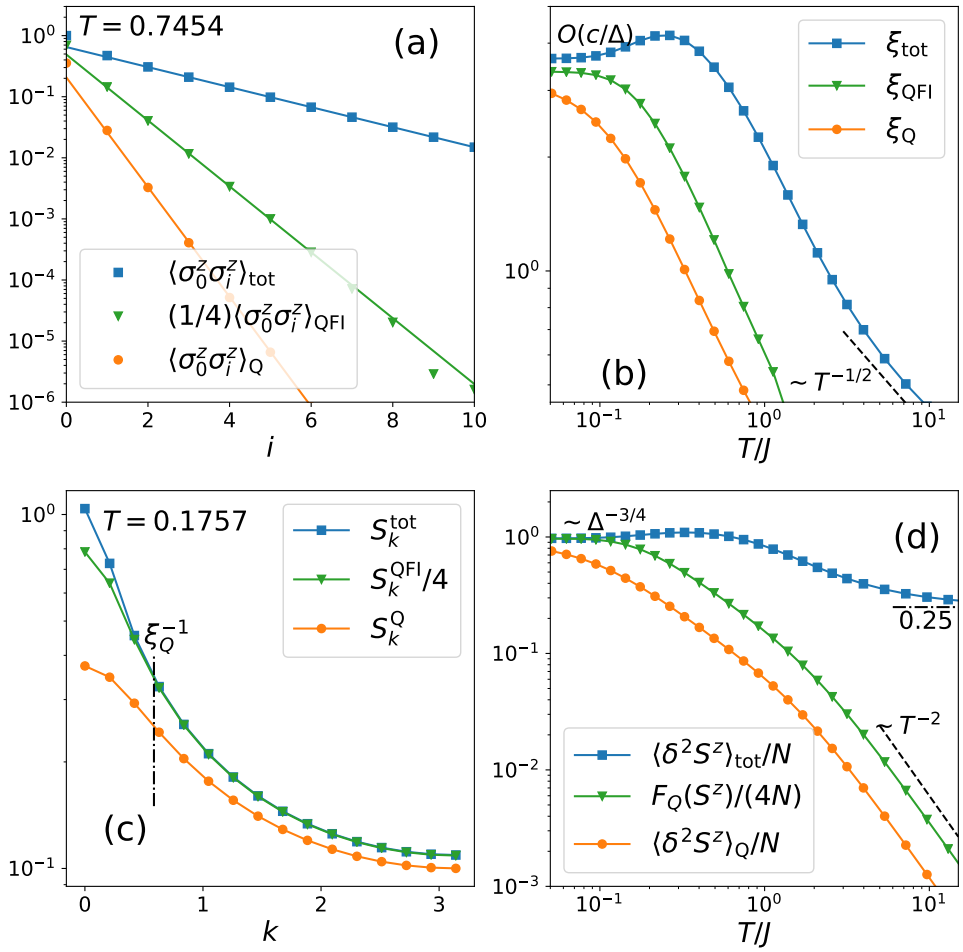

Figure 11.4: Structure of correlations in the paramagnetic phase ($g = 1.2$, $N = 30$). (a) Quantum, total and QFI covariance of σ^z between the first spin of the chain and a spin at position i. Solid lines are fits of the form $ae^{-i/\xi}$. The resulting correlation lengths ξ are plotted on panel (b) as a function of temperature. For $T \ll \Delta$, $\xi \sim 1/\sqrt{T}$, corresponding to the thermal de Broglie wavelength of the quasiparticles. (c) Structure factors. The vertical dashed line indicates a cross-over between thermal-dominated ($k\xi_Q < 1$) and quantum-dominated ($k\xi_Q > 1$) fluctuations. (d) $k = 0$ fluctuations as a function of temperature. For $T \gg \Delta$, total fluctuations are essentially uncorrelated, and assume the shot-noise value $\langle\delta^2 S^z\rangle = N/4$, while quantum fluctuations are proportional to $1/T^2$. A scaling regime, precursor of the quantum critical scaling, can be guessed at intermediate temperature for the QV and the QFI, but no clear power-law exponent can be extracted.

the same form as the one describing the (thermal) critical point of the $d = 2$ classical Ising model. In particular, correlation functions are invariant under rotation in the $(x, c\tau)$ plane, and their decay with distance is controlled by the exponent $\eta = 1/4$ of the $d = 2$ classical Ising model

$$\langle \sigma_x^z(\tau)\sigma_0^z(0)\rangle \sim \frac{1}{(x^2 + c^2\tau^2)^{1/8}} \tag{11.46}$$

(this rotational invariance in the $(x, c\tau)$ plane, which implies that the correlation function depends only on the distance $x^2 + c^2\tau^2$, is the consequence of the value $z = 1$ for the dynamical exponent, itself a consequence of the linear spectrum $\omega = ck$ at the critical point, see Eq. (11.15)). Equivalently, the real-time correlations display Lorentz invariance

$$\langle \sigma_x^z(t)\sigma_0^z(0)\rangle \sim \frac{1}{(x^2 - c^2t^2)^{1/8}} , \tag{11.47}$$

or in Fourier space

$$S(k, \omega) \sim \frac{1}{[k^2c^2 - (\omega + i0^+)^2]^{7/8}} . \tag{11.48}$$

At finite temperature, the $(x, c\tau)$ plane acquires the topology of a cylinder: fluctuations in imaginary time are periodic, of period β. Techniques of conformal field theory allow the $T = 0$ results to be extended at finite temperature along the critical trajectory $(g = 1, T \geq 0)$. It is remarkable that this field-theory approach to the quantum Ising chain gives not only the correct scaling laws, but also the exact expression of the scaling functions. The central result, which forms the starting point for the comparison of our numerical calculations with the field-theory predictions, is the following expression for the dynamical susceptibility (Sachdev, 2001)

$$\chi(k, \omega) = aT^{-7/4} \frac{\Gamma\left(\frac{1}{16} - i\frac{\omega+ck}{4\pi T}\right)\Gamma\left(\frac{1}{16} - i\frac{\omega-ck}{4\pi T}\right)}{\Gamma\left(\frac{15}{16} - i\frac{\omega+ck}{4\pi T}\right)\Gamma\left(\frac{15}{16} - i\frac{\omega-ck}{4\pi T}\right)} \tag{11.49}$$

where $a \approx 0.00501$ is known exactly, and where T is measured in units of J. Γ is Euler gamma function. This formula predicts a line of peaks for $\omega = ck$, whose width remains finite down to $T = 0$, where they acquire a singular shape (see Fig. 11.5(c)).

11.4.2 Dynamical correlations

On Fig. 11.5, we compare the field-theory prediction with an exact calculation on a open chain of $N = 50$ spins, for $T = 0.401$. On panel (a), we have compared the real-time dynamics of $\Re[S(k, t)]$ at a wave-vector $k = 4\pi/25$. The field-theory prediction is obtained by Fourier-transforming $S(k, \omega)$, obtained itself from the imaginary-part of $\chi(k, \omega)$ via the fluctuation-dissipation theorem $S(k, \omega) = 2\chi''(k, \omega)/(1 - e^{-\beta\omega})$. Although the initial time dependencies for the exact finite-size and the field-theory

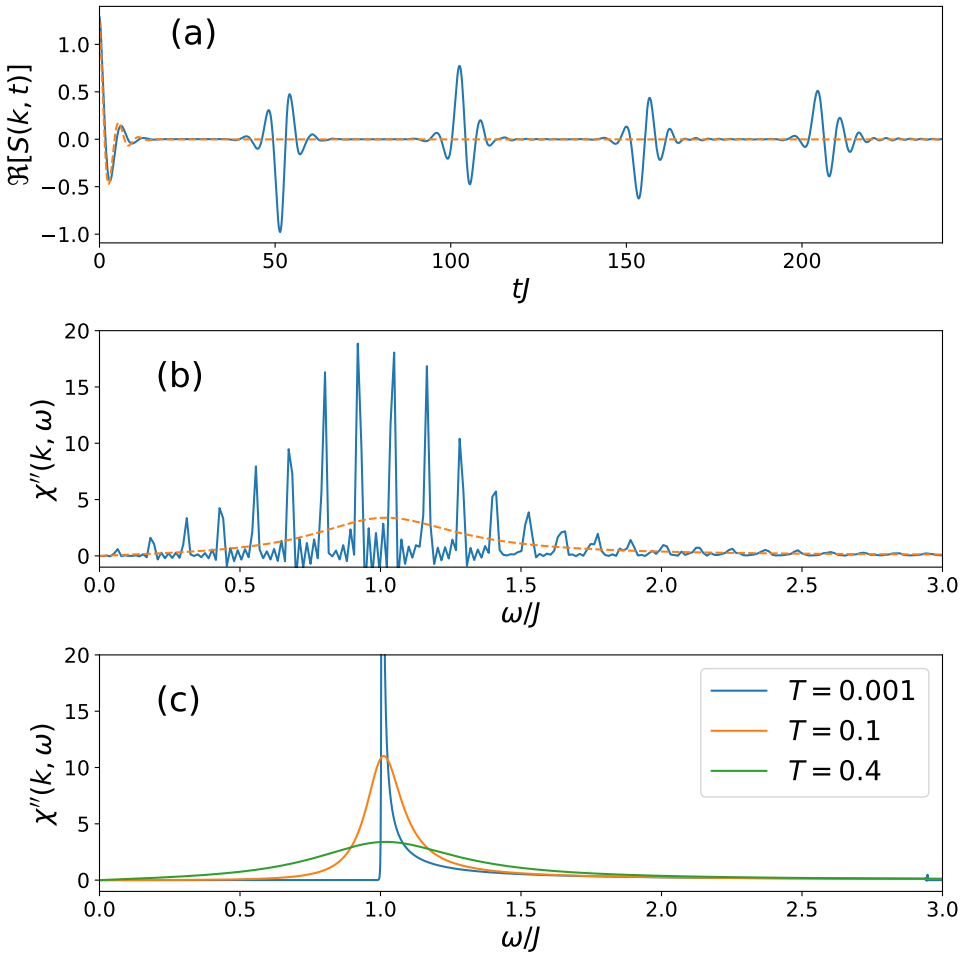

Figure 11.5: Dynamical correlations for $g = 1$, $T/J = 0.401$ and $N = 50$ spins. (a) Real part of the dynamic correlation $S(k,t)$ for $k = 4\pi/25$. Solid blue line: exact numerical calculation; dashed orange line: theoretical prediction from the scaling function of Eq. (11.49). On a finite open chain of N spins, the correlation is roughly periodic with a period $t/J = 2N$. (b) $\chi''(k,\omega)$ reconstructed from a numerical Fourier transform of (a) (solid blue line), and imaginary part of Eq. (11.49) (dashed orange line). For the finite chain, frequencies are roughly odd multiples of the fundamental frequency $\omega_0 = J\pi/N$. The resonance is a broad peak centered on $\omega = ck$, the broadening stemming from both thermal and quantum dissipation. (c) Theoretical prediction of Eq. (11.49) for $\chi''(k,\omega)$ at $k = 4\pi/25$, for $T/J = 0.001, 0.1, 0.4$. The resonance peak is completely asymmetric at $T = 0$, where an absorption of energy at $\omega \gtrsim ck$ decays into a continuum of excitations (there is no well-defined quasiparticle for S^z at the critical point).

calculations are in good agreement, the microscopic calculation shows finite-size revivals of the correlation signal with a periodicity $t_N = 2N/J$ (note that the signal is not exactly periodic). As shown on panel (b), it is clear that the frequency spectrum of $S(k,t)$ contains mainly odd multiples of the fundamental frequency $\omega_0 = 2\pi/t_N$

$$\omega_n \approx nJ\pi/N \quad n \text{ odd integer.} \tag{11.50}$$

We interpret this observation by remarking that the low-lying (fermionic) excitation spectrum of the open chain at $g = 1$, as obtained by the Jordan-Wigner and Bogoliubov transformation (Section 11.2.1), is also composed of these frequencies. Given that, for an arbitrary observable $\mathcal{O}$,

$$\langle \mathcal{O}(t)\mathcal{O}(0)\rangle = \frac{1}{Z}\sum_{n,m} e^{-\beta E_n} e^{it(E_n - E_m)} |\langle n|\mathcal{O}|m\rangle|^2 \,, \tag{11.51}$$

where the sum is over the (many-body) eigenstates of the Hamiltonian, it is clear that these frequencies must appear in the spectrum of $S(k,t)$ as stemming from matrix elements between the ground state and a state containing one fermionic excitation. In principle, we should also find all multiples and differences of the one-particle energies, but apparently the corresponding matrix elements are strongly suppressed.

In the end, a direct comparison of our numerical reconstruction of χ'' with the field-theory prediction is not easy, but as the quantities we focus on in the following result from integrating smooth "filters" multiplying $\chi''(k,\omega)$, the discrete nature of the frequency spectrum on a finite chain (as opposed to the continuous spectrum in the thermodynamic limit, and predicted by the field-theory) is not problematic.

Finally, on Fig. 11.5(c), we have plotted the field-theory prediction for $\chi''(k,\omega)$ at $k = 4\pi/25$, varying the temperature. We clearly see that the broad resonance observed at $T/J = 0.4$, corresponding to a very short lifetime of the magnetic excitations created around $\omega = ck$, sharpens upon decreasing the temperature. However, even at $T = 0$, the resonance is not a delta function (*i.e* there are no stable quasiparticles), and the peak is completely asymmetric with respect to $\omega = ck$: no absorption of energy is possible for $\omega < ck$, while the system absorbs energy for all $\omega \geq ck$.

11.4.3 Scaling of fluctuations

Static structure factors. Instead of comparing directly the dynamical structure factor as predicted by Eq. (11.49) and as calculated by exact diagonalization on a finite chain (Fig. 11.5), we can compare the spatial structure of correlations, contained in the corresponding static structure factors, which descends from $\chi''(k,\omega)$ as integrals over frequencies against the various filters $h_\alpha(\omega/T)$ (with $\alpha =$ T, tot, Q, QFI and so

on)

$$S_\alpha(k) = \int_0^\infty \frac{d\omega}{\pi} h_\alpha\left(\frac{\omega}{T}\right) \chi''(k,\omega) \tag{11.52}$$

where we recall that

$$\begin{cases} h_{\rm T}(x) &= 2/x \\ h_{\rm tot}(x) &= \mathrm{cotanh}(x/2) \\ h_{\rm Q}(x) &= \mathrm{cotanh}(x/2) - 2/x \\ h_{\rm QFI}(x) &= 4\tanh(x/2)\ . \end{cases} \tag{11.53}$$

$S_\alpha(k)$ is the structure factor for, respectively, thermal, total, quantum and QFI correlations. Note that the thermal structure factor is equivalently given by $S_{\rm T}(k) = T\chi(k,0)$.

Scaling form along the quantum critical trajectory. From the field-theory prediction of $\chi(k,\omega)$ [Eq. (11.49)], we see that χ'' assumes the following scaling form

$$\chi''(k,\omega) = T^{-7/4} f\left(\frac{ck}{T}, \frac{\omega}{T}\right)\ . \tag{11.54}$$

This implies, in passing, that the correlation length ξ and the characteristic relaxation time τ both scale according to

$$\tau,\ \xi \sim \frac{1}{T}\ . \tag{11.55}$$

We can immediately draw from the scaling form of χ'' a fundamental conclusion concerning the scaling of fluctuations along the quantum critical trajectory. Indeed, making the change of variable $x = \omega/T$ in the integral over ω in Eq. (11.52), we obtain

$$S_\alpha(k) = T^{-3/4} \int_0^\infty \frac{dx}{\pi} h_\alpha(x) f\left(\frac{ck}{T}, x\right)\ . \tag{11.56}$$

Focusing on $k = 0$ fluctuations, we conclude that

$$S_\alpha(0) = (T/J)^{-3/4} c_\alpha \tag{11.57}$$

where we recall that T is measured in units of J, and where the exact value of c_α is predicted by field theory

$$c_\alpha = \int_0^\infty \frac{dx}{\pi} h_\alpha(x) f(0,x) \tag{11.58}$$

and

$$f(0,x) = a\Im\left(\frac{\Gamma\left[\frac{1}{16} - i\frac{x}{4\pi}\right]^2}{\Gamma\left[\frac{15}{16} - i\frac{x}{4\pi}\right]^2}\right)\ . \tag{11.59}$$

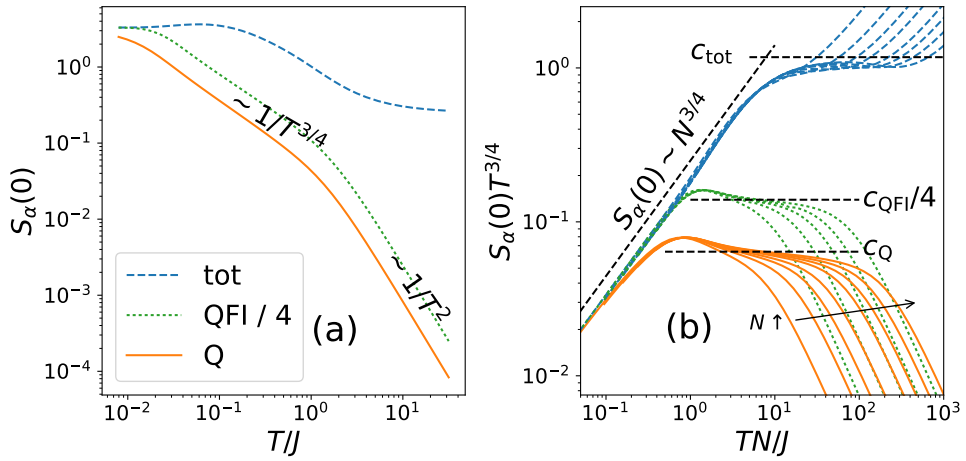

Figure 11.6: Scaling of fluctuations along the critical trajectory $g = 1$ of the quantum Ising chain. (a) Total (dashed line), QFI (dotted line) and QV (solid line) structure factors at $k = 0$ of S^z for a chain of $N = 50$ spins. At high temperature, the total structure factor equals the shot-noise limit for spins-1/2 ($\langle \delta^2 S^z \rangle = N/4$), while quantum fluctuations decrease as $1/T^2$. For temperatures $T \sim 1/N$, finite-size effects appear and all the structure factors are of order $N^{3/4}$. In the quantum critical regime, $k = 0$ fluctuations diverge proportionally to $1/T^{1-\eta}$ with $\eta = 1/4$. (b) Rescaled data for $N = 6, 12, 20, 30, 50$ for the QFI, and up to $N = 150$ for the QV and the total structure factor. The collapse of the curves for various values of N in these rescaled axes, and the flat plateau, prove the scaling behavior $S_\alpha(0) = T^{-3/4} f(N/\xi)$ in the critical regime, with $\xi \sim 1/T$. Horizontal dashed lines are the prediction of field theory for $f(\infty)$ [see Eq. (11.60)].

Performing the integration numerically, we obtain

$$\begin{cases} c_{\rm tot} & \approx & 1.175 \\ c_{\rm T} & \approx & 1.111 \\ c_{\rm Q} & \approx & 0.0640 \\ c_{\rm QFI} & \approx & 0.557 \end{cases} \tag{11.60}$$

Even though $c_{\rm T}$ contributes for $\approx 95\%$ to $c_{\rm tot}$, all quantities exhibit the same $(T/J)^{-3/4}$ divergence. This observation supports the statement according to which the quantum critical region involves quantum and thermal effects on a similar footing.

Comparison of the field-theory prediction with a microscopic calculation. Fig. 11.6 shows a very good agreement of this field-theory prediction with our finite-size calculations. Finite-size effects are apparent for T close to the finite-size gap $\Delta_{\text{finite size}} \sim 1/N$, or equivalently, for N close to $\xi \sim 1/T$. For $T \gtrsim 0.5J$, the critical regime terminates, and the physics is dominated by lattice effects (corresponding to

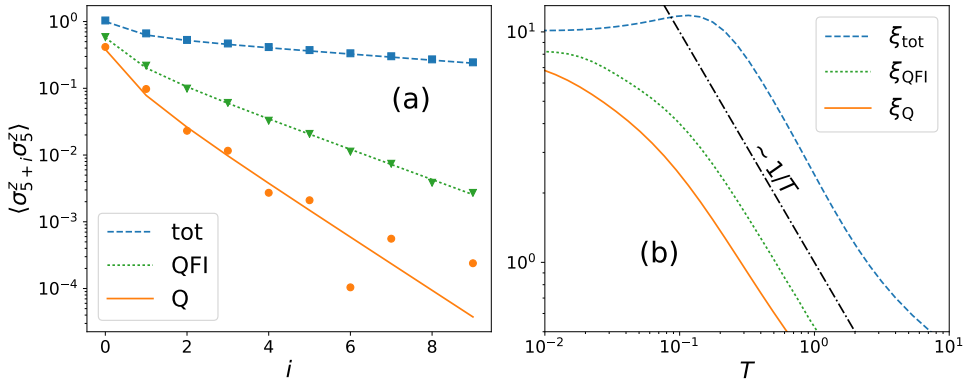

Figure 11.7: Quantum, total and QFI correlations (defined in Section 11.2.4) for $g = 1$, $T/J = 0.266$ and $N = 50$ spins. (a) Correlation function between the $5^{\rm th}$ site and the site at position $i + 5$. Lines are exact calculations, and symbols are given by Eq. (11.62). (b) Correlation lengths, extracted from fitting to an exponential the correlations function calculated on a system of $N = 50$ spins, as a function of temperature. Dashed-dotted line indicates the expected scaling behavior $\xi \sim 1/T$ along the critical trajectory.

the fact that $\xi \approx$ lattice spacing). Finally, at $T = 0$, fluctuations diverge as

$$\langle \delta^2 S^z \rangle_{\rm tot} = \langle \delta^2 S^z \rangle_{\rm Q} = (1/4) F_Q(S^z) \sim N^{7/4} \tag{11.61}$$

in agreement with the scaling prediction.

11.4.4 Correlation lengths

Divergence of the correlation lengths. We now focus on the behavior of the correlation lengths along the quantum critical trajectory. Such behavior can be predicted by field theory, as we can indeed evaluate the correlation functions as

$$\langle \sigma^z_i \sigma^z_j \rangle_\alpha = \frac{1}{N} \sum_k e^{ik(r_i - r_j)} S_\alpha(k) \tag{11.62}$$

where $S_\alpha(k)$ is obtained by a numerical integration of Eq. (11.56).

On Fig. 11.7(a), we show that the field-theory prediction (symbols) is in very good agreement with the exact calculation on a chain of $N = 50$ spins (lines), when considering the correlations with a spin not too close to the boundary (here the fifth spin of the chain). The agreement is better for the total and QFI covariance than for the quantum covariance. In particular, the field-theory predicts small oscillations, especially visible for the quantum covariance $\langle \sigma^z_i \sigma^z_j \rangle_Q$, which are not observed on our open-chain calculation, but the correlation length is closely captured. On Fig. 11.7(b),

the correlation lengths for these three correlation functions (as extracted from fitting data similar to those of panel (a) at various temperatures) are plotted as a function of temperature. As expected, for the three of them we observe the critical scaling

$$\xi \sim 1/T^{1/z} \tag{11.63}$$

with $z = 1$, but the prefactor for the total (and, hence, thermal) correlations is about one order of magnitude larger than for the quantum correlation lengths.

Correlation lengths and finite-size effects. This last observation is consistent with the picture obtained from the integrated correlation functions, namely the structure factors at $k = 0$ plotted on Fig. 11.6. Indeed the total structure factor shows much more pronounced finite-size effects than the quantum and QFI ones. As finite-size effects are apparent for $N \approx \xi$, this property must follow from the fact that the quantum correlation lengths ξ_Q and $\xi_{\rm QFI}$ are smaller than the total $\xi_{\rm tot}$ (although all of them diverge according to $\xi \sim 1/T$). This property allows one to extract the critical exponents more easily from quantum fluctuations than from total ones.

11.4.5 Quantum critical region

We conclude this section with a brief discussion of the structure of the quantum critical region, as witnessed by the scaling of total and quantum fluctuations.

Definition of the quantum critical region. Given the scaling of fluctuations around the QCP

$$\langle \delta^2 S^z \rangle_{\rm tot,Q} = T^{-3/4} f(\Delta/T) \tag{11.64}$$

where $\Delta = 2|1 - g|$ is the gap, the quantum critical region is defined as the region where $T \gg \Delta$, so that $f(\Delta/T) \approx f(0)$

$$\langle \delta^2 S^z \rangle_{\rm tot,Q} = \text{const.} \times T^{-3/4} \, . \tag{11.65}$$

Characterization of the quantum critical region through total or quantum fluctuations. On Fig. 11.8(a), we have plotted the total variance of S^z across the phase diagram for $N = 100$ spins. To quantify quantum fluctuations, we have chosen to compute the Wigner-Yanase "skew information" (Wigner and Yanase, 1963), defined as

$$I_{1/2}(S^z) = \langle (S^z)^2 \rangle - \langle S_z(\beta/2) S_z(0) \rangle \tag{11.66}$$

where $S_z(\beta/2) = e^{\beta/2} S^z e^{-\beta/2}$. The behavior of the skew information is very close to that of the QV and of the QFI, but is simpler to calculate. Indeed these quantities

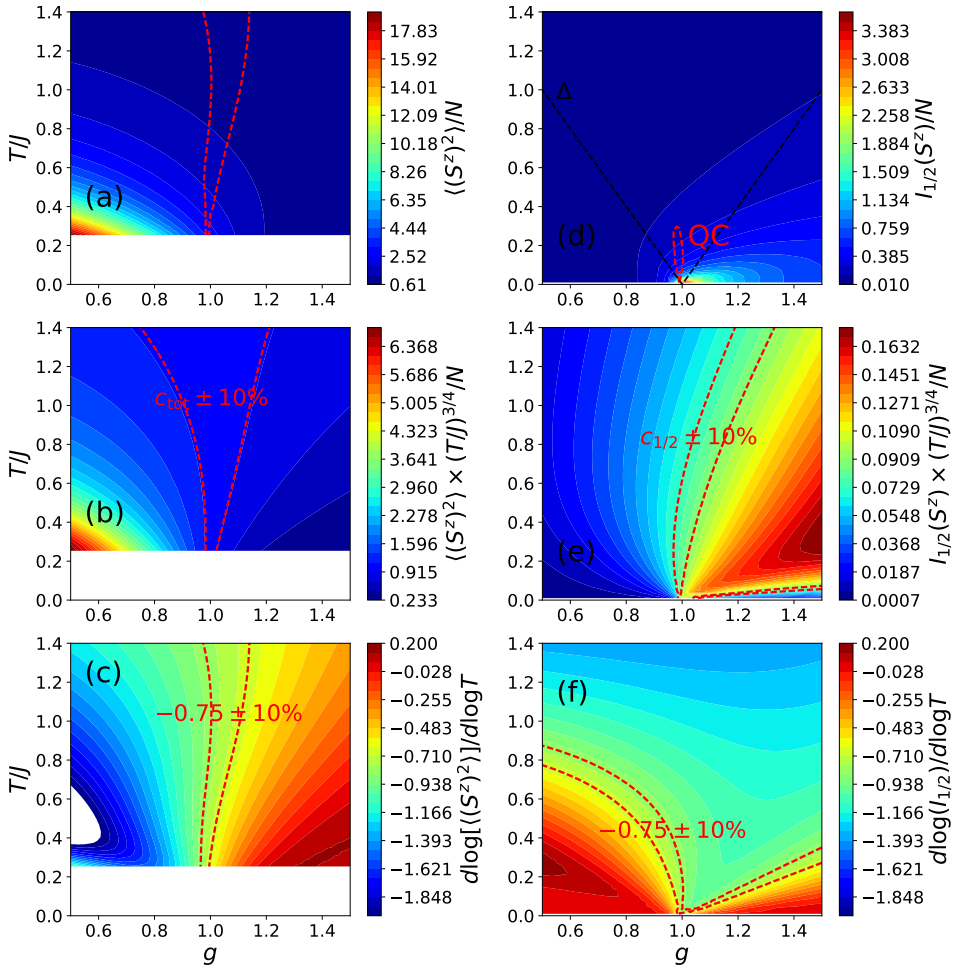

Figure 11.8: Quantum critical region of the Ising chain, for $N = 100$ spins. (a) Total variance of S^z; (b) total variance rescaled to $(T/J)^{-3/4}$; (d) logarithmic derivative $\frac{d \log \langle \delta^2 S^z \rangle}{d \log T}$; (d) skew information of S^z (see text) and (e) rescaled to $(T/J)^{-3/4}$; (f) logarithmic derivative $\frac{d \log I_{1/2}}{d \log T}$. On panels (b) and (e), the red dotted lines mark the region where the rescaled fluctuations are equal to the "plateau" value within 10% (the plateau value is approximated as the value for $g = 1$ and $T/J = 0.3$). On panels (c) and (f), they mark the region where the logarithmic derivative is equal to $\eta - 1 = -0.75$ within 10%. On panel (a) and (d), they mark the intersection of the two above-mentioned regions. The most conservative definition of the quantum critical region is for the quantum fluctuations, and the corresponding region is marked on panel (d), where the black dashed lines indicated the gap. For total fluctuations, data for $T < 0.23$ are not show because they are affected by finite-size effects.

are related by the chain of the inequalities (Section 1.8)

$$\langle \delta^2 S^z \rangle_Q \leq I_{1/2}(S^z) \leq F_Q(S^z)/2 \leq 2I_{1/2}(S^z) \leq 3\langle \delta^2 S^z \rangle_Q \, . \tag{11.67}$$

The skew information takes the form of Eq. (11.52) with the filter $h_{1/2}(x) = \tanh(x/4)$. The skew information is plotted on Fig. 11.8(d). When focusing on total fluctuations (panel a), the quantum critical point is not easy to identify. On the ferromagnetic side $g < 1$, the exponential increase of total fluctuations at low T, discussed in Section 11.3.1, make the QCP very difficult to isolate. Instead, the quantum fluctuations (panel d) are clearly maximal at the QCP. So is the QV (not shown), and the QFI (Hauke et al., 2016).

Multiplying these quantities by $T^{3/4}$ to test the validity of the scaling Ansatz of Eq. (11.64) (panels b and e), we expect to see levels of constant value for $T/|g-1| = \text{const}$. Such lines are indeed visible on the paramagnetic side $g > 1$ for both the total variance and the skew information, but we cannot identify a clear plateau signaling the quantum critical region, as was the case for the Ising model with infinite-range interactions (compare Fig. 11.8 with Fig. 10.6). On panels (b), we have indicated the region where

$$0.9 \, c_{\rm tot} \leq \langle \delta^2 S_z \rangle (T/J)^{3/4}/N \leq 1.1 \, c_{\rm tot} \tag{11.68}$$

with $c_{\rm tot}$ the plateau value given in Eq. 11.60. In practice, to limit finite-size effects, we approximated $c_{\rm tot}$ as $c_{\rm tot} \approx \langle \delta^2 S_z \rangle (T/J)^{3/4}/N$ for $T/J = 0.3$ and $g = 1$. We used a similar definition the skew-information [Fig. 11.8(d)].

To complete the identification of the quantum critical (QC) region, we plot on panels (c) and (f) the logarithmic derivative

$$\frac{d \log \langle \delta^2 S^z \rangle}{d \log T} \approx (\eta - 2)/z + 1 = -3/4 \tag{11.69}$$

in the QC region.

On panels (a), the QC region is then identified as the region where

$$\left| \frac{\langle \delta^2 S^z \rangle T^{3/4}}{N c_{\rm tot}} - 1 \right| < 0.1 \;\; \text{and} \;\; \left| \frac{1}{1 + (\eta - 2)/z} \frac{d \log \langle \delta^2 S^z \rangle}{d \log T} - 1 \right| < 0.1 \tag{11.70}$$

and similarly for panel (c), where the QC region is defined in terms of the skew information. As we see on Fig. 11.8, this naive definition of the QC region leads to overestimate its size. It is clear, for instance, that along $g = 1$, the critical regime terminates for $T/J \approx 0.5$ [see Fig. 11.6)(a)], and not above $T/J = 1.5$. Finite-size effects are also still present for the total fluctuations, which probably alter the prediction with respect to the thermodynamic limit. On the other hand, quantum

fluctuations identify a more restricted QC region. Our findings concerning the extent of the quantum critical region at finite temperature are consistent with the ones of Kopp and Chakravarty (2005), based on the scaling behavior of the free energy.

When going to $d \geq 2$, we recover a "predictive power" of the total and quantum fluctuations similar to the one observed in $d = \infty$ (unpublished quantum Monte Carlo results, courtesy of T. Roscilde).

11.5 QFI vs. spin squeezing

To conclude this chapter, we investigate the potential metrological implications of the strong coherent fluctuations in the vicinity of the quantum critical point (QCP).

Metrological gain and spin squeezing. For the Ising model with infinite-range interactions (which may also be viewed as the Ising model in $d = \infty$), we saw that the approximate equality

$$F_Q(S^z)/N \approx \xi_R^{-2} = \frac{\langle S^x \rangle^2}{N \langle \delta^2 S^y \rangle} \tag{11.71}$$

holds throughout the phase diagram (see Section 10.5, Fig. 10.7 and Fig. 11.9(a) below). The squeezing parameter (Wineland et al., 1994) quantifies the sensitivity of the mean orientation of the collective spin (here along the x axis) with respect to rotations (here, rotations around the z axis). In $d = \infty$, the "metrological usefulness" of the system, quantified in general by the QFI, is completely captured by the squeezing of fluctuations of the collective spin. We argued that this property holds in virtue of the gaussian nature of the fluctuations in $d = \infty$, including at the QCP. It is thus extremely interesting to contrast this $d = \infty$, gaussian behavior, with the behavior of the same model in the opposite $d = 1$ limit, where deviations from the mean-field behavior are expected to be extreme.

Absence of divergence of the squeezing parameter at the QCP. As we show on Fig. 11.9(b), it turns out that the system manifests nearly no squeezing down to the lowest temperatures along the critical trajectory $g = 1$ (or a very weak squeezing, $\xi_R^{-2} \lesssim 2$, which does not scale with N in the limit $N \to \infty$ at the QCP).

Beyond squeezing. The very important and natural question is then to identify the observable whose average value is extremely sensitive to rotations around the z axis. The QFI provides the ultimate sensitivity among all possible observables, but no information on the actual one which has to be measured. As already remarked, at

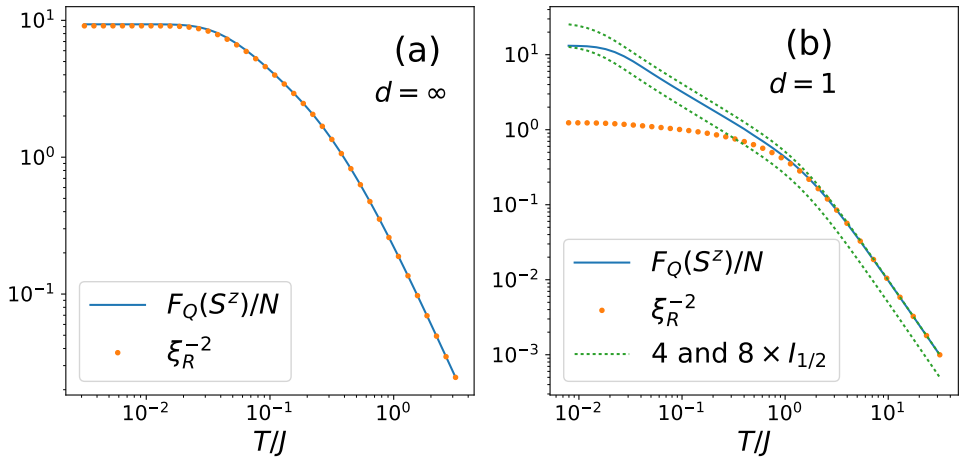

Figure 11.9: Spin squeezing vs. QFI along the quantum critical trajectory. (a) Ising model with infinite-range interactions (see Section 10) for $N = 1000$ spins. The QFI (solid blue line) is completely captured by the squeezing parameter ξ_R^{-2} (orange dots). (b) Ising chain for $N = 50$ spins. The quantum critical scaling is not exhibited by the squeezing parameter. Dashed lines show the "skew information" $I_{1/2} = \langle S^z(0)[S^z(0) - S^z(\beta/2)]\rangle/N$, which bounds the QFI ($4I_{1/2} \leq F_Q \leq 8I_{1/2}$, see Section 1.8), and is much simpler to calculate in practice. Here, we introduced $S^z(\tau) = e^{\tau\mathcal{H}} S^z e^{-\tau\mathcal{H}}$.

the QCP the QFI scales as $F_Q(S^z) \sim N^{7/4}$, almost saturating the Heisenberg limit $F_Q(S^z) = N^2$, obtained with a "Schrödinger-cat state"

$$|\Psi_{\rm cat}\rangle = \frac{1}{\sqrt{2}} \left(\otimes_{i=1}^N |\uparrow_z\rangle_i + \otimes_{i=1}^N |\downarrow_z\rangle_i \right) . \tag{11.72}$$

Actually, this Schrödinger-cat state is very close to the exact ground state for $g < 1$ on a finite-size system, and it is well-known that the metrological usefulness of this state may be exploited by measuring the evolution of the parity of S^x

$$P(\theta) = \langle \prod_{i=1}^N \sigma_i^x \rangle(\theta) \tag{11.73}$$

under rotations around z ($|\Psi_{\rm cat}\rangle(\theta) = e^{-i\theta S^z} |\Psi_{\rm cat}\rangle$) (Bollinger et al., 1996), as demonstrated in trapped-ions experiments (Monz et al., 2011; Leibfried et al., 2005). Indeed, $P(\theta)$ exhibits interference fringes oscillating at a frequency $2\pi/N$, to be compared with the 2π frequency obtained for the Rabi oscillations of uncorrelated spins polarized initially along the x axis. This remark suggests to investigate the evolution of $P(\theta)$ for the Ising chain, and compare the obtained sensitivity with the QFI. We postpone this study to a future work.

Chapter 12

Conclusions, perspectives

During this thesis, we have adopted a quantum statistical mechanics point of view in order to characterize coherent fluctuations and quantum correlations in many-body systems. Our conclusions are threefold.

12.1 General framework to quantify quantum correlations.

Focusing on equilibrium states, we have developed a general framework to quantify quantum fluctuations via standard thermodynamic quantities (namely fluctuations and response functions).

Quantum variance. In this context, the central quantity we have introduced is the *quantum variance* (QV) of an arbitrary observable $\mathcal{O}$

$$\langle \delta^2 \mathcal{O} \rangle_Q = \langle \delta^2 \mathcal{O} \rangle - T \chi_{\mathcal{O}\mathcal{O}} \, , \tag{12.1}$$

defined as difference between the total variance of $\mathcal{O}$ and (T times, with T the temperature) the static susceptibility of $\langle \mathcal{O} \rangle$ with respect to a small perturbation which couples to $\mathcal{O}$ in the Hamiltonian.

Coherent fluctuations. We have shown that the quantum fluctuations, as quantified by the QV, have a coherent nature, and could be probed by interferometric measurements. By doing so, we proved that the QV belongs to a larger family of so-called *coherence measures*, in the sense of quantum information theory. In particular, we argued that the QV of $\mathcal{O}$ is closely related to a central quantity for quantum metrology, the *quantum Fisher information* $F_Q(\mathcal{O})$, quantifying the potential metrological gain

that can be attained if a quantum-correlated many-body system is used as the input of an interferometer in which the unitary evolution is generated by the observable $\mathcal{O}$ in question. Indeed, we proved the following chain of inequalities

$$\langle \delta^2 \mathcal{O} \rangle_Q \leq \frac{F_Q(\mathcal{O})}{4} \leq 3 \langle \delta^2 \mathcal{O} \rangle_Q \, , \tag{12.2}$$

showing that the QV and the quantum Fisher information quantify the same physical property — the quantum uncertainty of $\mathcal{O}$.

Quantum covariance. As a natural extension of the concept of coherent fluctuations, we introduced a physical concept of quantum correlations, namely *correlations among coherent fluctuations*, as quantified by the *quantum covariance* of two observables $\mathcal{O}_1$ and $\mathcal{O}_2$:

$$\langle \delta \mathcal{O}_1 \delta \mathcal{O}_2 \rangle_Q = \frac{1}{2} \left(\langle \delta^2 \mathcal{O}_1 + \mathcal{O}_2 \rangle_Q - \langle \delta^2 \mathcal{O}_1 \rangle_Q - \langle \delta^2 \mathcal{O}_2 \rangle_Q \right) \, . \tag{12.3}$$

Although very natural from the point of view of coherent fluctuations, this physical concept of quantum correlations is independent of previous measures of quantum correlations proposed in the literature.

We can envision several directions for future work:

- To clarify the status of the quantum covariance within quantum information theory is an important perspective open to future studies.
- Once introduced theoretically, quantum correlations beyond (or alternative to) entanglement can be used to characterize both thermal equilibrium states (as done in this thesis) as well as non-equilibrium ones, such as the generalized Gibbs ensemble of integrable quantum systems, or stationary states of the evolution of driven-dissipative systems.
- Furthermore, one can speculate on the possibility to define, beyond the quantum variance, a *probability distribution for quantum fluctuations*. Such a definition is rather straightforward within the path-integral framework for equilibrium states, but in general, it is not obvious that a precise definition (and a precise physical meaning) can be given to this concept. If such a precise definition can be obtained, it would allow to study, *e.g.* possible universal traits in the quantum critical regime, at non-equilibrium quantum phase transitions, etc.

12.2 Entanglement thermodynamics

As a special case of equilibrium states, we have devoted a large part of this thesis to the study of zero-temperature quantum many-body systems. In this context, we have

explored the relationship between quantum fluctuations and entanglement entropy of extended subsystems from a thermodynamic perspective.

Local entanglement temperature. According to the physical picture we have developed, the reduced density matrix of a subsystem A is closely approximated by a thermal state, albeit with a spatially-varying *entanglement temperature* $T(x)$

$$\rho_A \approx \frac{1}{Z} \exp\left(- \int_{x\in A} \frac{\mathcal{H}(x)}{T(x)} \right) \tag{12.4}$$

where $\mathcal{H}(x)$ a uniform Hamiltonian which, under general assumptions, can be thought of as the physical Hamiltonian of the system. This physical picture is inspired by the Bisognano-Wichmann theorem for a Lorentz-invariant quantum field theory, according to which the local temperature is given by

$$T(x') = \frac{c}{2\pi x'} \tag{12.5}$$

with c the speed of light, and x' the distance to the boundary between x and the complement of A.

Local equilibrium approximation. Based on this physical picture, we have been able to relate entanglement entropy and quantum fluctuations via a *local equilibrium approximation*. Central to this approximation is the concept of entanglement and fluctuation *contours*, expressing the local contribution of a portion of a subsystem to the entanglement entropy or quantum fluctuations of extensive observables of the subsystem itself. According to the local equilibrium approximation, the contours at position x are related in the same manner as the corresponding bulk quantities (thermodynamic entropy and fluctuations) would be in an equilibrium state at temperature $T(x)$. Namely, we argued that

$$S \approx \int_{x\in A} s[T(x)] \tag{12.6}$$

where $s(T)$ is the entropy density at temperature T, and similarly for the variance of $\mathcal{O}$:

$$\langle \delta^2 \mathcal{O} \rangle \approx \int_{x\in A} \frac{\langle \delta^2 \mathcal{O} \rangle [T(x)]}{V} \,. \tag{12.7}$$

Reconstruction of the entanglement temperature. We have also shown how the entanglement temperature can be reconstructed from the knowledge of 1) the correlations $\langle \delta\mathcal{O}(x)\delta\mathcal{O}(y)\rangle$ in the ground state; 2) the temperature dependence of $\langle \delta^2\mathcal{O}\rangle(T)$. Indeed, the local temperature $T(x)$ can be extracted from

$$\mathcal{C}_{\mathcal{O}}(x) \equiv \int_{y\in A} \langle \delta\mathcal{O}(x)\delta\mathcal{O}(y)\rangle \approx \frac{\langle \delta^2 \mathcal{O} \rangle [T(x)]}{V} \,, \tag{12.8}$$

where $\mathcal{C}_{\mathcal{O}}(x)$ is the contour associated to the fluctuations of $\mathcal{O}$.

On the side of future perspectives, we observe that the experimental reconstruction of the entanglement temperature would provide a new characterization of quantum many-body systems, and can be envisioned in state-of-the-art cold-atom experiments based on quantum-gas microscopes which can measure, *e.g.* density correlations.

Microscopic understanding of the scaling laws of entanglement and fluctuations in the ground state. Focusing on basic examples of many-body systems (inspired by cold atom experiments), namely free fermions and interacting bosons on a lattice, our thermodynamic approach provided us with a microscopic explanation for the area-law scaling of entanglement entropy and particle-number fluctuations in a subsystem, and for the possible (logarithmic) violation of the area-law.

Free fermions. For free fermions in a gapless phase, we showed that, in compliance with the picture of local equilibrium, the contours for entanglement and for density fluctuations are tightly related by

$$\mathcal{C}_s(x) \approx \frac{\pi^2}{3}\mathcal{C}_N(x) \, . \tag{12.9}$$

Superfluid bosons. For bosons in a superfluid phase, we showed that the entanglement contour is made of two parts: 1) a large-distance universal part that we have predicted analytically, and confirmed numerically

$$\mathcal{C}_s^{\text{large dist.}}(x) \approx \frac{a_d}{x'^d} \tag{12.10}$$

where d is the number of spatial dimensions, and a_d is a universal constant that we have determined analytically; and 2) a short-distance exponential decay uniquely controlled by the healing length ξ_h

$$\mathcal{C}_s^{\text{short dist.}}(x) \sim e^{-x'/\xi_h} \, . \tag{12.11}$$

On the side of perspectives, in a recent work we have studied the consequences of power-law-decaying interactions ($1/r^\alpha$) onto the structure of entanglement and fluctuations in the ground state of the XXZ spin model (Frérot, Naldesi, and Roscilde, 2017a). We have shown that for $d < \alpha < d + 2$, the area-law of the entanglement entropy is preserved, while collective-spin fluctuations acquire a modified scaling behavior controlled by the exponent α. It would be extremely interesting to understand these results from the perspective of entanglement thermodynamics. It would be interesting to see if the local equilibrium hypothesis breaks down due to the non-locality of long-range interactions.

We can also envision the extension of the study of contours in out-of-equilibrium situations (as already discussed by Chen and Vidal (2014)), and define a local instantaneous entanglement temperature thanks to an instantaneous local equilibrium hypothesis. This point of view could shine light on the generic problem of correlation and entanglement spreading after a quantum quench, which we recently addressed in the particular case of a long-range interacting spin model (Frérot, Naldesi, and Roscilde, 2017b).

Entanglement across the superfluid-Mott insulator phase transition. Based on a controlled quadratic approximation to the Bose-Hubbard Hamiltonian (the *slave-boson* approach), we have studied the reorganization of quantum correlations across the paradigmatic superfluid-Mott insulator phase transition for interacting bosons on a lattice. Our main result in this context is the prediction of a sharp cusp for the entanglement entropy at the O(2) transition (namely the transition occurring at fixed, integer filling fraction), that we could attribute to the softening of amplitude fluctuations of the superfluid order parameter upon approaching the transition. This interpretation is based on the strong similarities between the physical spectrum (known to display such an extra soft mode) and the entanglement spectrum.

As future perspectives, we remark that the quantitative link between the cusp singularity of the entanglement entropy and the behavior of the contours remains to be understood. Most importantly, the definition of the entanglement contour beyond the quadratic models we have focused on also represents an important challenge for future works.

12.3 Quantum versus thermal criticality

Absence of divergence of quantum fluctuations at thermal critical points. The general framework we have developed to quantify coherent fluctuations and quantum correlations is especially suited to contrast the physical mechanisms at play close to *thermal* phase transitions (induced by thermal fluctuations), with those at play close to *quantum* phase transitions (induced by quantum fluctuations). In particular, resorting to generic scaling arguments, we have shown that quantum fluctuations are not expected to diverge at thermal critical points. Nonetheless, we showed that they are indeed singular, and that their singular part is governed by the *dynamical critical exponent*, associated to the so-called critical slowing down of the dynamics close to the thermal phase transition.

In the future, it would be very interesting to take advantage of the link between the

singular part of quantum fluctuations at a thermal phase transition and the dynamical critical exponent in order to extract the value of this exponent, either in numerical calculations, in field-theory calculations, or in experiments. This would provide an alternative to the methods probing directly the dynamics of the order parameter.

Divergence at quantum critical points. By focusing on two exactly solvable limits of the paradigmatic Ising model in a transverse field (namely the infinite-range limit and the $d = 1$ Ising chain with nearest-neighbor interactions), we have shown that quantum fluctuations diverge at the quantum critical point (QCP), and only there — in particular they do not diverge at thermal phase transitions, in agreement with the arguments of scaling theory.

Moreover, we have proposed to define the *quantum critical region* (namely the finite-temperature region in which the scaling of fluctuations is governed by the critical exponents of the QCP) in terms of the scaling behavior of quantum fluctuations, as captured *e.g.* by the quantum variance. This definition allowed us to identify in a clean manner the quantum critical region, in comparison to the characterization based on a similar definition for the total fluctuations — as the latter are also affected by thermal criticality, if present.

In this respect, the study of quantum critical regions from the perspective of quantum fluctuations for the Ising model in dimensions $d = 2, 3$, and for other classes of models, represents an exciting perspective open to future works.

Quantum versus total correlation length. The spatial structure of quantum correlations at finite temperature can be characterized by a *quantum correlation length* ξ_Q, defined through

$$\langle \delta\mathcal{O}_i \delta\mathcal{O}_j \rangle_Q \sim e^{-r_{ij}/\xi_Q} \ , \tag{12.12}$$

in a similar manner as what is done for total correlations:

$$\langle \delta\mathcal{O}_i \delta\mathcal{O}_j \rangle_{\rm tot} \sim e^{-r_{ij}/\xi_{\rm tot}} \ . \tag{12.13}$$

The comparison of the quantum and total correlation lengths shows the generic hierarchy

$$\xi_Q < \xi_{\rm tot} \ . \tag{12.14}$$

While the total correlation length diverges at thermal phase transitions, the quantum correlation length remains finite at such transitions. Approaching a quantum critical point, we have observed for the quantum Ising chain that the two correlation lengths diverge with the same critical exponents, and that the total correlation length is about one order of magnitude larger than the quantum one.

In principle, the quantum fluctuations could be studied in various experimental platforms. Cold atom experiments equipped with a quantum gas microscope, and where arbitrary-shape optical potentials can be engineered, could access the quantum variance and covariance. Bragg-scattering experiments, where the dynamical susceptibilities are measured, could as well access the coherent part of fluctuations.

Correlation-assisted interferometry with equilibrium many-body states? At a quantum critical point, quantum fluctuations diverge with the number of individual components of the system. As a consequence, we can predict that the corresponding quantum critical states are resources for interferometric measurements of very small fields which couple to the order parameter of the QCP, allowing to overcome the so-called standard quantum limit achievable with classically-correlated probes. In the case of the infinitely-connected Ising model, we showed that this can be realized by taking advantage of the *squeezing* of fluctuations in the direction transverse to the order parameter. For the $d = 1$ Ising chain, although the potential metrological gain is extremely large (as quantified by the quantum Fisher information), we could not identify the optimal protocol to exploit it.

Quantum critical points offer a largely unexplored playground for quantum interferometry. The perspective to characterize, both theoretically and experimentally, the strong quantum cooperative behaviors which develop close to quantum critical points, to do so in terms of quantities without a classical analog (namely quantum (co)-variances), via protocols which themselves lack of a classical analog (namely interferometric protocols), is evidently very exciting.

Bibliography

Adesso, Gerardo, Thomas R Bromley, and Marco Cianciaruso (2016). "Measures and applications of quantum correlations". In: *Journal of Physics A: Mathematical and Theoretical* 49.47, p. 473001. URL: http://stacks.iop.org/1751-8121/49/i=47/a=473001 (cit. on pp. 46, 50).

Alba, Vincenzo, Masudul Haque, and Andreas M. Läuchli (2013). "Entanglement Spectrum of the Two-Dimensional Bose-Hubbard Model". In: *Phys. Rev. Lett.* 110 (26), p. 260403. DOI: 10.1103/PhysRevLett.110.260403. URL: http://link.aps.org/doi/10.1103/PhysRevLett.110.260403 (cit. on pp. 105, 169).

Altman, Ehud and Assa Auerbach (2002). "Oscillating Superfluidity of Bosons in Optical Lattices". In: *Phys. Rev. Lett.* 89 (25), p. 250404. DOI: 10.1103/PhysRevLett.89.250404. URL: http://link.aps.org/doi/10.1103/PhysRevLett.89.250404 (cit. on p. 111).

Altman, Ehud et al. (2003). "Phase diagram of two-component bosons on an optical lattice". In: *New Journal of Physics* 5.1, p. 113. URL: http://stacks.iop.org/1367-2630/5/i=1/a=113 (cit. on p. 111).

Amico, Luigi et al. (2008). "Entanglement in many-body systems". In: *Rev. Mod. Phys.* 80 (2), pp. 517–576. DOI: 10.1103/RevModPhys.80.517. URL: https://link.aps.org/doi/10.1103/RevModPhys.80.517 (cit. on p. 56).

Anderson, P. W. (1966). "Considerations on the Flow of Superfluid Helium". In: *Rev. Mod. Phys.* 38 (2), pp. 298–310. DOI: 10.1103/RevModPhys.38.298. URL: https://link.aps.org/doi/10.1103/RevModPhys.38.298 (cit. on p. 108).

Araki, Huzihiro and Elliott H. Lieb (1970). “Entropy inequalities”. In: *Comm. Math. Phys.* 18.2, pp. 160–170. URL: http://projecteuclid.org/euclid.cmp/1103842506 (cit. on p. 60).

Arecchi, F. T. et al. (1972). “Atomic Coherent States in Quantum Optics”. In: *Phys. Rev. A* 6 (6), pp. 2211–2237. DOI: 10.1103/PhysRevA.6.2211. URL: https://link.aps.org/doi/10.1103/PhysRevA.6.2211 (cit. on p. 204).

Aspect, Alain, Philippe Grangier, and Gérard Roger (1982). “Experimental Realization of Einstein-Podolsky-Rosen-Bohm Gedankenexperiment: A New Violation of Bell’s Inequalities”. In: *Phys. Rev. Lett.* 49 (2), pp. 91–94. DOI: 10.1103/PhysRevLett.49.91. URL: http://link.aps.org/doi/10.1103/PhysRevLett.49.91 (cit. on p. 44).

Astrakharchik, G. E., R. Combescot, and L. P. Pitaevskii (2007). “Fluctuations of the number of particles within a given volume in cold quantum gases”. In: *Phys. Rev. A* 76 (6), p. 063616. DOI: 10.1103/PhysRevA.76.063616. URL: http://link.aps.org/doi/10.1103/PhysRevA.76.063616 (cit. on p. 68).

Augusiak, R., M. Demianowicz, and A. Acín (2014). “Local hiddenvariable models for entangled quantum states”. In: *Journal of Physics A: Mathematical and Theoretical* 47.42, p. 424002. URL: http://stacks.iop.org/1751-8121/47/i=42/a=424002 (cit. on p. 44).

Bakr, W. S. et al. (2009). “A quantum gas microscope for detecting single atoms in a Hubbard-regime optical lattice”. In: *Nature* 462, p. 74 (cit. on p. 100).

Bekenstein, J. D. (1973). “Black Holes and Entropy”. In: *Phys. Rev. B* 7, pp. 2333–2346. DOI: 10.1103/PhysRevD.7.2333 (cit. on p. 71).

Bell, John S. (1964). “On the Einstein Podolski Rosen paradox”. In: *Physics* 1 (3), pp. 195–200 (cit. on p. 44).

Bengtsson, I. and K. Zyczkowski (2007). *Geometry of Quantum States: An Introduction to Quantum Entanglement*. Cambridge University Press. ISBN: 9781139453462 (cit. on p. 26).

Bernigau, H, M J Kastoryano, and J Eisert (2015). “Mutual information area laws for thermal free fermions”. In: *Journal of Statistical Mechanics: Theory and Experiment* 2015.2, P02008. URL: http://stacks.iop.org/1742-5468/2015/i=2/a=P02008 (cit. on p. 187).

Bisognano, J.J. and E.W. Wichmann (1976). “On the duality condition for quantum fields”. In: *Journal of Mathematical Physics* 17.3, pp. 303–321. DOI: 10.1063/

1.522898. URL: http://aip.scitation.org/doi/abs/10.1063/1.522898 (cit. on pp. 71, 74).

Biswas, T., M. García Díaz, and A. Winter (2017). "Interferometric visibility and coherence". In: *ArXiv e-prints*. arXiv: 1701.05051 [quant-ph] (cit. on p. 18).

Blaizot, J.P. and G. Ripka (1986). *Quantum Theory of Finite Systems*. The MIT Press, Cambridge, MA. ISBN: 9780262022149 (cit. on pp. 79, 117–120, 124, 180, 229, 231).

Bloch, Immanuel, Jean Dalibard, and Wilhelm Zwerger (2008). "Many-body physics with ultracold gases". In: *Rev. Mod. Phys.* 80 (3), pp. 885–964. DOI: 10.1103/RevModPhys.80.885. URL: https://link.aps.org/doi/10.1103/RevModPhys.80.885 (cit. on pp. 103, 104).

Bohm, David (1952). "A Suggested Interpretation of the Quantum Theory in Terms of "Hidden" Variables. I and II". In: *Phys. Rev.* 85 (2), pp. 166–193. DOI: 10.1103/PhysRev.85.166. URL: http://link.aps.org/doi/10.1103/PhysRev.85.166 (cit. on p. 44).

Bohnet, Justin G. et al. (2016). "Quantum spin dynamics and entanglement generation with hundreds of trapped ions". In: *Science* 352.6291, pp. 1297–1301. ISSN: 0036-8075. DOI: 10.1126/science.aad9958. eprint: http://science.sciencemag.org/content/352/6291/1297.full.pdf. URL: http://science.sciencemag.org/content/352/6291/1297 (cit. on p. 224).

Bohr, Niels (1928). "The Quantum Postulate and the recent Development of Atomic Theory". In: *Nature* 121. Reprinted in Quantum Theory and Measurement, J. A. Wheeler and W. H. Zurek (Editors), Princeton University Press (1983), pp. 580–90 (cit. on p. 13).

Boll, Martin et al. (2016). "Spin- and density-resolved microscopy of antiferromagnetic correlations in Fermi-Hubbard chains". In: *Science* 353.6305, pp. 1257–1260. ISSN: 0036-8075. DOI: 10.1126/science.aag1635. eprint: http://science.sciencemag.org/content/353/6305/1257.full.pdf. URL: http://science.sciencemag.org/content/353/6305/1257 (cit. on p. 101).

Bollinger, J. J . et al. (1996). "Optimal frequency measurements with maximally correlated states". In: *Phys. Rev. A* 54 (6), R4649–R4652. DOI: 10.1103/PhysRevA.54.R4649. URL: https://link.aps.org/doi/10.1103/PhysRevA.54.R4649 (cit. on p. 251).

Born, Max (1926). “Zur Quantenmechanik der Stossvorgänge”. In: *Zeitschrift für Physik* 37. English translation in Quantum Theory and Measurement, J. A. Wheeler and W. H. Zurek (Editors), Princeton University Press (1983), pp. 863–67 (cit. on p. 13).

Botet, R., R. Jullien, and P. Pfeuty (1982). “Size Scaling for Infinitely Coordinated Systems”. In: *Phys. Rev. Lett.* 49 (7), pp. 478–481. DOI: 10.1103/PhysRevLett.49.478. URL: https://link.aps.org/doi/10.1103/PhysRevLett.49.478 (cit. on pp. 213, 215).

Brunner, Nicolas et al. (2014). “Bell nonlocality”. In: *Rev. Mod. Phys.* 86 (2), pp. 419–478. DOI: 10.1103/RevModPhys.86.419. URL: http://link.aps.org/doi/10.1103/RevModPhys.86.419 (cit. on pp. 44, 46).

Calabrese, Pasquale and John Cardy (2004). “Entanglement entropy and quantum field theory”. In: *Journal of Statistical Mechanics: Theory and Experiment* 2004.06, P06002. URL: http://stacks.iop.org/1742-5468/2004/i=06/a=P06002 (cit. on pp. 63, 67, 157, 170, 171).

Calabrese, Pasquale, Mihail Mintchev, and Ettore Vicari (2012). “Exact relations between particle fluctuations and entanglement in Fermi gases”. In: *EPL (Europhysics Letters)* 98.2, p. 20003. URL: http://stacks.iop.org/0295-5075/98/i=2/a=20003 (cit. on pp. 56, 66, 67).

Callen, Herbert B. and Theodore A. Welton (1951). “Irreversibility and Generalized Noise”. In: *Phys. Rev.* 83 (1), pp. 34–40. DOI: 10.1103/PhysRev.83.34. URL: http://link.aps.org/doi/10.1103/PhysRev.83.34 (cit. on pp. 29, 233).

Casini, H and M Huerta (2009). “Entanglement entropy in free quantum field theory”. In: *Journal of Physics A: Mathematical and Theoretical* 42.50, p. 504007. URL: http://stacks.iop.org/1751-8121/42/i=50/a=504007 (cit. on p. 137).

Cavalcanti, D. and P. Skrzypczyk (2017). “Quantum steering: a review with focus on semidefinite programming”. In: *Reports on Progress in Physics* 80.2, p. 024001. URL: http://stacks.iop.org/0034-4885/80/i=2/a=024001 (cit. on p. 44).

Chandran, Anushya, Vedika Khemani, and S. L. Sondhi (2014). “How Universal Is the Entanglement Spectrum?” In: *Phys. Rev. Lett.* 113 (6), p. 060501. DOI: 10.1103/PhysRevLett.113.060501. URL: https://link.aps.org/doi/10.1103/PhysRevLett.113.060501 (cit. on p. 92).

Chen, Y. and G. Vidal (2014). “Entanglement contour”. In: *Journal of Statistical Mechanics: Theory and Experiment* 10, 10011, p. 10011. DOI: 10.1088/1742-

5468/2014/10/P10011. arXiv: 1406.1471 [cond-mat.str-el] (cit. on pp. 57, 76, 80–82, 100, 125, 257).

Coletta, Tommaso, Nicolas Laflorencie, and Frédéric Mila (2012). "Semiclassical approach to ground-state properties of hard-core bosons in two dimensions". In: *Phys. Rev. B* 85 (10), p. 104421. DOI: 10.1103/PhysRevB.85.104421. URL: http://link.aps.org/doi/10.1103/PhysRevB.85.104421 (cit. on pp. 105, 110, 122, 133, 207, 208).

Collins, M.F. (1989). *Magnetic Critical Scattering*. Oxford Series on Neutron Scattering in Condensed Matter. Oxford University Press. ISBN: 9780195364408 (cit. on pp. 37–39, 189, 194).

Coser, A., C. De Nobili, and E. Tonni (2017). "A contour for the entanglement entropies in harmonic lattices". In: *ArXiv e-prints*. arXiv: 1701.08427 [cond-mat.stat-mech] (cit. on pp. 80, 125–127, 129, 139–141).

Das, Arnab et al. (2006). "Infinite-range Ising ferromagnet in a time-dependent transverse magnetic field: Quench and ac dynamics near the quantum critical point". In: *Phys. Rev. B* 74 (14), p. 144423. DOI: 10.1103/PhysRevB.74.144423. URL: https://link.aps.org/doi/10.1103/PhysRevB.74.144423 (cit. on pp. 205, 207).

Davisson, C J and L H Germer (1928). "Reflection of Electrons by a Crystal of Nickel". In: *Proceedings of the National Academy of Sciences of the United States of America* 14.4, pp. 317–322 (cit. on p. 13).

Dickerscheid, D. B. M. et al. (2003). "Ultracold atoms in optical lattices". In: *Phys. Rev. A* 68 (4), p. 043623. DOI: 10.1103/PhysRevA.68.043623. URL: http://link.aps.org/doi/10.1103/PhysRevA.68.043623 (cit. on p. 111).

Ding, Wenxin and Kun Yang (2009). "Entanglement entropy and mutual information in Bose-Einstein condensates". In: *Phys. Rev. A* 80 (1), p. 012329. DOI: 10.1103/PhysRevA.80.012329. URL: http://link.aps.org/doi/10.1103/PhysRevA.80.012329 (cit. on p. 169).

Diu, B., D. Lederer, and B. Roulet (1996). *Éléments de Physique Statistique*. Hermann. ISBN: 2705660658 (cit. on pp. 67, 68).

Dusuel, Sébastien and Julien Vidal (2004). "Finite-Size Scaling Exponents of the Lipkin-Meshkov-Glick Model". In: *Phys. Rev. Lett.* 93 (23), p. 237204. DOI: 10.1103/PhysRevLett.93.237204. URL: https://link.aps.org/doi/10.1103/PhysRevLett.93.237204 (cit. on pp. 206, 209, 210).

— (2005). “Continuous unitary transformations and finite-size scaling exponents in the Lipkin-Meshkov-Glick model”. In: *Phys. Rev. B* 71 (22), p. 224420. DOI: 10.1103/PhysRevB.71.224420. URL: https://link.aps.org/doi/10.1103/PhysRevB.71.224420 (cit. on pp. 206, 209, 210).

Einstein, A., B. Podolsky, and N. Rosen (1935). “Can Quantum-Mechanical Description of Physical Reality Be Considered Complete?” In: *Phys. Rev.* 47 (10), pp. 777–780. DOI: 10.1103/PhysRev.47.777. URL: http://link.aps.org/doi/10.1103/PhysRev.47.777 (cit. on p. 44).

Einstein, Albert (1905). “Über einen die Erzeugung und Verwandlung des Lichtes betreffenden heuristischen Gesichtspunkt”. In: *Annalen der Physik* 17. English translation in ”The Old Quantum Theory”, D. ter Haar, Pergamon press (1967), pp. 132–148 (cit. on p. 13).

Eisert, J., M. Cramer, and M. B. Plenio (2010). “*Colloquium* : Area laws for the entanglement entropy”. In: *Rev. Mod. Phys.* 82 (1), pp. 277–306. DOI: 10.1103/RevModPhys.82.277. URL: http://link.aps.org/doi/10.1103/RevModPhys.82.277 (cit. on pp. 56, 62).

Eisler, V. and I. Peschel (2017). “Analytical results for the entanglement Hamiltonian of a free-fermion chain”. In: *ArXiv e-prints*. arXiv: 1703.08126 [cond-mat.stat-mech] (cit. on p. 86).

Endres, Manuel et al. (2012). “The /‘Higgs/’ amplitude mode at the two-dimensional superfluid/Mott insulator transition”. In: *Nature* 487.7408, pp. 454–458. URL: http://dx.doi.org/10.1038/nature11255 (cit. on p. 122).

Feynman, R.P. and A.R. Hibbs (1965). *Quantum mechanics and path integrals*. International series in pure and applied physics. McGraw-Hill (cit. on pp. 32, 33).

Fisher, Matthew P. A. et al. (1989). “Boson localization and the superfluid-insulator transition”. In: *Phys. Rev. B* 40 (1), pp. 546–570. DOI: 10.1103/PhysRevB.40.546. URL: https://link.aps.org/doi/10.1103/PhysRevB.40.546 (cit. on pp. 104, 105, 109, 170).

Forster, D. (1995). *Hydrodynamic Fluctuations, Broken Symmetry, and Correlation Functions*. Advanced book classics. Avalon Publishing. ISBN: 9780201410495 (cit. on pp. 28, 29, 233).

Frérot, Irénée, Piero Naldesi, and Tommaso Roscilde (2017a). “Entanglement and fluctuations in the XXZ model with power-law interactions”. In: *Phys. Rev. B* 95 (24), p. 245111. DOI: 10.1103/PhysRevB.95.245111. URL: https://link.aps.org/doi/10.1103/PhysRevB.95.245111 (cit. on p. 256).

— (2017b). “Multi-speed prethermalization in spin models with power-law decaying interactions”. In: *ArXiv e-prints*. arXiv: 1704.04461 [cond-mat.quant-gas] (cit. on p. 257).

Frérot, Irénée and Tommaso Roscilde (2015). “Area law and its violation: A microscopic inspection into the structure of entanglement and fluctuations”. In: *Phys. Rev. B* 92 (11), p. 115129. DOI: 10.1103/PhysRevB.92.115129. URL: https://link.aps.org/doi/10.1103/PhysRevB.92.115129 (cit. on pp. 54, 57, 68, 76, 80–82, 87, 120, 125, 126, 129, 136, 137, 139–141, 144, 167, 169).

— (2016a). “Entanglement Entropy across the Superfluid-Insulator Transition: A Signature of Bosonic Criticality”. In: *Phys. Rev. Lett.* 116 (19), p. 190401. DOI: 10.1103/PhysRevLett.116.190401. URL: https://link.aps.org/doi/10.1103/PhysRevLett.116.190401 (cit. on pp. 54, 157, 169).

— (2016b). “Quantum variance: A measure of quantum coherence and quantum correlations for many-body systems”. In: *Phys. Rev. B* 94 (7), p. 075121. DOI: 10.1103/PhysRevB.94.075121. URL: http://link.aps.org/doi/10.1103/PhysRevB.94.075121 (cit. on pp. 32, 33, 89, 130, 186, 187).

Frésard, R. (1994). “Slave Boson Formulation for Interacting Boson Systems and the Superfluid-Insulator Transition”. In: *eprint arXiv:cond-mat/9405053*. eprint: cond-mat/9405053 (cit. on p. 111).

Gibilisco, P., D. Imparato, and T. Isola (2009). “Inequalities for quantum Fisher information”. In: *Proc. Amer. Math. Soc.* 137, pp. 317–27. (Cit. on p. 27).

Gioev, Dimitri and Israel Klich (2006). “Entanglement Entropy of Fermions in Any Dimension and the Widom Conjecture”. In: *Phys. Rev. Lett.* 96 (10), p. 100503. DOI: 10.1103/PhysRevLett.96.100503. URL: http://link.aps.org/doi/10.1103/PhysRevLett.96.100503 (cit. on p. 63).

Giustina, Marissa et al. (2015). “Significant-Loophole-Free Test of Bell’s Theorem with Entangled Photons”. In: *Phys. Rev. Lett.* 115 (25), p. 250401. DOI: 10.1103/PhysRevLett.115.250401. URL: http://link.aps.org/doi/10.1103/PhysRevLett.115.250401 (cit. on p. 44).

Greiner, Markus et al. (2002). “Quantum phase transition from a superfluid to a Mott insulator in a gas of ultracold atoms”. In: *Nature* 415.6867, pp. 39–44. URL: http://dx.doi.org/10.1038/415039a (cit. on pp. 103, 105).

Hansen, Frank (2008). “Metric adjusted skew information”. In: *Proceedings of the National Academy of Sciences* 105.29, pp. 9909–9916. DOI: 10.1073/pnas.

0803323105. eprint: http://www.pnas.org/content/105/29/9909.full.pdf. URL: http://www.pnas.org/content/105/29/9909.abstract (cit. on p. 34).

Hastings, Matthew B. et al. (2010). "Measuring Renyi Entanglement Entropy in Quantum Monte Carlo Simulations". In: *Phys. Rev. Lett.* 104 (15), p. 157201. DOI: 10.1103/PhysRevLett.104.157201. URL: http://link.aps.org/doi/10.1103/PhysRevLett.104.157201 (cit. on pp. 68, 137).

Hauke, Philipp et al. (2016). "Measuring multipartite entanglement through dynamic susceptibilities". In: *Nat Phys* 12.8, pp. 778–782. URL: http://dx.doi.org/10.1038/nphys3700 (cit. on pp. 28, 36, 194, 195, 215, 220, 225, 227, 232, 249).

Hawking, S. W. (1974). "Black hole explosions?" In: *Nature* 248, pp. 30–31. DOI: 10.1038/248030a0 (cit. on p. 71).

Heisenberg, Werner (1927). "Über der anschaulichen Inhalt der quantentheoretischen Kinematik und Mechanik". In: *Zeitschrift für Physik* 43. English translation in Quantum Theory and Measurement, J. A. Wheeler and W. H. Zurek (Editors), Princeton University Press (1983), pp. 172–98 (cit. on p. 13).

Helmes, Johannes and Stefan Wessel (2014). "Entanglement entropy scaling in the bilayer Heisenberg spin system". In: *Phys. Rev. B* 89 (24), p. 245120. DOI: 10.1103/PhysRevB.89.245120. URL: http://link.aps.org/doi/10.1103/PhysRevB.89.245120 (cit. on p. 171).

Henderson, L. and V. Vedral (2001). "Classical, quantum and total correlations". In: *Journal of Physics A Mathematical General* 34, pp. 6899–6905. DOI: 10.1088/0305-4470/34/35/315. eprint: quant-ph/0105028 (cit. on pp. 45, 46).

Hensen, B. et al. (2015). "Loophole-free Bell inequality violation using electron spins separated by 1.3 kilometers". In: *Nature* 526, pp. 682–686. DOI: 10.1038/nature15759 (cit. on p. 44).

Herdman, C. M. et al. (2016). "Entanglement area law in superfluid ^{4}He". In: *ArXiv e-prints*. arXiv: 1610.08518 [cond-mat.other] (cit. on p. 68).

Hohenberg, P. C. and B. I. Halperin (1977). "Theory of dynamic critical phenomena". In: *Rev. Mod. Phys.* 49 (3), pp. 435–479. DOI: 10.1103/RevModPhys.49.435. URL: https://link.aps.org/doi/10.1103/RevModPhys.49.435 (cit. on pp. 37–39, 189, 202).

Holstein, T. and H. Primakoff (1940). "Field Dependence of the Intrinsic Domain Magnetization of a Ferromagnet". In: *Phys. Rev.* 58 (12), pp. 1098–1113. DOI: 10.1103/PhysRev.58.1098. URL: http://link.aps.org/doi/10.1103/PhysRev.58.1098 (cit. on p. 133).

Horodecki, Ryszard and Michal/ Horodecki (1996). “Information-theoretic aspects of inseparability of mixed states”. In: *Phys. Rev. A* 54 (3), pp. 1838–1843. DOI: 10.1103/PhysRevA.54.1838. URL: https://link.aps.org/doi/10.1103/PhysRevA.54.1838 (cit. on p. 60).

Horodecki, Ryszard et al. (2009). “Quantum Entanglement”. In: *Rev. Mod. Phys.* 81 (2), pp. 865–942. DOI: 10.1103/RevModPhys.81.865. URL: http://link.aps.org/doi/10.1103/RevModPhys.81.865 (cit. on pp. 44, 60).

Huang, K. (1987). *Statistical mechanics*. Wiley. ISBN: 9780471815181 (cit. on pp. 67, 68).

Huber, S. D. et al. (2007). “Dynamical properties of ultracold bosons in an optical lattice”. In: *Phys. Rev. B* 75 (8), p. 085106. DOI: 10.1103/PhysRevB.75.085106. URL: http://link.aps.org/doi/10.1103/PhysRevB.75.085106 (cit. on p. 111).

Huerga, Daniel, Jorge Dukelsky, and Gustavo E. Scuseria (2013). “Composite Boson Mapping for Lattice Boson Systems”. In: *Phys. Rev. Lett.* 111 (4), p. 045701. DOI: 10.1103/PhysRevLett.111.045701. URL: http://link.aps.org/doi/10.1103/PhysRevLett.111.045701 (cit. on pp. 111, 117).

Humeniuk, Stephan and Tommaso Roscilde (2012). “Quantum Monte Carlo calculation of entanglement Rényi entropies for generic quantum systems”. In: *Phys. Rev. B* 86 (23), p. 235116. DOI: 10.1103/PhysRevB.86.235116. URL: http://link.aps.org/doi/10.1103/PhysRevB.86.235116 (cit. on pp. 68, 137).

Hyllus, Philipp et al. (2012). “Fisher information and multiparticle entanglement”. In: *Phys. Rev. A* 85 (2), p. 022321. DOI: 10.1103/PhysRevA.85.022321. URL: https://link.aps.org/doi/10.1103/PhysRevA.85.022321 (cit. on pp. 51, 196, 220).

Islam, R. et al. (2011). “Onset of a quantum phase transition with a trapped ion quantum simulator”. In: 2, 377 EP –. URL: http://dx.doi.org/10.1038/ncomms1374 (cit. on p. 224).

Islam, Rajibul et al. (2015). “Measuring entanglement entropy in a quantum many-body system”. In: *Nature* 528.7580, pp. 77–83. URL: http://dx.doi.org/10.1038/nature15750 (cit. on p. 60).

Jammer, Max (1966). *The Conceptual Development of Quantum Mechanics*. International series in pure and applied physics. McGraw-Hill (cit. on p. 13).

Kallin, Ann B. et al. (2011). “Anomalies in the entanglement properties of the square-lattice Heisenberg model”. In: *Phys. Rev. B* 84 (16), p. 165134. DOI: 10.1103/

PhysRevB.84.165134. URL: http://link.aps.org/doi/10.1103/PhysRevB.84.165134 (cit. on pp. 68, 137).

Kamenev, A. (2011). *Field Theory of Non-Equilibrium Systems*. Cambridge University Press. ISBN: 9781139500296 (cit. on pp. 37–39, 189, 202).

Kardar, M. (2007). *Statistical Physics of Fields*. Cambridge University Press. ISBN: 9780521873413 (cit. on p. 171).

Kim, K. et al. (2011). "Quantum simulation of the transverse Ising model with trapped ions". In: *New Journal of Physics* 13.10, p. 105003. URL: http://stacks.iop.org/1367-2630/13/i=10/a=105003 (cit. on p. 228).

Kinross, A. W. et al. (2014). "Evolution of Quantum Fluctuations Near the Quantum Critical Point of the Transverse Field Ising Chain System $CoNb_2O_6$". In: *Phys. Rev. X* 4 (3), p. 031008. DOI: 10.1103/PhysRevX.4.031008. URL: https://link.aps.org/doi/10.1103/PhysRevX.4.031008 (cit. on p. 228).

Klawunn, M. et al. (2011). "Local atom-number fluctuations in quantum gases at finite temperature". In: *Phys. Rev. A* 84 (3), p. 033612. DOI: 10.1103/PhysRevA.84.033612. URL: http://link.aps.org/doi/10.1103/PhysRevA.84.033612 (cit. on p. 68).

Kopp, Angela and Sudip Chakravarty (2005). "Criticality in correlated quantum matter". In: *Nat Phys* 1.1, pp. 53–56. URL: http://dx.doi.org/10.1038/nphys105 (cit. on p. 250).

Laflorencie, Nicolas (2016). "Quantum entanglement in condensed matter systems". In: *Physics Reports* 646, pp. 1–59. ISSN: 0370-1573. DOI: http://dx.doi.org/10.1016/j.physrep.2016.06.008. URL: http://www.sciencedirect.com/science/article/pii/S0370157316301582 (cit. on pp. 56, 68, 137).

Laflorencie, Nicolas and Stephan Rachel (2014). "Spin-resolved entanglement spectroscopy of critical spin chains and Luttinger liquids". In: *Journal of Statistical Mechanics: Theory and Experiment* 2014.11, P11013. URL: http://stacks.iop.org/1742-5468/2014/i=11/a=P11013 (cit. on pp. 56, 66).

Leibfried, D. et al. (2005). "Creation of a six-atom /'Schrodinger cat/' state". In: *Nature* 438.7068, pp. 639–642. URL: http://dx.doi.org/10.1038/nature04251 (cit. on p. 251).

Lewenstein, M., A. Sanpera, and V. Ahufinger (2012). *Ultracold Atoms in Optical Lattices: Simulating quantum many-body systems*. OUP Oxford. ISBN: 9780191627439 (cit. on p. 107).

Li, Hui and F. D. M. Haldane (2008). “Entanglement Spectrum as a Generalization of Entanglement Entropy: Identification of Topological Order in Non-Abelian Fractional Quantum Hall Effect States”. In: *Phys. Rev. Lett.* 101 (1), p. 010504. DOI: 10.1103/PhysRevLett.101.010504. URL: https://link.aps.org/doi/10.1103/PhysRevLett.101.010504 (cit. on p. 65).

Lieb, Elliott H. and Mary Beth Ruskai (1973). “Proof of the strong subadditivity of quantummechanical entropy”. In: *Journal of Mathematical Physics* 14.12, pp. 1938–1941. DOI: 10.1063/1.1666274. eprint: http://dx.doi.org/10.1063/1.1666274. URL: http://dx.doi.org/10.1063/1.1666274 (cit. on p. 59).

Lieb, Elliott, Theodore Schultz, and Daniel Mattis (1961). “Two soluble models of an antiferromagnetic chain”. In: *Annals of Physics* 16.3, pp. 407 –466. ISSN: 0003-4916. DOI: http://dx.doi.org/10.1016/0003-4916(61)90115-4. URL: http://www.sciencedirect.com/science/article/pii/0003491661901154 (cit. on pp. 228, 229).

Luitz, David J. et al. (2015). “Universal logarithmic corrections to entanglement entropies in two dimensions with spontaneously broken continuous symmetries”. In: *Phys. Rev. B* 91 (15), p. 155145. DOI: 10.1103/PhysRevB.91.155145. URL: http://link.aps.org/doi/10.1103/PhysRevB.91.155145 (cit. on pp. 68, 169).

Malpetti, Daniele (2016). “Thermodynamics of strongly interacting bosons on a lattice : new insights and numerical approaches”. PhD thesis. Université de Lyon. URL: https://tel.archives-ouvertes.fr/tel-01451352 (cit. on pp. 32, 33, 228).

Malpetti, Daniele and Tommaso Roscilde (2016). “Quantum Correlations, Separability, and Quantum Coherence Length in Equilibrium Many-Body Systems”. In: *Phys. Rev. Lett.* 117 (13), p. 130401. DOI: 10.1103/PhysRevLett.117.130401. URL: http://link.aps.org/doi/10.1103/PhysRevLett.117.130401 (cit. on pp. 49, 52, 196, 197, 228, 232, 234).

Marvian, Iman and Robert W. Spekkens (2014). “Extending Noether’s theorem by quantifying the asymmetry of quantum states”. In: *Nature Communications* 5, 3821 EP –. URL: http://dx.doi.org/10.1038/ncomms4821 (cit. on p. 24).

— (2016). “How to quantify coherence: Distinguishing speakable and unspeakable notions”. In: *Phys. Rev. A* 94 (5), p. 052324. DOI: 10.1103/PhysRevA.94.052324. URL: http://link.aps.org/doi/10.1103/PhysRevA.94.052324 (cit. on p. 23).

Metlitski, M. A. and T. Grover (2011). "Entanglement Entropy of Systems with Spontaneously Broken Continuous Symmetry". In: *ArXiv e-prints*. arXiv: 1112.5166 [cond-mat.str-el] (cit. on pp. 137, 154, 167, 169).

Metlitski, Max A., Carlos A. Fuertes, and Subir Sachdev (2009). "Entanglement entropy in the $O(N)$ model". In: *Phys. Rev. B* 80 (11), p. 115122. DOI: 10.1103/PhysRevB.80.115122. URL: http://link.aps.org/doi/10.1103/PhysRevB.80.115122 (cit. on pp. 157, 170, 171).

Modi, Kavan et al. (2012). "The classical-quantum boundary for correlations: Discord and related measures". In: *Rev. Mod. Phys.* 84 (4), pp. 1655–1707. DOI: 10.1103/RevModPhys.84.1655. URL: http://link.aps.org/doi/10.1103/RevModPhys.84.1655 (cit. on pp. 46, 47).

Monz, Thomas et al. (2011). "14-Qubit Entanglement: Creation and Coherence". In: *Phys. Rev. Lett.* 106 (13), p. 130506. DOI: 10.1103/PhysRevLett.106.130506. URL: https://link.aps.org/doi/10.1103/PhysRevLett.106.130506 (cit. on p. 251).

Nielsen, M. A. and I. L. Chuang (2000). *Quantum Computation and Quantum Information*. Cambridge University Press. ISBN: 9780521635035 (cit. on p. 61).

Nozieres, P. and D. Pines (1999). *Theory Of Quantum Liquids*. Advanced Books Classics. Avalon Publishing. ISBN: 9780813346533 (cit. on p. 100).

Ollivier, Harold and Wojciech H. Zurek (2001). "Quantum Discord: A Measure of the Quantumness of Correlations". In: *Phys. Rev. Lett.* 88 (1), p. 017901. DOI: 10.1103/PhysRevLett.88.017901. URL: http://link.aps.org/doi/10.1103/PhysRevLett.88.017901 (cit. on pp. 45, 46).

Parsons, Maxwell F. et al. (2016). "Site-resolved measurement of the spin-correlation function in the Fermi-Hubbard model". In: *Science* 353.6305, pp. 1253–1256. ISSN: 0036-8075. DOI: 10.1126/science.aag1430. eprint: http://science.sciencemag.org/content/353/6305/1253.full.pdf. URL: http://science.sciencemag.org/content/353/6305/1253 (cit. on p. 101).

Pekker, D. et al. (2012). "Signatures of the superfluid to Mott insulator transition in equilibrium and in dynamical ramps". In: *Phys. Rev. B* 86 (14), p. 144527. DOI: 10.1103/PhysRevB.86.144527. URL: http://link.aps.org/doi/10.1103/PhysRevB.86.144527 (cit. on p. 111).

Penrose, Oliver and Lars Onsager (1956). "Bose-Einstein Condensation and Liquid Helium". In: *Phys. Rev.* 104 (3), pp. 576–584. DOI: 10.1103/PhysRev.104.576. URL: https://link.aps.org/doi/10.1103/PhysRev.104.576 (cit. on p. 108).

Peschel, Ingo and Viktor Eisler (2009). “Reduced density matrices and entanglement entropy in free lattice models”. In: *Journal of Physics A: Mathematical and Theoretical* 42.50, p. 504003. URL: http://stacks.iop.org/1751-8121/42/i=50/a=504003 (cit. on pp. 69, 77, 79).

Petz, Dénes (1996). “Monotone Metrics On Matrix Spaces”. In: *Linear Algebra and its Applications* 244, pp. 81 –96. ISSN: 0024-3795. DOI: http://dx.doi.org/10.1016/0024-3795(94)00211-8. URL: http://www.sciencedirect.com/science/article/pii/0024379594002118 (cit. on pp. 26, 277).

Pezzè, L. and A. Smerzi (2014). “Quantum theory of phase estimation”. In: *Proceedings of the International School of Physics "Enrico Fermi"*. Ed. by G.M. Tino and M.A. Kasevich. IOS Press, Amsterdam, p. 691. URL: https://arxiv.org/abs/1411.5164 (cit. on pp. 18, 19, 21, 27, 186, 196, 211).

Pezzè, L. et al. (2016). “Non-classical states of atomic ensembles: fundamentals and applications in quantum metrology”. In: *ArXiv e-prints*. arXiv: 1609.01609 [quant-ph] (cit. on pp. 18, 196, 204, 210, 220).

Pezzé, Luca and Augusto Smerzi (2009). “Entanglement, Nonlinear Dynamics, and the Heisenberg Limit”. In: *Phys. Rev. Lett.* 102 (10), p. 100401. DOI: 10.1103/PhysRevLett.102.100401. URL: https://link.aps.org/doi/10.1103/PhysRevLett.102.100401 (cit. on pp. 21, 221).

Pfeuty, Pierre (1970). “The one-dimensional Ising model with a transverse field”. In: *Annals of Physics* 57.1, pp. 79 –90. ISSN: 0003-4916. DOI: http://dx.doi.org/10.1016/0003-4916(70)90270-8. URL: http://www.sciencedirect.com/science/article/pii/0003491670902708 (cit. on pp. 228, 229).

Pires, Diego Paiva et al. (2016). “Generalized Geometric Quantum Speed Limits”. In: *Phys. Rev. X* 6 (2), p. 021031. DOI: 10.1103/PhysRevX.6.021031. URL: http://link.aps.org/doi/10.1103/PhysRevX.6.021031 (cit. on p. 21).

Pitaevskii, L.P. and S. Stringari (2003). *Bose-Einstein Condensation*. International Series of Monographs on Physics. Clarendon Press. ISBN: 9780198507192 (cit. on pp. 67, 104, 110, 136).

Preiss, Philipp M. et al. (2015). “Quantum gas microscopy with spin, atom-number, and multilayer readout”. In: *Phys. Rev. A* 91 (4), p. 041602. DOI: 10.1103/PhysRevA.91.041602. URL: http://link.aps.org/doi/10.1103/PhysRevA.91.041602 (cit. on p. 100).

Preiss, Philipp (2015). “Atomic Bose-Hubbard systems with single -particle atomic control”. PhD thesis. Harvard University. URL: http://greiner.physics.harvard.edu/Theses/ppreiss_thesis.pdf (cit. on pp. 100, 104).

Sachdev, S. (2001). *Quantum Phase Transitions*. Cambridge University Press. ISBN: 9780521004541 (cit. on pp. 191, 192, 194, 195, 199, 215, 217, 226, 228, 234, 236, 238, 239, 241).

Sachdev, Subir and Jinwu Ye (1992). “Universal quantum-critical dynamics of two-dimensional antiferromagnets”. In: *Phys. Rev. Lett.* 69 (16), pp. 2411–2414. DOI: 10.1103/PhysRevLett.69.2411. URL: https://link.aps.org/doi/10.1103/PhysRevLett.69.2411 (cit. on p. 194).

Schrödinger, Erwin (1926). “An Undulatory Theory of the Mechanics of Atoms and Molecules”. In: *Physical Review* 28, pp. 1049–70. DOI: 10.1103/PhysRev.28.1049 (cit. on p. 13).

Schrödinger, Erwin (1935). “Die gegenwärtiger Situation in der Quantenmechanik”. In: *Naturwissenschaften* 23. English translation by John D. Trimmer reprinted in Quantum Theory and Measurement, J. A. Wheeler and W. H. Zurek (Editors), Princeton University Press (1983), pp. 807–812 ; 823–828 ; 844–849 (cit. on pp. 44, 60).

Sengupta, K. and N. Dupuis (2005). “Mott-insulator to superfluid transition in the Bose-Hubbard model: A strong-coupling approach”. In: *Phys. Rev. A* 71 (3), p. 033629. DOI: 10.1103/PhysRevA.71.033629. URL: http://link.aps.org/doi/10.1103/PhysRevA.71.033629 (cit. on p. 111).

Shalm, Lynden K. et al. (2015). “Strong Loophole-Free Test of Local Realism”. In: *Phys. Rev. Lett.* 115 (25), p. 250402. DOI: 10.1103/PhysRevLett.115.250402. URL: http://link.aps.org/doi/10.1103/PhysRevLett.115.250402 (cit. on p. 44).

Singh, Rajiv R. P., Roger G. Melko, and Jaan Oitmaa (2012). “Thermodynamic singularities in the entanglement entropy at a two-dimensional quantum critical point”. In: *Phys. Rev. B* 86 (7), p. 075106. DOI: 10.1103/PhysRevB.86.075106. URL: http://link.aps.org/doi/10.1103/PhysRevB.86.075106 (cit. on p. 171).

Song, H. Francis et al. (2011). “Entanglement entropy of the two-dimensional Heisenberg antiferromagnet”. In: *Phys. Rev. B* 83 (22), p. 224410. DOI: 10.1103/PhysRevB.83.224410. URL: http://link.aps.org/doi/10.1103/PhysRevB.83.224410 (cit. on pp. 68, 137, 139, 169).

Song, H. Francis et al. (2012). “Bipartite fluctuations as a probe of many-body entanglement”. In: *Phys. Rev. B* 85 (3), p. 035409. DOI: 10.1103/PhysRevB.85.

035409. URL: http://link.aps.org/doi/10.1103/PhysRevB.85.035409 (cit. on pp. 56, 61).

Sørensen, Anders S. and Klaus Mølmer (2001). "Entanglement and Extreme Spin Squeezing". In: *Phys. Rev. Lett.* 86 (20), pp. 4431–4434. DOI: 10.1103/PhysRevLett.86.4431. URL: https://link.aps.org/doi/10.1103/PhysRevLett.86.4431 (cit. on pp. 220, 224).

Streltsov, A., G. Adesso, and M. B. Plenio (2016). "Quantum Coherence as a Resource". In: *ArXiv e-prints*. arXiv: 1609.02439 [quant-ph] (cit. on pp. 23, 24, 50).

Susskind, L. and J. Lindesay (2005). *An Introduction to Black Holes, Information and the String Theory Revolution: The Holographic Universe*. World Scientific. ISBN: 9789812560834 (cit. on pp. 71, 74).

Swingle, B. (2013). "Structure of entanglement in regulated Lorentz invariant field theories". In: *ArXiv e-prints*. arXiv: 1304.6402 [cond-mat.stat-mech] (cit. on pp. 74, 154).

Swingle, B. and J. McGreevy (2015). "Area Law for Gapless States from Local Entanglement Thermodynamics". In: *ArXiv e-prints*. arXiv: 1505.07106 [cond-mat.str-el] (cit. on pp. 57, 70, 71, 74, 75).

Swingle, Brian (2010). "Entanglement Entropy and the Fermi Surface". In: *Phys. Rev. Lett.* 105 (5), p. 050502. DOI: 10.1103/PhysRevLett.105.050502. URL: https://link.aps.org/doi/10.1103/PhysRevLett.105.050502 (cit. on pp. 96, 99).

Täuber, U.C. (2014). *Critical Dynamics: A Field Theory Approach to Equilibrium and Non-Equilibrium Scaling Behavior*. Cambridge University Press. ISBN: 9780521842235 (cit. on pp. 28, 37–39, 189, 193, 194, 199, 201, 202).

Tóth, Géza (2012). "Multipartite entanglement and high-precision metrology". In: *Phys. Rev. A* 85 (2), p. 022322. DOI: 10.1103/PhysRevA.85.022322. URL: https://link.aps.org/doi/10.1103/PhysRevA.85.022322 (cit. on pp. 51, 196, 220).

Unruh, W. G. (1976). "Notes on black-hole evaporation". In: *Phys. Rev. D* 14, pp. 870–892. DOI: 10.1103/PhysRevD.14.870 (cit. on p. 71).

Vedral, V. (2002). "The role of relative entropy in quantum information theory". In: *Rev. Mod. Phys.* 74 (1), pp. 197–234. DOI: 10.1103/RevModPhys.74.197. URL: https://link.aps.org/doi/10.1103/RevModPhys.74.197 (cit. on pp. 19, 59).

Werner, Reinhard F. (1989). "Quantum states with Einstein-Podolsky-Rosen correlations admitting a hidden-variable model". In: *Phys. Rev. A* 40 (8), pp. 4277–4281.

DOI: 10.1103/PhysRevA.40.4277. URL: http://link.aps.org/doi/10.1103/PhysRevA.40.4277 (cit. on pp. 44, 46).

Wigner, E. P. and Mutsuo M. Yanase (1963). "Information Contents of Distributions". In: *Proceedings of the National Academy of Sciences* 49.6, pp. 910–918. eprint: http://www.pnas.org/content/49/6/910.full.pdf. URL: http://www.pnas.org/content/49/6/910.short (cit. on pp. 34, 36, 247).

Wimmer, M. (2012). "Algorithm 923: Efficient Numerical Computation of the Pfaffian for Dense and Banded Skew-Symmetric Matrices". In: *ACM Trans. Math. Softw.* 38.4, 30:1–30:17. ISSN: 0098-3500. DOI: 10.1145/2331130.2331138. URL: http://doi.acm.org/10.1145/2331130.2331138 (cit. on p. 231).

Wineland, D. J. et al. (1994). "Squeezed atomic states and projection noise in spectroscopy". In: *Phys. Rev. A* 50 (1), pp. 67–88. DOI: 10.1103/PhysRevA.50.67. URL: https://link.aps.org/doi/10.1103/PhysRevA.50.67 (cit. on pp. 221, 226, 250).

Wiseman, H.M. and G.J. Milburn (2010). *Quantum Measurement and Control*. Cambridge University Press. ISBN: 9780521804424 (cit. on p. 24).

Wolf, Michael M. (2006). "Violation of the Entropic Area Law for Fermions". In: *Phys. Rev. Lett.* 96 (1), p. 010404. DOI: 10.1103/PhysRevLett.96.010404. URL: http://link.aps.org/doi/10.1103/PhysRevLett.96.010404 (cit. on p. 63).

Wong, G. et al. (2013). "Entanglement temperature and entanglement entropy of excited states". In: *Journal of High Energy Physics* 12, 20, p. 20. DOI: 10.1007/JHEP12(2013)020. arXiv: 1305.3291 [hep-th] (cit. on pp. 72, 74, 140, 150).

Yang, C. N. (1962). "Concept of Off-Diagonal Long-Range Order and the Quantum Phases of Liquid He and of Superconductors". In: *Rev. Mod. Phys.* 34 (4), pp. 694–704. DOI: 10.1103/RevModPhys.34.694. URL: https://link.aps.org/doi/10.1103/RevModPhys.34.694 (cit. on p. 108).

Zhang, C. et al. (2016). "Determining the speed of multipartite quantum systems by few local measurements". In: *ArXiv e-prints*. arXiv: 1611.02004 [quant-ph] (cit. on p. 27).

de Broglie, Louis (1924). "Recherches sur la théorie des Quanta". Theses. URL: https://tel.archives-ouvertes.fr/tel-00006807 (cit. on p. 13).

von Prillwitz, Kai, Łukasz Rudnicki, and Florian Mintert (2015). “Contrast in multipath interference and quantum coherence”. In: *Phys. Rev. A* 92 (5), p. 052114. DOI: 10.1103/PhysRevA.92.052114. URL: http://link.aps.org/doi/10.1103/PhysRevA.92.052114 (cit. on p. 18).

Appendix A

A classical-quantum state has vanishing quantum covariance

In this appendix, we show that a classical-quantum state has a vanishing quantum f-covariance. We are considering a family of coherence measures (see Section 1.5)

$$\mathcal{C}_f(\rho, H) = \frac{f(0)}{2} \sum_{ij} \frac{(p_i - p_j)^2}{p_i f(p_j/p_i)} \langle i|H|j\rangle\langle j|H|i\rangle \tag{A.1}$$

Where f are functions classified by Petz (1996). Here, $\rho = \sum_i p_i |i\rangle\langle i|$ and H is some observable. Among these coherence measures are the quantum Fisher information, the Wigner-Yanase skew informations, and the quantum variance. Then, the f-quantum covariance of O_A and O_B is defined as :

$$2\text{covar}_Q^f(\rho, O_A, O_B) = \mathcal{C}_f(\rho, O_A + O_B) - \mathcal{C}_f(\rho, O_A) - \mathcal{C}_f(\rho, O_B) \tag{A.2}$$

or equivalently

$$\text{covar}_Q^f(\rho, O_A, O_B) = \frac{f(0)}{2} \sum_{ij} \frac{(p_i - p_j)^2}{p_i f(p_j/p_i)} \langle i|O_A|j\rangle\langle j|O_B|i\rangle \tag{A.3}$$

where we used that $p_i f(p_j/p_i) = p_j f(p_i/p_j)$. Then, we consider a classical-quantum state

$$\rho^{CQ} = \sum_\mu p_\mu |\mu^A\rangle\langle\mu^A| \otimes \sigma_\mu^B \tag{A.4}$$

with $\langle\mu^A|\nu^A\rangle = \delta_{\mu\nu}$. We also introduce :

$$\sigma_\mu^B = \sum_k p_{k|\mu} |\psi_{\mu,k}^B\rangle\langle\psi_{\mu,k}^B| \tag{A.5}$$

$$\forall\mu \ \langle\psi_{\mu,k}^B|\psi_{\mu,k'}^B\rangle = \delta_{k,k'} \tag{A.6}$$

Then, the diagonal form of ρ^{CQ} is given by :

$$\rho^{CQ} = \sum_{\mu,k} p_{\mu,k} |\mu^A\rangle |\psi^B_{\mu,k}\rangle \langle \mu^A| \langle \psi^B_{\mu,k}| \tag{A.7}$$

with the notation $p_{\mu,k} = p_\mu p_{k|\mu}$. Given all that, the proof that $\mathrm{covar}^f_Q(\rho^{CQ}, O_A, O_B) = 0$ is immediate:

$$\begin{aligned} \mathrm{covar}^f_Q(\rho^{CQ}, O_A, O_B) = \sum_{\mu,\nu,k,k'} g(p_{\mu,k}, p_{\nu,k'}) \quad & \langle \mu^A | \langle \psi^B_{\mu,k} | O_A | \nu^A \rangle | \psi^B_{\nu,k'} \rangle \\ \times \quad & \langle \nu^A | \langle \psi^B_{\nu,k'} | O_B | \mu^A \rangle | \psi^B_{\mu,k} \rangle \end{aligned} \tag{A.8}$$

with $g(p_i, p_j) = \frac{f(0)(p_i - p_j)^2}{2 p_i f(p_j/p_i)} = 0$ if $p_i = p_j$. First, the matrix element of O_B gives a $\delta_{\mu,\nu}$, then, the matrix element of O_A gives a $\delta_{k,k'}$ (because we must have $\mu = \nu$) and since $g(p_{\mu,k}, p_{\mu,k}) = 0$, we conclude that $\mathrm{covar}^f_Q(\rho^{CQ}, O_A, O_B) = 0$.